
On the Renormalization of
the Two-Higgs-Doublet Model

Masterarbeit
von

Marcel Krause

An der Fakultät für Physik
Institut für Theoretische Physik

Referent: Prof. Dr. M. M. Mühlleitner (KIT, Karlsruhe)

Korreferent: Prof. Dr. R. Santos (ISEL & ULISBOA, Lissabon)

Bearbeitungszeit: 11. Mai 2015 – 11. Mai 2016

Hiermit versichere ich, dass ich die vorliegende Arbeit selbständig verfasst und keine anderen als die angegebenen Hilfsmittel benutzt, die wörtlich oder inhaltlich übernommenen Stellen als solche kenntlich gemacht und die Satzung des Karlsruher Instituts für Technologie (KIT) zur Sicherung guter wissenschaftlicher Praxis in der aktuell gültigen Fassung beachtet habe.

Karlsruhe, den 11. Mai 2016

.....
(Marcel Krause)

Als Masterarbeit anerkannt.

Karlsruhe, den 11. Mai 2016

.....
(Prof. Dr. M. M. Mühlleitner)

*“Es irrt der Mensch
so lang er strebt.”*

Johann Wolfgang von Goethe
(Faust. Der Tragödie erster Teil)

Contents

1. Introduction	1
2. Introduction to the Two-Higgs-Doublet Model	5
2.1. Motivation	5
2.2. Constraints on Theories Beyond the Standard Model	6
2.2.1. The ρ Parameter	6
2.2.2. Flavor-Changing Neutral Currents	7
2.2.3. Unitarity Constraints	7
2.3. The Electroweak 2HDM Lagrangian	7
2.4. The Scalar 2HDM Potential	8
2.5. The Scalar Lagrangian	12
2.6. The Yukawa Lagrangian and FCNCs	14
2.7. Gauge-Fixing Procedure and Faddeev-Popov Ghosts	15
2.8. Set of Independent Parameters	16
3. Partial Decay Widths of One-to-Two Processes at Next-to-Leading Order	17
3.1. Kinematics of Decay Processes at Leading-Order	17
3.2. Partial Decay Width at Next-to-Leading Order	19
4. Renormalization of the Two-Higgs-Doublet Model	21
4.1. Divergences in Classical and Quantum Field Theories	21
4.2. Regularization and Renormalization	23
4.3. On-Shell Renormalization	24
4.4. Tadpole Renormalization	29
4.4.1. Standard Tadpole Scheme	30
4.4.2. Alternative Tadpole Scheme	32
4.5. Renormalization of the Gauge Sector	39
4.6. Renormalization of the Fermion Sector	41
4.7. Renormalization of the Scalar Fields and Masses	43
4.8. Renormalization of the Scalar Mixing Angles α and β	45
4.8.1. Minimal Subtraction Scheme	46
4.8.2. Kanemura's Scheme	46
4.8.3. Pinched Scheme	50
4.8.4. Process-Dependent Scheme	53
4.9. Renormalization of Λ_5	58
4.9.1. $\overline{\text{MS}}$ Scheme	59
4.9.2. Improved $\overline{\text{MS}}$ Scheme	59
4.9.3. Process-Dependent Scheme	60
4.10. Renormalization of the Gauge-Fixing Lagrangian	64

5. The Decays $H^+ \rightarrow W^+ h^0/H^0$ at Next-to-Leading Order	65
5.1. The Partial Decay Width at LO	66
5.2. NLO Virtual Corrections	66
5.3. IR Divergences and Real Corrections	69
5.4. Gauge-Dependence of the NLO Amplitude	71
6. The Decay $H^0 \rightarrow Z^0 Z^0$ at Next-to-Leading Order	75
6.1. The Partial Decay Width at LO	76
6.2. The Partial Decay Width at NLO	76
6.3. Gauge-Dependence of the NLO Amplitude	79
7. The Decay $H^0 \rightarrow h^0 h^0$ at Next-to-Leading Order	81
7.1. The Partial Decay Width at LO	82
7.2. The Partial Decay Width at NLO	82
7.3. Gauge-Dependence of the NLO Amplitude	84
8. Numerical Results	87
8.1. Used Software Packages	87
8.2. Input Parameter Sets	88
8.3. Numerical Results for the Decays $H^+ \rightarrow W^+ h^0/H^0$	92
8.4. Numerical Results for the Decay $H^0 \rightarrow Z^0 Z^0$	96
8.5. Numerical Results for the Decay $H^0 \rightarrow h^0 h^0$	97
9. Conclusion and Outlook	103
A. Alternative Parametrization of the 2HDM Potential	107
B. Introduction to the Pinch Technique	109
B.1. Motivation	109
B.2. Basic Principles of the Pinch Technique	110
B.2.1. Cancellation of Gauge-Dependences within One-Loop Amplitudes	110
B.2.2. The Pinch Technique in Practice	112
B.3. Gauge-Independent Quark-Quark Scattering Amplitude	113
B.3.1. Preliminary Remarks	113
B.3.2. The Scattering Amplitude at LO	113
B.3.3. Pinch Contributions from the Box Diagrams	114
B.3.4. Pinch Contributions from the Triangle Diagrams	117
B.3.5. Pinch Contributions from the Quark Self-Energy Diagrams	120
B.3.6. Pinch Contributions from the Gluon Self-Energy Diagrams	120
B.3.7. The Full One-Loop Scattering Amplitude	121
B.3.8. Additional Pinch Contributions from the Three-Gluon Vertex	123
B.3.9. Creation of a Pinched Gluon Self-Energy	126
C. The Pinch Technique in the 2HDM	129
C.1. The Pinch Technique in the 2HDM in Practice	129
C.2. The Pinch Technique in the CP-Even Sector	131
C.2.1. Gauge-Dependence of the CP-Even Self-Energies	131
C.2.2. Derivation of the CP-Even Pinched Self-Energies	134
C.3. The Pinch Technique in the CP-Odd and Charged Sectors	139
Acknowledgement / Danksagungen	141
References	143

CHAPTER 1

Introduction

Even centuries before the advent of high-energy physics, the concept that ordinary matter might consist of smaller building blocks has driven scientific and philosophic curiosity alike. The ancient Greek word *átomos*, literally translated to “indivisible” [1], is a remnant of this belief which was applied in the last two centuries in chemistry by structuring the atoms of the periodic table of elements as the fundamental components of all matter. It was not until the end of the 19th century that scientists realized that atoms are not truly indivisible, but consist of smaller building blocks themselves. The electron was the first of these sub-atomic particles to be discovered and the detection of protons and neutrons soon followed, enabling a complete explanation of the inner structure of atoms in the picture of the *Rutherford model* [2, 3].

Due to the development of quantum mechanics in the early 20th century, the duality between particles and waves became clear, and the division between particles according to one of their intrinsic quantum mechanical properties, called the spin, was presented in a mathematically rigorous way. Subsequently, the unification of quantum mechanics with the theory of physical fields was achieved in the form of quantum field theories. The first of these theories to be mathematically complete, called *quantum electrodynamics*, explains among other phenomena the electromagnetic interaction of charged particles and photons [4, 5].

The enormous success of quantum electrodynamics led to the search for more general field theories, trying to explain not only the electromagnetic interaction, but additionally, the *weak interaction*, which explains radioactive decays, and the inner structure of the nuclei, described by the *strong interaction*. In the middle of the 20th century, the development of particle accelerators allowed for the observation of particle collisions at higher energies. This in turn led to the observation that all baryons, e.g. protons and neutrons, are composed of quarks as their fundamental elementary particles, and the interaction between those particles is mediated by photons γ , electroweak gauge bosons Z^0 , W^\pm and gluons g as the carriers of the fundamental forces [3].

In order to arrive at a more fundamental theory of particle physics, the electromagnetic and weak interactions were unified to the so-called *electroweak interactions*. This theory, together with quantum electrodynamics, was used in the late 1970s to build up the *Standard Model* (SM) of particle physics [6–8]. Within the SM, all interactions and particles of nature known to date (apart from gravity) arise in a mathematically rigorous way [3, 5].

Through the course of the second half of the 20th century, every component of the SM was observed at a variety of collider experiments, and with the discovery of the top quark in 1995 [9, 10] and of the τ neutrino in 2000 [11], the observation of the lepton, hadron and gauge boson sectors of the SM was completed. The last missing piece of the SM was a scalar particle, called the Higgs boson, being predicted as a fundamental building block of the SM as early as 1968 [12–16]. Over four centuries later, such a scalar particle was discovered at the Large Hadron Collider (LHC) in 2012 [17, 18], finally completing the Standard Model of particle physics.

Although the theory of the SM turned out to be successful in the last decades and electroweak precision measurements suggest a so-far very good agreement with SM predictions [19–26], several phenomena exist that are not explainable with our current understanding of particle physics. Among these is the dominance of matter over antimatter in our universe [27] and the absence of a valid candidate for dark matter within the SM framework, while experimental data establish an abundance of dark matter with respect to ordinary matter in our universe [28]. Therefore, it is necessary to explore physics beyond the Standard Model (BSM) in order to propose solutions to the so-far open problems within the SM.

The Two-Higgs-Doublet Model (2HDM), which is investigated in this thesis, is a BSM theory which is capable of solving some of the problems mentioned above while still preserving the good agreement between the SM and experiments. The 2HDM provides a simple extension of the SM through the introduction of an additional scalar doublet in the Higgs sector, giving rise to a possible candidate for dark matter [29, 30] and mechanisms to explain the dominance of matter over antimatter [31]. Due to the second Higgs doublet, the phenomenology and scalar particle content is extended in comparison to the SM, containing one light and one heavy neutral CP-even Higgs boson (h^0 and H^0 , respectively), one neutral CP-odd Higgs A^0 and two charged scalar Higgs bosons H^\pm [32, 33].

With the LHC now being operated in run II at 13 TeV, the exploration of the scalar sector is expected to reveal more details. In a theory with an extended Higgs sector like the 2HDM, the decay of charged Higgs bosons is expected to produce good signals at the LHC. The comparison between theory and data requires precise predictions obtained through higher-order calculations. To achieve this goal, the first important step is the complete renormalization of the 2HDM.

This thesis focuses on the electroweak sector of the 2HDM and its renormalization. Due to the rotation of the scalar fields from the gauge basis to their mass eigenstates, the 2HDM requires the renormalization of two scalar mixing angles α and β [34, 35]. The renormalization of these mixing angles is a subtle task, since there is no natural way of defining them through a physically motivated renormalization scheme. Additionally, an unsuitable choice of scheme might introduce gauge-dependences in the one-loop amplitude and consequently in physical observables, thus breaking gauge-invariance of next-to-leading order calculations [36].

Within the Minimal Supersymmetric Standard Model (MSSM), where the scalar mixing angle β needs to be renormalized, a “no-go theorem” was discussed [36] which states that a renormalization scheme for β may not be simultaneously gauge-independent, process-independent and numerically stable. Within this thesis, this discussion is extended to the two scalar mixing angles and different renormalization schemes for α and β are analyzed with respect to these three properties. Additionally, we consider different renormalization schemes for the 2HDM parameter Λ_5 , which is proportional to the fields in the 2HDM potential that softly violate a discrete \mathbb{Z}_2 symmetry. Hence, the purpose of this thesis is to compare different renormalization schemes and propose a numerically stable, gauge- and process-independent renormalization scheme of the scalar mixing angles for the 2HDM, as well as a suitable renormalization scheme for Λ_5 .

The thesis is structured as follows.

Chapter 2 presents an introduction to the Two-Higgs-Doublet Model. In Sec. 2.1, we will motivate the exploration of physics beyond the Standard Model and particularly the 2HDM. To that end, it is necessary to take care of several theoretical and experimental constraints on any new physical theory, as discussed in Sec. 2.2. In Sec. 2.3, the complete electroweak Lagrangian of the 2HDM is presented. It contains the scalar potential of the 2HDM, whose parametrization, rich vacuum structure and particle content is presented in Sec. 2.4 as the main part of the introduction to the 2HDM. In the subsequent Sec. 2.5, the full scalar Lagrangian and the electroweak symmetry breaking within the 2HDM are analyzed. The interaction with fermions is discussed in Sec. 2.6, where additionally, mechanisms for avoiding flavor-changing neutral currents are introduced. The necessary gauge-fixing of the Lagrangian is implemented in Sec. 2.7, followed by the full set of parameters of the 2HDM.

In Chapter 3, we discuss the connection between decay amplitudes, following from field theoretical calculations, and partial decay widths as observables at a collider experiment for one-to-two decay processes. This discussion is presented for tree-level calculations in Sec. 3.1 and at next-to-leading order in Sec. 3.2 in a generic way, so that it can be applied to a variety of decay processes.

The renormalization of the Two-Higgs-Doublet Model in Chapter 4 forms the main part of this thesis. We start with an overview of the appearance of divergences in higher-order calculations in Sec. 4.1 and their regularization and renormalization in Sec. 4.2. In Sec. 4.3, we present the on-shell renormalization of scalar fields for the 2HDM as an exemplary renormalization method. In spontaneously broken gauge symmetries, special care has to be taken with respect to the renormalization of the tadpole terms in order to preserve the minimum conditions of the potential to all orders. This is discussed in Sec. 4.4. In the subsequent Sec. 4.5 to Sec. 4.7, the generic results of the on-shell renormalization procedure are applied to the gauge boson, fermion and scalar sector of the 2HDM. In Sec. 4.8, different renormalization schemes for the 2HDM-specific scalar mixing angles α and β are discussed with respect to gauge-dependence of the one-loop amplitude. The last independent parameter of our parametrization of the 2HDM, Λ_5 , is renormalized in two different schemes in Sec. 4.9, and the chapter closes with a discussion about the renormalization of the gauge-fixing Lagrangian in Sec. 4.10.

The subsequent three chapters introduce 2HDM-specific decays of the heavy CP-even Higgs H^0 and the charged Higgs H^+ , namely the decays $H^+ \rightarrow W^+ h^0/H^0$ in Chapter 5, $H^0 \rightarrow Z^0 Z^0$ in Chapter 6 and $H^0 \rightarrow h^0 h^0$ in Chapter 7. For all processes, the calculation of the tree-level and next-to-leading order partial decay width is presented and the gauge-dependence of the one-loop amplitude for the different renormalization schemes of the scalar angles and Λ_5 are discussed. In the case of the first process, we additionally discuss the infrared divergence of the one-loop amplitude and its regularization as well as the cancellation of all infrared divergences through the inclusion of real corrections.

In Chapter 8, the numerical evaluation of the next-to-leading order partial decay widths is presented. To this end, we present the software packages as well as the 2HDM input parameter sets that we use for our analysis. Subsequently, the numerical results for all processes introduced in the previous three chapters are presented. The different renormalization schemes for the scalar mixing angles and Λ_5 are compared with respect to numerical stability of the next-to-leading order partial decay width.

Chapter 9 gives a summary of the previous chapters and the results that were obtained. A renormalization scheme for the 2HDM is presented that is gauge-independent, process-independent as well as numerically stable. Finally, suggestions are proposed for a further investigation of the renormalization schemes, especially of Λ_5 , as well as for a subsequent numerical analysis of the results.

Introduction to the Two-Higgs-Doublet Model

2.1. Motivation

The phenomenology of the gauge boson and fermion sector of the electroweak Standard Model of particle physics has been well investigated so far. The detection of the Higgs boson in 2012 [17, 18] enabled the exploration of the scalar sector of the theory for the first time, and with run II of the LHC now being in full swing, taking data at a center-of-mass energy of 13 TeV, the Higgs couplings will be measured in even greater detail.

The SM uses the simplest of all possible scalar structures (apart from a singlet), namely one complex $SU(2)_L$ doublet [14, 37], being referred to as the *minimal Higgs structure* [32]. From an experimental point of view, the detected Higgs boson is so far well compatible with this minimal Higgs structure [25, 26] and electroweak precision measurements show a very good agreement with the SM [19–21], so naturally, the question arises why investigations of any BSM physics should be strived. Despite good agreement between theory and experiment, there are several reasons speaking for the existence of an extended BSM sector.

From a theoretical point of view, the introduction of the Higgs mechanism is an elegant way to explain the generation of mass in the otherwise massless gauge theory of the SM [12] while still preserving its gauge symmetry. However, higher-order corrections to the physical Higgs boson mass introduce a strong dependence on the renormalization scale of the theory [38]. As a consequence, the Higgs boson mass is expected to be of the order of a scale where new physics appears, for instance the Planck scale, but instead, the Higgs mass differs from this scale by astonishing 17 orders of magnitude. This so-called *hierarchy problem* can be solved through the cancellation of the large loop contributions in the framework of supersymmetry (SUSY), which is amongst the most popular and well studied theories for BSM physics. Due to the structure of the SUSY superpotential, it is not sufficient to consider only one Higgs doublet. Instead, two doublets are needed in order to give mass to both up- and down-type quarks [32, 39, 40]. Within the scope of this thesis, we do not consider a SUSY theory but restrict ourselves to an extension of the scalar sector in the form of two $SU(2)_L$ doublets, giving rise to the 2HDM, without any additional SUSY relations or particles. While the 2HDM does not have the advantage of SUSY models to solve the hierarchy problem, the theory is still interesting, since it offers solutions to other unsolved problems of the SM.

Measurements show that the ordinary baryonic matter accounts only for roughly 15% of the total matter in the universe, with the other 85% being so-called *dark matter* [28, 41]. A special case of a 2HDM, the *Inert Two-Higgs-Doublet Model* (IDM) establishes an unbroken \mathbb{Z}_2 symmetry for one of the two Higgs doublets, so that the vacuum expectation value of this doublet vanishes. As a consequence, one of the doublets provides the SM-like Higgs boson, while the other doublet does not couple to quarks and leptons, but still has a non-vanishing mass. This *inert* doublet serves as the dark matter candidate of the IDM [29, 30].

Another cosmological observation that is not explicable within the SM is the dominance of matter over antimatter in our universe. As one of the three *Sakharov conditions* necessary for baryogenesis in the universe, the gauge theory describing nature must provide methods for violation of charge and parity (CP) symmetries that are strong enough to account for the dominance of matter over antimatter [27]. Within the SM, a source of CP-violation comes through the non-vanishing phase in the Cabibbo-Kobayashi-Maskawa (CKM) matrix [42, 43], however, it is not strong enough to fully explain baryogenesis [44]. Through the extended scalar sector of the 2HDM, it is possible to introduce new sources of explicit and spontaneous CP-violation in order to explain baryogenesis [31, 45].

2.2. Constraints on Theories Beyond the Standard Model

2.2.1. The ρ Parameter

Focusing on an extension of the scalar structure of the SM, one has to be careful not to violate several theoretical and experimental constraints. If we consider the electroweak $SU(2)_L \times U(1)_Y$ gauge theory with n scalar Higgs doublets Φ_i , with their weak hypercharges Y_i , weak isospins I_i and vacuum expectation values v_i ($i = 1, \dots, n$), then one of the most restrictive constraints can be formulated by introducing the ρ parameter [32]

$$\rho = \frac{\sum_{i=1}^n v_i [4I_i(I_i + 1) - Y_i^2]}{\sum_{i=1}^n 2Y_i^2 v_i} . \quad (2.1)$$

The constraint on any scalar extension of the Standard Model is the experimental fact that the ρ parameter is very close to 1 [46]:

$$\rho_{\text{exp}} = 1.00040 \pm 0.00024 . \quad (2.2)$$

For the Standard Model with only one complex $SU(2)_L$ doublet with weak isospin $I = 1/2$ and hypercharge $Y = 1$, Eq. (2.1) reduces to

$$\rho_{\text{SM}} = \frac{m_W^2}{m_Z^2 \cos^2(\Theta_W)} = 1 , \quad (2.3)$$

with m_Z and m_W being the masses of the Z^0 and W^\pm gauge bosons and Θ_W being the Weinberg angle. In the SM, Eq. (2.3) is automatically fulfilled by the theory [47]. However, the minimal Higgs sector of the Standard Model is not the only way to realize $\rho = 1$ from a theoretical point of view. In fact, there are infinitely many possible realizations of the Higgs sector [32], as long as the combination of isospins, hypercharges and vacuum expectation values are such that the ρ parameter in Eq. (2.1) is within current experimental bounds.

While in principle there are complicated extensions possible, e.g. by adding the representation $I = 3$ and $Y = 4$ [32], the simplest extensions are those where doublets with weak isospin $I_i = 1/2$ and hypercharge $Y_i = 1$ are added. In that sense, the simplest extension of the scalar sector of the SM is the addition of just one other complex $SU(2)_L$ doublet, giving rise to the 2HDM.

2.2.2. Flavor-Changing Neutral Currents

Many BSM theories introduce the possibility of *flavor-changing neutral current* (FCNC) processes, i.e. processes that involve the change of the particle flavor without a coincident alteration of its electric charge. Experimental data puts very strict constraints on the branching ratios of FCNC processes [48, 49]. Within the Standard Model, FCNC reactions are automatically ruled out on tree level and appear only in higher-order calculations, where they are suppressed by the Glashow–Iliopoulos–Maiani (GIM) mechanism [50]. Therefore, any new physical theory beyond the SM must either prohibit the existence of FCNC at tree level or provide mechanisms to suppress FCNC reactions. The 2HDM provides such a mechanism, thus ensuring not to violate the strict experimental constraints on the observation of flavor-changing neutral currents [32], as will be discussed in Sec. 2.6.

2.2.3. Unitarity Constraints

While the constraints mentioned so far are set up mostly due to experimental data, there is another constraint that emerges purely from theoretical aspects of electroweak symmetry breaking, called the *unitarity constraints* of the theory. The scattering of longitudinal vector bosons $V_L V_L \rightarrow V_L V_L$ (with $V \in \{Z^0, W^\pm\}$) and fermions to longitudinal vector bosons $f_+ \bar{f}_+ \rightarrow V_L V_L$ (where the subscript + stands for fermions with positive helicity) leads to partial decay widths that potentially grow infinitely with an increase of the center-of-mass energy, thus violating the unitarity of the scattering. Within the SM, this problem is solved through electroweak symmetry breaking, which leads to a set of non-trivial cancellations between Feynman diagrams containing the vector bosons, fermions and the Higgs boson. Since electroweak symmetry breaking gives rise to the Higgs coupling g_{HWW} (with H being the SM Higgs boson), these cancellations are ensured automatically by the theory, thus preserving the unitarity constraint [32].

In a theory with an extended Higgs sector composed of additional doublet and singlet Higgs fields, the unitarity constraints still have to be preserved. For this it is sufficient that the Higgs sector (with the BSM Higgs bosons h_i) fulfills the following sum rules of the couplings between fermions, vector bosons and Higgs particles [51]:

$$\sum_i g_{h_i VV}^2 = g_{HVV}^2, \quad (2.4)$$

$$\sum_i g_{h_i VV} g_{h_i f \bar{f}} = g_{HVV} g_{Hf \bar{f}}. \quad (2.5)$$

Through the structure of the electroweak symmetry breaking, the 2HDM exhibits the sum rules given above, thus preserving the unitarity constraints.

2.3. The Electroweak 2HDM Lagrangian

In comparison to the Standard Model, the 2HDM consists of two complex $SU(2)_L$ doublets Φ_i ($i = 1, 2$) with hypercharge $Y = +1$ instead of just one. In this thesis, the focus lies on electroweak corrections to 2HDM-specific decays, only. Therefore, it is sufficient to give the full electroweak Lagrangian of the 2HDM and quantum chromodynamics (QCD) is not considered. Explicitly, the fully quantized electroweak Lagrangian reads

$$\mathcal{L}_{2\text{HDM}}^{\text{EW}} = \mathcal{L}_{\text{YM}} + \mathcal{L}_{\text{F}} + \mathcal{L}_{\text{S}} + \mathcal{L}_{\text{Yuk}} + \mathcal{L}_{\text{GF}} + \mathcal{L}_{\text{FP}}. \quad (2.6)$$

The first two terms consist of the *Yang-Mills Lagrangian* \mathcal{L}_{YM} and the kinematic terms of the fermion sector and the couplings between fermions and gauge bosons, \mathcal{L}_{F} . Since they do

not introduce any new physics when changing from the SM to the 2HDM and their explicit form is not needed later, these terms will be kept implicit in the Lagrangian. For reference, their explicit form can be found e.g. in [5, 52].

The third term of Eq. (2.6) introduces the 2HDM-specific scalar Lagrangian \mathcal{L}_S , which contains the kinetic terms of the two Higgs doublets and the scalar potential $V_{2\text{HDM}}$. Given its rich vacuum structure and particle content, the scalar potential will be investigated separately from the scalar Lagrangian in Sec. 2.4. The full scalar Lagrangian, as well as the mechanism of electroweak symmetry breaking within the 2HDM, is discussed in Sec. 2.5.

In analogy to the SM, the interaction between the extended scalar sector of the 2HDM and the fermionic fields is described within the *Yukawa Lagrangian* \mathcal{L}_{Yuk} . In contrast to the SM, however, the Yukawa theory of the 2HDM potentially gives rise to flavor-changing neutral currents at tree level. Since FCNCs serve as a strict constraint for any BSM theory, as discussed in the previous section, the procedure of isolating and eliminating FCNCs from the 2HDM will be discussed in Sec. 2.6.

Lastly, the quantization of the electroweak Lagrangian requires the introduction of a *gauge-fixing* term \mathcal{L}_{GF} in order to isolate unphysical degrees of freedom, as well as the corresponding *Faddeev-Popov Lagrangian* \mathcal{L}_{FP} which removes these redundant degrees of freedom from the theory. Both Lagrangians will be discussed in Sec. 2.7.

2.4. The Scalar 2HDM Potential

The most general 2HDM potential is constructed out of all possible combinations of $SU(2)_L$ invariants $((\Phi_1^\dagger \Phi_1), (\Phi_2^\dagger \Phi_1), (\Phi_2^\dagger \Phi_2), \dots)$ of the two complex $SU(2)_L$ doublets Φ_i ($i = 1, 2$) such that the potential is still renormalizable. In the most general form, such a potential contains 14 free parameters, is explicitly CP-violating and exhibits minima that can be CP-conserving, CP-violating or charge-violating [33]. While a CP-violating 2HDM potential gives rise to a possible explanation for baryogenesis [53], as it was mentioned in Sec. 2.1, the phenomenological analysis of this thesis restricts itself to a CP-conserving 2HDM. Additionally, a discrete \mathbb{Z}_2 symmetry of the form $\Phi_1 \rightarrow -\Phi_1$ is imposed on the potential to suppress FCNCs in the tree-level Yukawa couplings [32], as discussed in further detail in Sec. 2.6. With these restrictions in mind, one way of parametrizing a general CP-conserving 2HDM potential is given by [33]

$$\begin{aligned} V_{2\text{HDM}}(\Phi_1, \Phi_2) = & m_{11}^2 (\Phi_1^\dagger \Phi_1) + m_{22}^2 (\Phi_2^\dagger \Phi_2) - m_{12}^2 \left[(\Phi_1^\dagger \Phi_2) + (\Phi_2^\dagger \Phi_1) \right] \\ & + \frac{\lambda_1}{2} (\Phi_1^\dagger \Phi_1)^2 + \frac{\lambda_2}{2} (\Phi_2^\dagger \Phi_2)^2 + \lambda_3 (\Phi_1^\dagger \Phi_1) (\Phi_2^\dagger \Phi_2) \\ & + \lambda_4 (\Phi_1^\dagger \Phi_2) (\Phi_2^\dagger \Phi_1) + \frac{\lambda_5}{2} \left[(\Phi_1^\dagger \Phi_2)^2 + (\Phi_2^\dagger \Phi_1)^2 \right]. \end{aligned} \quad (2.7)$$

The potential contains five real-valued, dimensionless parameters λ_i ($i = 1, \dots, 5$) and three real-valued mass parameters m_{11} , m_{22} and m_{12} , so that the full CP-conserving 2HDM potential has eight free real-valued parameters [33]. For convenience, the parameters λ_3 , λ_4 and λ_5 are often combined to a single parameter

$$\lambda_{345} := \lambda_3 + \lambda_4 + \lambda_5. \quad (2.8)$$

Although a discrete \mathbb{Z}_2 symmetry was imposed on the 2HDM potential to avoid FCNCs, Eq. (2.7) still contains a term that explicitly breaks this symmetry. If m_{12} is non-vanishing, the potential is not invariant under the transformation $\Phi_1 \rightarrow -\Phi_1$. But since m_{12} has mass-dimension, this form of symmetry breaking is only soft. Therefore, the parameter may be kept in the potential as long as phenomenologically its effect on FCNC is limited [54].

The parametrization of the potential in Eq. (2.7) exhibits several phenomena of the 2HDM in an elegant way and is thus used in this and the next chapter to explore the vacuum structure and scalar sector in detail. For calculations of 2HDM-specific processes, we will switch to an alternative form of the 2HDM potential given in App. A. It is this form of the potential that is also implemented in the tool `FeynArts` [55], which will be used later on in the computation of the decay amplitudes.

The 2HDM potential in Eq. (2.7) exhibits two CP-conserving, neutral minima $\langle \Phi_1 \rangle$, $\langle \Phi_2 \rangle$ of the form

$$\langle \Phi_1 \rangle = \begin{pmatrix} 0 \\ \frac{v_1}{\sqrt{2}} \end{pmatrix}, \quad \langle \Phi_2 \rangle = \begin{pmatrix} 0 \\ \frac{v_2}{\sqrt{2}} \end{pmatrix}, \quad (2.9)$$

with v_1 and v_2 being the *vacuum expectation values* (vevs) of the doublets Φ_1 and Φ_2 , respectively. By introducing eight real fields ω_i^\pm , ρ_i and η_i ($i = 1, 2$), the doublets may be expanded around these minima, taking the form

$$\Phi_1 = \begin{pmatrix} \omega_1^+ \\ \frac{v_1 + \rho_1 + i\eta_1}{\sqrt{2}} \end{pmatrix}, \quad \Phi_2 = \begin{pmatrix} \omega_2^+ \\ \frac{v_2 + \rho_2 + i\eta_2}{\sqrt{2}} \end{pmatrix}. \quad (2.10)$$

The mechanism of breaking $SU(2)_L \times U(1)_Y$ down to $U(1)_{\text{em}}$ is equivalent to breaking three gauge symmetries, analogous to the Higgs mechanism of the SM [12, 14]. Each broken symmetry corresponds to the existence of a would-be Goldstone boson, through which the gauge bosons acquire mass (and thus, their longitudinal polarizations) [5]. In contrast to the SM, where only one free Higgs field is left after the spontaneous symmetry breaking, there are five fields in the 2HDM, corresponding to five Higgs particles. Two of them form a CP-even doublet, two are charged and one is CP-odd.

Inserting Eq. (2.10) into the 2HDM potential in Eq. (2.7) generates, among others, terms that are linear in the two fields ρ_i . In order for the doublets Φ_i to have their minima truly at $\langle \Phi_i \rangle$, the two minimum conditions

$$\left. \frac{\partial V_{2\text{HDM}}}{\partial \Phi_1^\dagger} \right|_{\langle \Phi_1 \rangle, \langle \Phi_2 \rangle} = 0, \quad \left. \frac{\partial V_{2\text{HDM}}}{\partial \Phi_2^\dagger} \right|_{\langle \Phi_1 \rangle, \langle \Phi_2 \rangle} = 0. \quad (2.11)$$

have to be fulfilled. This is equivalent to the requirement that the two terms linear in the fields ρ_1 and ρ_2 ,

$$\begin{aligned} T_1 &:= m_{11}^2 v_1 - m_{12}^2 v_2 + \frac{1}{2} \lambda_1 v_1^3 + \frac{1}{2} \lambda_{345} v_1 v_2^2, \\ T_2 &:= m_{22}^2 v_2 - m_{12}^2 v_1 + \frac{1}{2} \lambda_2 v_2^3 + \frac{1}{2} \lambda_{345} v_1^2 v_2, \end{aligned} \quad (2.12)$$

called the *tadpole terms* of the potential, must vanish at tree level:

$$T_1|_{\text{tree}} = T_2|_{\text{tree}} = 0. \quad (2.13)$$

This requirement is analogous to the statement that the vacuum expectation values represent the true minima of the two Higgs doublets Φ_1 and Φ_2 in the tree-level potential. Note that there are no terms linear in the fields ω_1^+ and ω_2^+ due to charge conservation, and since we are considering a CP-conserving 2HDM, terms linear in the fields η_1 and η_2 are absent as well.

The tadpole conditions in Eq. (2.13) allow for the elimination of two parameters of the 2HDM potential in favor of the other parameters of the 2HDM. The parameters m_{11}^2 and m_{22}^2 can therefore be replaced as

$$\begin{aligned} m_{11}^2 &= m_{12}^2 \frac{v_2}{v_1} - \frac{1}{2} \lambda_1 v_1^2 - \frac{1}{2} \lambda_{345} v_2^2, \\ m_{22}^2 &= m_{12}^2 \frac{v_1}{v_2} - \frac{1}{2} \lambda_2 v_2^2 - \frac{1}{2} \lambda_{345} v_1^2. \end{aligned} \quad (2.14)$$

Additionally to the terms that are linear in the fields, the insertion of the doublet expansions in Eq. (2.10) into the 2HDM potential generates terms that are bilinear in the fields ω_i^\pm , ρ_i and η_i . Since these bilinear terms contribute to the propagators of the eight fields, they give rise to mass terms. All bilinear terms in the 2HDM potential can be brought into the form

$$\begin{aligned} V_{2\text{HDM}} \Big|_{\text{bilin}} &= \frac{1}{2} \begin{pmatrix} \rho_1 & \rho_2 \end{pmatrix} M_\rho^2 \begin{pmatrix} \rho_1 \\ \rho_2 \end{pmatrix} + \frac{1}{2} \begin{pmatrix} \eta_1 & \eta_2 \end{pmatrix} M_\eta^2 \begin{pmatrix} \eta_1 \\ \eta_2 \end{pmatrix} \\ &+ \frac{1}{2} \begin{pmatrix} \omega_1^+ & \omega_2^+ \end{pmatrix} M_\omega^2 \begin{pmatrix} \omega_1^- \\ \omega_2^- \end{pmatrix}, \end{aligned} \quad (2.15)$$

with the explicit form of the non-diagonal mass matrices given by

$$M_\rho^2 = \begin{pmatrix} m_{12}^2 \frac{v_2}{v_1} + \lambda_1 v_1^2 & -m_{12}^2 + \lambda_{345} v_1 v_2 \\ -m_{12}^2 + \lambda_{345} v_1 v_2 & m_{12}^2 \frac{v_1}{v_2} + \lambda_2 v_2^2 \end{pmatrix} + \begin{pmatrix} \frac{T_1}{v_1} & 0 \\ 0 & \frac{T_2}{v_2} \end{pmatrix}, \quad (2.16)$$

$$M_\eta^2 = \begin{pmatrix} m_{12}^2 - \lambda_5 \\ v_1 v_2 \end{pmatrix} \begin{pmatrix} v_2^2 & -v_1 v_2 \\ -v_1 v_2 & v_1^2 \end{pmatrix} + \begin{pmatrix} \frac{T_1}{v_1} & 0 \\ 0 & \frac{T_2}{v_2} \end{pmatrix}, \quad (2.17)$$

$$M_\omega^2 = \begin{pmatrix} m_{12}^2 - \frac{\lambda_4 + \lambda_5}{2} \\ v_1 v_2 \end{pmatrix} \begin{pmatrix} v_2^2 & -v_1 v_2 \\ -v_1 v_2 & v_1^2 \end{pmatrix} + \begin{pmatrix} \frac{T_1}{v_1} & 0 \\ 0 & \frac{T_2}{v_2} \end{pmatrix}. \quad (2.18)$$

Note the explicit appearance of the tadpole terms in the mass matrices. Usually, the tree-level condition in Eq. (2.13) is applied, so that the mass matrices simplify and the tadpole terms T_i do not have to be taken into account. However, a correct treatment beyond tree level requires to keep the tadpole terms explicitly in the mass matrices. This will be investigated in more detail in Sec. 4.4.

To have physical, propagating particles in the 2HDM, it is necessary to consider eigenstates with specific masses. This can be achieved by diagonalizing the matrices in Eqs. (2.16) – (2.18), which means that for any of the matrices M_ρ^2 , M_η^2 and M_ω^2 , matrices R_α and R_β must be found such that

$$D_\rho^2 = R_\alpha^T M_\rho^2 R_\alpha, \quad (2.19)$$

$$D_\eta^2 = R_\beta^T M_\eta^2 R_\beta, \quad (2.20)$$

$$D_\omega^2 = R_\beta^T M_\omega^2 R_\beta, \quad (2.21)$$

are diagonal matrices (note that M_η^2 and M_ω^2 are proportional to each other, therefore, the transformation matrix R_β is the same for both). The spectral theorem ensures that for the

real-valued, symmetric matrices in Eqs. (2.16) – (2.18), the transformation matrices R_α and R_β are orthogonal. The matrices can be parametrized by two angles α and β , defined over the explicit form of the transformation matrices¹,

$$R_\alpha = \begin{pmatrix} c_\alpha & -s_\alpha \\ s_\alpha & c_\alpha \end{pmatrix}, \quad R_\beta = \begin{pmatrix} c_\beta & -s_\beta \\ s_\beta & c_\beta \end{pmatrix} \quad (2.22)$$

By applying the diagonalizing procedure to the 2HDM potential, the bilinear terms can be cast into the form

$$\begin{aligned} V_{2\text{HDM}} \Big|_{\text{bilin}} &= \frac{1}{2} \begin{pmatrix} H^0 & h^0 \end{pmatrix} D_\rho^2 \begin{pmatrix} H^0 \\ h^0 \end{pmatrix} + \frac{1}{2} \begin{pmatrix} G^0 & A^0 \end{pmatrix} D_\eta^2 \begin{pmatrix} G^0 \\ A^0 \end{pmatrix} \\ &+ \frac{1}{2} \begin{pmatrix} G^\pm & H^\pm \end{pmatrix} D_\omega^2 \begin{pmatrix} G^\pm \\ H^\pm \end{pmatrix}. \end{aligned} \quad (2.23)$$

The fields ω_i^\pm , ρ_i and η_i in the *gauge basis* have been transformed into physical fields

$$\begin{pmatrix} H^0 \\ h^0 \end{pmatrix} = R_\alpha^T \begin{pmatrix} \rho_1 \\ \rho_2 \end{pmatrix} = \begin{pmatrix} c_\alpha & s_\alpha \\ -s_\alpha & c_\alpha \end{pmatrix} \begin{pmatrix} \rho_1 \\ \rho_2 \end{pmatrix}, \quad (2.24)$$

$$\begin{pmatrix} G^0 \\ A^0 \end{pmatrix} = R_\beta^T \begin{pmatrix} \eta_1 \\ \eta_2 \end{pmatrix} = \begin{pmatrix} c_\beta & s_\beta \\ -s_\beta & c_\beta \end{pmatrix} \begin{pmatrix} \eta_1 \\ \eta_2 \end{pmatrix}, \quad (2.25)$$

$$\begin{pmatrix} G^\pm \\ H^\pm \end{pmatrix} = R_\beta^T \begin{pmatrix} \omega_1^\pm \\ \omega_2^\pm \end{pmatrix} = \begin{pmatrix} c_\beta & s_\beta \\ -s_\beta & c_\beta \end{pmatrix} \begin{pmatrix} \omega_1^\pm \\ \omega_2^\pm \end{pmatrix}. \quad (2.26)$$

The mass matrices in Eqs. (2.19) – (2.21) are diagonal in this basis, therefore, the corresponding fields are commonly referred to as the *mass basis* of the 2HDM potential. The entries of the mass matrices are then interpreted as the masses of these physical fields,

$$D_\rho^2 = \begin{pmatrix} m_{H^0}^2 & 0 \\ 0 & m_{h^0}^2 \end{pmatrix}, \quad D_\eta^2 = \begin{pmatrix} m_{G^0}^2 & 0 \\ 0 & m_{A^0}^2 \end{pmatrix}, \quad D_\omega^2 = \begin{pmatrix} m_{G^\pm}^2 & 0 \\ 0 & m_{H^\pm}^2 \end{pmatrix}. \quad (2.27)$$

Since they are needed in Sec. 4.4, the explicit dependences of the masses on the 2HDM parameters shall be given. Their form is automatically determined through the diagonalization procedure as the eigenvalues of the mass matrices in Eqs. (2.16) – (2.18). With the definition

$$v^2 = v_1^2 + v_2^2, \quad (2.28)$$

¹Here and in the following, the short-hand notation $s_x := \sin(x)$, $c_x := \cos(x)$ and $t_x := \tan(x)$ will be used.

the tree-level masses of the particles in the mass basis are given by

$$m_{H^0}^2 = \frac{1}{2} \left[(M_\rho^2)_{11} + (M_\rho^2)_{22} + \sqrt{((M_\rho^2)_{11} - (M_\rho^2)_{22})^2 + 4(M_\rho^2)_{12}^2} \right], \quad (2.29)$$

$$m_{h^0}^2 = \frac{1}{2} \left[(M_\rho^2)_{11} + (M_\rho^2)_{22} - \sqrt{((M_\rho^2)_{11} - (M_\rho^2)_{22})^2 + 4(M_\rho^2)_{12}^2} \right], \quad (2.30)$$

$$m_{G^0}^2 = 0, \quad (2.31)$$

$$m_{A^0}^2 = v^2 \left(\frac{m_{12}^2}{v_1 v_2} - \lambda_5 \right), \quad (2.32)$$

$$m_{G^\pm}^2 = 0, \quad (2.33)$$

$$m_{H^\pm}^2 = v^2 \left(\frac{m_{12}^2}{v_1 v_2} - \frac{\lambda_4 + \lambda_5}{2} \right), \quad (2.34)$$

with $(M_\rho^2)_{ij}$ ($i, j = 1, 2$) being the entries of the first part of the mass matrix M_ρ^2 in Eq. (2.16), i.e. without the tadpole parameters. The massless particles G^0 and G^\pm are the three would-be Goldstone bosons of the 2HDM. The particles H^0 and h^0 form the CP-even doublet, A^0 is the CP-odd Higgs and the two particles H^\pm are the charged Higgs bosons.

For completeness, it should be noted that the diagonalization procedure connects the two angles α and β , introduced in the transformation matrices in Eq. (2.22), with the 2HDM parameters through the following tree-level relations: [32]

$$\mathfrak{t}_\beta = \frac{v_2}{v_1}, \quad (2.35)$$

$$\mathfrak{t}_{2\alpha} = \frac{s_{2\beta} (M^2 - \lambda_{345} v^2)}{c_\beta^2 (M^2 - \lambda_1 v^2) - s_\beta^2 (M^2 - \lambda_2 v^2)}, \quad (2.36)$$

where we introduced the parameter

$$M^2 := \frac{m_{12}^2}{s_\beta c_\beta} \quad (2.37)$$

which is often used as an alternative to m_{12}^2 for the parametrization of the 2HDM [56].

The inverse of the transformation in Eqs. (2.24) – (2.26) can be used to transform the whole 2HDM potential to the mass basis. This also generates terms that are trilinear and quartic in the physical fields. Such terms give rise to trilinear and quartic couplings in the scalar sector. Examples of this will be presented in Sec. 4.9.3 and Sec. 7.2.

2.5. The Scalar Lagrangian

The condensation of the two scalar $SU(2)_L$ doublets Φ_i into symmetry-breaking vacua with non-vanishing vacuum expectation values v_i , cf. Eq. (2.9), gives rise to the rich vacuum structure and particle content of the 2HDM, as described in the previous section. The symmetry breaking further induces the mass generation in the gauge sector, in analogy to the Higgs mechanism of the Standard Model [12]. Local gauge-invariance of the 2HDM Lagrangian is implemented through the covariant derivative²

$$D_\mu = \partial_\mu + ig \frac{\sigma^a}{2} W_\mu^a(x) + ig' \frac{Y}{2} B_\mu(x), \quad (2.38)$$

where W_μ^a ($a = 1, 2, 3$) and B_μ are the $SU(2)_L$ and $U(1)_Y$ gauge boson fields in the gauge basis, respectively. Note that we use Einstein's sum convention for the index a . The constants

²Note that our sign convention for the covariant derivative follows the sign convention for MSSM and 2HDM models that is used in [57], while the Standard Model usually introduces opposite signs for the $SU(2)_L$ term [52].

g and g' are the coupling constants of the gauge boson fields W_μ^a and B_μ , respectively, and the Pauli matrices σ^a and the weak isospin Y are, together with a factor of $1/2$, the generators of the respective groups. The scalar Lagrangian of the 2HDM is then given by

$$\mathcal{L}_S = (D_\mu \Phi_1)^\dagger (D^\mu \Phi_1) + (D_\mu \Phi_2)^\dagger (D^\mu \Phi_2) - V_{2\text{HDM}}(\Phi_1, \Phi_2) . \quad (2.39)$$

In order to preserve local gauge-invariance, the 2HDM Lagrangian is not allowed to contain explicit mass terms for the gauge bosons. Instead, the generation of mass is achieved through spontaneous symmetry breaking. By inserting Eq. (2.9) into Eq. (2.39), the terms bilinear in the gauge boson fields can be isolated in the scalar Lagrangian,

$$\begin{aligned} \mathcal{L}_S|_{\text{bilin}} &= \sum_{i=1}^2 \begin{pmatrix} 0 & \frac{v_i}{\sqrt{2}} \end{pmatrix} \left(g \frac{\sigma^a}{2} W_\mu^a + g' \frac{Y}{2} B_\mu \right)^\dagger \left(g \frac{\sigma^b}{2} W^{\mu,b} + g' \frac{Y}{2} B^\mu \right) \begin{pmatrix} 0 \\ \frac{v_i}{\sqrt{2}} \end{pmatrix} \\ &= \sum_{i=1}^2 \frac{1}{2} \frac{v_i^2}{4} \begin{pmatrix} 0 & 1 \end{pmatrix} \left| \begin{pmatrix} g' B_\mu + g W_\mu^3 & g (W_\mu^1 - i W_\mu^2) \\ g (W_\mu^1 + i W_\mu^2) & g' B_\mu - g W_\mu^3 \end{pmatrix} \right|^2 \begin{pmatrix} 0 \\ 1 \end{pmatrix} \\ &= \frac{1}{2} \frac{v^2}{4} \left[g^2 |W_\mu^1|^2 + g^2 |W_\mu^2|^2 + |-g W_\mu^3 + g' B_\mu|^2 \right] , \end{aligned} \quad (2.40)$$

which is the same as the result of spontaneous symmetry breaking in the Standard Model [5] as long as the vacuum expectation value v , introduced in Eq. (2.28), is interpreted as the measured value of $v \approx 246$ GeV [46]. By diagonalizing the last line of Eq. (2.40), the gauge boson fields are shifted from the gauge basis to the mass basis through the relations

$$W_\mu^\pm = \frac{1}{\sqrt{2}} (W_\mu^1 \mp i W_\mu^2) , \quad (2.41)$$

$$\begin{pmatrix} Z_\mu^0 \\ \gamma_\mu \end{pmatrix} = \begin{pmatrix} c_W & -s_W \\ s_W & c_W \end{pmatrix} \begin{pmatrix} W_\mu^3 \\ B_\mu \end{pmatrix} , \quad (2.42)$$

with the short-hand notation $c_W := \cos(\Theta_W)$ and $s_W := \sin(\Theta_W)$ for the Weinberg angle Θ_W . The four physical fields W_μ^\pm , Z_μ^0 and γ_μ correspond to the W^\pm and Z^0 boson and the photon γ . The diagonalized form of Eq. (2.40) exhibits the mass matrices of the physical fields, with the squared masses of the gauge bosons given by

$$m_W^2 = g^2 \frac{v^2}{4} , \quad (2.43)$$

$$m_Z^2 = (g^2 + g'^2) \frac{v^2}{4} , \quad (2.44)$$

$$m_\gamma^2 = 0 . \quad (2.45)$$

The diagonalization procedure further gives a mathematical definition of the Weinberg angle as a derived parameter,

$$c_W \equiv \frac{m_W}{m_Z} , \quad (2.46)$$

which ensures the ρ parameter to be unity at tree level, cf. Eq. (2.3). For completeness, we note that the electric charge e may be expressed through the coupling constants of the gauge groups by

$$e = \frac{g g'}{\sqrt{g^2 + g'^2}} = g s_W . \quad (2.47)$$

2.6. The Yukawa Lagrangian and FCNCs

The interaction of the fermions and scalar bosons of the 2HDM is determined by the form of the Yukawa Lagrangian. The fermionic particle content of the 2HDM is the same as of the Standard Model. The fermions can be grouped into triplets in flavor space in the form

$$\Psi \in \left\{ U := \begin{pmatrix} u \\ c \\ t \end{pmatrix}, \quad D := \begin{pmatrix} d \\ s \\ b \end{pmatrix}, \quad N := \begin{pmatrix} \nu_e \\ \nu_\mu \\ \nu_\tau \end{pmatrix}, \quad L := \begin{pmatrix} e \\ \mu \\ \tau \end{pmatrix} \right\}, \quad (2.48)$$

where L stands for the charged leptons, N for the neutrinos and U and D for up- and down-type quarks, respectively. In order to correspond to the gauge structure of the electroweak Lagrangian, all fermionic fields Ψ are projected onto their left-handed (LH) and right-handed (RH) states³ via $\Psi_L = \omega_- \Psi$ and $\Psi_R = \omega_+ \Psi$. The chiral projection operators have the explicit form

$$\omega_\mp = \frac{\mathbb{1} \mp \gamma_5}{2}, \quad (2.49)$$

where the subscript $-$ stands for LH and $+$ for RH chirality. In analogy to the SM, all RH fermions of the 2HDM are grouped into $SU(2)_L$ singlets of the form

$$U_R = \begin{pmatrix} u_R \\ c_R \\ t_R \end{pmatrix}, \quad D_R = \begin{pmatrix} d_R \\ s_R \\ b_R \end{pmatrix}, \quad L_R = \begin{pmatrix} e_R \\ \mu_R \\ \tau_R \end{pmatrix}, \quad (2.50)$$

while the LH fermions are grouped into $SU(2)_L$ doublets

$$Q_L := \begin{pmatrix} U_L \\ D_L \end{pmatrix} = \begin{pmatrix} (u_L, c_L, t_L)^T \\ (d_L, s_L, b_L)^T \end{pmatrix}, \quad L_L := \begin{pmatrix} N_L \\ E_L \end{pmatrix} = \begin{pmatrix} (\nu_{e,L}, \nu_{\mu,L}, \nu_{\tau,L})^T \\ (e_L, \mu_L, \tau_L)^T \end{pmatrix}. \quad (2.51)$$

The most general Yukawa Lagrangian is formed out of all possible charge-conserving combinations of the $SU(2)_L$ doublets Ψ_L from the fermionic and $\Phi_{1,2}$ from the Higgs sector as well as the $SU(2)_L$ singlets Ψ_R in such a way that the Lagrangian remains invariant under $SU(2)_L$ transformations. If we denote with ε_{ij} the totally antisymmetric tensor in two dimensions in matrix form,

$$(\varepsilon_{ij}) = \begin{pmatrix} 0 & 1 \\ -1 & 0 \end{pmatrix}, \quad (2.52)$$

and use the short-hand notation $\tilde{\Phi}_k := (\varepsilon_{ij})\Phi_k^*$ ($k = 1, 2$), the most general Yukawa Lagrangian fulfilling these criteria is given by [58]

$$\begin{aligned} \mathcal{L}_{\text{Yuk}} = & -\bar{Q}_L \left[Y_{U,1} \tilde{\Phi}_1 + Y_{U,2} \tilde{\Phi}_2 \right] U_R - \bar{Q}_L \left[Y_{D,1} \Phi_1 + Y_{D,2} \Phi_2 \right] D_R \\ & - \bar{L}_L \left[Y_{L,1} \Phi_1 + Y_{L,2} \Phi_2 \right] E_R + (\text{h.c.}), \end{aligned} \quad (2.53)$$

with the Yukawa coupling matrices $Y_{\Psi,1}, Y_{\Psi,2} \in \mathbb{C}^{3 \times 3}$ in flavor space and with (h.c.) being the Hermitian conjugate of the three preceding terms.

³Apart from the neutrinos, which are considered to be massless for simplicity. As such, they exist in a LH state, only.

In the SM, the Yukawa matrices appearing in the mass terms of the fermions are proportional to those appearing as the coupling matrices between the flavor triplets. As a result, the matrices can be diagonalized simultaneously, giving rise to the masses m_Ψ of the fermions as well as ruling out any FCNCs at tree level. In contrast to that, a general 2HDM introduces the possibility of having flavor-changing neutral currents even at tree level. The diagonalized form of the Yukawa matrices $Y_{\Psi,1}, Y_{\Psi,2}$ appearing in the mass terms will, in general, differ from the diagonalized form of the Yukawa coupling matrices. As a consequence, the Yukawa coupling matrix will not be diagonal in flavor space, which results in tree-level couplings like $\bar{d}sh_i$ (where h_i is a neutral Higgs boson), leading to FCNC reactions e.g. in the form of Kaon mixing [33].

While it is still possible to construct a viable 2HDM with FCNC being present at tree level [33], within the scope of this thesis we restrict ourselves to a model which prohibits FCNCs. The transformation from a general to a flavor-conserving 2HDM can be achieved naturally⁴ by imposing a discrete or continuous symmetry. This follows from the observation that the FCNCs vanish at tree level if fermions with the same quantum numbers, i.e. those that potentially mix, couple only to the same Higgs doublet [59]. Mathematically, this is achieved by imposing \mathbb{Z}_2 symmetries on the Higgs doublets Φ_1 and Φ_2 , additionally to the $SU(2)_L \times U(1)_Y$ symmetry that is demanded from the Lagrangian. In the 2HDM, there are four independent possibilities to implement such symmetries, out of which the two most commonly used shall be presented here [32, 33].

Type I 2HDM: Imposing the discrete \mathbb{Z}_2 symmetry $\Phi_1 \rightarrow -\Phi_1$ enforces all quarks and leptons to couple only to the Higgs doublet Φ_2 , but not to Φ_1 .

Type II 2HDM: Imposing the \mathbb{Z}_2 symmetries $\Phi_1 \rightarrow -\Phi_1$, $D_R \rightarrow -D_R$ and $E_R \rightarrow -E_R$ simultaneously enforces all RH up-type quarks to couple only to Φ_2 , while the RH down-type quarks and RH charged leptons couple only to Φ_1 .

The scalar sector of the MSSM contains a type II 2HDM. Choosing one of the types fixes the Yukawa couplings between the fermions and the Higgs bosons. In tools like `FeynArts`, the coupling constants are kept in a generic form, so that the decision of choosing a type I or II 2HDM is postponed until an actual numerical evaluation.

2.7. Gauge-Fixing Procedure and Faddeev-Popov Ghosts

The Yang-Mills Lagrangian contains the gauge bosons in the form of vector fields. The degrees of freedom exhibited by these vector fields exceeds the degrees of freedom of the physical gauge fields, thus giving rise to gauge-freedom. The quantization procedure of the electroweak 2HDM Lagrangian requires the specification of a gauge in order to parametrize the redundant degrees of freedom. For the calculations performed in this thesis, the set of linear R_ξ gauges is the most convenient one, since the set is also implemented in tools like `FeynArts`. If we introduce the terms [52]

$$\begin{aligned} F_{W^\pm} &= \frac{1}{\sqrt{\xi_W}} \left[\partial^\mu W_\mu^\pm \mp i\xi_W m_W G^\pm \right], \\ F_Z &= \frac{1}{\sqrt{\xi_Z}} \left[\partial^\mu Z_\mu^0 - \xi_Z m_Z G^0 \right], \\ F_\gamma &= \frac{1}{\sqrt{\xi_\gamma}} \partial^\mu A_\mu, \end{aligned} \tag{2.54}$$

⁴The term ‘‘naturally’’ is used in the sense that the flavor-conservation is not achieved by fine-tuning the parameters of the theory in order to rule out FCNCs.

the gauge for each field is fixed through the gauge-fixing-parameters (gfp) ξ_W for the W^\pm and G^\pm bosons, ξ_Z for the Z^0 and G^0 bosons and ξ_γ for the photon γ . Gauge-fixing is implemented in the full electroweak Lagrangian in the form of the gauge-fixing Lagrangian [52]

$$\mathcal{L}_{\text{GF}} = -\frac{1}{2} \left[2F_{W^+}F_{W^-} + |F_Z|^2 + |F_\gamma|^2 \right]. \quad (2.55)$$

The functional integral of the electroweak theory remains unchanged under a shear in field configuration space that corresponds to the local gauge transformations [5]. In order to compensate the effect of the unphysical degrees of freedom in the gauge-fixing Lagrangian, the method developed by L. Faddeev and V. Popov [60] can be used. The introduction of the Faddeev-Popov-Lagrangian via a variation of the gauge-fixing terms F_α in Eq. (2.54) with respect to corresponding Grassmann fields $\theta_\beta(x)$ ($\alpha, \beta \in \{W^\pm, Z, \gamma\}$),

$$\mathcal{L}_{\text{FP}} = \bar{u}_\alpha(x) \frac{\delta F_\alpha}{\delta \theta_\beta(x)} u_\beta(x), \quad (2.56)$$

enables the separation of the physical part of the functional integral from the one that remains unchanged under gauge transformations [52]. Note that Einstein's sum convention is used in Eq. (2.56). This introduces so-called *Faddeev-Popov ghost fields* u_{W^\pm} , u_Z and u_γ to the electroweak theory, with their own set of corresponding Feynman rules. These ghost particles violate the spin-statistic theorem, since they are defined over scalar, yet anticommuting fields. As such, they are considered to be unphysical particles, appearing only internally in loop calculations. Nevertheless, the ghost particles are necessary to restore unitarity within the theory, since they serve as negative degrees of freedom to ensure the cancellation of the unphysical gauge-freedom of the vector fields [5].

2.8. Set of Independent Parameters

The discussions in the previous sections allow us to give the full set of independent parameters of the CP-conserving 2HDM. It is most convenient to have such a set at hand when turning from tree-level calculations to higher-order corrections, since it enables an efficient bookkeeping of all parameters that need to be renormalized.

The full set of 2HDM parameters is given by the form of the potential in Eq. (2.7), together with all free parameters of the Standard Model as well as the Yukawa couplings Y_Ψ of Sec. 2.6. Additionally, the minimum conditions in Eq. (2.12) can be exploited to replace m_{11}^2 and m_{22}^2 with the tadpole parameters, as shown in Eq. (2.14). This gives the full set of free parameters in the gauge basis of the 2HDM:

$$\left\{ \lambda_1, \lambda_2, \lambda_3, \lambda_4, \lambda_5, m_{12}, T_1, T_2, v_1, v_2, g, g', Y_\Psi \right\}. \quad (2.57)$$

While renormalizing the 2HDM in the gauge basis is in principle possible, it is more practical to transform the parameters to the mass basis. Doing so enables us to use as many physical parameters (i.e. masses) as possible as input parameters. Additionally, we use the alternative form of the potential, given in App. A, since it is this form of the potential that is implemented in the `FeynArts` model file, which will be used later on for the calculation of the decay amplitudes. Denoting with m_Ψ all fermion masses and with T_{h^0} and T_{H^0} the tadpole parameters T_1 and T_2 in the mass basis, the full set of free 2HDM parameters in the mass basis is given by:

$$\left\{ m_{h^0}, m_{H^0}, m_{A^0}, m_{H^\pm}, \alpha, \beta, \Lambda_5, T_{h^0}, T_{H^0}, e, m_W, m_Z, m_\Psi \right\}. \quad (2.58)$$

Partial Decay Widths of One-to-Two Processes at Next-to-Leading Order

If we wish to make theoretical predictions of observables at the LHC, we have to find a way to connect the results of calculations of a field theory, e.g. decay amplitudes, with observables at a collider, i.e. partial decay widths. In the following, this connection shall be presented in a generic way, so that it can be applied to all decay processes that were considered within the scope of this thesis. The generic formula for calculating the partial decay width can be generalized from leading-order to next-to-leading order without dealing with renormalization first. Therefore, we want to present this generic result in this chapter and postpone the renormalization of the 2HDM to Chapter 4.

3.1. Kinematics of Decay Processes at Leading-Order

Consider a generic decay process of one initial particle f_1 into two final states f_2 and f_3 , with their four-momenta and masses being p_i and m_i ($i = 1, 2, 3$), respectively, as depicted in Fig. 3.1. The four-momentum conservation holds, so that we have

$$p_1 = p_2 + p_3 . \quad (3.1)$$

Additionally, we consider the decay process to be on-shell, so that $p_i^2 = m_i^2$ holds.

At leading-order (LO), the decay amplitude for the process $f_1 \rightarrow f_2 f_3$,

$$i\mathcal{A}_{f_1 f_2 f_3}^{\text{LO}} := i\mathcal{A}^{\text{LO}}(f_1 \rightarrow f_2 f_3) , \quad (3.2)$$

is obtained by applying the Feynman rules for the three-particle vertex, taking into account the respective Lorentz or spinor structure of the decay. It is common practice to drop a global factor of i in the amplitude, so that here and in the following, $\mathcal{A}_{f_1 f_2 f_3}^{\text{LO}}$ will stand for the LO amplitude reduced by a factor of i , as it would be generated by `FeynArts` when using the default configuration.

The complex-valued decay amplitude delivers the absolute square, $|\mathcal{A}_{f_1 f_2 f_3}^{\text{LO}}|^2$, which, in the center-of-mass frame, is proportional to the differential cross-section [5], and thus a necessary ingredient for the calculation of the decay probability. If the external particles allow for additional degrees of freedom, e.g. spins for fermions or polarizations for vector bosons, which

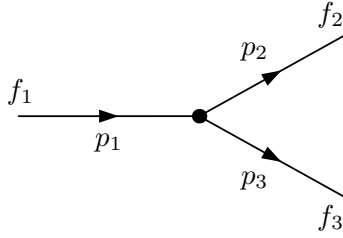


Figure 3.1.: Generic one-to-two decay. Feynman diagram of a generic decay of one initial particle f_1 into two final states f_2, f_3 , with masses m_i and four-momenta p_i ($i = 1, 2, 3$), respectively. The arrows indicate the flow of momentum.

are neither prepared in the initial nor observed in the final state in an experiment, we have to average over all initial and sum over all final degrees of freedom. Additionally, if particles in the final state are indistinguishable, a statistical factor S has to be taken into account (e.g. $S = 1/n! \cdot 1/m!$ for n photons and m neutral Higgs bosons h^0 in the final state) [61]. For this, we will use the short-hand notation

$$S \sum_{\text{d.o.f.}} |\mathcal{A}_{f_1 f_2 f_3}^{\text{LO}}|^2 . \quad (3.3)$$

The partial decay width of the process is connected to the decay amplitude by an integration over the two-body Lorentz-invariant phase space [5]

$$\int d\Pi_2 = \prod_{f=f_2, f_3} \int \frac{d^3 p_f}{(2\pi)^3} \frac{1}{2E_f} (2\pi)^4 \delta^{(4)}(p_1 - p_2 - p_3) , \quad (3.4)$$

with E_f being the energy of the final particle $f \in \{f_2, f_3\}$. For all decay processes considered in this thesis, the integrand, Eq. (3.3), is independent of the four-momenta p_i after applying all polarization or spin sums and assuming on-shell external particles. Therefore, the Lorentz-invariant phase space can be integrated out,

$$\begin{aligned} \int d\Pi_2 &= \int d\Omega \frac{1}{16\pi^2} \frac{|\vec{p}_1|}{m_1} \\ &\equiv \frac{1}{8\pi m_1^2} \lambda(m_1^2, m_2^2, m_3^2) , \end{aligned} \quad (3.5)$$

where we introduced the Källén phase space function

$$\lambda(x, y, z) := \sqrt{x^2 + y^2 + z^2 - 2xy - 2xz - 2yz} . \quad (3.6)$$

The partial decay width for the process $f_1 \rightarrow f_2 f_3$ is given by the integration of the squared amplitude, Eq. (3.3), over the two-body Lorentz-invariant phase space [5]:

$$\begin{aligned} \Gamma_{f_1 f_2 f_3}^{\text{LO}} &= \frac{1}{2m_1} \int d\Pi_2 S \sum_{\text{d.o.f.}} |\mathcal{A}_{f_1 f_2 f_3}^{\text{LO}}|^2 \\ &= S \frac{\lambda(m_1^2, m_2^2, m_3^2)}{16\pi m_1^3} \sum_{\text{d.o.f.}} |\mathcal{A}_{f_1 f_2 f_3}^{\text{LO}}|^2 . \end{aligned} \quad (3.7)$$

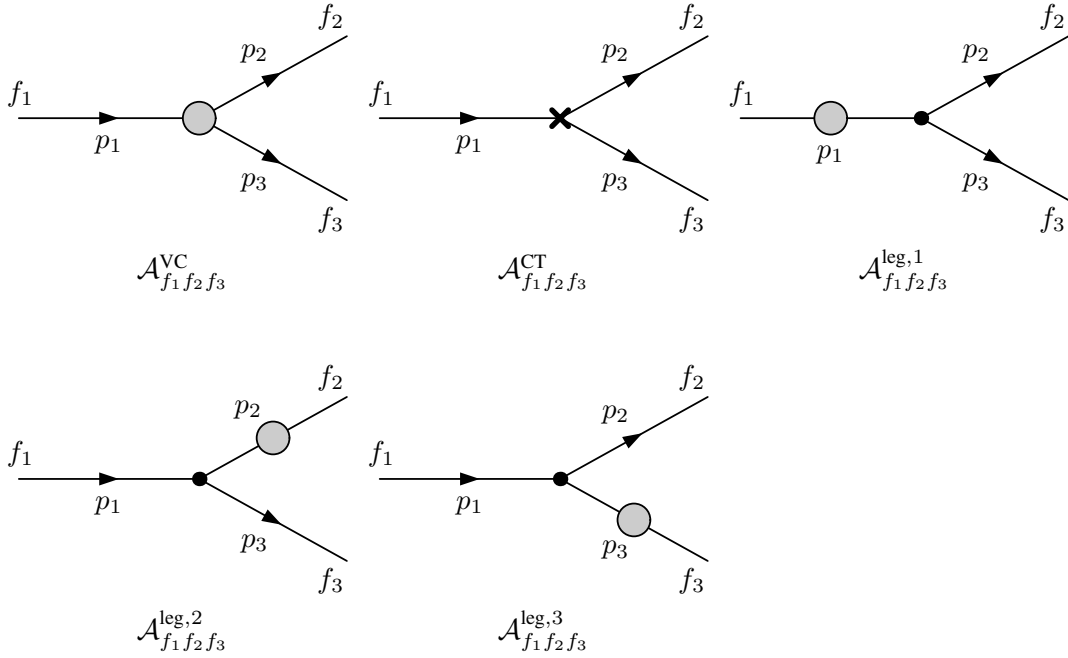


Figure 3.2.: NLO virtual contributions to a generic one-to-two decay. Generic diagrams contributing to the NLO corrections $\mathcal{A}_{f_1 f_2 f_3}^{\text{NLO}}$: virtual vertex corrections $\mathcal{A}_{f_1 f_2 f_3}^{\text{VC}}$, the counterterm $\mathcal{A}_{f_1 f_2 f_3}^{\text{CT}}$ and external leg corrections $\mathcal{A}_{f_1 f_2 f_3}^{\text{leg},i}$ ($i = 1, 2, 3$).

3.2. Partial Decay Width at Next-to-Leading Order

At next-to-leading order (NLO) the LO decay amplitude receives additional one-loop contributions as depicted in Fig. 3.2. These are the sum of all virtual vertex corrections $\mathcal{A}_{f_1 f_2 f_3}^{\text{VC}}$, the vertex counterterm $\mathcal{A}_{f_1 f_2 f_3}^{\text{CT}}$ and virtual external leg corrections $\mathcal{A}_{f_1 f_2 f_3}^{\text{leg},i}$ that contribute at the one-loop level,

$$\mathcal{A}_{f_1 f_2 f_3}^{\text{1loop}} := \mathcal{A}_{f_1 f_2 f_3}^{\text{VC}} + \mathcal{A}_{f_1 f_2 f_3}^{\text{CT}} + \sum_i \mathcal{A}_{f_1 f_2 f_3}^{\text{leg},i}. \quad (3.8)$$

Although the corrections of the external legs have to be considered in general, these contributions will vanish in all three processes that are considered in this thesis, either due to the on-shell renormalization conditions as presented in Sec. 4.3 or due to Ward and Slavnov-Taylor identities. This will be investigated in more detail in the following sections, as soon as we consider specific processes. In general, the full NLO amplitude to the generic decay process $f_1 \rightarrow f_2 f_3$ reads

$$\mathcal{A}_{f_1 f_2 f_3}^{\text{NLO}} := \mathcal{A}_{f_1 f_2 f_3}^{\text{LO}} + \mathcal{A}_{f_1 f_2 f_3}^{\text{1loop}}. \quad (3.9)$$

In order to calculate the partial decay width at NLO, the absolute square of Eq. (3.9) has to be taken. Doing so generates NLO contributions of order $\mathcal{O}(\alpha^2)$, where the fine-structure constant α is the coupling in which the perturbative expansion is performed. Additionally, the absolute square of the NLO amplitude contains next-to-next-to-leading order (NNLO) terms $\mathcal{O}_{\text{NNLO}}$ which are above the order $\mathcal{O}(\alpha^2)$. These terms will be neglected at NLO,

$$\begin{aligned} |\mathcal{A}_{f_1 f_2 f_3}^{\text{NLO}}|^2 &= |\mathcal{A}_{f_1 f_2 f_3}^{\text{LO}}|^2 + \left[\mathcal{A}_{f_1 f_2 f_3}^{\text{LO}} \left(\mathcal{A}_{f_1 f_2 f_3}^{\text{1loop}} \right)^* + \left(\mathcal{A}_{f_1 f_2 f_3}^{\text{LO}} \right)^* \mathcal{A}_{f_1 f_2 f_3}^{\text{1loop}} \right] + \mathcal{O}_{\text{NNLO}} \\ &\approx |\mathcal{A}_{f_1 f_2 f_3}^{\text{LO}}|^2 + 2 \operatorname{Re} \left[\left(\mathcal{A}_{f_1 f_2 f_3}^{\text{LO}} \right)^* \mathcal{A}_{f_1 f_2 f_3}^{\text{1loop}} \right], \end{aligned} \quad (3.10)$$

so that the squared NLO amplitude consists solely of the squared LO amplitude and the interference term between the LO and NLO amplitude. For the calculation of the partial decay width, the sum and average over all degrees of freedom has to be taken,

$$S \sum_{\text{d.o.f.}} |\mathcal{A}_{f_1 f_2 f_3}^{\text{NLO}}|^2, \quad (3.11)$$

which is the NLO equivalent of Eq. (3.3), with the same statistical factor S to account for indistinguishable particles in the final state. If it turns out that Eq. (3.11) is independent of all momenta p_i after integrating out all degrees of freedom and applying the on-shell conditions, as it is the case for all processes considered in this thesis, then Eq. (3.7) can be directly generalized to the one-loop level, giving the NLO partial decay width

$$\begin{aligned} \Gamma_{f_1 f_2 f_3}^{\text{NLO}} &= \frac{1}{2m_1} \int d\Pi_2 S \sum_{\text{d.o.f.}} |\mathcal{A}_{f_1 f_2 f_3}^{\text{NLO}}|^2 \\ &= S \frac{\lambda(m_1^2, m_2^2, m_3^2)}{16\pi m_1^3} \sum_{\text{d.o.f.}} \left(|\mathcal{A}_{f_1 f_2 f_3}^{\text{LO}}|^2 + 2 \operatorname{Re} \left[(\mathcal{A}_{f_1 f_2 f_3}^{\text{LO}})^* \mathcal{A}_{f_1 f_2 f_3}^{\text{1loop}} \right] \right) \\ &= \Gamma_{f_1 f_2 f_3}^{\text{LO}} + S \frac{\lambda(m_1^2, m_2^2, m_3^2)}{16\pi m_1^3} \sum_{\text{d.o.f.}} 2 \operatorname{Re} \left[(\mathcal{A}_{f_1 f_2 f_3}^{\text{LO}})^* \mathcal{A}_{f_1 f_2 f_3}^{\text{1loop}} \right]. \end{aligned} \quad (3.12)$$

In case that some of the external particles are charged, the NLO amplitude $\mathcal{A}_{f_1 f_2 f_3}^{\text{NLO}}$ will in general contain infrared divergences which stem from internal photon propagators. Since the photon is a massless particle, its propagator develops a pole at vanishing loop momentum. These infrared divergences have to be regularized and incoherently summed with additional real corrections in the form of soft photons in such a way that it is consistent with the NLO of the squared amplitude. This procedure will be illustrated in Sec. 5.3, when dealing with a 2HDM-specific process that contains external charged particles.

In general, this incoherent sum leads to a modification of the observable partial decay width in the form

$$\Gamma_{f_1 f_2 f_3}^{\text{NLO}} \longrightarrow \Gamma_{f_1 f_2 f_3}^{\text{NLO}} + \Gamma_{f_1 f_2 f_3}^{\text{real}}, \quad (3.13)$$

where $\Gamma_{f_1 f_2 f_3}^{\text{real}}$ is the additional contribution to the NLO partial decay width due to real corrections, necessary for the cancellation of all IR divergences.

Renormalization of the Two-Higgs-Doublet Model

It is a general feature of quantum field theories to contain divergent amplitudes as soon as higher order corrections are taken into account. Without proper treatment, these divergences manifest themselves at the worst possible place of the theory, namely in the calculated results of scattering amplitudes or decay widths. Since any physical quantity should be free of singularities, the powerful tool of renormalization has to be used to make sense of the divergent results, leading to finite observables in a self-consistent way.

4.1. Divergences in Classical and Quantum Field Theories

Before presenting the renormalization program for the 2HDM, we want to give a brief historical overview of the appearance of divergences which persist in physical theories since the late 19th century. Applying classical electrodynamics to a point particle, e.g. an electron, allows for the calculation of its classical electromagnetic mass in natural units,

$$m_e^{\text{class}} = \frac{e^2}{4\pi r_e} , \quad (4.1)$$

with the classical electron radius r_e [62]. Although classical electrodynamics is a consistent theory explaining many different phenomena, it is obvious that the theory has its flaws if the electron is considered as a point particle. As such, the electron radius vanishes, leading to a divergence in Eq. (4.1), although the electron mass at the left-hand side of the equation remains a finite, observable parameter.

With the development of quantum electrodynamics (QED), this problem was partly solved by giving the classical theory a new interpretation. Within QED, the electron is consistently treated as a point particle [63] with a bare electric charge e_0 . Due to higher-order corrections, the vacuum around the electron gets polarized. This leads to the creation of electric dipoles that align along the electric field that is induced by the bare charge, as it is shown in Fig. 4.1. What is observed by an experiment is not the bare charge, which would be infinite due to the electron being a point particle, but rather the charge cloud around the bare charge that is induced by vacuum polarization. This way, the electron is given an effective, classical radius and an effective, finite charge. Increasing the momentum in scattering experiments is, through Heisenberg's uncertainty principle, equivalent to resolving the electron at a smaller

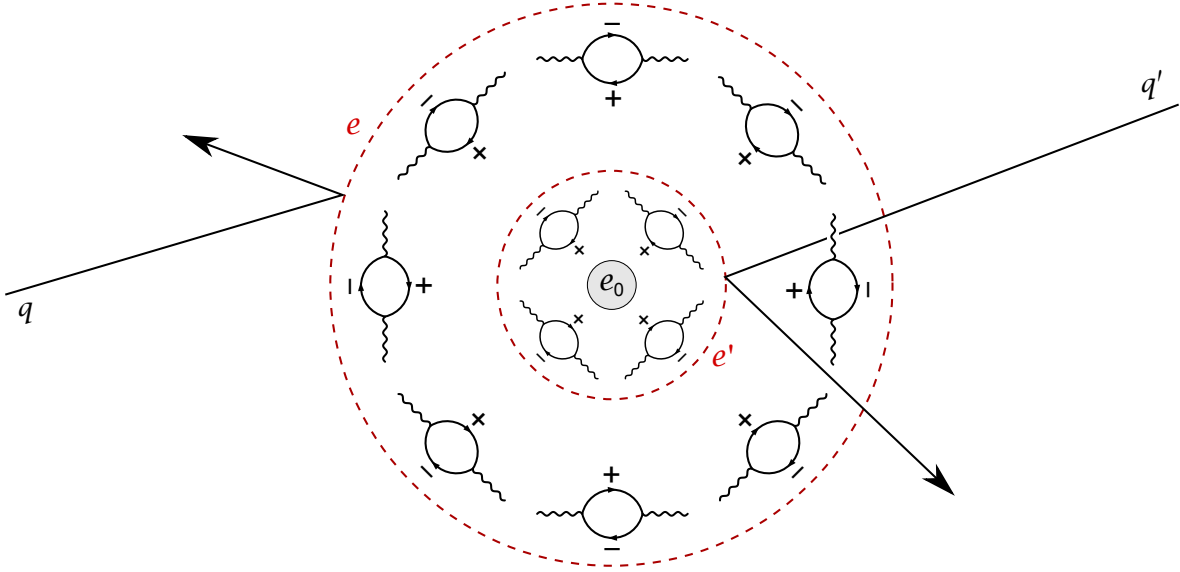


Figure 4.1.: Screening of the electron charge. The infinite bare charge e_0 of the point-like electron is screened by vacuum polarization contributions due to higher-order corrections in QED, depicted as one-loop bubble diagrams. Increasing the scattering momentum $q' > q$ enables the penetration of the charge cloud, leading to the measurement of a higher electric charge $|e'| > |e|$. The dependence of the electric charge on the scattering momentum is called the running of the coupling constant.

length scale. Doing so enables us to penetrate the charge cloud around the bare electric charge, which leads to a measurable increase in the physical electric charge. In QED, this phenomenon is called the running coupling constant of the theory [5].

While QED enables us to give sense to the divergences appearing in classical electrodynamics, the theory itself is not free of divergences, either. In fact, divergences are omnipresent in quantum field theories, showing up in most higher-order corrections to physical observables. Consider the following integral that has to be solved in a quantum field theory, like QED, at the one-loop level:

$$\int \frac{d^4 l}{(2\pi)^4} \frac{1}{l^2}. \quad (4.2)$$

If we naively try to solve the integral, we realize that it diverges as soon as the loop momentum l goes towards infinity. Since this divergence appears in the region of high momentum, or equivalently, high frequency, the integral contains a so-called ultraviolet (UV) divergence, referencing to the famous ultraviolet Rayleigh–Jeans paradox appearing in the classical treatment of blackbody radiation [64]. The integral in Eq. (4.2) contains an additional divergence in the region of integration where $l \rightarrow 0$. Since this region corresponds to low momenta or low frequency, it is called an infrared (IR) divergence. The IR and UV divergences are of a very different nature within quantum field theories and have to be treated separately from each other. In this chapter, we focus on the treatment of UV divergences, while in Sec. 5.3, the nature and cancellation of IR divergences is discussed.

In a sense, the problem of divergence was not solved by QED, but it was rather shifted from the classical to a more fundamental theory. Although many physicists, most prominently Paul Dirac, openly criticized the treatment of divergences in QED [65], it was pointed out by Freeman Dyson [66] that UV divergences are of a very basic nature in a quantum field theory and as such, their appearance is inevitable. To some extent, the existence of these divergences is a result of our lack of a more fundamental theory that would enable us to

describe physics at the smallest length scales in a non-continuous way [4]. Nevertheless, quantum field theories led to successful theoretical predictions, and especially QED counts as one of the most stringently tested physical theories to date [67–69].

4.2. Regularization and Renormalization

As we have seen in the previous section, the appearance of divergences is in general inevitable for higher-order calculations in quantum field theories. In order to still calculate sensible predictions out of these theories, we must find a way to eliminate the divergences in a mathematically well-defined and self-consistent way. To that end, it is first necessary to isolate the divergences and make them explicit. This process is called *regularization*.

Considering again the typical loop integral in Eq. (4.2), it was already pointed out that the divergence occurs in the region where the loop momentum goes to infinity. One way of treating this UV divergence is to regularize the integral by adding an additional term,

$$\int \frac{d^4 l}{(2\pi)^4} \frac{1}{l^2} \xrightarrow{\text{regularized}} \int \frac{d^4 l}{(2\pi)^4} \left[\frac{1}{l^2} - \frac{1}{l^2 - \Lambda^2} \right], \quad (4.3)$$

where Λ is an additional mass term that is arbitrarily high, yet finite. It is exactly this mass term that serves as the regulator, and the divergence becomes explicit in the limit $\Lambda \rightarrow \infty$. In the region of low loop momentum, this regularization method gives $(l^2 - \Lambda^2)^{-1} \approx -\Lambda^{-2} \approx 0$, so that the second term that was added in Eq. (4.3) vanishes again. In the region of high loop momentum however, this gives $(l^2 - \Lambda^2)^{-1} \approx l^{-2}$, so that both terms cancel, thus leading to a finite result of the integral. This procedure is called *Pauli-Villars regularization* [70], and it leads in fact to the proper isolation of all UV divergences in some theories. However, due to the introduction of the artificial high mass Λ , the Pauli-Villars regularization breaks gauge covariance [5], and can therefore not be used in all theories.

Another method of isolating the UV divergences is the so-called *cutoff regularization*, where the integrals are evaluated only up to an upper bound l_{\max} in the loop momentum. In this case, the chosen upper bound is the regulator, and the divergence becomes explicit in the form of terms that diverge when taking the limit $l_{\max} \rightarrow \infty$. This form of regularization has the side effect of breaking translational invariance in the loop integrals, which renders their calculation more complicated. Due to this, the method is not widely used. However, it still leads to a correct cancellation of all UV divergences if applied consistently [71].

Among the most commonly used schemes today is *dimensional regularization* [72]. If the integration over the loop momentum in integrals like Eq. (4.2) is not performed in physical four space-time dimensions, but instead in $D = 4 - 2\varepsilon$ dimensions (with ε being arbitrarily small), then it turns out that the integrals become well-defined and may be formally solved, without running into immediate singularities. In this scheme, the dimensional shift ε serves as the regulator. The UV divergence becomes explicit in the limit of $\varepsilon \rightarrow 0$ due to the appearance of the term

$$\Delta = \frac{1}{\varepsilon} - \gamma_E + \ln(4\pi) \quad (4.4)$$

in the solution of the integral, where γ_E stands for the Euler-Mascheroni constant. Dimensional regularization preserves gauge covariance, unitarity and allows for shifts in the loop momentum [73], therefore avoiding the problems of the other regularization schemes above. If the integral contains a spinor structure, the momentum shift leads to a change of the Dirac algebra, which has to be applied consistently [5]. The only subtlety one has to be aware of is the case in which the integrand contains the Dirac matrix γ_5 . Since this matrix cannot be converted trivially from four to D dimensions [74], it is possible to run into axial anomalies that have to be treated appropriately [75, 76].

As soon as all divergences are regulated, they have to be cancelled against each other in a consistent way in order to obtain a finite result. This procedure is called *renormalization* of the field theory. The main idea of renormalization is that each parameter of the field theory is to be considered a bare parameter that has to be fixed order-by-order by experimental data to render the field theory calculations finite.

In practice, this means that each of the n free bare parameters $\rho_{i,0}$ ($i = 1, \dots, n$) of a renormalizable field theory is split up into n renormalized parameters ρ_i and n counterterms $\delta\rho_i$ according to

$$\rho_{i,0} = \rho_i + \delta\rho_i . \quad (4.5)$$

Both the bare parameters as well as the counterterms are considered infinite, while the renormalized parameter is finite. After splitting up all n free parameters, n renormalization conditions have to be applied. It is exactly the demand that the renormalization conditions hold, that leads to the cancellation of all divergent terms, giving a finite result [5].

Consistently applying this procedure to a renormalizable field theory will render all S matrix calculations finite, to every order of perturbation theory, separately [5]. In addition to the free parameters, the k different bare fields $\phi_{j,0}$ ($j = 1, \dots, k$) can be renormalized by a similar procedure. Using the factorization

$$\phi_{j,0} = \sqrt{Z_{\phi_j}} \phi_j \approx \left(1 + \frac{\delta Z_{\phi_j}}{2} \right) \phi_j , \quad (4.6)$$

the bare fields are multiplicatively split up into physical fields ϕ_j and the field strength renormalization constants $\sqrt{Z_{\phi_j}}$. On the right-hand side of Eq. (4.6), we expanded $\sqrt{Z_{\phi_j}}$ around unity up to NLO, introducing the NLO counterterms δZ_{ϕ_j} . Fixing these counterterms by k renormalization conditions leads to the cancellation of all UV divergences in the fields, as well [5].

Before turning to the renormalization conditions, it should be noted that the procedure for cancelling all UV divergences as described above can only be applied for renormalizable field theories¹. If the theory is unrenormalizable, an infinite number of counterterms would be needed in order to render the calculations finite [77]. However, it has been shown that QED, based on the gauge group $U(1)_{\text{em}}$, is renormalizable [78], and so is the Standard Model of particle physics, based on the gauge group $SU(3)_C \times SU(2)_L \times U(1)_Y$ [73]. Since the 2HDM differs from the SM only in the scalar potential, where all additional terms are renormalizable, the 2HDM is renormalizable, as well [79].

4.3. On-Shell Renormalization

In order to consistently remove the UV divergences from the field theory, it is not enough to regularize them. The second step necessary for achieving a field theory with finite predictions and calculations is the specification of a renormalization program of the field theory. Within the scope of this thesis, we adopt the so-called *on-shell* (OS) renormalization of the 2HDM. The name of the renormalization scheme refers to the particles of the theory being on their mass-shell, i.e. the particles are considered to be physical in the sense that they obey Einstein's energy-momentum relation, which describes hyperbolas (the "shells") in momentum-space [80]. The OS renormalization scheme can be applied throughout almost all sectors of the 2HDM. Therefore, a general description of the scheme is given in this section and the application of it to the scalar, fermion and gauge boson sectors is explicitly stated in the following sections.

¹Strictly speaking, the procedure can be applied to unrenormalizable field theories as well. However, in such theories the number of counterterms needed for the cancellation of all divergences increases order-by-order.

$$i\Sigma(p^2) := \text{---} \circ \text{1PI} \text{---} = \text{---} \text{---} \text{---} + \text{---} \text{---} \text{---} + \dots$$

Figure 4.2.: Definition of the one-particle irreducible self-energy. The 1PI self-energy $i\Sigma(p^2)$ consists of all self-energy diagrams that cannot be split into two distinct diagrams by cutting a single internal line. While $i\Sigma(p^2)$ contains contributions from all orders of perturbation theory, the two diagrams shown are the only relevant diagrams at the one-loop level for our toy theory with only one scalar particle.

In order to illustrate the OS renormalization scheme, we consider a simple field theory with only one spin 0 particle with bare mass m_0 , represented by the bare scalar field ϕ_0 . The motion of the particle through space-time can be described by the so-called bare *propagator* $G_0(p^2)$ of the particle in momentum space p , which corresponds to the causal Green's function of the equations of motion of the scalar field. In that sense, the propagator represents the probability of the particle to move from one point in space-time to another [5]. If we denote by $|\Omega\rangle$ the vacuum state of the scalar field theory and T the time-ordering operator, then the bare propagator is given as the integral over all space-time configurations x ,

$$\begin{aligned} G_0(p^2) &= \int d^4x \langle \Omega | T \phi_0(x) \phi_0^*(0) | \Omega \rangle \\ &= \sqrt{Z_\phi^*} \int d^4x \langle \Omega | T \phi(x) \phi^*(0) | \Omega \rangle \sqrt{Z_\phi} \\ &\equiv \sqrt{Z_\phi^*} \hat{G}(p^2) \sqrt{Z_\phi}. \end{aligned} \quad (4.7)$$

In the second line, the field strength renormalization constants according to Eq. (4.6) have been inserted and as a consequence, in the third line, the renormalized propagator $\hat{G}(p^2)$ has been introduced. In order to distinguish physical from bare quantities, renormalized quantities are indicated with the hat symbol $\hat{}$ in this section.

On the other hand, the bare propagator can be described by the two-point function. In the language of Feynman diagrams, this can be identified as the all-order self-energy contributions of the scalar particle ϕ . We denote with $i\Sigma$ the sum of all truncated *one-particle irreducible* (1PI) self-energy diagrams depicted in Fig. 4.2, i.e. diagrams that cannot be separated into two distinct diagrams by a simple cut of one internal line² [5]. With this definition, the full bare propagator, to all orders of perturbation theory, is expressed through a geometric series by³

$$\begin{aligned} G_0(p^2) &= \text{---} + \text{---} \text{---} \text{---} + \text{---} \text{---} \text{---} \text{---} \text{---} + \dots \\ &= \frac{i}{p^2 - m_0^2} + \frac{i}{p^2 - m_0^2} i\Sigma(p^2) \frac{i}{p^2 - m_0^2} + \frac{i}{p^2 - m_0^2} \left(i\Sigma(p^2) \frac{i}{p^2 - m_0^2} \right)^2 + \dots \quad (4.8) \\ &= \frac{i}{p^2 - m_0^2} \left[1 + \frac{-\Sigma(p^2)}{p^2 - m_0^2} + \left(\frac{-\Sigma(p^2)}{p^2 - m_0^2} \right)^2 + \dots \right] = \frac{i}{p^2 - m_0^2 + \Sigma(p^2)}. \end{aligned}$$

²This definition is not completely accurate: tadpole diagrams, which could be separated into two distinct diagrams by a single cut, are part of 1PI topologies, as well [5]. However, in most cases they are removed through an appropriate renormalization condition, as explained in Sec. 4.4. Therefore, it is convenient to exclude them from the 1PI self-energies from the start.

³Throughout this thesis, the necessary contour-shifting parameter $+i\epsilon$ is not explicitly stated in the denominator of the propagator, since it does not contribute to the derivation of the renormalization program.

The bare propagator still contains the bare mass squared m_0^2 , which, according to Eq. (4.5), has to be split up into the physical mass squared m^2 and a mass counterterm δm^2 . With this modification in mind, the full renormalized propagator is obtained in a compact form by inserting Eq. (4.8) into Eq. (4.7) and solving for $\widehat{G}(p^2)$:

$$\begin{aligned}\widehat{G}(p^2) &= \frac{i}{\sqrt{Z_\phi^*} \left[p^2 - m^2 + \Sigma(p^2) - \delta m^2 \right] \sqrt{Z_\phi}} \\ &\approx \frac{i}{p^2 - m^2 + \widehat{\Sigma}(p^2)}.\end{aligned}\quad (4.9)$$

In the second line, we inserted the expansion of Eq. (4.6) for the field strength renormalization constants and combined all quantities into the renormalized self-energy $\widehat{\Sigma}(p^2)$. Within the scope of this thesis, we consider only NLO corrections at the one-loop level. Therefore, terms of order $\mathcal{O}(\delta^2)$ as well as interference terms of renormalization constants and the 1PI self-energy (that is at the one-loop level by itself) have to be neglected. This fixes the renormalized self-energy to be of the form

$$\widehat{\Sigma}(p^2) = \Sigma(p^2) - \delta m^2 + \frac{\delta Z_\phi^*}{2}(p^2 - m^2) + (p^2 - m^2) \frac{\delta Z_\phi}{2}.\quad (4.10)$$

With this compact result at hand, the inverse of the renormalized propagator, called the *two-point correlation function* of the scalar particle, is directly given by (the minus sign follows from the normalization of the propagator):

$$\begin{aligned}\widehat{\Gamma}(p^2) &= -\widehat{G}^{-1}(p^2) = i \left[p^2 - m^2 + \widehat{\Sigma}(p^2) \right] \\ &\approx i(p^2 - m^2) \left(1 + \frac{\partial \widehat{\Sigma}(p^2)}{\partial p^2} \Big|_{p^2=m^2} \right) \equiv i(p^2 - m^2) (-i) \frac{\partial \widehat{\Gamma}(p^2)}{\partial p^2} \Big|_{p^2=m^2}.\end{aligned}\quad (4.11)$$

The second line is an expansion of the correlation function around its root, corresponding to an expansion around the pole of the propagator at the on-shell value $p^2 = m^2$.

Up until now, we considered a toy theory with a single scalar field. The 2HDM, on the other hand, offers an extended scalar sector with eight scalar fields that are paired into the doublets of Eqs. (2.24) – (2.26). The scalar particles within each doublet have the same quantum numbers and thus, they can mix at the one-loop level. In order to account for this mixing, the structure of the field strength renormalization constant in Eq. (4.6) has to be adjusted to the doublet structure of the fields. To keep the notation generic, we denote with ϕ_1 and ϕ_2 two scalar particles of the same doublet. For these, the field strength renormalization constant is in general a matrix $\sqrt{Z_\phi} \in \mathbb{C}^{2 \times 2}$, which multiplicatively separates the bare field doublet from the renormalized one:

$$\begin{pmatrix} \phi_1 \\ \phi_2 \end{pmatrix}_0 = \sqrt{Z_\phi} \begin{pmatrix} \phi_1 \\ \phi_2 \end{pmatrix} \approx \left(\mathbb{1}_{2 \times 2} + \frac{\delta Z_\phi}{2} \right) \begin{pmatrix} \phi_1 \\ \phi_2 \end{pmatrix}.\quad (4.12)$$

The NLO expansion involves the 2×2 matrix δZ_ϕ , which has four distinct field renormalization constants as its entries:

$$\frac{\delta Z_\phi}{2} = \begin{pmatrix} \frac{\delta Z_{\phi_1 \phi_1}}{2} & \frac{\delta Z_{\phi_1 \phi_2}}{2} \\ \frac{\delta Z_{\phi_2 \phi_1}}{2} & \frac{\delta Z_{\phi_2 \phi_2}}{2} \end{pmatrix}.\quad (4.13)$$

At NLO, it is sufficient to consider the real matrix $\delta Z_\phi \in \mathbb{R}^{2 \times 2}$ as the most general form of the field strength renormalization. Each scalar doublet of the 2HDM contains four distinct renormalization constants $\delta Z_{\phi_i \phi_j}$ ($i, j = 1, 2$), which have to be fixed by four renormalization conditions.

It is straightforward to generalize the two-point correlation function of Eq. (4.11) to account for the matrix structure of the fields:

$$\begin{aligned} \widehat{\Gamma}_\phi(p^2) &:= \begin{pmatrix} \widehat{\Gamma}_{\phi_1 \phi_1}(p^2) & \widehat{\Gamma}_{\phi_1 \phi_2}(p^2) \\ \widehat{\Gamma}_{\phi_1 \phi_2}(p^2) & \widehat{\Gamma}_{\phi_2 \phi_2}(p^2) \end{pmatrix} \\ &= i \sqrt{Z_\phi}^\dagger \left[p^2 \mathbb{1}_{2 \times 2} - D_\phi^2 + \Sigma_\phi(p^2) - \delta D_\phi^2 \right] \sqrt{Z_\phi} \approx i \left[p^2 \mathbb{1}_{2 \times 2} - D_\phi^2 + \widehat{\Sigma}_\phi(p^2) \right], \end{aligned} \quad (4.14)$$

where the diagonal mass matrices D_ϕ^2 are given in Eq. (2.27). The expansion of the correlation function around its root in the second line of Eq. (4.11) is generalized to the matrix structure, as well:

$$\begin{aligned} \widehat{\Gamma}_\phi(p^2) &\approx i (p^2 \mathbb{1}_{2 \times 2} - D_\phi^2) \left(\mathbb{1}_{2 \times 2} + \left. \frac{\partial \widehat{\Sigma}_\phi(p^2)}{\partial p^2} \right|_{p^2=m_\phi^2} \right) \\ &\equiv i (p^2 \mathbb{1}_{2 \times 2} - D_\phi^2) (-i) \left. \frac{\partial \widehat{\Gamma}_\phi(p^2)}{\partial p^2} \right|_{p^2=m_\phi^2}. \end{aligned} \quad (4.15)$$

Note that the two-point correlation function in Eq. (4.14) is explicitly symmetric. The matrix form of the renormalized self-energy in Eq. (4.14) is given by

$$\begin{aligned} \widehat{\Sigma}_\phi(p^2) &:= \begin{pmatrix} \widehat{\Sigma}_{\phi_1 \phi_1}(p^2) & \widehat{\Sigma}_{\phi_1 \phi_2}(p^2) \\ \widehat{\Sigma}_{\phi_2 \phi_1}(p^2) & \widehat{\Sigma}_{\phi_2 \phi_2}(p^2) \end{pmatrix} \\ &= \Sigma_\phi(p^2) - \delta D_\phi^2 + \frac{\delta Z_\phi^\dagger}{2} (p^2 \mathbb{1}_{2 \times 2} - D_\phi^2) + (p^2 \mathbb{1}_{2 \times 2} - D_\phi^2) \frac{\delta Z_\phi}{2}, \end{aligned} \quad (4.16)$$

where δD_ϕ^2 is a symmetric 2×2 matrix whose specific form is determined in Sec. 4.4 and Σ_ϕ is a symmetric 2×2 matrix containing the 1PI self-energies of the scalar doublet (ϕ_1, ϕ_2) . Since the two-point correlation function is now a matrix, the propagator is obtained by inverting the negative of the matrix structure:

$$\widehat{G}_\phi(p^2) = -\widehat{\Gamma}_\phi^{-1}(p^2) = \frac{i}{(-i) \det(\widehat{\Gamma}_\phi(p^2))} \begin{pmatrix} \widehat{\Gamma}_{\phi_2 \phi_2}(p^2) & -\widehat{\Gamma}_{\phi_1 \phi_2}(p^2) \\ -\widehat{\Gamma}_{\phi_1 \phi_2}(p^2) & \widehat{\Gamma}_{\phi_1 \phi_1}(p^2) \end{pmatrix}, \quad (4.17)$$

with the determinant of the two-point correlation function given by

$$(-i) \det(\widehat{\Gamma}_\phi(p^2)) = -i \left[\widehat{\Gamma}_{\phi_1 \phi_1}(p^2) \widehat{\Gamma}_{\phi_2 \phi_2}(p^2) - \left(\widehat{\Gamma}_{\phi_1 \phi_2}(p^2) \right)^2 \right]. \quad (4.18)$$

After splitting up all fields and masses into physical parameters and counterterms and expressing the two-point correlation function and the propagator in terms of these quantities, the last necessary step for a successful renormalization is to fix the counterterms with a set of *renormalization conditions*. In the OS scheme, the mass parameters are fixed through the fact that the physical masses of particles are the poles in their correlation functions, which directly follows from the Källén–Lehmann spectral representation of the field theory [5, 81, 82]. For the 2HDM, these OS renormalization conditions can be formulated as follows:

- 1) Mixing of fields:** The mixing of fields of particles with the same quantum numbers vanishes at $p^2 = m_{\phi_j}^2$ ($j = 1, 2$).
- 2) Physical mass:** The mass parameters m_{ϕ_j} ($j = 1, 2$) are defined as being the real parts of the poles of the renormalized propagator $\widehat{G}_\phi(p^2)$.
- 3) Field normalization:** The physical fields ϕ_j ($j = 1, 2$) are properly normalized through fixing the residue of the propagator at its pole to i .

The first of the three conditions can be applied to the explicit form of the propagator in Eq. (4.17), which translates to the following two conditions for the off-diagonal two-point correlation functions:

$$\operatorname{Re} \left[(-i) \widehat{\Gamma}_{\phi_1 \phi_2}(m_{\phi_1}^2) \right] = \operatorname{Re} \left[(-i) \widehat{\Gamma}_{\phi_1 \phi_2}(m_{\phi_2}^2) \right] \stackrel{!}{=} 0 \quad (4.19)$$

$$\stackrel{(4.14)}{\iff} \operatorname{Re} \left[\widehat{\Sigma}_{\phi_1 \phi_2}(m_{\phi_1}^2) \right] = \operatorname{Re} \left[\widehat{\Sigma}_{\phi_1 \phi_2}(m_{\phi_2}^2) \right] = 0 . \quad (4.20)$$

The second renormalization condition is equivalent to the vanishing of the real part⁴ of the determinant in Eq. (4.18) on the mass shell, which, together with Eq. (4.19), delivers the following two conditions for the diagonal parts of the renormalized self-energies:

$$\operatorname{Re} \left[(-i) \widehat{\Gamma}_{\phi_1 \phi_1}(m_{\phi_1}^2) \right] = \operatorname{Re} \left[(-i) \widehat{\Gamma}_{\phi_2 \phi_2}(m_{\phi_2}^2) \right] \stackrel{!}{=} 0 \quad (4.21)$$

$$\iff \operatorname{Re} \left[\widehat{\Sigma}_{\phi_1 \phi_1}(m_{\phi_1}^2) \right] = \operatorname{Re} \left[\widehat{\Sigma}_{\phi_2 \phi_2}(m_{\phi_2}^2) \right] = 0 . \quad (4.22)$$

The effect of the third renormalization condition is best observed by considering the residue of the two-point correlation function in Eq. (4.15), where the proper field normalization, equivalent to the residue being equal to i , leads to the following two conditions:

$$\operatorname{Re} \left[(-i) \frac{\partial \widehat{\Gamma}_{\phi_1 \phi_1}(p^2)}{\partial p^2} \Big|_{p^2=m_{\phi_1}^2} \right] = \operatorname{Re} \left[(-i) \frac{\partial \widehat{\Gamma}_{\phi_2 \phi_2}(p^2)}{\partial p^2} \Big|_{p^2=m_{\phi_2}^2} \right] \stackrel{!}{=} 1 \quad (4.23)$$

$$\iff \operatorname{Re} \left[\frac{\partial \widehat{\Sigma}_{\phi_1 \phi_1}(p^2)}{\partial p^2} \Big|_{p^2=m_{\phi_1}^2} \right] = \operatorname{Re} \left[\frac{\partial \widehat{\Sigma}_{\phi_2 \phi_2}(p^2)}{\partial p^2} \Big|_{p^2=m_{\phi_2}^2} \right] = 0 . \quad (4.24)$$

The two renormalization conditions in Eq. (4.22) can be used to fix the diagonal elements of the counterterm δD_ϕ^2 :

$$\operatorname{Re} \left[\delta D_{\phi_1 \phi_1}^2 \right] = \operatorname{Re} \left[\Sigma_{\phi_1 \phi_1}(m_{\phi_1}^2) \right] , \quad (4.25)$$

$$\operatorname{Re} \left[\delta D_{\phi_2 \phi_2}^2 \right] = \operatorname{Re} \left[\Sigma_{\phi_2 \phi_2}(m_{\phi_2}^2) \right] . \quad (4.26)$$

The four independent conditions in Eqs. (4.20) and (4.24) are used to obtain explicit expressions for the four field strength renormalization constants $\delta Z_{\phi_i \phi_j}$ by inserting Eq. (4.16):

⁴The imaginary part accounts for the finite width of the particles [5], which is of no interest in the scope of this thesis. A detailed analysis can be found e.g. in [83].

$$\delta Z_{\phi_1\phi_1} = -\text{Re} \left[\frac{\partial \Sigma_{\phi_1\phi_1}(p^2)}{\partial p^2} \right]_{p^2=m_{\phi_1}^2}, \quad (4.27)$$

$$\delta Z_{\phi_1\phi_2} = \frac{2}{m_{\phi_1}^2 - m_{\phi_2}^2} \text{Re} \left[\Sigma_{\phi_1\phi_2}(m_{\phi_2}^2) - \delta D_{\phi_1\phi_2}^2 \right], \quad (4.28)$$

$$\delta Z_{\phi_2\phi_1} = \frac{2}{m_{\phi_2}^2 - m_{\phi_1}^2} \text{Re} \left[\Sigma_{\phi_1\phi_2}(m_{\phi_1}^2) - \delta D_{\phi_1\phi_2}^2 \right], \quad (4.29)$$

$$\delta Z_{\phi_2\phi_2} = -\text{Re} \left[\frac{\partial \Sigma_{\phi_2\phi_2}(p^2)}{\partial p^2} \right]_{p^2=m_{\phi_2}^2}. \quad (4.30)$$

While we use the conditions in Eq. (4.22) to explicitly fix $\delta D_{\phi_1\phi_1}$ and $\delta D_{\phi_2\phi_2}$, so far we did not elaborate what these counterterms actually mean. Since δD_ϕ^2 is a direct generalization of the mass counterterm introduced in the sense of Eq. (4.5), it is expected that the diagonal parts of δD_ϕ^2 appear as the counterterms of the physical masses, as well. However, the meaning of the off-diagonal parts of δD_ϕ^2 is far from clear. It turns out that the exact form of δD_ϕ^2 depends on the treatment of the renormalization program of the tadpoles, which is elaborated in the next section.

The renormalization of fermion and gauge boson fields is achieved in an analogous way as for the scalar fields presented in this section. In many cases, the expressions for the field strength renormalization constants is formally the same as in Eqs. (4.25) – (4.30), apart from slight modifications that account for the different Lorentz structure of the fermions or gauge bosons. In Sec. 4.5 and Sec. 4.6, we will take a look at the gauge boson and fermion sector, respectively.

4.4. Tadpole Renormalization

In order to derive counterterms of physical observables that are manifestly gauge-independent, it is crucial to treat the renormalization of tadpole contributions at higher orders properly. To this end, the tadpole terms in Eq. (2.12) that are linear in the fields ρ_1 and ρ_2 in the tree-level potential are considered as bare parameters $T_{1,0}$ and $T_{2,0}$. At NLO, they receive a shift that corresponds to the change of the vacuum state of the potential through electroweak corrections. While such a shift by itself is not problematic and may take an arbitrary value, it is most convenient to renormalize the tadpoles in such a way that the vacuum expectation values represent the same minimum as at tree level. This can be achieved by applying a renormalization condition in the form that the one-loop renormalized one-point function vanishes again:

$$i\widehat{T}_1 = iT_1 - i\delta T_1 \stackrel{!}{=} 0, \quad i\widehat{T}_2 = iT_2 - i\delta T_2 \stackrel{!}{=} 0. \quad (4.31)$$

The terms iT_1 and iT_2 represent the sum of all one-loop tadpole contributions to the fields ρ_1 and ρ_2 in the gauge basis. The application of the renormalization condition fixes the counterterms to

$$\delta T_1 = T_1, \quad \delta T_2 = T_2. \quad (4.32)$$

In Fig. 4.3 (a), this renormalization condition is stated pictorially for the fields in the gauge basis. Since we perform all calculations in the mass basis, it is convenient to transform the tadpole parameters according to the inverse of Eq. (2.24):

$$\begin{pmatrix} \delta T_1 \\ \delta T_2 \end{pmatrix} = \begin{pmatrix} c_\alpha & -s_\alpha \\ s_\alpha & c_\alpha \end{pmatrix} \begin{pmatrix} \delta T_{H^0} \\ \delta T_{h^0} \end{pmatrix} = \begin{pmatrix} c_\alpha \delta T_{H^0} - s_\alpha \delta T_{h^0} \\ s_\alpha \delta T_{H^0} + c_\alpha \delta T_{h^0} \end{pmatrix}. \quad (4.33)$$

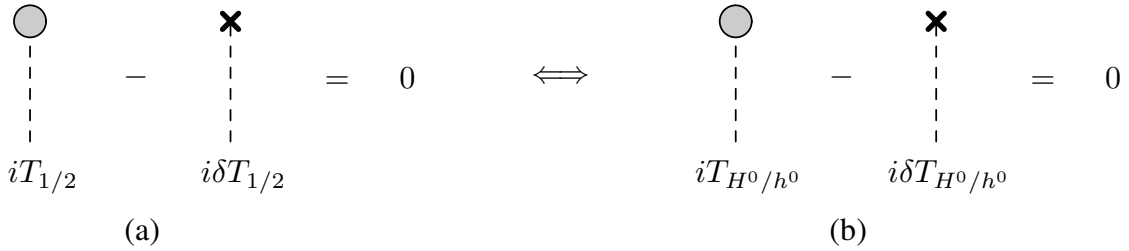


Figure 4.3.: Renormalization condition for the tadpoles. The tadpoles are renormalized such that the tadpole counterterms $i\delta T$ precisely cancel against all one-loop tadpole contributions iT (depicted by a gray blob) in the (a) gauge and (b) mass basis.

The renormalization conditions in Eq. (4.32) are transformed to the mass basis accordingly, where the tadpole terms iT_{H^0} and iT_{h^0} represent the tadpole diagrams of the physical Higgs fields H^0 and h^0 . In the mass basis, the renormalization condition is shown in Fig. 4.3 (b).

The renormalization conditions depicted in Fig. 4.3, namely that the *proper vacuum expectation values* v_1 and v_2 represent the true minimum states of the potential, are gauge-invariant to all orders of perturbation theory [84]. Therefore, the counterterms of physical quantities that are fixed through these conditions would be expected to be gauge-independent. The question, however, is what the proper vevs of the potential actually are. There are two distinct approaches to solve this problem, which lead to two distinct ways of renormalization of the tadpoles. These schemes, and their differences, shall be explored in the next two subsections.

4.4.1. Standard Tadpole Scheme

The first possibility of treating the tadpoles can be found in a variety of literature for the SM (e.g. [52]) and for the 2HDM (e.g. [56, 85]), therefore, we refer to this as the *standard tadpole scheme*. In order to keep the discussion clear, we limit ourselves to the scalar sector.

The bare mass of every particle of the 2HDM is split up into a physical mass and a counterterm, as presented generically in Eq. (4.5). The vacuum expectation values v_1 and v_2 (and, through Eq. (2.28), consequently v) are fixed at the one-loop level such that their values in the tree-level mass relations for the scalars in Eqs. (2.29) – (2.34) lead to the proper physical masses of the particles at the one-loop level. Therefore, the shift from the bare parameter to the physical one-loop value is fully contained inside the mass counterterms.

For the scalar particles of the 2HDM, there is an additional subtlety that has to be taken into account in order to derive the correct form of the mass counterterms in this scheme. The form of the mass matrices in Eqs. (2.16) – (2.18) reveals that the tadpole parameters appear explicitly in the diagonalized mass matrices for all three scalar doublets ϕ ,

$$D_{\phi,0}^2 = \begin{pmatrix} m_{\phi_1,0}^2 & 0 \\ 0 & m_{\phi_2,0}^2 \end{pmatrix} + R_\varphi^T \begin{pmatrix} \frac{T_{1,0}}{v_1} & 0 \\ 0 & \frac{T_{2,0}}{v_2} \end{pmatrix} R_\varphi \quad (4.34)$$

where $\varphi = \alpha$ for the CP-even or $\varphi = \beta$ for the CP-odd and charged doublets, respectively. At NLO, the bare masses and tadpole parameters are replaced by their physical values together with their respective counterterms. Taking into account our renormalization condition for the tadpole parameters in Eq. (4.32), this generates a counterterm for the mass matrix,

$$\delta D_\phi^2 \approx \begin{pmatrix} \delta m_{\phi_1}^2 & 0 \\ 0 & \delta m_{\phi_2}^2 \end{pmatrix} + R_\varphi^T \begin{pmatrix} \frac{\delta T_1}{v_1} & 0 \\ 0 & \frac{\delta T_2}{v_2} \end{pmatrix} R_\varphi \equiv \begin{pmatrix} \delta m_{\phi_1}^2 & 0 \\ 0 & \delta m_{\phi_2}^2 \end{pmatrix} + \begin{pmatrix} \delta T_{\phi_1\phi_1} & \delta T_{\phi_1\phi_2} \\ \delta T_{\phi_1\phi_2} & \delta T_{\phi_2\phi_2} \end{pmatrix}, \quad (4.35)$$

where we neglected all terms of order $\mathcal{O}(\delta\varphi\delta T_i)$ ($i = 1, 2$), since they contribute only from the two-loop order onwards. Note that the mass matrix counterterm in Eq. (4.35) is symmetric and consequently, $\delta T_{\phi_1\phi_2} = \delta T_{\phi_2\phi_1}$ holds. The explicit form of the second matrix depends on the scalar doublet. After rotating the tadpole parameters from the gauge to the mass basis with the help of Eq. (4.33), the tadpole counterterms explicitly read:

$$\delta T_{H^0 H^0} = \frac{c_\alpha^3 s_\beta + s_\alpha^3 c_\beta}{vs_\beta c_\beta} \delta T_{H^0} - \frac{s_{2\alpha} s_{\beta-\alpha}}{vs_{2\beta}} \delta T_{h^0}, \quad (4.36)$$

$$\delta T_{H^0 h^0} = -\frac{s_{2\alpha} s_{\beta-\alpha}}{vs_{2\beta}} \delta T_{H^0} + \frac{s_{2\alpha} c_{\beta-\alpha}}{vs_{2\beta}} \delta T_{h^0}, \quad (4.37)$$

$$\delta T_{h^0 h^0} = \frac{s_{2\alpha} c_{\beta-\alpha}}{vs_{2\beta}} \delta T_{H^0} - \frac{s_\alpha^3 s_\beta - c_\alpha^3 c_\beta}{vs_\beta c_\beta} \delta T_{h^0}, \quad (4.38)$$

$$\delta T_{G^0 G^0} = \frac{c_{\beta-\alpha}}{v} \delta T_{H^0} + \frac{s_{\beta-\alpha}}{v} \delta T_{h^0}, \quad (4.39)$$

$$\delta T_{G^0 A^0} = -\frac{s_{\beta-\alpha}}{v} \delta T_{H^0} + \frac{c_{\beta-\alpha}}{v} \delta T_{h^0}, \quad (4.40)$$

$$\delta T_{A^0 A^0} = \frac{c_\alpha s_\beta^3 + s_\alpha c_\beta^3}{vs_\beta c_\beta} \delta T_{H^0} - \frac{s_\alpha s_\beta^3 - c_\alpha c_\beta^3}{vs_\beta c_\beta} \delta T_{h^0}, \quad (4.41)$$

$$\delta T_{G^+ G^+} = \frac{c_{\beta-\alpha}}{v} \delta T_{H^0} + \frac{s_{\beta-\alpha}}{v} \delta T_{h^0}, \quad (4.42)$$

$$\delta T_{G^+ H^+} = -\frac{s_{\beta-\alpha}}{v} \delta T_{H^0} + \frac{c_{\beta-\alpha}}{v} \delta T_{h^0}, \quad (4.43)$$

$$\delta T_{H^+ H^+} = \frac{c_\alpha s_\beta^3 + s_\alpha c_\beta^3}{vs_\beta c_\beta} \delta T_{H^0} - \frac{s_\alpha s_\beta^3 - c_\alpha c_\beta^3}{vs_\beta c_\beta} \delta T_{h^0}. \quad (4.44)$$

Inserting Eq. (4.35) into our results given in Eqs. (4.25) – (4.30) gives the generic form of the field strength renormalization constants and mass counterterms for the scalar sector:

$$\delta Z_{\phi_1\phi_1} = -\text{Re} \left[\frac{\partial \Sigma_{\phi_1\phi_1}(p^2)}{\partial p^2} \right]_{p^2=m_{\phi_1}^2}, \quad (4.45)$$

$$\delta Z_{\phi_1\phi_2} = \frac{2}{m_{\phi_1}^2 - m_{\phi_2}^2} \text{Re} \left[\Sigma_{\phi_1\phi_2}(m_{\phi_2}^2) - \delta T_{\phi_1\phi_2} \right], \quad (4.46)$$

$$\delta Z_{\phi_2\phi_1} = \frac{2}{m_{\phi_2}^2 - m_{\phi_1}^2} \text{Re} \left[\Sigma_{\phi_1\phi_2}(m_{\phi_1}^2) - \delta T_{\phi_1\phi_2} \right], \quad (4.47)$$

$$\delta Z_{\phi_2\phi_2} = -\text{Re} \left[\frac{\partial \Sigma_{\phi_2\phi_2}(p^2)}{\partial p^2} \right]_{p^2=m_{\phi_2}^2}, \quad (4.48)$$

$$\delta m_{\phi_1}^2 = \text{Re} \left[\Sigma_{\phi_1\phi_1}(m_{\phi_1}^2) - \delta T_{\phi_1\phi_1} \right], \quad (4.49)$$

$$\delta m_{\phi_2}^2 = \text{Re} \left[\Sigma_{\phi_2\phi_2}(m_{\phi_2}^2) - \delta T_{\phi_2\phi_2} \right]. \quad (4.50)$$

It is straightforward to generalize these formula to the fermion and gauge boson sector. There, the tadpole counterterms disappear, since the tadpole terms are not part of the tree-level mass relations. Additionally, the formulas are adjusted in order to account for the additional degrees of freedom in the form of chirality for fermions and polarizations for vector bosons.

The standard tadpole scheme is a valid approach for the renormalization of the field theory, since it leads to a successful cancellation of all UV divergences in the scattering amplitude. However, the counterterms introduced in Eqs. (4.45) – (4.50) are in general gauge-dependent. This, by itself, is not a problem of the theory, as long as in the end, all gauge-dependences cancel against each other to deliver an overall gfp-independent amplitude.

This cancellation is normally ensured by the Becchi-Rouet-Stora-Tyutin (BRST) formalism of the gauge theory [5, 86]. In the 2HDM however, it is possible to introduce additional gauge-dependences in the angle counterterms, which spoil the overall gfp-independence of the one-loop amplitude. Additionally, terms like Eqs. (4.49) and (4.50) serve as counterterms to physical masses, i.e. observables, which are by definition gauge-invariant. As a consequence, the unobservable bare mass becomes gauge-dependent, as well (cf. Eq. (4.5)). From a theoretical point of view, it would be more appealing if the bare mass, the physical mass and the mass counterterm are gauge-independent, by themselves, since it would simplify the book-keeping of all gauge-dependences in a one-loop amplitude. It turns out that these problems are tightly connected to the treatment of the tadpoles, and by means of an alternative tadpole treatment, these problems can be solved.

4.4.2. Alternative Tadpole Scheme

An alternative treatment of the tadpoles, the *alternative tadpole scheme*, is based on the work of J. Fleischer and F. Jegerlehner [84]. Since their work is based on the Standard Model, and the 2HDM provides an extended scalar sector, this alternative treatment shall be worked out for the latter model in detail in the following.

The alternative tadpole scheme uses the same renormalization condition for the tadpoles, depicted in Fig. 4.3. As it was already mentioned at the beginning of this section, this renormalization condition is manifestly gauge-invariant to all orders of perturbation theory. However, the counterterms that are defined by this condition, e.g. mass counterterms, are gauge-independent if and only if the bare mass appearing in Eq. (4.5) is given the *proper value*. Since all masses in the 2HDM are generated through the mechanism of electroweak symmetry breaking, this proper value is determined by the proper vacuum expectation values v_1 and v_2 , which have to be determined order-by-order in perturbation theory [84]. To that end, we consider a shift of the vevs when going from leading-order to the one-loop level⁵

$$v_1 \rightarrow v_1 + \delta v_1, \quad v_2 \rightarrow v_2 + \delta v_2. \quad (4.51)$$

The tadpole parameters in Eq. (2.12) explicitly depend on the vevs. Taking seriously that the position of the minima is changed when turning from tree level to NLO, this leads to shifts⁶ in the tadpole parameters T_1 and T_2 , themselves. After the shifts have been performed consistently in the parameters, the tree-level relations in Eq. (2.14) can be applied to eliminate

⁵For better readability, the shift from tree level to the one-loop level is indicated by a replacement rule in this subsection instead of using subscripts as in Eq. (4.5). As a consequence, the parameters appearing after the replacement rule are considered to be the physical parameters.

⁶We emphasize that the term “shift” strictly refers to the application of the shift of the vevs in Eq. (4.51) to the parameters that we consider in the following, i.e. to the tadpole terms and masses of the 2HDM particles. Hence, these shifts have to be differed from the counterterms of the parameters, which are considered later on after having worked out all effects of the vev shifts.

the redundant parameters m_{11}^2 and m_{22}^2 again from the parameter set. The vev shifts induce the following shifts of the tadpole parameters at NLO:

$$T_1 \rightarrow T_1 + \left(m_{12}^2 \frac{v_2}{v_1} + \lambda_1 v_1^2 \right) \delta v_1 + \left(-m_{12}^2 + \lambda_{345} v_1 v_2 \right) \delta v_2 \equiv T_1 + \delta T_1, \quad (4.52)$$

$$T_2 \rightarrow T_2 + \left(-m_{12}^2 + \lambda_{345} v_1 v_2 \right) \delta v_1 + \left(m_{12}^2 \frac{v_1}{v_2} + \lambda_2 v_2^2 \right) \delta v_2 \equiv T_2 + \delta T_2. \quad (4.53)$$

On the right-hand side of both equations, we identified the shift of the tadpole parameters, as induced by the shift of the vevs, with the counterterms δT_1 and δT_2 which are fixed through the renormalization conditions stated in Eq. (4.32). The diagrammatic form of the counterterms δT_1 and δT_2 is given by Fig. 4.3. In order to derive expressions for the vev shifts δv_1 and δv_2 , we compare the coefficients of the shifts in Eqs. (4.52) and (4.53) with the elements of the CP-even mass matrix in Eq. (2.16), which reveals the following identity:

$$\begin{pmatrix} \delta T_1 \\ \delta T_2 \end{pmatrix} = M_\rho^2|_{T_i=0} \begin{pmatrix} \delta v_1 \\ \delta v_2 \end{pmatrix}. \quad (4.54)$$

Therefore, the tadpole shifts are diagonalized by the same matrix R_α in Eq. (2.22) that diagonalizes the mass matrix of the CP-even fields ρ_1 and ρ_2 , so that the vev shifts can be expressed in the mass basis of the CP-even Higgs fields:

$$\begin{pmatrix} \delta v_{H^0} \\ \delta v_{h^0} \end{pmatrix} = \begin{pmatrix} \frac{\delta T_{H^0}}{m_{H^0}^2} \\ \frac{\delta T_{h^0}}{m_{h^0}^2} \end{pmatrix}. \quad (4.55)$$

By applying the renormalization condition depicted diagrammatically in Fig. 4.3, this shift can be interpreted as an explicit appearance of a diagram containing the Higgs tadpole or, equivalently, a *connected tadpole diagram* which contains not only the Higgs tadpole, but additionally the Higgs propagator with zero momentum transfer,

$$\delta v_{h_i} = \frac{-i}{m_{h_i}^2} i \delta T_{h_i} = \frac{-i}{m_{h_i}^2} \left(\begin{array}{c} \text{---} \textcircled{\bullet} \text{---} \\ | \\ h_i \end{array} \right) = \left(\begin{array}{c} \text{---} \textcircled{\bullet} \text{---} \\ | \\ h_i \\ \bullet \end{array} \right), \quad (4.56)$$

where $h_i \in \{H^0, h^0\}$ stands for the physical Higgs particles. In order to consistently apply the alternative tadpole scheme, the vev shifts introduced in Eq. (4.51) have to be applied to all sectors of the 2HDM where the vacuum expectation values explicitly appear. Since the calculation of the tadpole diagrams is usually performed in the mass basis, but the shift of the vevs appear most conveniently in the gauge basis, it is useful to state the transformation between the two basis. With the inverse of Eq. (2.24), we get:

$$\begin{pmatrix} \delta v_1 \\ \delta v_2 \end{pmatrix} = \begin{pmatrix} \frac{\delta T_{H^0}}{m_{H^0}^2} c_\alpha - \frac{\delta T_{h^0}}{m_{h^0}^2} s_\alpha \\ \frac{\delta T_{H^0}}{m_{H^0}^2} s_\alpha + \frac{\delta T_{h^0}}{m_{h^0}^2} c_\alpha \end{pmatrix}. \quad (4.57)$$

The consequences of the alternative tadpole scheme are best observed by considering a specific example. From that, we can generalize the result to the whole scalar sector and eventually, to the complete Two-Higgs-Doublet Model.

Let us consider the NLO effects of the vev shifts on the mass matrix of the CP-odd doublet in Eq. (2.17). Inserting the relations from Eqs. (4.51) – (4.53), this produces several terms in each of the four entries of the mass matrix as a consequence of the shift:

$$\begin{aligned}
M_\eta^2 \rightarrow M_\eta^2 + & \begin{pmatrix} \frac{\delta T_1}{v_1} & 0 \\ 0 & \frac{\delta T_2}{v_2} \end{pmatrix} + \left(\frac{m_{12}^2}{v_1 v_2} - \lambda_5 \right) \begin{pmatrix} 2v_2 \delta v_2 & -v_1 \delta v_2 - v_2 \delta v_1 \\ -v_1 \delta v_2 - v_2 \delta v_1 & 2v_1 \delta v_1 \end{pmatrix} \\
& - \frac{m_{12}^2}{v_1 v_2} \left(\frac{\delta v_1}{v_1} + \frac{\delta v_2}{v_2} \right) \begin{pmatrix} v_2^2 & -v_1 v_2 \\ -v_1 v_2 & v_1^2 \end{pmatrix} - \begin{pmatrix} \frac{T_1 \delta v_1}{v_1^2} & 0 \\ 0 & \frac{T_2 \delta v_2}{v_2^2} \end{pmatrix}.
\end{aligned} \tag{4.58}$$

In order to determine the effect of the vev shifts on the physical mass matrix of the CP-odd sector, we have to rotate Eq. (4.58) into the mass basis. To that end we note that since we have applied the vev shifts completely in the CP-odd mass matrix, the minimum conditions of the tadpole parameters given in Eq. (2.13) can be applied again and as a consequence, the last matrix in the second line of Eq. (4.58) vanishes. Additionally, we demand that the tree-level angle β diagonalizes the CP-odd matrix M_η^2 again in the sense that the physical masses $m_{G^0}^2$ and $m_{A^0}^2$ appear as its diagonal elements.

Therefore, the effect of the vev shift on the physical (i.e. diagonalized) CP-odd mass matrix can be observed by inserting Eq. (4.58) into Eq. (2.20). In order to bring the expression for the shift into a compact form, we use the fact that only after the shifts have been performed completely, the relations between the tree-level masses, parameters of the potential and the vevs, given in Eqs. (2.29) – (2.34), hold again. Additionally, we use the relations from Eq. (A.4) to transform the remaining potential parameter m_{12}^2 to Λ_5 , as discussed in Sec. 2.8. In total, the mass shift of the diagonal CP-odd mass matrix is given by:

$$\begin{aligned}
D_\eta = R_\beta^T M_\eta^2 R_\beta \rightarrow D_\eta + & \begin{pmatrix} \delta T_{G^0 G^0} & \delta T_{G^0 A^0} \\ \delta T_{G^0 A^0} & \delta T_{A^0 A^0} \end{pmatrix} - \frac{\Lambda_5 v}{s_2 \beta} (s_\beta \delta v_1 + c_\beta \delta v_2) \begin{pmatrix} 0 & 0 \\ 0 & 1 \end{pmatrix} \\
& + \frac{m_{A^0}^2}{v} \begin{pmatrix} 0 & s_\beta \delta v_1 - c_\beta \delta v_2 \\ s_\beta \delta v_1 - c_\beta \delta v_2 & 2(c_\beta \delta v_1 + s_\beta \delta v_2) \end{pmatrix} \\
\equiv D_\eta + & \begin{pmatrix} \Delta D_{G^0 G^0} & \Delta D_{G^0 A^0} \\ \Delta D_{G^0 A^0} & \Delta D_{A^0 A^0} \end{pmatrix}.
\end{aligned} \tag{4.59}$$

In the last line, we introduced the terms $\Delta D_{G^0 G^0}$, $\Delta D_{G^0 A^0}$ and $\Delta D_{A^0 A^0}$ which contain all effects of the vev shifts on the physical mass matrix D_η . Their explicit form will be further evaluated below. Note that when we inserted the second matrix from Eq. (4.58) containing the tadpole parameter shifts δT_1 and δT_2 into Eq. (2.20), we gained an expression which is analogous to the rotation of the tadpole counterterms, as performed in Eq. (4.35) in the previous subsection. Therefore, we identify the physical tadpole parameter shifts $\delta T_{G^0 G^0}$, $\delta T_{G^0 A^0}$ and $\delta T_{A^0 A^0}$ in the first line of Eq. (4.59) with the tadpole counterterms given in Eqs. (4.39) – (4.41).

Finally, the off-diagonal part $\Delta D_{G^0 A^0}$ receives a non-vanishing contribution as well,

$$\begin{aligned}
\Delta D_{G^0 A^0} &= \delta T_{G^0 A^0} + \frac{m_{A^0}^2}{v} (s_\beta \delta v_1 - c_\beta \delta v_2) \\
&= i \frac{-is_{\beta-\alpha}}{v} (m_{A^0}^2 - m_{H^0}^2) \frac{-i}{m_{H^0}^2} i \delta T_{H^0} + i \frac{ic_{\beta-\alpha}}{v} (m_{A^0}^2 - m_{h^0}^2) \frac{-i}{m_{h^0}^2} i \delta T_{h^0} \\
&= i \left(\begin{array}{ccc} & \textcircled{\bullet} & \\ & | & \\ G^0 & H^0 & A^0 \\ \text{---} & \bullet & \text{---} \end{array} \right) + i \left(\begin{array}{ccc} & \textcircled{\bullet} & \\ & | & \\ G^0 & h^0 & A^0 \\ \text{---} & \bullet & \text{---} \end{array} \right), \tag{4.68}
\end{aligned}$$

where we again identified the connected tadpole diagrams with the help of Eq. (4.56) and the coupling constants according to Eqs. (4.64) and (4.65) in order to derive the diagrammatic representation.

This result can be easily generalized to the whole scalar sector of the 2HDM. If we consider the full shift of the mass matrices (including the counterterm insertion for the bare masses), then the mass matrix counterterm δD_ϕ^2 for the scalar doublet ϕ in the alternative tadpole scheme reads

$$\delta D_\phi^2 = \begin{pmatrix} \delta m_{\phi_1}^2 & 0 \\ 0 & \delta m_{\phi_2}^2 \end{pmatrix} + \begin{pmatrix} \Delta D_{\phi_1 \phi_1} & \Delta D_{\phi_1 \phi_2} \\ \Delta D_{\phi_1 \phi_2} & \Delta D_{\phi_2 \phi_2} \end{pmatrix}, \tag{4.69}$$

with the explicit form of the additional mass shifts

$$\Delta D_{\phi_i \phi_j} = i \left(\begin{array}{ccc} & \textcircled{\bullet} & \\ & | & \\ \phi_i & H^0 & \phi_j \\ \text{---} & \bullet & \text{---} \end{array} \right) + i \left(\begin{array}{ccc} & \textcircled{\bullet} & \\ & | & \\ \phi_i & h^0 & \phi_j \\ \text{---} & \bullet & \text{---} \end{array} \right), \tag{4.70}$$

where $i, j = 1, 2$. Note that in the alternative tadpole scheme, the tadpole counterterms δT_1 and δT_2 , introduced through the vev shifts in Eqs. (4.52) and (4.53), are part of the shift parameters $\Delta D_{\phi_i \phi_j}$ of the physical mass matrices of the scalar sector. Therefore, in the alternative scheme they do not appear explicitly as counterterms in Eq. (4.69). This is in contrast to the standard scheme, where we considered δT_1 and δT_2 as counterterms, appearing explicitly in δD_ϕ^2 , cf. Eq. (4.35). Consequently, the tadpole counterterms in Eqs. (4.36) – (4.44) do not appear in the definition of mass counterterms and wave function renormalization constants within the alternative tadpole scheme.

In order to further illustrate the effect of the mass shifts, we recall the form of the renormalized two-point correlation function in Eq. (4.14), where the renormalized self-energy $\widehat{\Sigma}_\phi(p^2)$ explicitly appears. If we redefine the 1PI self-energy as

$$i \Sigma_{\phi_i \phi_j}^{\text{tad}}(p^2) := i \Sigma_{\phi_i \phi_j}(p^2) - i \Delta D_{\phi_i \phi_j}, \tag{4.71}$$

then it is straightforward to see that the insertion of Eq. (4.69) into Eq. (4.16) yields the following form of the renormalized self-energy in the alternative tadpole scheme:

$$\widehat{\Sigma}_\phi(p^2) = \Sigma_\phi^{\text{tad}}(p^2) - \begin{pmatrix} \delta m_{\phi_1}^2 & 0 \\ 0 & \delta m_{\phi_2}^2 \end{pmatrix} + \frac{\delta Z_\phi^\dagger}{2} (p^2 \mathbb{1}_{2 \times 2} - D_\phi^2) + (p^2 \mathbb{1}_{2 \times 2} - D_\phi^2) \frac{\delta Z_\phi}{2}. \tag{4.72}$$

As a consequence, the counterterms and wave function renormalization constants derived at the end of Sec. 4.3, namely Eqs. (4.25) – (4.30), change to:

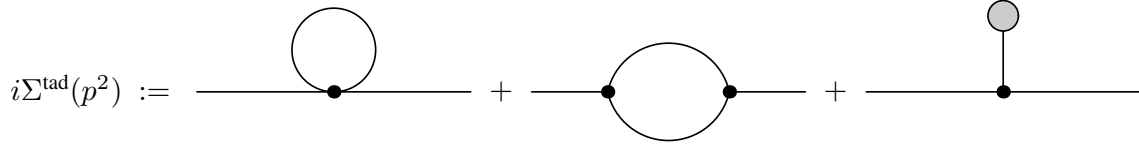


Figure 4.4.: Modified self-energy in the alternative tadpole scheme. The self-energy $i\Sigma^{\text{tad}}(p^2)$ consists of all 1PI self-energy diagrams together with the one-loop tadpole diagrams, indicated by a gray blob. The self-energy is depicted in a generic topological way and has to be replaced with the actual particle content and vertices of the 2HDM.

$$\delta Z_{\phi_1\phi_1} = -\text{Re} \left[\frac{\partial \Sigma_{\phi_1\phi_1}^{\text{tad}}(p^2)}{\partial p^2} \right]_{p^2=m_{\phi_1}^2}, \quad (4.73)$$

$$\delta Z_{\phi_1\phi_2} = \frac{2}{m_{\phi_1}^2 - m_{\phi_2}^2} \text{Re} \left[\Sigma_{\phi_1\phi_2}^{\text{tad}}(m_{\phi_2}^2) \right], \quad (4.74)$$

$$\delta Z_{\phi_2\phi_1} = \frac{2}{m_{\phi_2}^2 - m_{\phi_1}^2} \text{Re} \left[\Sigma_{\phi_1\phi_2}^{\text{tad}}(m_{\phi_1}^2) \right], \quad (4.75)$$

$$\delta Z_{\phi_2\phi_2} = -\text{Re} \left[\frac{\partial \Sigma_{\phi_2\phi_2}^{\text{tad}}(p^2)}{\partial p^2} \right]_{p^2=m_{\phi_2}^2}, \quad (4.76)$$

$$\delta m_{\phi_1}^2 = \text{Re} \left[\Sigma_{\phi_1\phi_1}^{\text{tad}}(m_{\phi_1}^2) \right], \quad (4.77)$$

$$\delta m_{\phi_2}^2 = \text{Re} \left[\Sigma_{\phi_2\phi_2}^{\text{tad}}(m_{\phi_2}^2) \right]. \quad (4.78)$$

This result can be generalized to the fermion and gauge boson sectors. In general, the change from the standard to the alternative tadpole scheme leads to a redefinition of the self-energy in the form of Fig. 4.4. Additionally, the tadpole counterterms $\delta T_{\phi_i\phi_j}$ in the scalar sector drop out of the definition of the field strength renormalization constants and mass counterterms.

The alternative tadpole treatment has another important implication. Consider e.g. the coupling constants $g_{H^0 Z^0 Z^0}$ and $g_{H^0 H^0 Z^0 Z^0}$ for the coupling of two vector bosons Z^0 with one or two heavy Higgses H^0 , respectively (for simplicity, we omit the Lorentz structure of the associated Feynman rule):

$$ig_{H^0 Z^0 Z^0} = \frac{ig^2 v c_{\beta-\alpha}}{2c_W^2} = \frac{ig^2}{2c_W^2} (c_\alpha v_1 + s_\alpha v_2), \quad ig_{H^0 H^0 Z^0 Z^0} = \frac{ig^2}{2c_W^2}. \quad (4.79)$$

The shifts from Eq. (4.51) introduce a shift in coupling constants as well. In order to perform this shift consistently, the couplings have to be expressed in terms of the vacuum expectation values v_1 and v_2 . Note however that when performing the shifts in the coupling constants, we carefully have to differentiate between the angles α and β in the sense of mixing angles and β in the sense of the ratio of the vevs, cf. Eq. (2.35), and α as the ratio of 2HDM potential parameters⁷, cf. Eq. (2.36). The vev shifts from Eq. (4.51) only affect the latter two.

The quartic coupling in Eq. (4.79) does not contain the vevs. Therefore, it does not receive a shift. In contrast to that, the trilinear coupling given in Eq. (4.79) contains α as a mixing

⁷The angle α only appears in the trilinear and quartic Higgs couplings partly in the sense of a ratio of 2HDM potential parameters, cf. Eq. (2.36). In all other couplings, α is the mixing angle.

angle, but β is precisely defined over the ratio of the vevs and thus receives a shift. At NLO, this shift yields

$$\begin{aligned}
ig_{H^0 Z^0 Z^0} &\rightarrow ig_{H^0 Z^0 Z^0} + \frac{ig^2}{2c_W^2} (c_\alpha \delta v_1 + s_\alpha \delta v_2) \\
&= ig_{H^0 Z^0 Z^0} + \frac{ig^2}{2c_W^2} \left[(c_\alpha^2 + s_\alpha^2) \frac{\delta T_{H^0}}{m_{H^0}^2} + (s_\alpha c_\alpha - s_\alpha c_\alpha) \frac{\delta T_{h^0}}{m_{h^0}^2} \right] \\
&= ig_{H^0 Z^0 Z^0} + \frac{ig^2}{2c_W^2} \frac{-i}{m_{H^0}^2} i\delta T_{H^0} \\
&= ig_{H^0 Z^0 Z^0} + \left(\text{Diagram} \right)_{\text{trunc}} .
\end{aligned} \tag{4.80}$$

The subscript ‘‘trunc’’ stands for the truncated Feynman diagram, meaning that the external Lorentz structure of the vector bosons as well as the Lorentz structure of the quartic coupling is not explicitly stated in the diagram. Note that we used the explicit form of the quartic coupling constant in Eq. (4.79) together with the form of the connected tadpole diagram according to Eq. (4.56) to identify the calculated shift in the third line of Eq. (4.80) with the diagram in the last line.

The shift of the vevs, which is induced by the alternative tadpole scheme, leads to a modification of the Feynman rules of the vertex in the form of the explicit appearance of a Higgs tadpole. As a result, the tadpole diagram depicted in the last line of Eq. (4.80) has to be taken into account, even though the tadpoles were renormalized away by our renormalization conditions in Eq. (4.31).

This result can be generalized to the whole 2HDM. The change from the standard to the alternative tadpole scheme introduces additional virtual vertex corrections in the form of tadpole vertex diagrams. As a rule of thumb, every 2HDM trilinear vertex receives these additional tadpole vertex corrections if the resulting quartic coupling constant, consisting of the three original particles of the trilinear vertex and additionally, the Higgs tadpoles, exists within the 2HDM. In the case discussed above, the trilinear coupling constant $g_{H^0 Z^0 Z^0}$ in Eq. (4.79) receives an additional tadpole contribution with the heavy CP-even Higgs H^0 , since the resulting quartic coupling $g_{H^0 H^0 Z^0 Z^0}$ exists within the 2HDM. But note that the vev shifts do not lead to the appearance of a tadpole diagram containing the lighter CP-even Higgs h^0 , since the coupling $g_{H^0 h^0 Z^0 Z^0}$ does not exist within the 2HDM due to internal symmetry relations. These symmetries make their appearance in Eq. (4.80) as well and lead to the cancellation of the term proportional to δT_{h^0} , thus preventing the lighter CP-even Higgs from appearing as a vertex tadpole diagram in the last line of Eq. (4.80).

As another example, consider the coupling constant of the charged Higgs boson H^+ , the W^- boson and the light Higgs h^0 , which reads

$$ig_{h^0 W^- H^+} = \frac{-ig c_{\beta-\alpha}}{2} , \tag{4.81}$$

where the Lorentz structure of the associated Feynman rule has been omitted again for simplicity. The coupling constant does not explicitly contain the vevs v_1 and v_2 and both angles α and β which are contained in Eq. (4.81) appear in the coupling in the sense of mixing angles. Therefore, the coupling constant is unaffected by the shift of the vevs and the coupling in Eq. (4.81) receives no additional tadpole contributions when changing from the standard to the alternative tadpole scheme.

The only difference between the two tadpole renormalization schemes is the exact definition of the bare mass and its counterterm. In the standard scheme, the mass counterterms are generated through the mass relations in Eqs. (2.29) – (2.34) *after* the minimum conditions of the potential have been applied. The tadpole terms appearing explicitly in the tree-level mass matrices receive tadpole counterterms at NLO.

In the alternative scheme however, the proper vacuum state is taken into account. The shift of the vacuum expectation values generates additional terms through the proper tree-level values of the mass matrix *before* the minimum conditions are applied. As a result, the tadpole parameters do not appear in the counterterms any more, but the 1PI self-energies, over which the counterterms are defined, are shifted to self-energies that contain the tadpole contributions. Additionally, tadpole contributions to the vertex corrections have to be taken into account. In summary, the change to the alternative tadpole scheme has the following implications on higher-order calculations in the Two-Higgs-Doublet Model:

Self-energies: The self-energies appearing in the definitions of the wave function renormalization constants and counterterms are changed such that they contain additional tadpole contributions: $\Sigma(p^2) \rightarrow \Sigma^{\text{tad}}(p^2)$.

Tadpole counterterms: The tadpole counterterms $\delta T_{\phi_i \phi_j}$ ($i, j = 1, 2$) in the scalar sector vanish: $\delta T_{\phi_i \phi_j} \rightarrow 0$.

Vertex corrections: The virtual vertex corrections change to contain additional tadpole contributions if the resulting coupling exists within the 2HDM.

Both schemes use the manifestly gauge-invariant renormalization condition shown pictorially in Fig. 4.3, however, only the alternative tadpole scheme, that considers the proper vacuum state of the 2HDM, yields mass counterterms, cf. Eqs. (4.77) and (4.78), that are manifestly gauge-independent, as well. This will be investigated further in the following sections, when we consider the actual particle content of the 2HDM.

4.5. Renormalization of the Gauge Sector

The renormalization of the gauge sector encompasses the fixation of all counterterms to the coupling constants that belong to the weak sector. With the chosen parameter set of Eq. (2.58), this introduces the three counterterms

$$m_{W,0}^2 = m_W^2 + \delta m_W^2, \quad (4.82)$$

$$m_{Z,0}^2 = m_Z^2 + \delta m_Z^2, \quad (4.83)$$

$$e_0 = (1 + \delta Z_e) e, \quad (4.84)$$

$$g_0 = g + \delta g \quad (4.85)$$

Note that the weak coupling constant g_0 is a redundant parameter in this list, since it can be expressed through the other three parameters by means of Eqs. (2.46) and (2.47). Nevertheless, it is practical to keep it in the list, since it is often more convenient to express the couplings through g instead of e .

Additionally, in higher-order calculations, the gauge bosons fields acquire field strength renormalization constants. Keeping in mind that the Z^0 boson and the photon γ form a doublet

which allows for mixing, the field strength renormalization constants at next-to-leading order are introduced through

$$W_{\mu,0}^{\pm} \approx \left(1 + \frac{\delta Z_{WW}}{2}\right) W_{\mu}^{\pm}, \quad (4.86)$$

$$\begin{pmatrix} Z_{\mu}^0 \\ \gamma_{\mu} \end{pmatrix}_0 \approx \begin{pmatrix} 1 + \frac{\delta Z_{ZZ}}{2} & \frac{\delta Z_{Z\gamma}}{2} \\ \frac{\delta Z_{\gamma Z}}{2} & 1 + \frac{\delta Z_{\gamma\gamma}}{2} \end{pmatrix} \begin{pmatrix} Z_{\mu}^0 \\ \gamma_{\mu} \end{pmatrix} \quad (4.87)$$

The form of the field strength renormalization constants and mass counterterms in the gauge boson sector depends on the chosen tadpole scheme. In order to present the explicit form of the counterterms in a convenient way, it is necessary to introduce the two-point correlation function of the gauge bosons. In general R_{ξ} gauge, the renormalized two-point correlation function of the gauge bosons $V_i, V_j \in \{W^{\pm}, Z^0, \gamma\}$ can be written as [5]

$$\begin{aligned} \widehat{\Gamma}_{ij}^{\mu\nu}(p) = & -i \left(g^{\mu\nu} - \frac{p^{\mu}p^{\nu}}{p^2} \right) (p^2 - m_V^2) \delta_{ij} - i \frac{p^{\mu}p^{\nu}}{p^2} \frac{1}{\xi_V} (p^2 - \xi_V m_V^2) \delta_{ij} \\ & - i \left(g^{\mu\nu} - \frac{p^{\mu}p^{\nu}}{p^2} \right) \widehat{\Sigma}_{ij}^T(p^2) - i \frac{p^{\mu}p^{\nu}}{p^2} \widehat{\Sigma}_{ij}^L(p^2), \end{aligned} \quad (4.88)$$

where the superscripts T and L denote the transverse and longitudinal components of the renormalized gauge boson self-energies, respectively.

In order to fix all renormalization constants, the on-shell prescription from Sec. 4.3 can be applied directly to the gauge sector. However, in order to fix the counterterm δZ_e in Eq. (4.84), an additional condition is needed. Since the electric charge e has been well-observed before the rise of quantum electrodynamics, the physical value is usually fixed in the so-called *Thomson limit*, i.e. the limit of vanishing photon momentum in the Thomson scattering between a photon and an electron [5].

The application of the two tadpole schemes of Sec. 4.4 reveals that only the mass counterterms depend on the choice of scheme. All other field strength renormalization constants, as well as the counterterms of the electric charge and weak coupling constant, are *tadpole-invariant*, i.e. invariant under the change of tadpole scheme⁸. In order to illustrate the effect of the alternative tadpole scheme, we consider the effect on the tree-level mass of the W^{\pm} bosons as given in Eq. (2.43). Performing the shift, we get⁹

$$m_W^2 \rightarrow m_W^2 + i \left(\text{diagram with } H^0 \text{ tadpole} \right) + i \left(\text{diagram with } h^0 \text{ tadpole} \right). \quad (4.89)$$

Considering the form of the two-point correlation function in Eq. (4.88), this leads to a modification of the 1PI self-energies shown pictorially in Fig. 4.4

$$\Sigma_{ij}^T(p^2) \rightarrow \Sigma_{ij}^{\text{tad},T}(p^2), \quad \Sigma_{ij}^L(p^2) \rightarrow \Sigma_{ij}^{\text{tad},L}(p^2). \quad (4.90)$$

In summary, the field strength renormalization constants and counterterms of the gauge sector read: [52]

⁸The self-energies involving $\gamma\gamma$ and γZ^0 are invariant since the photons do not couple to the CP-even Higgs bosons. The diagonal field strength constants δZ_{WW} and δZ_{ZZ} are invariant since the derivative of the tadpole diagrams vanishes, and finally, δg is invariant due to an invariant combination of δm_W^2 and δm_Z^2 .

⁹Note that for the calculation of Eq. (4.89), we use that the polarization vectors of the gauge bosons are normalized as $\varepsilon(p) \cdot \varepsilon^*(p) = -1$.

Standard tadpole scheme

$$\delta m_W^2 = \widetilde{\text{Re}} \left[\Sigma_{WW}^T (m_W^2) \right] , \quad \delta m_Z^2 = \text{Re} \left[\Sigma_{ZZ}^T (m_Z^2) \right] . \quad (4.91)$$

Alternative tadpole scheme

$$\delta m_W^2 = \widetilde{\text{Re}} \left[\Sigma_{WW}^{\text{tad},T} (m_W^2) \right] , \quad \delta m_Z^2 = \text{Re} \left[\Sigma_{ZZ}^{\text{tad},T} (m_Z^2) \right] . \quad (4.92)$$

Tadpole-invariant

$$\delta Z_e = \frac{1}{2} \left. \frac{\partial \Sigma_{\gamma\gamma}^T (p^2)}{\partial p^2} \right|_{p^2=0} + \frac{s_W}{c_W} \frac{\Sigma_{\gamma Z}^T (0)}{m_Z^2} , \quad (4.93)$$

$$\frac{\delta g}{g} = \delta Z_e + \frac{1}{2} \frac{1}{m_Z^2 - m_W^2} (\delta m_W^2 - c_W^2 \delta m_Z^2) , \quad (4.94)$$

$$\delta Z_{WW} = -\text{Re} \left[\left. \frac{\partial \Sigma_{WW}^T (p^2)}{\partial p^2} \right]_{p^2=m_W^2} \right] , \quad (4.95)$$

$$\begin{pmatrix} \delta Z_{ZZ} & \delta Z_{Z\gamma} \\ \delta Z_{\gamma Z} & \delta Z_{\gamma\gamma} \end{pmatrix} = \begin{pmatrix} -\text{Re} \left[\left. \frac{\partial \Sigma_{ZZ}^T (p^2)}{\partial p^2} \right]_{p^2=m_Z^2} \right] & \frac{2}{m_Z^2} \Sigma_{Z\gamma}^T (0) \\ -\frac{2}{m_Z^2} \text{Re} \left[\Sigma_{Z\gamma}^T (m_Z^2) \right] & -\text{Re} \left[\left. \frac{\partial \Sigma_{\gamma\gamma}^T (p^2)}{\partial p^2} \right]_{p^2=0} \right] \end{pmatrix} . \quad (4.96)$$

Note that the sign in front of the second term of Eq. (4.93) is equivalent to the sign of the $SU(2)_L$ term in the covariant derivative in Eq. (2.38). Therefore, a change of the sign of this term is required if one chooses to follow the SM convention of the covariant derivative. The modified real part $\widetilde{\text{Re}}$ takes the real part of the loop integrals, but not of any coupling constants (like CKM matrix elements for quark mixing). If these are chosen to be real, the replacement $\widetilde{\text{Re}} \rightarrow \text{Re}$ is valid at the one-loop order [52].

The wave function renormalization constants in Eq. (4.95) and Eq. (4.96) contain gauge-dependent parts, while the counterterms δg and δZ_e are manifestly gauge-independent. The mass counterterms δm_W^2 and δm_Z^2 are gauge-independent only if the alternative tadpole scheme is chosen, which has been checked both numerically and analytically. In the standard tadpole scheme, the mass counterterms in Eq. (4.91) contain a residual gauge-dependence.

4.6. Renormalization of the Fermion Sector

For the renormalization of the fermion sector of the Two-Higgs-Doublet Model, in principle all constants and fields introduced in Sec. 2.6 have to be considered. However, the renormalization of the fermion sector does not differ much between the SM and the 2HDM. Hence, we restrict ourselves only to the τ^\pm particle, since we need the results later in Sec. 4.8.4 for a process-dependent definition of the scalar mixing angles. A treatment of the complete fermion sector can be found e.g. in [52].

In the on-shell basis, the relevant parameter that needs to be renormalized is the mass of the τ^\pm particle:

$$m_{\tau,0} = m_\tau + \delta m_\tau . \quad (4.97)$$

The mixing between charged lepton fields is either absent in nature or strongly suppressed [87, 88]. Therefore, we consider the τ field to be a lepton number eigenstate, so that the left- and right-handed bare fields are split up according to

$$\tau_{L,0} = \left(1 + \frac{\delta Z_{\tau\tau}^L}{2}\right) \tau_L, \quad (4.98)$$

$$\tau_{R,0} = \left(1 + \frac{\delta Z_{\tau\tau}^R}{2}\right) \tau_R. \quad (4.99)$$

The two-point correlation function of the τ particle accounts for the spinor structure of the fermionic field. Using Feynman slash notation, it is given by

$$\widehat{\Gamma}_{\tau\tau}(p) = i(\not{p} - m_\tau) + i\left[\not{p}\omega_- \widehat{\Sigma}_{\tau\tau}^L(p^2) + \not{p}\omega_+ \widehat{\Sigma}_{\tau\tau}^R(p^2) + m_\tau(\omega_- + \omega_+) \widehat{\Sigma}_{\tau\tau}^S(p^2)\right], \quad (4.100)$$

where the superscripts L , R and S stand for the left-handed, right-handed and scalar parts of the renormalized self-energies, respectively [52]. The explicit form of the spinor structure in the correlation function is instructive for an unambiguous extraction of the three different self-energies $\Sigma_{\tau\tau}^L(p^2)$, $\Sigma_{\tau\tau}^R(p^2)$ and $\Sigma_{\tau\tau}^S(p^2)$ of the τ fields.

In general, the renormalization of the fermion sector depends on the chosen tadpole scheme. In the previous section, we saw that the change from the standard to the alternative tadpole scheme shifted the tree-level vertex couplings such that they contain additional tadpole contributions. In the 2HDM (as in any other renormalizable field theory) however, no vertex of two fermions, one CP-even Higgs boson and one additional particle exists. Therefore, the change from the standard to the alternative tadpole scheme does not introduce any additional tadpole diagrams to the tree-level couplings of the fermion sector.

By applying the shift of the vacuum expectation values of Eq. (4.51), the mass of the τ particle receives a shift, as well. Independently on the type of the 2HDM, this shift reads

$$m_\tau \rightarrow m_\tau + i \left(\text{trunc} \left[\begin{array}{c} \text{---} \bullet \text{---} \\ | \\ \text{---} \text{H}^0 \text{---} \\ | \\ \text{---} \bullet \text{---} \\ | \\ \tau^+ \end{array} \right] + i \left(\text{trunc} \left[\begin{array}{c} \text{---} \bullet \text{---} \\ | \\ \text{---} h^0 \text{---} \\ | \\ \text{---} \bullet \text{---} \\ | \\ \tau^+ \end{array} \right] \right) \right), \quad (4.101)$$

in complete analogy to the scalar and gauge boson sector. Note the subscript “trunc”, indicating that the external spinor structure is omitted in the diagrams. Inserting this mass shift into the two-point correlation function in Eq. (4.100) reveals the modification of the τ self-energies in the alternative tadpole scheme:

$$\Sigma_{\tau\tau}^L(p^2) \rightarrow \Sigma_{\tau\tau}^L(p^2), \quad \Sigma_{\tau\tau}^R(p^2) \rightarrow \Sigma_{\tau\tau}^R(p^2), \quad \Sigma_{\tau\tau}^S(p^2) \rightarrow \Sigma_{\tau\tau}^{\text{ad},S}(p^2), \quad (4.102)$$

since the tadpole diagrams that have to be added to the fermion self-energies contain no spinor structures of the form $\not{p}\omega_-$ or $\not{p}\omega_+$ and hence, are purely scalar. Consequently, the left-handed and right-handed components of the τ self-energies are invariant under a change of the tadpole scheme, and only the scalar component differs between the two schemes.

The full set of field strength renormalization constants and mass counterterms for the τ particle in the standard tadpole scheme is derived in [52], while for the alternative tadpole scheme, Eq. (4.102) can be applied. In summary, the explicit form of the renormalization constants is given by:

Standard tadpole scheme	
$\delta m_\tau = \frac{m_\tau}{2} \widetilde{\text{Re}} \left[\Sigma_{\tau\tau}^L(m_\tau^2) + \Sigma_{\tau\tau}^R(m_\tau^2) + 2\Sigma_{\tau\tau}^S(m_\tau^2) \right]. \quad (4.103)$	

Alternative tadpole scheme

$$\delta m_\tau = \frac{m_\tau}{2} \widetilde{\text{Re}} \left[\Sigma_{\tau\tau}^L(m_\tau^2) + \Sigma_{\tau\tau}^R(m_\tau^2) + 2\Sigma_{\tau\tau}^{\text{tad},S}(m_\tau^2) \right]. \quad (4.104)$$

Tadpole-invariant

$$\delta Z_{\tau\tau}^L = -\widetilde{\text{Re}} \left[\Sigma_{\tau\tau}^L(m_\tau^2) \right] - m_\tau^2 \widetilde{\text{Re}} \left[\frac{\partial \Sigma_{\tau\tau}^L(p^2)}{\partial p^2} + \frac{\partial \Sigma_{\tau\tau}^R(p^2)}{\partial p^2} + 2 \frac{\partial \Sigma_{\tau\tau}^S(p^2)}{\partial p^2} \right]_{p^2=m_\tau^2}, \quad (4.105)$$

$$\delta Z_{\tau\tau}^R = -\widetilde{\text{Re}} \left[\Sigma_{\tau\tau}^R(m_\tau^2) \right] - m_\tau^2 \widetilde{\text{Re}} \left[\frac{\partial \Sigma_{\tau\tau}^L(p^2)}{\partial p^2} + \frac{\partial \Sigma_{\tau\tau}^R(p^2)}{\partial p^2} + 2 \frac{\partial \Sigma_{\tau\tau}^S(p^2)}{\partial p^2} \right]_{p^2=m_\tau^2}. \quad (4.106)$$

As it was the case for the gauge boson sector, the wave function renormalization constants of the τ particle as well as the mass counterterm δm_τ in the standard tadpole scheme contain gauge-dependent parts. The mass counterterm in the alternative tadpole scheme, Eq. (4.104), is manifestly gauge-independent.

4.7. Renormalization of the Scalar Fields and Masses

The renormalization of the scalar sector of the 2HDM introduces the counterterms of all scalar masses:

$$m_{H^0,0}^2 = m_{H^0}^2 + \delta m_{H^0}^2, \quad (4.107)$$

$$m_{h^0,0}^2 = m_{h^0}^2 + \delta m_{h^0}^2, \quad (4.108)$$

$$m_{A^0,0}^2 = m_{A^0}^2 + \delta m_{A^0}^2, \quad (4.109)$$

$$m_{H^\pm,0}^2 = m_{H^\pm}^2 + \delta m_{H^\pm}^2. \quad (4.110)$$

The scalar fields of the Two-Higgs-Doublet Model are transformed to the NLO expansion, introducing the field strength renormalization constants. Since the scalar sector forms doublets that allow for mixing (cf. Sec. 4.3), the field strength renormalization is most conveniently presented in a matrix structure:

$$\begin{pmatrix} H^0 \\ h^0 \end{pmatrix}_0 = \begin{pmatrix} 1 + \frac{\delta Z_{H^0 H^0}}{2} & \frac{\delta Z_{H^0 h^0}}{2} \\ \frac{\delta Z_{h^0 H^0}}{2} & 1 + \frac{\delta Z_{h^0 h^0}}{2} \end{pmatrix} \begin{pmatrix} H^0 \\ h^0 \end{pmatrix}, \quad (4.111)$$

$$\begin{pmatrix} G^0 \\ A^0 \end{pmatrix}_0 = \begin{pmatrix} 1 + \frac{\delta Z_{G^0 G^0}}{2} & \frac{\delta Z_{G^0 A^0}}{2} \\ \frac{\delta Z_{A^0 G^0}}{2} & 1 + \frac{\delta Z_{A^0 A^0}}{2} \end{pmatrix} \begin{pmatrix} G^0 \\ A^0 \end{pmatrix}, \quad (4.112)$$

$$\begin{pmatrix} G^\pm \\ H^\pm \end{pmatrix}_0 = \begin{pmatrix} 1 + \frac{\delta Z_{G^\pm G^\pm}}{2} & \frac{\delta Z_{G^\pm H^\pm}}{2} \\ \frac{\delta Z_{H^\pm G^\pm}}{2} & 1 + \frac{\delta Z_{H^\pm H^\pm}}{2} \end{pmatrix} \begin{pmatrix} G^\pm \\ H^\pm \end{pmatrix}. \quad (4.113)$$

The renormalization procedure of the scalar sector was discussed extensively in Sec. 4.3 in a generic way. Additionally, in 4.4 we investigated the differences between the standard and alternative tadpole scheme regarding the form of the counterterms. This generic discussion allows us to give the explicit form of all renormalization constants for both schemes:

Standard tadpole scheme

$$\delta Z_{H^0 h^0} = \frac{2}{m_{H^0}^2 - m_{h^0}^2} \text{Re} \left[\Sigma_{H^0 h^0}(m_{h^0}^2) - \delta T_{H^0 h^0} \right], \quad (4.114)$$

$$\delta Z_{h^0 H^0} = -\frac{2}{m_{H^0}^2 - m_{h^0}^2} \text{Re} \left[\Sigma_{H^0 h^0}(m_{H^0}^2) - \delta T_{H^0 h^0} \right], \quad (4.115)$$

$$\delta Z_{G^0 A^0} = -\frac{2}{m_{A^0}^2} \text{Re} \left[\Sigma_{G^0 A^0}(m_{A^0}^2) - \delta T_{G^0 A^0} \right], \quad (4.116)$$

$$\delta Z_{A^0 G^0} = \frac{2}{m_{A^0}^2} \text{Re} \left[\Sigma_{G^0 A^0}(0) - \delta T_{G^0 A^0} \right], \quad (4.117)$$

$$\delta Z_{G^\pm H^\pm} = -\frac{2}{m_{H^\pm}^2} \widetilde{\text{Re}} \left[\Sigma_{G^\pm H^\pm}(m_{H^\pm}^2) - \delta T_{G^\pm H^\pm} \right], \quad (4.118)$$

$$\delta Z_{H^\pm G^\pm} = \frac{2}{m_{H^\pm}^2} \widetilde{\text{Re}} \left[\Sigma_{G^\pm H^\pm}(0) - \delta T_{G^\pm H^\pm} \right], \quad (4.119)$$

$$\delta m_{H^0}^2 = \text{Re} \left[\Sigma_{H^0 H^0}(m_{H^0}^2) - \delta T_{H^0 H^0} \right], \quad (4.120)$$

$$\delta m_{h^0}^2 = \text{Re} \left[\Sigma_{h^0 h^0}(m_{h^0}^2) - \delta T_{h^0 h^0} \right], \quad (4.121)$$

$$\delta m_{A^0}^2 = \text{Re} \left[\Sigma_{A^0 A^0}(m_{A^0}^2) - \delta T_{A^0 A^0} \right], \quad (4.122)$$

$$\delta m_{H^\pm}^2 = \widetilde{\text{Re}} \left[\Sigma_{H^\pm H^\pm}(m_{H^\pm}^2) - \delta T_{H^\pm H^\pm} \right]. \quad (4.123)$$

Alternative tadpole scheme

$$\delta Z_{H^0 h^0} = \frac{2}{m_{H^0}^2 - m_{h^0}^2} \text{Re} \left[\Sigma_{H^0 h^0}^{\text{tad}}(m_{h^0}^2) \right], \quad (4.124)$$

$$\delta Z_{h^0 H^0} = -\frac{2}{m_{H^0}^2 - m_{h^0}^2} \text{Re} \left[\Sigma_{H^0 h^0}^{\text{tad}}(m_{H^0}^2) \right], \quad (4.125)$$

$$\delta Z_{G^0 A^0} = -\frac{2}{m_{A^0}^2} \text{Re} \left[\Sigma_{G^0 A^0}^{\text{tad}}(m_{A^0}^2) \right], \quad (4.126)$$

$$\delta Z_{A^0 G^0} = \frac{2}{m_{A^0}^2} \text{Re} \left[\Sigma_{G^0 A^0}^{\text{tad}}(0) \right], \quad (4.127)$$

$$\delta Z_{G^\pm H^\pm} = -\frac{2}{m_{H^\pm}^2} \widetilde{\text{Re}} \left[\Sigma_{G^\pm H^\pm}^{\text{tad}}(m_{H^\pm}^2) \right], \quad (4.128)$$

$$\delta Z_{H^\pm G^\pm} = \frac{2}{m_{H^\pm}^2} \widetilde{\text{Re}} \left[\Sigma_{G^\pm H^\pm}^{\text{tad}}(0) \right], \quad (4.129)$$

$$\delta m_{H^0}^2 = \text{Re} \left[\Sigma_{H^0 H^0}^{\text{tad}}(m_{H^0}^2) \right], \quad (4.130)$$

$$\delta m_{h^0}^2 = \text{Re} \left[\Sigma_{h^0 h^0}^{\text{tad}}(m_{h^0}^2) \right], \quad (4.131)$$

$$\delta m_{A^0}^2 = \text{Re} \left[\Sigma_{A^0 A^0}^{\text{tad}}(m_{A^0}^2) \right], \quad (4.132)$$

$$\delta m_{H^\pm}^2 = \widetilde{\text{Re}} \left[\Sigma_{H^\pm H^\pm}^{\text{tad}}(m_{H^\pm}^2) \right]. \quad (4.133)$$

Tadpole-invariant	
$\delta Z_{H^0 H^0} = -\text{Re} \left[\frac{\partial \Sigma_{H^0 H^0}(p^2)}{\partial p^2} \right]_{p^2=m_{H^0}^2},$	(4.134)
$\delta Z_{h^0 h^0} = -\text{Re} \left[\frac{\partial \Sigma_{h^0 h^0}(p^2)}{\partial p^2} \right]_{p^2=m_{h^0}^2},$	(4.135)
$\delta Z_{G^0 G^0} = -\text{Re} \left[\frac{\partial \Sigma_{G^0 G^0}(p^2)}{\partial p^2} \right]_{p^2=0},$	(4.136)
$\delta Z_{A^0 A^0} = -\text{Re} \left[\frac{\partial \Sigma_{A^0 A^0}(p^2)}{\partial p^2} \right]_{p^2=m_{A^0}^2},$	(4.137)
$\delta Z_{G^\pm G^\pm} = -\widetilde{\text{Re}} \left[\frac{\partial \Sigma_{G^\pm G^\pm}(p^2)}{\partial p^2} \right]_{p^2=0},$	(4.138)
$\delta Z_{H^\pm H^\pm} = -\widetilde{\text{Re}} \left[\frac{\partial \Sigma_{H^\pm H^\pm}(p^2)}{\partial p^2} \right]_{p^2=m_{H^\pm}^2}.$	(4.139)

The scalar wave function renormalization constants are in general explicitly gauge-dependent. The mass counterterms in the alternative tadpole scheme in Eqs. (4.130) – (4.133) are manifestly gauge-independent.

4.8. Renormalization of the Scalar Mixing Angles α and β

Until now, the renormalization of the parameters and fields of the Two-Higgs-Doublet Model was achieved entirely through the on-shell scheme, enabling us to provide physical masses as sensible input parameters. If we choose to perform the rotation from the gauge to the mass basis of the fields in the tree-level 2HDM potential of Sec. 2.4 before turning to higher-order calculations, it is necessary to renormalize α and β in the sense of mixing angles, as well.

Another choice would be to first renormalize and then rotate to the gauge basis. In that case, the angles α and β do not appear in the sense of mixing angles, but rather as functions of the parameters of the 2HDM potential. Therefore, they are only renormalized as such, but not in the sense of angles that diagonalize the mass matrices of the scalar doublets. While the latter approach is perfectly valid and possible within the 2HDM, we choose to perform the renormalization after rotating to the mass eigenstates of the scalar fields. Hence, the scalar mixing angles are split up at next-to-leading order according to

$$\alpha_0 = \alpha + \delta\alpha, \quad (4.140)$$

$$\beta_0 = \beta + \delta\beta. \quad (4.141)$$

The renormalization of the scalar mixing angles is a subtle task within the 2HDM. In contrast to the masses, the angles are not considered as physical parameters in a sense that they can be directly observed. Consequently, there is no suitable way of fixing them with the help of physical observables, as it was done in the on-shell renormalization procedure of Sec. 4.3. Due to the renormalizability of the Two-Higgs-Doublet Model, the UV-divergent parts of $\delta\alpha$ and $\delta\beta$ necessarily have to be the same for all schemes. However, the UV-finite parts may differ between the schemes, and due to the choice of an unsuitable scheme, it is possible

to introduce additional gauge-dependences into the UV-finite parts. In the following, we will present different renormalization schemes for the scalar mixing angles, and discuss the gauge-dependence that is introduced through them in the one-loop amplitudes.

4.8.1. Minimal Subtraction Scheme

Among the most intuitive schemes for renormalizing the scalar mixing angles is the *minimal subtraction* (MS) scheme [89]. It relies on the fact that in dimensional regularization, divergences of one-loop integrals appear explicitly as poles in the regulator ε , cf. Sec. 4.2. In any one-loop amplitude, where apart from the angle counterterms, all fields strength renormalization constants and physical counterterms are fixed, the angle counterterms are determined such that they exactly cancel the residual divergence in the amplitude.

The *modified minimal subtraction* ($\overline{\text{MS}}$) scheme is a more widely implemented adoption of the MS scheme. Within the $\overline{\text{MS}}$ scheme, the counterterms are chosen such that they cancel the residual Δ term of the amplitude, with Δ being defined in Eq. (4.4). Therefore, the counterterms do not only cancel the pole, but additionally some finite constants which appear universally in all one-loop integrals [90].

The $\overline{\text{MS}}$ scheme is per definition a suitable scheme for achieving an overall UV-finite decay amplitude at higher-order calculations. However, it has been shown in a previous work [91] that within the 2HDM, the application of the scheme to the scalar mixing angles leads to one-loop corrections to partial decay widths which are orders of magnitude higher than in other schemes. It has been checked explicitly that this happens for a large set of possible 2HDM parameters. The reason behind this is that in general, the wave function renormalization constants introduce large finite contributions to the one-loop amplitude, which need to be cancelled by the finite parts of the angle counterterms. However, the latter are set to zero in the $\overline{\text{MS}}$ scheme, thus preventing the cancellation [91]. Additionally, the angle counterterms might contain an explicit gauge-dependence, according to whether the residual amplitude (i.e. the amplitude without the angle counterterms) contains a gauge-dependence that needs to be cancelled or not. Since the $\overline{\text{MS}}$ scheme is potentially gauge-dependent as well as numerically unstable in most cases, it will not be used in this thesis as a renormalization scheme for the mixing angles.

4.8.2. Kanemura's Scheme

One idea of defining the angle counterterms was formulated by S. Kanemura *et al.* [56, 85], which we refer to as *Kanemura's scheme*. It enables the derivation of the angle counterterms by connecting the usual OS conditions of the scalar fields with the internal relations between the gauge and mass basis of the 2HDM.

Consider the scalar doublet (ϕ_1, ϕ_2) in the mass basis, which is connected with its gauge basis $(\tilde{\phi}_1, \tilde{\phi}_2)$ through the rotation matrix R_{θ}^T with mixing angle θ (cf. Eq. (2.22)). At next-to-leading order, the approximation

$$R_{\theta,0}^T \approx R_{\delta\theta}^T R_{\theta}^T \quad (4.142)$$

is valid. By temporarily switching between the two bases, the NLO expansion yields [56, 91]:

$$\begin{pmatrix} \phi_1 \\ \phi_2 \end{pmatrix}_0 = R_{\theta,0}^T \begin{pmatrix} \tilde{\phi}_1 \\ \tilde{\phi}_2 \end{pmatrix}_0 \approx R_{\delta\theta}^T R_{\theta}^T \sqrt{Z_{\tilde{\phi}}} R_{\theta} R_{\theta}^T \begin{pmatrix} \tilde{\phi}_1 \\ \tilde{\phi}_2 \end{pmatrix} \equiv \sqrt{Z_{\phi}^{\text{Kan}}} \begin{pmatrix} \phi_1 \\ \phi_2 \end{pmatrix}, \quad (4.143)$$

where the matrix $\sqrt{Z_{\phi}^{\text{Kan}}}$ connects the bare and renormalized fields in the mass basis. The field strength renormalization matrix of the scalar fields in the gauge basis, $\sqrt{Z_{\tilde{\phi}}}$, is considered

to be a real symmetric matrix, therefore containing three free parameters for each scalar doublet at NLO that need to be fixed through renormalization conditions. Alternatively, the Kanemura field strength renormalization matrix $\sqrt{Z_\phi^{\text{Kan}}}$ can be considered, which is defined through Eq. (4.143) as an NLO expansion [56, 91]:

$$\begin{aligned} \sqrt{Z_\phi^{\text{Kan}}} &\approx R_{\delta\theta}^T R_\theta^T \sqrt{Z_\phi} R_\theta = R_{\delta\theta}^T \begin{pmatrix} 1 + \frac{\delta Z_{\phi_1\phi_1}}{2} & \delta C_{\phi_2} \\ \delta C_{\phi_2} & 1 + \frac{\delta Z_{\phi_2\phi_2}}{2} \end{pmatrix} \\ &\approx \begin{pmatrix} 1 + \frac{\delta Z_{\phi_1\phi_1}}{2} & \delta C_{\phi_2} + \delta\theta \\ \delta C_{\phi_2} - \delta\theta & 1 + \frac{\delta Z_{\phi_2\phi_2}}{2} \end{pmatrix}. \end{aligned} \quad (4.144)$$

The wave function renormalization matrix $\sqrt{Z_\phi}$ has been rotated to the mass basis, so that $\sqrt{Z_\phi^{\text{Kan}}}$ contains the three free parameters $\delta Z_{\phi_1\phi_1}$, $\delta Z_{\phi_2\phi_2}$ and δC_{ϕ_2} that need to be fixed through renormalization conditions, together with the counterterm $\delta\theta$ of the mixing angle. For the scalar fields of the 2HDM, this translates to the following explicit forms of the field strength renormalization:

$$\begin{pmatrix} H^0 \\ h^0 \end{pmatrix}_0 = \begin{pmatrix} 1 + \frac{\delta Z_{H^0 H^0}}{2} & \delta C_{h^0} + \delta\alpha \\ \delta C_{h^0} - \delta\alpha & 1 + \frac{\delta Z_{h^0 h^0}}{2} \end{pmatrix} \begin{pmatrix} H^0 \\ h^0 \end{pmatrix}, \quad (4.145)$$

$$\begin{pmatrix} G^0 \\ A^0 \end{pmatrix}_0 = \begin{pmatrix} 1 + \frac{\delta Z_{G^0 G^0}}{2} & \delta C_{A^0} + \delta\beta \\ \delta C_{A^0} - \delta\beta & 1 + \frac{\delta Z_{A^0 A^0}}{2} \end{pmatrix} \begin{pmatrix} G^0 \\ A^0 \end{pmatrix}, \quad (4.146)$$

$$\begin{pmatrix} G^\pm \\ H^\pm \end{pmatrix}_0 = \begin{pmatrix} 1 + \frac{\delta Z_{G^\pm G^\pm}}{2} & \delta C_{H^\pm} + \delta\beta \\ \delta C_{H^\pm} - \delta\beta & 1 + \frac{\delta Z_{H^\pm H^\pm}}{2} \end{pmatrix} \begin{pmatrix} G^\pm \\ H^\pm \end{pmatrix}. \quad (4.147)$$

In order to remain within the framework of on-shell renormalization as much as possible, the diagonal field strength renormalization constants can be fixed via the pole conditions from Eq. (4.23). This leads to the same form of these constants as given in Eqs. (4.134) – (4.139), all of which are explicitly tadpole-invariant.

The other counterterms appearing in the off-diagonal matrix elements can be fixed by demanding the field mixing to vanish on the mass shell, which is equivalent to identifying the off-diagonal elements of the Kanemura field renormalization matrix with the ones from Eq. (4.13). For the CP-even sector, this leads to the identities [56, 91]

$$\frac{\delta Z_{H^0 h^0}}{2} \stackrel{!}{=} \delta C_{h^0} + \delta\alpha, \quad \frac{\delta Z_{h^0 H^0}}{2} \stackrel{!}{=} \delta C_{h^0} - \delta\alpha, \quad (4.148)$$

where $\delta Z_{H^0 h^0}$ and $\delta Z_{h^0 H^0}$ are the tadpole-dependent field strength renormalization constants given in Eqs. (4.114) and (4.115) or Eqs. (4.124) and (4.125), depending on the tadpole scheme that is chosen. The two equations allow to solve for δC_{h^0} , which is not present in any one-loop calculation and may therefore be omitted, and the angle counterterm $\delta\alpha$.

For the CP-odd and charged sector, Kanemura's scheme requires fixing three free parameters δC_{A^0} , δC_{H^\pm} and $\delta\beta$, since both sectors are diagonalized by the same mixing angle. The amount of free parameters in the off-diagonal parts of Eqs. (4.112) and (4.113) for the CP-odd and charged sector is four, however. If we choose to apply the on-shell renormalization

conditions to the CP-odd and charged sectors, it is necessary to choose which off-diagonal two-point correlation functions shall vanish, since not all CP-odd and charged fields can be on-shell at the same time. Out of four possible options, the same two as in [91] are chosen. Which of the definitions is used within the renormalization of a decay process depends on the external CP-odd or charged particles that are present in the considered process and that hence shall be renormalized OS. In summary, the angle counterterms in Kanemura's scheme are given by:

Standard tadpole scheme

$$\delta\alpha = \frac{1}{2(m_{H^0}^2 - m_{h^0}^2)} \text{Re} \left[\Sigma_{H^0 h^0}(m_{H^0}^2) + \Sigma_{H^0 h^0}(m_{h^0}^2) - 2\delta T_{H^0 h^0} \right], \quad (4.149)$$

$$\delta\beta^{(1)} = -\frac{1}{2m_{A^0}^2} \text{Re} \left[\Sigma_{G^0 A^0}(m_{A^0}^2) + \Sigma_{G^0 A^0}(0) - 2\delta T_{G^0 A^0} \right], \quad (4.150)$$

$$\delta\beta^{(2)} = -\frac{1}{2m_{H^\pm}^2} \text{Re} \left[\Sigma_{G^\pm H^\pm}(m_{H^\pm}^2) + \Sigma_{G^\pm H^\pm}(0) - 2\delta T_{G^\pm H^\pm} \right]. \quad (4.151)$$

Alternative tadpole scheme

$$\delta\alpha = \frac{1}{2(m_{H^0}^2 - m_{h^0}^2)} \text{Re} \left[\Sigma_{H^0 h^0}^{\text{tad}}(m_{H^0}^2) + \Sigma_{H^0 h^0}^{\text{tad}}(m_{h^0}^2) \right], \quad (4.152)$$

$$\delta\beta^{(1)} = -\frac{1}{2m_{A^0}^2} \text{Re} \left[\Sigma_{G^0 A^0}^{\text{tad}}(m_{A^0}^2) + \Sigma_{G^0 A^0}^{\text{tad}}(0) \right], \quad (4.153)$$

$$\delta\beta^{(2)} = -\frac{1}{2m_{H^\pm}^2} \text{Re} \left[\Sigma_{G^\pm H^\pm}^{\text{tad}}(m_{H^\pm}^2) + \Sigma_{G^\pm H^\pm}^{\text{tad}}(0) \right]. \quad (4.154)$$

Among the considered processes in this thesis in Chapter 5 to Chapter 7, only one contains an external H^+ particle, while all other processes do not contain external CP-odd or charged Higgs bosons in the initial or final state. Therefore, we choose the charged fields to be completely on-shell, which results in the usage of $\delta\beta^{(2)}$ in this thesis.

The angle counterterms defined according to Kanemura's scheme are explicitly gauge-dependent, both for the standard as well as the alternative tadpole scheme. If we use the notation of Eq. (C.8) and Eq. (C.9) for the reduced scalar integrals, one way of presenting the gauge-dependence¹⁰ of $\delta\beta^{(2)}$ is

$$\begin{aligned} \delta\beta^{(2)} &= \delta\beta^{(2)} \Big|_{\xi=1} \\ &+ (1 - \xi_W) \frac{g^2 c_{\beta-\alpha} s_{\beta-\alpha}}{128\pi^2} \left\{ m_{h^0}^2 \left[\beta_{Wh^0}(m_{H^\pm}^2) - \beta_{Wh^0}(0) \right] \right. \\ &\left. + m_{H^\pm}^2 \left[\beta_{WH^0}(m_{H^\pm}^2) - \beta_{Wh^0}(m_{H^\pm}^2) \right] + m_{H^0}^2 \left[\beta_{WH^0}(0) - \beta_{WH^0}(m_{H^\pm}^2) \right] \right\}, \end{aligned} \quad (4.155)$$

where the short-hand notation $\xi \in \{\xi_W, \xi_Z, \xi_\gamma\}$ is used here and in the following. The form of the gauge-dependence is independent of the tadpole scheme that is chosen. Due to the structure of the integrals in the second and third line of Eq. (4.155), the gauge-dependent part is UV-finite by itself. Therefore, Kanemura's scheme introduces a gauge-dependence through $\delta\beta^{(2)}$ in the UV-finite part of the amplitude only.

¹⁰The decomposition into gauge-dependent and -independent parts is not unique. Therefore, the presented form is only one of many possible ways of isolating the gauge-dependence.

For $\delta\alpha$, the gauge-dependence is more intricate and depends on the chosen tadpole scheme. In the standard tadpole scheme, the gauge-dependent parts can be isolated in the form

$$\begin{aligned}
\delta\alpha^{\text{sta}} &= \delta\alpha^{\text{sta}} \Big|_{\xi=1} \\
&- (1 - \xi_W) \frac{\Lambda_5 m_W^2 c_{\beta-\alpha} s_{\beta-\alpha}}{16\pi^2 (m_{H^0}^2 - m_{h^0}^2)} \alpha_W - (1 - \xi_Z) \frac{\Lambda_5 m_Z^2 c_{\beta-\alpha} s_{\beta-\alpha}}{32\pi^2 (m_{H^0}^2 - m_{h^0}^2)} \alpha_Z \\
&+ (1 - \xi_Z) \frac{g^2 c_{\beta-\alpha} s_{\beta-\alpha}}{256\pi^2 c_W^2} \left\{ 2m_{A^0}^2 \left[\beta_{ZA^0}(m_{H^0}^2) - \beta_{ZA^0}(m_{h^0}^2) \right] \right. \\
&\quad \left. + m_{H^0}^2 \left[\beta_{Z\xi Z}(m_{H^0}^2) - 2\beta_{ZA^0}(m_{H^0}^2) \right] - m_{h^0}^2 \left[\beta_{Z\xi Z}(m_{h^0}^2) - 2\beta_{ZA^0}(m_{h^0}^2) \right] \right\} \quad (4.156) \\
&+ (1 - \xi_W) \frac{g^2 c_{\beta-\alpha} s_{\beta-\alpha}}{128\pi^2} \left\{ 2m_{H^\pm}^2 \left[\beta_{WH^\pm}(m_{H^0}^2) - \beta_{WH^\pm}(m_{h^0}^2) \right] \right. \\
&\quad \left. + m_{H^0}^2 \left[\beta_{W\xi W}(m_{H^0}^2) - 2\beta_{WH^\pm}(m_{H^0}^2) \right] - m_{h^0}^2 \left[\beta_{W\xi W}(m_{h^0}^2) - 2\beta_{WH^\pm}(m_{h^0}^2) \right] \right\},
\end{aligned}$$

where the superscript ‘‘sta’’ indicates the standard tadpole scheme. When changing from the standard to the alternative tadpole scheme, the gauge-dependence reduces to

$$\begin{aligned}
\delta\alpha^{\text{alt}} &= \delta\alpha^{\text{alt}} \Big|_{\xi=1} \\
&+ (1 - \xi_Z) \frac{g^2 c_{\beta-\alpha} s_{\beta-\alpha}}{256\pi^2 c_W^2} \left\{ 2m_{A^0}^2 \left[\beta_{ZA^0}(m_{H^0}^2) - \beta_{ZA^0}(m_{h^0}^2) \right] \right. \\
&\quad \left. + m_{H^0}^2 \left[\beta_{Z\xi Z}(m_{H^0}^2) - 2\beta_{ZA^0}(m_{H^0}^2) \right] - m_{h^0}^2 \left[\beta_{Z\xi Z}(m_{h^0}^2) - 2\beta_{ZA^0}(m_{h^0}^2) \right] \right\} \quad (4.157) \\
&+ (1 - \xi_W) \frac{g^2 c_{\beta-\alpha} s_{\beta-\alpha}}{128\pi^2} \left\{ 2m_{H^\pm}^2 \left[\beta_{WH^\pm}(m_{H^0}^2) - \beta_{WH^\pm}(m_{h^0}^2) \right] \right. \\
&\quad \left. + m_{H^0}^2 \left[\beta_{W\xi W}(m_{H^0}^2) - 2\beta_{WH^\pm}(m_{H^0}^2) \right] - m_{h^0}^2 \left[\beta_{W\xi W}(m_{h^0}^2) - 2\beta_{WH^\pm}(m_{h^0}^2) \right] \right\},
\end{aligned}$$

where the superscript ‘‘alt’’ now indicates $\delta\alpha$ in the alternative tadpole scheme. Compared to the standard tadpole scheme, the second line in Eq. (4.156) is cancelled by the shift of the vevs.

The explicit appearance of gauge-dependent terms in the angle counterterms threatens the necessary gauge-independence of the one-loop amplitude. In the processes that are considered in this thesis, the gauge-dependence in the angle counterterms as defined in Kanemura’s scheme will not cancel completely, as we will see e.g. in Sec. 5.4. Consequently, the angle counterterms in Kanemura’s scheme are not only explicitly gauge-dependent by themselves, but additionally, they lead to a gauge-dependent one-loop partial decay width.

A later paper [85] proposes a way to remove the gauge-dependence from the angle counterterms¹¹. The condition that the field strength renormalization matrix $\sqrt{Z_{\tilde{\phi}}}$ introduced in Eq. (4.143) is symmetric is omitted. This increases the number of free parameters in the Kanemura field strength renormalization matrix of Eq. (4.144), effectively leading to two different off-diagonal renormalization constants δC_{ϕ_1} and δC_{ϕ_2} .

In [85], it is suggested to use the additional degree of freedom to define $\delta\beta$ in such a way that it contains only the gauge-independent parts. All gauge-dependent parts are shifted into the two constants δC_{ϕ_1} and δC_{ϕ_2} which do not appear in any one-loop calculation and are thus not observable. A look at Eq. (4.155) shows that this approach would in principle work,

¹¹This paper discusses the gauge-dependence of $\delta\beta$, only.

since all gauge-dependent parts of $\delta\beta$ form a UV-finite subset, and can thus be removed from the angle counterterm. However, the isolation of the gauge-dependent parts is not unique and [85] presents no unambiguous way of defining what parts should be contained in $\delta\beta$ and what parts are shifted into δC_{ϕ_1} and δC_{ϕ_2} .

An even more serious problem arises when trying to apply this approach to the angle counterterm $\delta\alpha$. The second line of Eq. (4.156) contains integrals that are UV-divergent by themselves. Therefore, the gauge-dependent parts of $\delta\alpha$ in the standard tadpole scheme are UV-divergent. Due to the renormalizability of the 2HDM, these UV-divergent terms have to appear in any other renormalization scheme of $\delta\alpha$, as well. Defining these UV-divergent parts into the unobservable counterterms δC_{ϕ_1} and δC_{ϕ_2} , which are not part of any one-loop calculation, thus inevitably leads to an overall UV-divergent one-loop amplitude. Therefore, the approach to remove the gauge-dependence of the angle counterterms presented in [85] cannot be applied to $\delta\alpha$ in the standard tadpole scheme. In the alternative tadpole scheme, it is possible to remove the gauge-dependence from $\delta\alpha$, since all integrals from the second to the last line of Eq. (4.157) are UV-finite. However, the same problem as in $\delta\beta$ remains, namely that the division of gauge-dependent and -independent parts is ambiguous.

4.8.3. Pinched Scheme

Eradicating the deficiencies of Kanemura's scheme is equivalent to using a renormalization scheme that leads to an overall UV-finite and gauge-independent one-loop amplitude on the one hand and stating an unambiguous definition of the gauge-independent parts of the angle counterterms on the other hand. This can be achieved by using the *pinched scheme* which is based on the pinch technique (PT) [92–97]. A short introduction to the PT is presented in App. B.

In [98], the sfermion mixing angle counterterm $\delta\theta$ was defined through the requirement of a gauge-independent residuum in a one-loop scattering amplitude of sfermions and Z^0 bosons within the MSSM, which is analogous to the argumentation presented in [99]. In [100], $\delta\theta$ is defined in a completely different approach by use of the pinch technique. However, both schemes lead to the same form of the sfermion mixing angle counterterm, indicating the equivalence of both approaches within the MSSM. Additionally, a method for the definition of the CP-even mixing angle counterterm $\delta\alpha$ within the MSSM is presented in [100] with the help of the PT.

Since the PT has been analyzed thoroughly in the SM [93, 94] and in the MSSM [100], we want to use it to derive an unambiguous gauge-independent definition of the scalar mixing angle counterterms. In order to keep the discussion clear, we will present the application of the PT within the 2HDM in App. C. In this subsection, we will only use the results of this discussion for a definition of the angle counterterms over the pinched self-energies.

The main idea of the pinched scheme is to improve the definition of the angle counterterms in Kanemura's scheme by using the pinched self-energies of the scalar sector instead of the self-energies Σ^{tad} in the tadpole scheme. In general, the pinched self-energies of the scalar doublet (ϕ_1, ϕ_2) have the form

$$\Sigma_{\phi_1\phi_2}^{\text{pinch}}(p^2) = \left[\Sigma_{\phi_1\phi_2}^{\text{tad}}(p^2) \right]_{\xi=1} + \Sigma_{\phi_1\phi_2}^{\text{add}}(p^2), \quad (4.158)$$

where the superscript “add” denotes additional terms whose explicit forms depend on the scalar doublets that are chosen. The proper derivation of the pinched self-energies requires self-energy contributions from all topologies shown in Fig. 4.4, cf. App. C. Therefore, the PT is only consistent in a scheme which uses the alternative tadpole renormalization of Sec. 4.4.2, but not the standard tadpole scheme [93].

The explicit form of the additional terms for the CP-even, CP-odd and charged off-diagonal self-energies, which are needed for the definitions of $\delta\alpha$ and $\delta\beta$, read

$$\begin{aligned} \Sigma_{H^0 h^0}^{\text{add}}(p^2) &= \frac{g^2 s_{\beta-\alpha} c_{\beta-\alpha}}{32\pi^2 c_W^2} \left(p^2 - \frac{m_{H^0}^2 + m_{h^0}^2}{2} \right) \left\{ [B_0(p^2; m_Z^2, m_{A^0}^2) - B_0(p^2; m_Z^2, m_Z^2)] \right. \\ &\quad \left. + 2c_W^2 [B_0(p^2; m_W^2, m_{H^\pm}^2) - B_0(p^2; m_W^2, m_W^2)] \right\}, \end{aligned} \quad (4.159)$$

$$\Sigma_{G^0 A^0}^{\text{add}}(p^2) = \frac{g^2 s_{\beta-\alpha} c_{\beta-\alpha}}{32\pi^2 c_W^2} \left(p^2 - \frac{m_{A^0}^2}{2} \right) [B_0(p^2; m_Z^2, m_{H^0}^2) - B_0(p^2; m_Z^2, m_{h^0}^2)], \quad (4.160)$$

$$\Sigma_{G^\pm H^\pm}^{\text{add}}(p^2) = \frac{g^2 s_{\beta-\alpha} c_{\beta-\alpha}}{16\pi^2} \left(p^2 - \frac{m_{H^\pm}^2}{2} \right) [B_0(p^2; m_W^2, m_{H^0}^2) - B_0(p^2; m_W^2, m_{h^0}^2)]. \quad (4.161)$$

The only freedom in the definition of the angle counterterms through the PT arises in the choice of scale at which the self-energies are evaluated, which is nothing else than the definition of what finite parts the angle counterterms will contain. If one sticks to the on-shell approach, a suitable scale would be the masses of the scalar bosons. We will refer to this scheme as *OS-pinched* scheme. A look at the momentum dependence of the additional terms in Eqs. (4.159) – (4.161) suggests another scale, namely

$$p_*^2 = \frac{m_{\phi_1}^2 + m_{\phi_2}^2}{2}. \quad (4.162)$$

This sum of mass squares scale is especially convenient, since all additional terms vanish at $p^2 = p_*^2$. In reference to [100], we refer to this choice of scale as the p_* -*pinched* scheme. In summary, the angle counterterms for both schemes explicitly read:

Alternative tadpole scheme, OS-pinched

$$\delta\alpha = \frac{\text{Re} \left[[\Sigma_{H^0 h^0}^{\text{tad}}(m_{H^0}^2) + \Sigma_{H^0 h^0}^{\text{tad}}(m_{h^0}^2)]_{\xi=1} + \Sigma_{H^0 h^0}^{\text{add}}(m_{H^0}^2) + \Sigma_{H^0 h^0}^{\text{add}}(m_{h^0}^2) \right]}{2(m_{H^0}^2 - m_{h^0}^2)}, \quad (4.163)$$

$$\delta\beta^{(1)} = - \frac{\text{Re} \left[[\Sigma_{G^0 A^0}^{\text{tad}}(m_{A^0}^2) + \Sigma_{G^0 A^0}^{\text{tad}}(0)]_{\xi=1} + \Sigma_{G^0 A^0}^{\text{add}}(m_{A^0}^2) + \Sigma_{G^0 A^0}^{\text{add}}(0) \right]}{2m_{A^0}^2}, \quad (4.164)$$

$$\delta\beta^{(2)} = - \frac{\text{Re} \left[[\Sigma_{G^\pm H^\pm}^{\text{tad}}(m_{H^\pm}^2) + \Sigma_{G^\pm H^\pm}^{\text{tad}}(0)]_{\xi=1} + \Sigma_{G^\pm H^\pm}^{\text{add}}(m_{H^\pm}^2) + \Sigma_{G^\pm H^\pm}^{\text{add}}(0) \right]}{2m_{H^\pm}^2}. \quad (4.165)$$

Alternative tadpole scheme, p_* -pinched

$$\delta\alpha = \frac{1}{m_{H^0}^2 - m_{h^0}^2} \text{Re} \left[\Sigma_{H^0 h^0}^{\text{tad}} \left(\frac{m_{H^0}^2 + m_{h^0}^2}{2} \right) \right]_{\xi=1}, \quad (4.166)$$

$$\delta\beta^{(1)} = - \frac{1}{m_{A^0}^2} \text{Re} \left[\Sigma_{G^0 A^0}^{\text{tad}} \left(\frac{m_{A^0}^2}{2} \right) \right]_{\xi=1}, \quad (4.167)$$

$$\delta\beta^{(2)} = - \frac{1}{m_{H^\pm}^2} \text{Re} \left[\Sigma_{G^\pm H^\pm}^{\text{tad}} \left(\frac{m_{H^\pm}^2}{2} \right) \right]_{\xi=1}. \quad (4.168)$$

The angle counterterms in the pinched schemes are per construction manifestly gauge-independent, although a look at Eqs. (4.163) – (4.168) might suggest the opposite, since the

Feynman-'t Hooft gauge is emphasized in the definition of the angle counterterms. This however is a direct result of the application of the PT. In App. C, it is discussed that the pinched self-energy is the result of adding all pinch parts to the usual self-energy Σ^{tad} calculated in general R_ξ gauge. The parts on the right-hand side of Eq. (4.158) are exactly the parts that remain *after* all gauge-dependences have been cancelled. In that sense, the emphasis of the Feynman-'t Hooft gauge is not a result of choosing a specific gauge, but rather the outcome of the cancellation of the gauge-dependences. Additionally, it shows the deep connection between the PT and the *background field method* (BFM) [101–104] for a specific choice of background-field gauge-fixing-parameters [93], cf. App. B.

The usage of the PT for the calculation of S -matrix elements has been discussed and criticized [105, 106]. The major points of criticism include that

- the extension of the PT from one-loop to higher orders is neither unique nor trivial,
- the process-independence of the PT is not generally proven, but only shown for specific examples,
- the PT is not generally applicable to all possible one-loop Green's functions,
- the PT is technically involved.

The aforementioned papers suggest to use the BFM instead of the PT in order to avoid these problems from the start, since the BFM is by construction applicable to all orders of perturbation theory. Additionally, it serves as a generalization of the PT and delivers an infinite set of possible vertex functions fulfilling QED-like Ward identities [105]. Since this criticism affects our choice of using the pinched schemes for renormalizing the scalar mixing angles, we want to discuss the points mentioned above.

Within the scope of this thesis, we deal with the gauge-independent renormalization of the angle counterterms only at the one-loop level. While the extension of the PT to the two-loop level and above is of no interest for us, it should be mentioned that the PT has been applied not only at two-loop level for the SM [107], but an unambiguous generalization to all orders of perturbation theory in the electroweak sector for the SM has been presented, as well [93, 108].

The process-independence of the PT is indeed not proven in general, which has to be accepted as one of the major weak points when using the technique. While the gauge-independence of the pinched self-energies is ensured by the BRST symmetry [93], a process-dependence of the PT might result in different forms of the additional gauge-independent terms presented in Eqs. (4.159) – (4.161). However, the PT was applied to a variety of different toy processes, so far yielding a universal result [109]. As a consequence, the process-independence of the PT is postulated until falsified with a suitable counter-example.

Lastly, the PT is indeed technically involved even at the one-loop level, especially when dealing with the CP-odd and charged scalar sector of the 2HDM, but nevertheless, it is possible to unambiguously derive the pinched scalar self-energies, as presented in App. C. While the PT might not be suitable for deriving all possible gauge-invariant Green's functions, it is applicable to the scalar sector of the 2HDM. In conclusion, the PT can be used for an unambiguous manifestly gauge-independent definition of the mixing angle counterterms at the one-loop level.

It should be mentioned that the BFM has some drawbacks on its own. If one considers the calculation of current correlation functions or Wilson loops, the BFM cannot be applied [93]. The PT on the other hand is suitable for such calculations and delivers unambiguous results [95, 110].

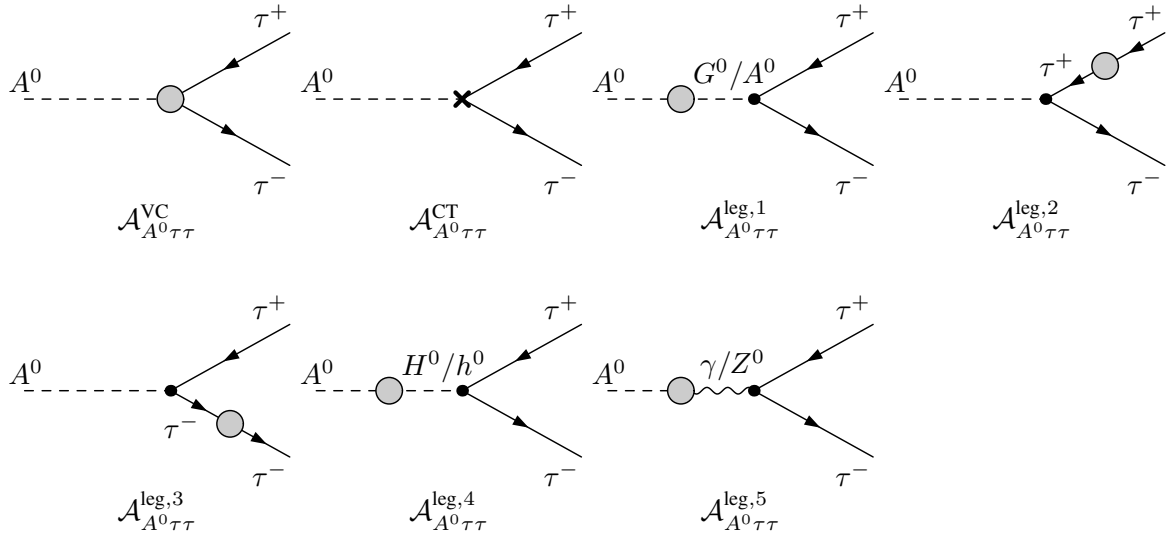


Figure 4.5.: NLO virtual corrections to the decays $A^0 \rightarrow \tau^+ \tau^-$. The one-loop amplitude $\mathcal{A}_{A^0\tau\tau}^{\text{1loop}}$ consists of all virtual vertex corrections $\mathcal{A}_{A^0\tau\tau}^{\text{VC}}$, the vertex counterterm $\mathcal{A}_{A^0\tau\tau}^{\text{CT}}$ as well as the external leg corrections $\mathcal{A}_{A^0\tau\tau}^{\text{leg},i}$ ($i = 1, \dots, 5$).

Additionally, while the BFM provides n -point functions that are manifestly gauge-invariant (i.e. they fulfill tree-level-like Ward identities), they are still gauge-dependent, since the n -point functions contain an explicit dependence on the background-field gauge-fixing-parameter. In theories with spontaneous symmetry breaking, this dependence induces unphysical thresholds in the BFM Green's functions for any other background-field gauge than the Feynman-'t Hooft gauge. But in this gauge, the BFM Green's functions usually coincide with the PT Green's functions [93].

As a conclusion, the PT and the BFM should not be considered as two rivaling approaches of defining gauge-invariant Green's functions, but rather as complementary tools. If the PT Green's functions coincide with the BFM Green's functions for the Feynman-'t Hooft gauge of the background-fields, which has to be checked explicitly for any possible Green's function [93], then the PT automatically adopts all desirable properties of the BFM Green's functions, e.g. process-independence and gauge-invariance, since these properties are independent of the choice of the gauge-fixing-parameter within the BFM framework [106]. The connection between the Green's functions in the PT and the BFM has been analyzed in detail in QCD [111], in the electroweak theory of the SM [93, 97] and in the MSSM [100, 112].

4.8.4. Process-Dependent Scheme

The last renormalization scheme of the scalar mixing angles presented in the scope of this thesis is a process-dependent scheme. The main motivation for such a renormalization scheme is the fact that the definition of the mixing angles over a process allows for a more physical interpretation of the otherwise unphysical (i.e. unobservable) mixing angles. In this sense, the process-dependent scheme is analogous to the renormalization of the electric charge in the Thomson limit in Sec. 4.5.

Within the MSSM, a definition of the angle counterterm $\delta\beta$ via the process $H^+ \rightarrow \tau^+ \nu_\tau$ was proposed in order to decouple the definition of the counterterm from the vevs of the scalar potential [113]. However, this process has the disadvantage of containing IR divergences which need to be combined with real corrections in order to gain an IR-finite result. Due to the tight connection of the process with the underlying $SU(2)_L$ symmetry, the IR-divergent and UV-divergent parts of the one-loop amplitude are intertwined. Thus, the definition of the

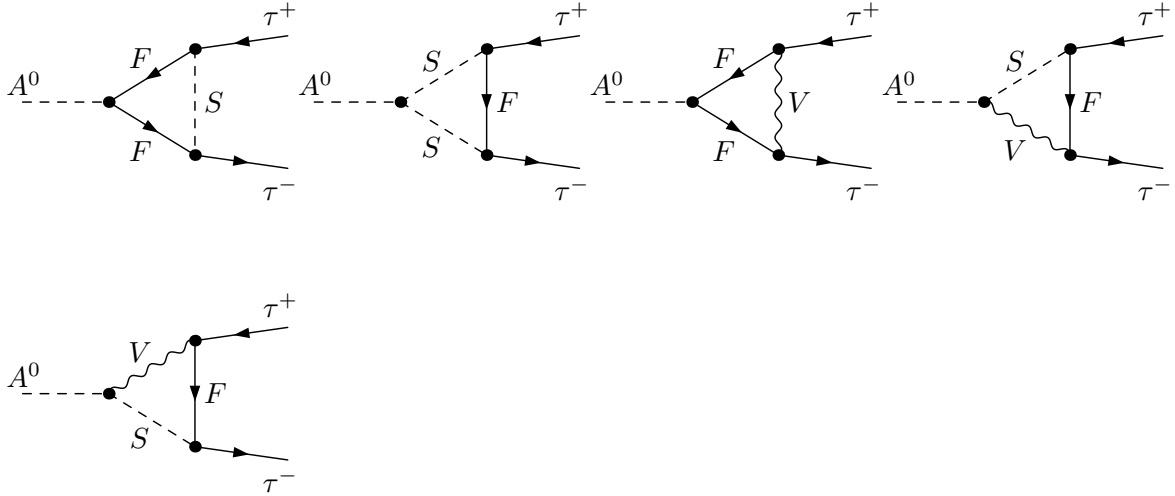


Figure 4.6.: All NLO vertex corrections to the decays $A^0 \rightarrow \tau^+ \tau^-$. All virtual vertex corrections $\mathcal{A}_{A^0\tau^+\tau^-}^{\text{VC}}$ are shown, grouped by their topological structure. The diagrams contain contributions from fermions F , scalar bosons S and gauge bosons V . Diagrams involving an internal photon contain IR divergences.

angle counterterm $\delta\beta$ over this process will contain IR-divergent parts. As a consequence, $\delta\beta$ will depend on experimental cuts on the phase-space of the real photon emissions, cf. Sec. 5.3, which is unacceptable [36].

In the 2HDM, the process $H^+ \rightarrow W^+ H^0$ was used as a process-dependent definition of the combination of mixing angle counterterms $\delta(\beta - \alpha)$ in the approximation of heavy top and bottom quarks [114]. While such a scheme works fine as long as the one-loop vertex corrections contain only the top and bottom quarks, it introduces the same difficulty as the process mentioned above as soon as the full electroweak vertex corrections are taken into account. In that case, the definition of $\delta(\beta - \alpha)$ would again necessarily contain IR-divergent parts.

What has instead been proposed in [36] is the definition of $\delta\beta$ over the process $A^0 \rightarrow \tau^+ \tau^-$. While in the paper the process is considered within the MSSM, we will adopt the scheme in order to renormalize $\delta\beta$ in the 2HDM. The process has the advantage that the QED corrections form a UV-finite subset by themselves. Since it is exactly the QED subset of the amplitude that contains the IR divergences, the idea is to isolate the purely weak corrections from the QED corrections and only use the former for the process-dependent definition of the angle counterterm.

We consider the on-shell process $A^0 \rightarrow \tau^+ \tau^-$. Using the generic notation of Chapter 3, we denote with $\bar{u}(p_3)$ the adjoint spinor of the outgoing τ^- with momentum p_3 and spin s_3 and with $v(p_2)$ the spinor of the outgoing τ^+ with momentum p_2 and spin s_2 . The LO decay amplitude is given by

$$\mathcal{A}_{A^0\tau\tau}^{\text{LO}} = \frac{iem_\tau Y_3}{2m_{WSW}} \bar{u}(p_3) \gamma^5 v(p_2) . \quad (4.169)$$

The factor Y_3 contains the Yukawa coupling as given in Sec. 8.2 whose specific form depends on the 2HDM type that is chosen. In order to calculate the LO partial decay width, we insert the LO amplitude into Eq. (3.3). The spin configuration of the fermions in the final state is of no interest for us, therefore, we use the spin sum [5]

$$\sum_{s_2, s_3} \bar{u}(p_3) \gamma^5 v(p_2) \bar{v}(p_2) (-\gamma^5) u(p_3) = \text{Tr} \left[-(\not{p}_2 - m_\tau) \gamma^5 (\not{p}_3 + m_\tau) \gamma^5 \right] = 2m_{A^0}^2 \quad (4.170)$$

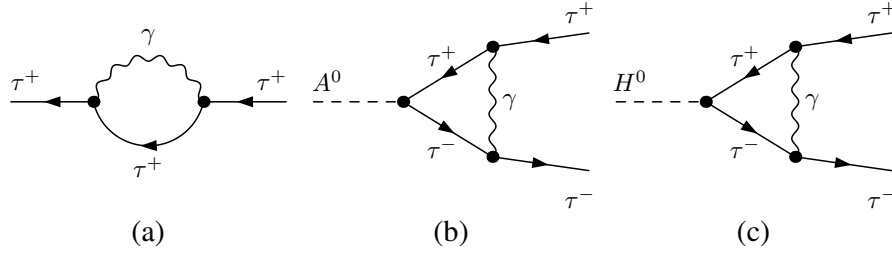


Figure 4.7.: Diagrammatic contributions to the UV-finite QED subset. Shown are all diagrams of the QED sector that have to be excluded in the process-dependent definition of the mixing angles. Diagram (a) appears in the definition of the counterterms δm_τ , $\delta Z_{\tau\tau}^L$ and $\delta Z_{\tau\tau}^R$, while (b) and (c) are parts of the vertex corrections $\mathcal{A}_{A^0\tau\tau}^{\text{1loop}}$ and $\mathcal{A}_{H^0\tau\tau}^{\text{1loop}}$, respectively.

to sum over all degrees of freedom. Inserting the LO amplitude into Eq. (3.7) and using this spin sum yields the LO partial decay width of the process $A^0 \rightarrow \tau^+ \tau^-$:

$$\Gamma_{A^0\tau\tau}^{\text{LO}} = \frac{g^2 Y_3^2 m_\tau^2 m_{A^0}}{32\pi m_W^2} \sqrt{1 - \frac{4m_\tau^2}{m_{A^0}^2}}. \quad (4.171)$$

At NLO, the one-loop amplitude consists of all virtual vertex corrections $\mathcal{A}_{A^0\tau\tau}^{\text{VC}}$, the vertex counterterm $\mathcal{A}_{A^0\tau\tau}^{\text{CT}}$ and all virtual external leg corrections $\mathcal{A}_{A^0\tau\tau}^{\text{leg},i}$ ($i = 1, \dots, 5$) as shown in Fig. 4.5. The first three external leg corrections vanish due to the on-shell renormalization conditions presented in Sec. 4.5 and Sec. 4.6. The fourth external leg corrections vanishes due to CP-conservation for the on-shell A^0 boson and the fifth correction vanishes because of a Slavnov-Taylor identity [115]. Hence, the one-loop amplitude consists of the virtual vertex corrections and the vertex counterterm. In both amplitudes, the LO amplitude of Eq. (4.169) factorizes out, yielding

$$\mathcal{A}_{A^0\tau\tau}^{\text{1loop}} = \mathcal{A}_{A^0\tau\tau}^{\text{VC}} + \mathcal{A}_{A^0\tau\tau}^{\text{CT}} = \mathcal{A}_{A^0\tau\tau}^{\text{LO}} [\mathcal{F}_{A^0\tau\tau}^{\text{VC}} + \mathcal{F}_{A^0\tau\tau}^{\text{CT}}]. \quad (4.172)$$

The form factor $\mathcal{F}_{A^0\tau\tau}^{\text{VC}}$ of the vertex corrections is determined by the sum of the diagrams shown in Fig. 4.6, while the form factor of the vertex counterterm has the explicit form [52, 79]

$$\mathcal{F}_{A^0\tau\tau}^{\text{CT}} = \frac{\delta g}{g} + \frac{\delta m_\tau}{m_\tau} - \frac{\delta m_W^2}{2m_W^2} + \frac{1 + Y_3^2}{Y_3} \delta\beta + \frac{\delta Z_{A^0 A^0}}{2} - \frac{1}{Y_3} \frac{\delta Z_{G^0 A^0}}{2} + \frac{\delta Z_{\tau\tau}^L}{2} + \frac{\delta Z_{\tau\tau}^R}{2}. \quad (4.173)$$

Note that we demand that both form factors contain contributions from the weak sector only [36], meaning that for the definition of the counterterms δm_τ , $\delta Z_{\tau\tau}^L$ and $\delta Z_{\tau\tau}^R$, the self-energy diagram of Fig. 4.7 (a) has to be excluded, while for the vertex corrections, the diagram of Fig. 4.7 (b) is omitted. The sum of these diagrams contains all IR divergences of the process and forms a UV-finite subset in Eq. (4.172), which has been checked analytically and numerically. Therefore, this subset can be omitted without spoiling the overall UV-finiteness of the process, thus removing all IR divergences from the amplitude.

Inserting the LO and one-loop amplitude into Eq. (3.12) yields the NLO partial decay width, which simplifies due to the fact that the LO amplitude factorizes completely:

$$\Gamma_{A^0\tau\tau}^{\text{NLO,weak}} = \Gamma_{A^0\tau\tau}^{\text{LO}} \left(1 + 2 \operatorname{Re} \left[\mathcal{F}_{A^0\tau\tau}^{\text{VC}} + \mathcal{F}_{A^0\tau\tau}^{\text{CT}} \right] \right). \quad (4.174)$$

The superscript “weak” indicates that the form factors contain contributions from the weak sector only, with all QED contributions being omitted. The counterterm $\delta\beta$ can be defined via the process by demanding that the one-loop contributions to the partial decay width shall vanish, so that

$$\Gamma_{A^0\tau\tau}^{\text{LO}} \stackrel{!}{=} \Gamma_{A^0\tau\tau}^{\text{NLO,weak}} \quad (4.175)$$

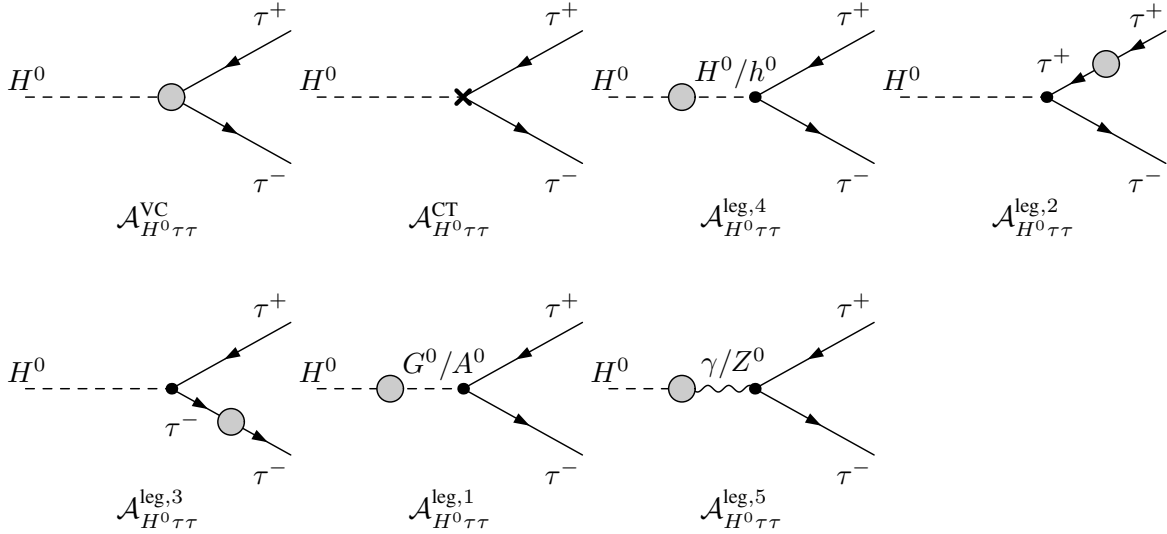


Figure 4.8.: NLO virtual corrections to the decays $H^0 \rightarrow \tau^+ \tau^-$. The one-loop amplitude $\mathcal{A}_{H^0\tau\tau}^{\text{1loop}}$ consists of all virtual vertex corrections $\mathcal{A}_{H^0\tau\tau}^{\text{VC}}$, the vertex counterterm $\mathcal{A}_{H^0\tau\tau}^{\text{CT}}$ as well as the external leg corrections $\mathcal{A}_{H^0\tau\tau}^{\text{leg},i}$ ($i = 1, \dots, 5$).

holds. Inserting Eqs. (4.173) and (4.174) into this renormalization condition allows us to solve for the angle counterterm:

$$\delta\beta = \frac{-Y_3}{1 + Y_3^2} \left[\mathcal{F}_{A^0\tau\tau}^{\text{VC}} + \frac{\delta g}{g} + \frac{\delta m_\tau}{m_\tau} - \frac{\delta m_W^2}{2m_W^2} + \frac{\delta Z_{A^0 A^0}}{2} - \frac{1}{Y_3} \frac{\delta Z_{G^0 A^0}}{2} + \frac{\delta Z_{\tau\tau}^{\text{L}}}{2} + \frac{\delta Z_{\tau\tau}^{\text{R}}}{2} \right]. \quad (4.176)$$

In contrast to the MSSM, where only the mixing angle β needs to be renormalized, the 2HDM requires an additional process in order to fix the angle counterterm $\delta\alpha$. Following the same arguments as above, we choose the decay $H^0 \rightarrow \tau^+ \tau^-$, since the QED contributions form a UV-finite subset in this process as well. The LO amplitude of the decay is given by

$$\mathcal{A}_{H^0\tau\tau}^{\text{LO}} = \frac{-em_\tau Y_2}{2m_W s_W} \bar{u}(p_3) v(p_2), \quad (4.177)$$

where Y_2 is the Yukawa coupling constant defined in Sec. 8.2. For the calculation of the LO partial decay width, we use the spin sum [5]

$$\sum_{s_2, s_3} \bar{u}(p_3) v(p_2) \bar{v}(p_2) u(p_3) = \text{Tr} \left[(\not{p}_2 - m_\tau)(\not{p}_3 + m_\tau) \right] = 2m_{H^0}^2 - 8m_\tau^2. \quad (4.178)$$

Inserting the LO amplitude into Eq. (3.7) and using the spin sum, the LO partial decay width explicitly reads

$$\Gamma_{H^0\tau\tau}^{\text{LO}} = \frac{g^2 Y_2^2 m_\tau^2 m_{H^0}}{32\pi m_W^2} \left(1 - \frac{4m_\tau^2}{m_{A^0}^2} \right)^{3/2}. \quad (4.179)$$

Analogous to the decay of the pseudoscalar Higgs boson A^0 , the one-loop amplitude of the process $H^0 \rightarrow \tau^+ \tau^-$ consists of the virtual vertex corrections, the vertex counterterm and virtual external leg corrections, all shown in Fig. 4.8. The latter vanish completely due to the same reasons as for the external leg corrections of the process $A^0 \rightarrow \tau^+ \tau^-$, and again, the LO amplitude factorizes from the vertex corrections as well as the counterterm, giving:

$$\mathcal{A}_{H^0\tau\tau}^{\text{1loop}} = \mathcal{A}_{H^0\tau\tau}^{\text{VC}} + \mathcal{A}_{H^0\tau\tau}^{\text{CT}} = \mathcal{A}_{H^0\tau\tau}^{\text{LO}} \left[\mathcal{F}_{H^0\tau\tau}^{\text{VC}} + \mathcal{F}_{H^0\tau\tau}^{\text{CT}} \right]. \quad (4.180)$$

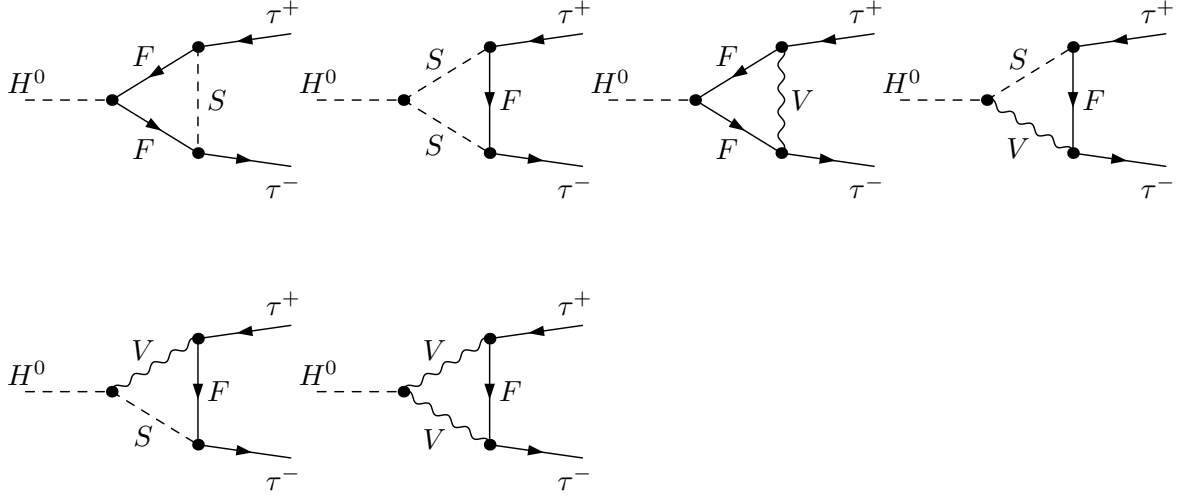


Figure 4.9.: All NLO vertex corrections to the decays $H^0 \rightarrow \tau^+ \tau^-$. All virtual vertex corrections $\mathcal{A}_{H^0\tau^+\tau^-}^{\text{VC}}$ are shown, grouped by their topological structure. The diagrams contain contributions from fermions F , scalar bosons S and gauge bosons V . Diagrams involving an internal photon contain IR divergences.

The form factor of the vertex corrections, $\mathcal{F}_{H^0\tau\tau}^{\text{VC}}$, has to be determined via the calculation of all diagrams shown in Fig. 4.9, while the form factor of the counterterm explicitly reads [52, 79]

$$\begin{aligned} \mathcal{F}_{H^0\tau\tau}^{\text{CT}} = & \frac{\delta g}{g} + \frac{\delta m_\tau}{m_\tau} - \frac{\delta m_W^2}{2m_W^2} + \frac{Y_1}{Y_2}\delta\alpha + Y_3\delta\beta + \frac{\delta Z_{H^0H^0}}{2} + \frac{Y_1}{Y_2} \frac{\delta Z_{h^0H^0}}{2} \\ & + \frac{\delta Z_{\tau\tau}^{\text{L}}}{2} + \frac{\delta Z_{\tau\tau}^{\text{R}}}{2}, \end{aligned} \quad (4.181)$$

with the Yukawa coupling Y_1 being defined in Sec. 8.2. The counterterm $\delta\beta$ appearing in the vertex counterterm is fixed through Eq. (4.176). As it was the case for the previous process, we exclude all QED contributions to the one-loop amplitude [36], meaning that for the definitions of δm_τ , $\delta Z_{\tau\tau}^{\text{L}}$ and $\delta Z_{\tau\tau}^{\text{R}}$, the self-energy in Fig. 4.7 (a) has to be excluded, while the vertex corrections do not contain the diagram in Fig. 4.7 (c). Applying the renormalization condition

$$\Gamma_{H^0\tau\tau}^{\text{LO}} \stackrel{!}{=} \Gamma_{H^0\tau\tau}^{\text{NLO,weak}} \quad (4.182)$$

allows for a process-dependent definition of the scalar mixing angle by solving for $\delta\alpha$. In summary, the two angle counterterms read:

Standard / alternative tadpole scheme
$\delta\beta = \frac{-Y_3}{1+Y_3^2} \left[\mathcal{F}_{A^0\tau\tau}^{\text{VC}} + \frac{\delta g}{g} + \frac{\delta m_\tau}{m_\tau} - \frac{\delta m_W^2}{2m_W^2} + \frac{\delta Z_{A^0A^0}}{2} - \frac{1}{Y_3} \frac{\delta Z_{G^0A^0}}{2} + \frac{\delta Z_{\tau\tau}^{\text{L}}}{2} + \frac{\delta Z_{\tau\tau}^{\text{R}}}{2} \right], \quad (4.183)$
$\delta\alpha = \frac{-Y_2}{Y_1} \left[\mathcal{F}_{H^0\tau\tau}^{\text{VC}} + \frac{\delta g}{g} + \frac{\delta m_\tau}{m_\tau} - \frac{\delta m_W^2}{2m_W^2} + Y_3\delta\beta + \frac{\delta Z_{H^0H^0}}{2} + \frac{Y_1}{Y_2} \frac{\delta Z_{h^0H^0}}{2} + \frac{\delta Z_{\tau\tau}^{\text{L}}}{2} + \frac{\delta Z_{\tau\tau}^{\text{R}}}{2} \right]. \quad (4.184)$

The headline in the box indicates that the definition of $\delta\alpha$ and $\delta\beta$ is valid for both the standard and the alternative tadpole scheme. So far, we did not specify which tadpole scheme is used for the process-dependent definition of the angle counterterms. The form factors $\mathcal{F}_{A^0\tau\tau}^{\text{VC}}$ and

$\mathcal{F}_{H^0\tau\tau}^{\text{VC}}$ of the virtual vertex corrections are invariant under a change of the tadpole scheme, cf. Sec. 4.6. However, the counterterms δm_τ , δm_W^2 , $\delta Z_{G^0 A^0}$ and $\delta Z_{h^0 H^0}$ depend on the chosen scheme and as a consequence, the actual expressions appearing in $\delta\alpha$ and $\delta\beta$ change with the chosen tadpole scheme as well. The form of the angle counterterms stated in Eqs. (4.183) and (4.184) is kept in a generic way, so that the choice of tadpole scheme is kept implicit through the actual form of the counterterms δm_τ , δm_W^2 , $\delta Z_{G^0 A^0}$ and $\delta Z_{h^0 H^0}$ appearing in those equations.

After having derived the explicit forms of $\delta\alpha$ and $\delta\beta$, we want to discuss their gauge-dependence. Since these counterterms are defined over a physical process, one might intuitively assume that they should be manifestly gauge-independent. This is the case for $\delta\beta$, as it was already mentioned in [36]. The form of $\delta\beta$ changes when switching from the standard to the alternative tadpole scheme, and with the change of the scheme, some of the counterterms in the definition of $\delta\beta$ receive additional gauge-dependent contributions. However, the combination of counterterms in Eq. (4.183) is such that all gauge-dependent parts precisely cancel. Therefore, the identity

$$\delta\beta = \delta\beta|_{\xi=1} \quad (4.185)$$

holds for *all* gauge-fixing-parameters $\xi \in \{\xi_W, \xi_Z, \xi_\gamma\}$ and independently of the tadpole scheme that is chosen, so that the gauge-independence becomes manifest. This has been checked both analytically and numerically.

The gauge-dependence of $\delta\alpha$ on the other hand differs in the two tadpole schemes. In the standard tadpole scheme, the definition of $\delta\alpha$ in Eq. (4.184) contains a residual gauge-dependence which is not cancelled. Explicitly, the gauge-dependence in this scheme reads

$$\delta\alpha^{\text{sta}} = \delta\alpha^{\text{sta}}|_{\xi=1} - (1 - \xi_W) \frac{\Lambda_5 m_W^2 c_{\beta-\alpha} s_{\beta-\alpha}}{16\pi^2 (m_{H^0}^2 - m_{h^0}^2)} \alpha_W - (1 - \xi_Z) \frac{\Lambda_5 m_Z^2 c_{\beta-\alpha} s_{\beta-\alpha}}{32\pi^2 (m_{H^0}^2 - m_{h^0}^2)} \alpha_Z, \quad (4.186)$$

with the superscript “sta” indicating the standard tadpole scheme. Note that this is equivalent to the second line of the gauge-dependence of $\delta\alpha$ in Kanemura’s scheme, Eq. (4.156). The fact that this line was cancelled in Kanemura’s scheme when switching from the standard to the alternative tadpole scheme foreshadows what will happen when we consider the process-dependent definition of $\delta\alpha$ in the alternative tadpole scheme. Indeed, the shift of the vevs in the alternative scheme is such that all gauge-dependences in $\delta\alpha$ cancel, yielding

$$\delta\alpha^{\text{alt}} = \delta\alpha^{\text{alt}}|_{\xi=1}, \quad (4.187)$$

valid for all $\xi \in \{\xi_W, \xi_Z, \xi_\gamma\}$, with the superscript “alt” now indicating the alternative tadpole scheme.

As a summary, the process-dependent definition of $\delta\beta$ is manifestly gauge-independent for both tadpole schemes, while $\delta\alpha$ is gauge-independent if and only if the alternative tadpole scheme is chosen. The fact that $\delta\alpha$ is gauge-dependent in the standard tadpole scheme does not necessarily spoil the overall gauge-independence of the one-loop calculation. It just means that the residual gauge-dependence in Eq. (4.186) must be cancelled by other gauge-dependences within the one-loop amplitude. That this is in fact the case will be discussed in Sec. 5.4, Sec. 6.3 and Sec. 7.3 for three different processes.

4.9. Renormalization of Λ_5

The last missing parameter of the 2HDM parameter set in Eq. (2.58) that needs to be renormalized is Λ_5 , appearing in the scalar sector of the 2HDM, i.e. in Higgs-to-Higgs decays. One

such decay will be considered in Chapter 7. At NLO, the bare parameter is split up according to

$$\Lambda_{5,0} = \Lambda_5 + \delta\Lambda_5 . \quad (4.188)$$

Similarly to the mixing angles, the renormalized Λ_5 is a residual parameter of the potential and as such, it has no physical meaning in the sense of e.g. masses. Therefore, there is no intuitive way of fixing the counterterm $\delta\Lambda_5$ through an on-shell condition. In the following, we present three different renormalization schemes for Λ_5 .

4.9.1. $\overline{\text{MS}}$ Scheme

Fixing the parameter $\delta\Lambda_5$ over an $\overline{\text{MS}}$ condition is analogous to the $\overline{\text{MS}}$ condition of the scalar mixing angles presented in Sec. 4.8.1. Such a renormalization scheme for $\delta\Lambda_5$ has been adopted e.g. in [56]¹².

The counterterm $\delta\Lambda_5$ is chosen such that it cancels any residual UV divergence in a one-loop amplitude. Since we consider an $\overline{\text{MS}}$ scheme instead of an MS scheme, this means that the remaining terms proportional to Δ , as defined in Eq. (4.4), will be absorbed in $\delta\Lambda_5$, thus leading to a UV-finite NLO amplitude. We will not state the explicit form of the counterterm, since it is rather lengthy, and use instead the symbolic notation

Standard / alternative tadpole scheme
$\delta\Lambda_5 = \delta\Lambda_5(\Delta) _{\overline{\text{MS}}} , \quad (4.189)$

where the right-hand side of the equation indicates all terms proportional to Δ that are necessary to cancel the dependence on Δ of the rest of the amplitude.

The gauge-dependence of $\delta\Lambda_5$ depends on the tadpole scheme that is chosen. Since the counterterm is directly proportional to Δ and thus contains no UV-finite parts per definition, any gauge-dependence in $\delta\Lambda_5$ manifests itself in the UV-divergent part of the counterterm. When considering the gauge-dependence of the Higgs-to-Higgs decay amplitude in Sec. 7.3, we will realize that the residual amplitude without $\delta\Lambda_5$ contains gauge-dependent UV-finite and UV-divergent parts within the standard tadpole scheme. Consequently, the pure $\overline{\text{MS}}$ condition of $\delta\Lambda_5$ cannot cancel the UV-finite gauge-dependent parts and has to be modified to contain those terms as well in order to yield a gauge-independent NLO amplitude. If instead the alternative tadpole scheme is chosen, then the $\overline{\text{MS}}$ condition will lead to a manifestly gauge-independent definition of $\delta\Lambda_5$.

4.9.2. Improved $\overline{\text{MS}}$ Scheme

While the renormalization of the parameter Λ_5 in an $\overline{\text{MS}}$ scheme works fine with respect to the cancellation of all UV divergences, it could lead to numerical instability, as it was the case for the mixing angle counterterms if defined over an $\overline{\text{MS}}$ condition, cf. Sec. 4.8.1. In Chapter 7, we will consider the 2HDM decay process $H^0 \rightarrow h^0 h^0$ that involves $\delta\Lambda_5$ at NLO. As it will turn out in the numerical evaluation of the process in Sec. 8.5, the $\overline{\text{MS}}$ condition of Λ_5 can be considered numerically stable if the standard tadpole scheme is chosen. However, a change to the alternative tadpole scheme will reveal that the $\overline{\text{MS}}$ scheme for $\delta\Lambda_5$ is not a suitable scheme, since it leads to numerical instability.

¹²Note that in this paper, the soft- \mathbb{Z}_2 -breaking mass M of Eq. (2.37) is renormalized instead of the parameter Λ_5 . However, both parameters are proportional to each other according to Eq. (A.4).

As soon as we look at the NLO decay amplitude of the Higgs-to-Higgs decay in Sec. 7.2, we will realize that the whole amplitude is not invariant under a shift of the vevs when changing from the standard to the alternative tadpole scheme if Λ_5 is renormalized in the usual $\overline{\text{MS}}$ approach. Since $\delta\Lambda_5$ is renormalized by an $\overline{\text{MS}}$ condition, containing only UV-divergent parts, the UV-finite part of $\delta\Lambda_5$ is unaffected by the shifts of the vevs and still equals zero after the shifts have been performed. Since the residual amplitude, with $\delta\Lambda_5$ being set to zero, will receive large UV-finite terms through the A_0 integrals contained in Eq. (4.57) when performing the shift, this means that these large additional contributions cannot be cancelled by the counterterm $\delta\Lambda_5$ in a pure $\overline{\text{MS}}$ scheme.

Therefore, we will improve the $\overline{\text{MS}}$ condition in a way that is consistent within the internal relations of the 2HDM, so that the scheme can be considered numerically stable even within the alternative tadpole treatment. To that end, we use Eqs. (2.43) and (A.4) in order to express the parameter Λ_5 through m_W , g , β and the parameter m_{12} of the 2HDM potential given in Eq. (2.7), noting that the angle β appearing in this expression has to be considered as defined over the ratio of the vevs, cf. Eq. (2.35), but not as a mixing angle:

$$\Lambda_5 = \frac{g^2 m_{12}^2}{m_W^2 s_{2\beta}}. \quad (4.190)$$

In order to consider the shifts that $\delta\Lambda_5$ receives when changing from the standard to the alternative tadpole scheme, we use not only $\delta\Lambda_5$ as a purely $\overline{\text{MS}}$ defined counterterm, but we include the counterterms δm_W^2 , $\delta\beta$ and δg which appear in Eq. (4.190) when changing from LO to NLO¹³. Consequently, the $\overline{\text{MS}}$ counterterm $\delta\Lambda_5$ in the alternative tadpole scheme explicitly reads

Alternative tadpole scheme

$$\delta\Lambda_5 = \delta\Lambda_5(\Delta)|_{\overline{\text{MS}}} + \Lambda_5 \left[2 \frac{\delta g}{g} - \frac{2c_{2\beta}}{s_{2\beta}} \delta\beta - \frac{\delta m_W^2}{m_W^2} \right]. \quad (4.191)$$

Through the appearance of the counterterms δg , $\delta\beta$ and δm_W^2 , the large contributions appearing in the NLO amplitude when changing from the standard to the alternative tadpole scheme are cancelled, leading to a numerically stable result. The term $\delta\Lambda_5(\Delta)|_{\overline{\text{MS}}}$ is defined to cancel any residual UV-divergent parts in the NLO amplitude. The counterterm $\delta\beta$ can be chosen to be defined in the gauge-independent pinched scheme of Sec. 4.8.3 and all other counterterms appearing in Eq. (4.191) are all gauge-independent in the alternative tadpole scheme, as well. Therefore, $\delta\Lambda_5$ is manifestly gauge-independent if the residual UV divergence of the amplitude is gauge-independent. That this is the case will be discussed in Sec. 7.3.

4.9.3. Process-Dependent Scheme

In order to define the counterterm in a more physical way, it is possible to use a process to fix $\delta\Lambda_5$. Demanding the decay process to occur on-shell, the scalar sector of the 2HDM provides four processes¹⁴ that can be used to fix $\delta\Lambda_5$:

$$\begin{aligned} H^0 &\longrightarrow h^0 h^0, \\ H^0 &\longrightarrow H^+ H^-, \\ h^0 &\longrightarrow A^0 A^0, \\ H^0 &\longrightarrow A^0 A^0. \end{aligned} \quad (4.192)$$

¹³By choosing m_{12}^2 instead of Λ_5 as our independent parameter, we could have avoided this problem from the start. Nevertheless, we stick to Λ_5 since this parameter is included in the 2HDM model file in **FeynArts**.

¹⁴A fifth 2HDM process, namely $h^0 \longrightarrow H^+ H^-$, is ruled out on-shell, since experimental data restrict the scalar masses to $m_{H^\pm} > m_{h^0}$, see e.g. [116] for a type II 2HDM.

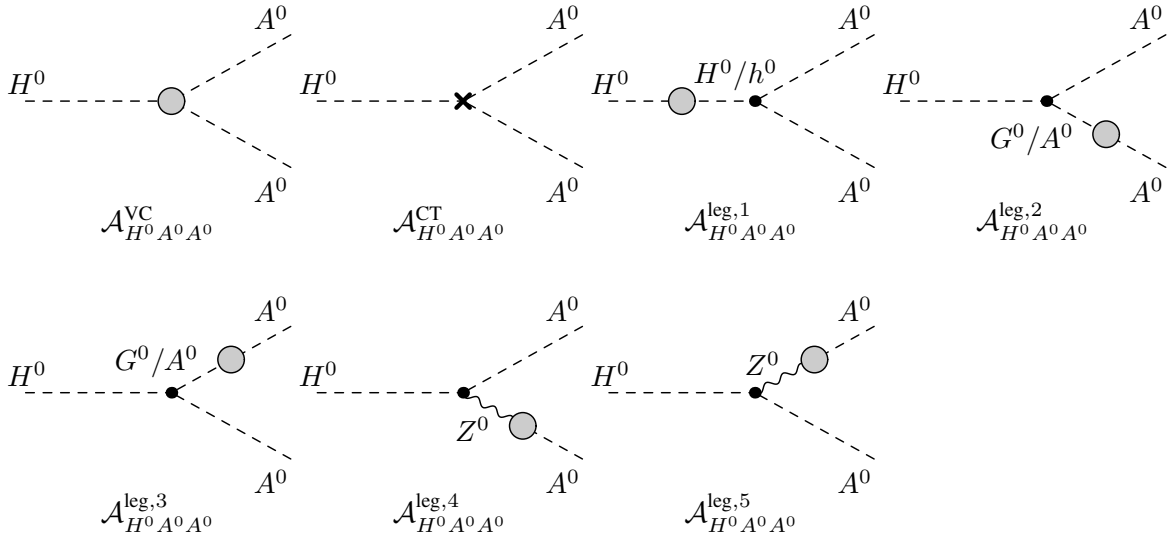


Figure 4.10.: NLO virtual corrections to the decays $H^0 \rightarrow A^0 A^0$. The one-loop amplitude $\mathcal{A}_{H^0 A^0 A^0}^{\text{1loop}}$ consists of all virtual vertex corrections $\mathcal{A}_{H^0 A^0 A^0}^{\text{VC}}$, the vertex counterterm $\mathcal{A}_{H^0 A^0 A^0}^{\text{CT}}$ as well as the external leg corrections $\mathcal{A}_{H^0 A^0 A^0}^{\text{leg},i}$ ($i = 1, \dots, 5$).

The first process is the one we want to renormalize in Chapter 7, therefore we cannot use it in order to fix the counterterm of Λ_5 . The second process should be avoided due to the appearance of IR divergences, while the third gives a very strict kinematical bound to the mass of the pseudoscalar Higgs boson A^0 . Therefore, we will use the decay $H^0 \rightarrow A^0 A^0$ as the least-restrictive process in order to fix $\delta\Lambda_5$.

The LO decay amplitude of the process is given by the coupling constant of the heavy Higgs H^0 to the two CP-odd Higgses A^0 , which reads

$$\mathcal{A}_{H^0 A^0 A^0}^{\text{LO}} = g_{H^0 A^0 A^0} = -\frac{g}{2m_W} \left[c_{\beta-\alpha} (2m_{A^0}^2 - m_{H^0}^2) + \frac{s_{\alpha+\beta}}{s_{2\beta}} \left(2m_{H^0}^2 - 4\frac{m_W^2}{g^2} \Lambda_5 \right) \right]. \quad (4.193)$$

The LO partial decay width is determined by inserting this amplitude into Eq. (3.7). The scalar particles of the process have no additional degrees of freedom. However, the two final A^0 bosons are indistinguishable, therefore the statistical factor $S = 1/2$ has to be considered. This yields the LO partial decay width

$$\Gamma_{H^0 A^0 A^0}^{\text{LO}} = \frac{|g_{H^0 A^0 A^0}|^2}{32\pi m_{H^0}} \sqrt{1 - \frac{4m_{A^0}^2}{m_{H^0}^2}}. \quad (4.194)$$

At NLO, the one-loop amplitude consists of all contributions shown in Fig. 4.10. The first three virtual external leg corrections vanish due to the on-shell renormalization of the scalar fields, presented in Sec. 4.7, while the last two leg corrections vanish due to a Slavnov-Taylor identity [115]. Therefore, the full one-loop amplitude is given by:

$$\mathcal{A}_{H^0 A^0 A^0}^{\text{1loop}} = \mathcal{A}_{H^0 A^0 A^0}^{\text{VC}} + \mathcal{A}_{H^0 A^0 A^0}^{\text{CT}}. \quad (4.195)$$

The virtual vertex corrections $\mathcal{A}_{H^0 A^0 A^0}^{\text{VC}}$ are the sum of all diagrams shown in Fig. 4.11. Note that the last four tadpole diagrams have to be included only if one chooses to use

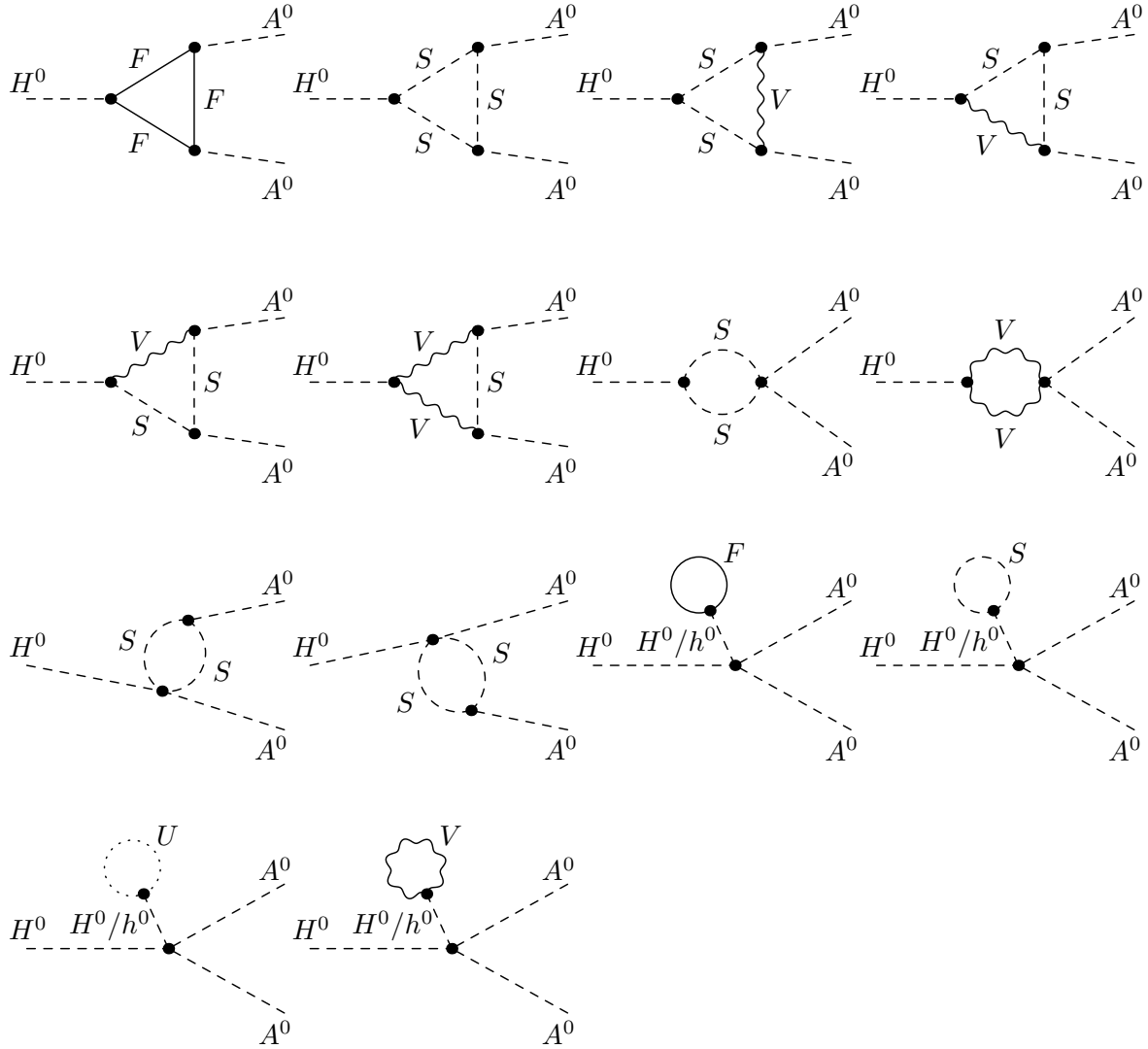


Figure 4.11.: All NLO vertex corrections to the decays $H^0 \rightarrow A^0 A^0$. All virtual vertex corrections $\mathcal{A}_{H^0 A^0 A^0}^{\text{VC}}$ are shown, grouped by their topological structure. The diagrams contain contributions from fermions F , scalar bosons S and gauge bosons V . The tadpole diagrams are included only if the alternative tadpole scheme is chosen.

the alternative tadpole scheme. Otherwise, they are omitted. In order to derive the vertex counterterm, we introduce the two Higgs couplings

$$g_{h^0 A^0 A^0} = -\frac{g}{2m_W} \left[s_{\beta-\alpha} (2m_{A^0}^2 - m_{h^0}^2) + \frac{c_{\alpha+\beta}}{s_{2\beta}} \left(2m_{h^0}^2 - 4\frac{m_W^2}{g^2} \Lambda_5 \right) \right], \quad (4.196)$$

$$g_{H^0 G^0 A^0} = -\frac{g^{S\beta-\alpha}}{2m_W} (m_{A^0}^2 - m_{H^0}^2). \quad (4.197)$$

The counterterm is generated from the relevant part of the bare Lagrangian that, after the field renormalization has been performed, is proportional to the renormalized fields $H^0 A^0 A^0$,

$$\begin{aligned} \mathcal{L}_{\text{int,rel}} &= \frac{-ig_{h^0 A^0 A^0}}{2!} h_0^0 A_0^0 A_0^0 + \frac{-ig_{H^0 A^0 A^0}}{2!} H_0^0 A_0^0 A_0^0 + \frac{-ig_{H^0 G^0 A^0}}{1!} H_0^0 G_0^0 A_0^0 \\ &\stackrel{\text{NLO}}{\approx} \left[\frac{-ig_{h^0 A^0 A^0}}{2!} \frac{\delta Z_{h^0 H^0}}{2} + \frac{-ig_{H^0 A^0 A^0}}{2!} \left(\delta Z_{A^0 A^0} + \frac{\delta Z_{H^0 H^0}}{2} \right) \right. \\ &\quad \left. + \frac{-ig_{H^0 G^0 A^0}}{1!} \frac{\delta Z_{G^0 A^0}}{2} \right] H^0 A^0 A^0. \end{aligned} \quad (4.198)$$

In order to derive the counterterm, we perform a functional derivative,

$$\frac{\delta}{\delta H^0} \frac{\delta}{\delta A^0} \frac{\delta}{\delta A^0} (i\mathcal{L}_{\text{int,rel}}) \quad (4.199)$$

and add to it the counterterm of the tree-level coupling,

$$\begin{aligned} \delta g_{H^0 A^0 A^0} = & \left(g_{H^0 A^0 A^0} - \frac{4m_W \Lambda_5 s_{\alpha+\beta}}{g s_{2\beta}} \right) \left[\frac{\delta g}{g} - \frac{\delta m_W^2}{2m_W^2} \right] \\ & - \frac{g}{2m_W} \left[\left(\frac{2s_{\alpha+\beta}}{s_{2\beta}} - c_{\beta-\alpha} \right) \delta m_{H^0}^2 + 2c_{\beta-\alpha} \delta m_{A^0}^2 - \frac{4m_W^2 s_{\alpha+\beta}}{g^2 s_{2\beta}} \delta \Lambda_5 \right. \\ & + \left(s_{\beta-\alpha} (2m_{A^0}^2 - m_{H^0}^2) + \frac{c_{\alpha+\beta}}{s_{2\beta}} \left(2m_{H^0}^2 - \frac{4m_W^2 \Lambda_5}{g^2} \right) \right) \delta \alpha \\ & \left. + \left(-s_{\beta-\alpha} (2m_{A^0}^2 - m_{H^0}^2) + \left(\frac{c_{\alpha+\beta}}{s_{2\beta}} - \frac{2s_{\alpha+\beta} c_{2\beta}}{s_{2\beta}^2} \right) \left(2m_{H^0}^2 - \frac{4m_W^2 \Lambda_5}{g^2} \right) \right) \delta \beta \right]. \end{aligned} \quad (4.200)$$

In total, the full vertex counterterm to the process $H^0 \rightarrow A^0 A^0$ at NLO reads:

$$\begin{aligned} \mathcal{A}_{H^0 A^0 A^0}^{\text{CT}} = & g_{h^0 A^0 A^0} \frac{\delta Z_{h^0 H^0}}{2} + g_{H^0 A^0 A^0} \left(\delta Z_{A^0 A^0} + \frac{\delta Z_{H^0 H^0}}{2} \right) + g_{H^0 G^0 A^0} \delta Z_{G^0 A^0} \\ & + \delta g_{H^0 A^0 A^0} . \end{aligned} \quad (4.201)$$

The NLO partial decay width is now given by inserting the virtual vertex corrections and the counterterm into Eq. (3.12):

$$\Gamma_{H^0 A^0 A^0}^{\text{NLO}} = \Gamma_{H^0 A^0 A^0}^{\text{LO}} + \frac{\lambda(m_{H^0}^2, m_{A^0}^2, m_{A^0}^2)}{32\pi m_{H^0}^3} 2 \text{Re} \left[(\mathcal{A}_{H^0 A^0 A^0}^{\text{LO}})^* \mathcal{A}_{H^0 A^0 A^0}^{\text{1loop}} \right]. \quad (4.202)$$

In order to fix the counterterm $\delta \Lambda_5$, we use the process-dependent renormalization condition

$$\Gamma_{H^0 A^0 A^0}^{\text{LO}} \stackrel{!}{=} \Gamma_{H^0 A^0 A^0}^{\text{NLO}}, \quad (4.203)$$

which finally translates to the definition of the counterterm:

Standard / alternative tadpole scheme
$\delta \Lambda_5 = -\frac{g s_{2\beta}}{2m_W s_{\alpha+\beta}} \text{Re} \left[\mathcal{A}_{H^0 A^0 A^0}^{\text{VC}} + [\mathcal{A}_{H^0 A^0 A^0}^{\text{CT}}]_{\delta \Lambda_5=0} \right]. \quad (4.204)$

The gauge-dependence of the counterterm of Λ_5 depends not only on the chosen tadpole scheme, but additionally, on the choice of renormalization scheme of the angle counterterms $\delta \alpha$ and $\delta \beta$. Using the alternative tadpole scheme and e.g. one of the pinched schemes of Sec. 4.8.3 or the process-dependent definition of the angle-counterterms presented in Sec. 4.8.4, the definition of $\delta \Lambda_5$ in Eq. (4.204) becomes manifestly gauge-independent, which has been checked numerically.

In the standard tadpole scheme, $\delta \Lambda_5$ is gauge-dependent. Due to the complicated structure of the scalar self-interactions in the 2HDM, the explicit form of the gauge-dependence is rather intricate and will thus not be presented here.

4.10. Renormalization of the Gauge-Fixing Lagrangian

For the renormalization of the gauge-fixing Lagrangian in Eq. (2.55), we follow the arguments presented in [79]. In the SM, the scalar Lagrangian produces a kinetic term of the form $im_W(\partial^\mu W_\mu^-)G^+$, which spoils the proper definition of the propagators of the charged sector. However, the mixing term arising from the gauge-fixing Lagrangian contains a term of the form $-im_W(\partial^\mu W_\mu^-)G^+$, which precisely cancels the one from the scalar Lagrangian. In the SM, this cancellation holds for the bare and the renormalized Lagrangian, to all orders in perturbation theory.

In the 2HDM however, the situation changes, since (4.113) introduces a mixing of the charged scalar doublet when the fields are renormalized. If the same approach as in the SM is applied to the 2HDM, the terms arising in the gauge-fixing and scalar Lagrangian would cancel against each other again. However, this would also cancel a counterterm that is necessary for the W^+H^+ two-point correlation function to vanish on-shell [79, 91].

To circumvent this problem, it is possible to consider the gauge-fixing Lagrangian of Eq. (2.55) as being already renormalized, i.e. to contain only renormalized fields [117]. Doing so ensures that the mixing terms of the scalar Lagrangian still produce the necessary counterterm for the W^+H^+ propagator to vanish on-shell, while the other non-mixing terms in the renormalized fields cancel against each other again. The same arguments hold for the CP-odd sector, as well. As a consequence, the vanishing of the on-shell W^+H^+ and Z^0A^0 propagators can be expressed through the use of Slavnov-Taylor identities [115].

 The Decays $H^+ \rightarrow W^+ h^0/H^0$ at Next-to-Leading Order

The decays $H^+ \rightarrow W^+ h^0/H^0$ at NLO have been discussed extensively in [91], where the full electroweak corrections were calculated in Feynman-'t Hooft gauge and different renormalization schemes were presented. Among those renormalization schemes are Kanemura's scheme as well as an $\overline{\text{MS}}$ scheme. As discussed in Sec. 4.8.2, the former scheme is explicitly gauge-dependent, while the latter is numerically unstable in most cases, cf. Sec. 4.8.1. Therefore, the task is to implement the other renormalization schemes from Sec. 4.8.3 and Sec. 4.8.4 that are both gauge-independent, and check for numerical stability. In order to compare these schemes with results presented in [91], the decays $H^+ \rightarrow W^+ h^0/H^0$ are considered within the scope of this thesis, as well.

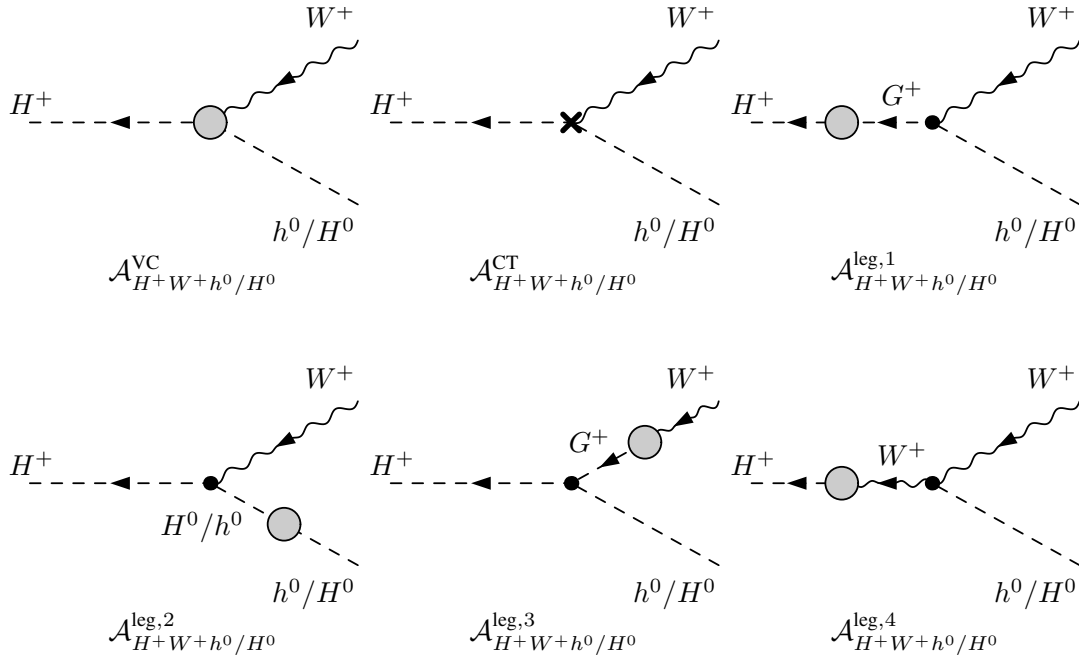


Figure 5.1.: NLO virtual corrections to the decays $H^+ \rightarrow W^+ h^0/H^0$. The one-loop amplitude $\mathcal{A}_{H^+W^+h^0/H^0}^{\text{1loop}}$ consists of all virtual vertex corrections $\mathcal{A}_{H^+W^+h^0/H^0}^{\text{VC}}$, the vertex counterterm $\mathcal{A}_{H^+W^+h^0/H^0}^{\text{CT}}$ as well as external leg corrections $\mathcal{A}_{H^+W^+h^0/H^0}^{\text{leg},i}$ ($i = 1, \dots, 4$).

5.1. The Partial Decay Width at LO

At LO, the decay amplitudes are given by the application of the Feynman rules for the scalar-scalar-vector vertices of the 2HDM. Using the generic notation of Sec. 3.1, we refer to p_1 as the momentum of the incoming H^+ , p_2 as the momentum of the outgoing W^+ boson and p_3 as the momentum of the Higgs bosons h^0/H^0 , depending on the process that is chosen. As a vector boson, the W^+ has additional degrees of freedom in the form of the polarization λ_2 , which is accounted for with a polarization vector $\varepsilon_2^* := \varepsilon_{\lambda_2}^*(p_2)$. The LO decay amplitudes for the processes $H^+ \rightarrow W^+ h^0/H^0$ are given by [79]

$$\begin{aligned} \mathcal{A}_{H^+W^+h^0}^{\text{LO}} &= \frac{-g c_{\beta-\alpha}}{2} (p_1 + p_3)^\mu \varepsilon_{2,\mu}^* \\ &= -g c_{\beta-\alpha} (p_1 \cdot \varepsilon_2^*) , \end{aligned} \quad (5.1)$$

$$\begin{aligned} \mathcal{A}_{H^+W^+H^0}^{\text{LO}} &= \frac{g s_{\beta-\alpha}}{2} (p_1 + p_3)^\mu \varepsilon_{2,\mu}^* \\ &= g s_{\beta-\alpha} (p_1 \cdot \varepsilon_2^*) , \end{aligned} \quad (5.2)$$

where in the second line of both equations, we used the four-momentum conservation, Eq. (3.1), as well as the transversality of the on-shell W^+ boson, leading to $p_2 \cdot \varepsilon_2^* = 0$. In order to calculate the LO partial decay width, we take the absolute square of the amplitudes and sum over all degrees of freedom. Since the polarization of the W^+ boson in the final state is of no interest, the degrees of freedom can be summed up by using the polarization sum [5]

$$\begin{aligned} \sum_{\text{d.o.f.}} (p_1 \cdot \varepsilon_2) (p_1 \cdot \varepsilon_2^*) &= p_1^\mu p_1^\nu \sum_{\lambda_2} \varepsilon_{2,\mu} \varepsilon_{2,\nu}^* = p_1^\mu p_1^\nu \left(-g_{\mu\nu} + \frac{p_{2,\mu} p_{2,\nu}}{m_W^2} \right) \\ &= \frac{1}{4m_W^2} \lambda^2 (m_{H^\pm}^2, m_W^2, p_3^2) . \end{aligned} \quad (5.3)$$

The statistical factor of the process is $S = 1$, since the W^+ boson is distinguishable from the CP-even Higgs bosons in the final state. Inserting the amplitudes into Eq. (3.7) and using Eq. (5.3) gives the LO partial decay widths for both processes:

$$\Gamma_{H^+W^+h^0}^{\text{LO}} = \frac{g^2 c_{\beta-\alpha}^2}{64\pi m_W^2 m_{H^\pm}^3} \lambda^3(m_{H^\pm}^2, m_W^2, m_{h^0}^2) , \quad (5.4)$$

$$\Gamma_{H^+W^+H^0}^{\text{LO}} = \frac{g^2 s_{\beta-\alpha}^2}{64\pi m_W^2 m_{H^\pm}^3} \lambda^3(m_{H^\pm}^2, m_W^2, m_{H^0}^2) . \quad (5.5)$$

5.2. NLO Virtual Corrections

At next-to-leading order, the decay amplitude receives contributions from all virtual corrections that appear at the one-loop level. Specifically, the amplitude is the sum of all virtual vertex corrections, the counterterm and external leg corrections, as depicted in Fig. 5.1.

As it was mentioned in Sec. 3.2, the corrections to the external legs vanish in most cases. In this case, the corrections $\mathcal{A}_{H^+W^+h^0/H^0}^{\text{leg},1}$ and $\mathcal{A}_{H^+W^+h^0/H^0}^{\text{leg},2}$, which introduce a mixing of the fields H^+G^+ , h^0H^0 and H^0h^0 , vanish according to the on-shell renormalization conditions presented in Sec. 4.7. The amplitude $\mathcal{A}_{H^+W^+h^0/H^0}^{\text{leg},3}$ vanishes due to the transversality of the external on-shell W^+ boson and the last external leg correction $\mathcal{A}_{H^+W^+h^0/H^0}^{\text{leg},4}$ vanishes due to a Slavnov-Taylor identity [115]. Therefore, the one-loop contribution to the decay amplitude reduces to:

$$\mathcal{A}_{H^+W^+h^0/H^0}^{\text{1loop}} = \mathcal{A}_{H^+W^+h^0/H^0}^{\text{VC}} + \mathcal{A}_{H^+W^+h^0/H^0}^{\text{CT}} . \quad (5.6)$$

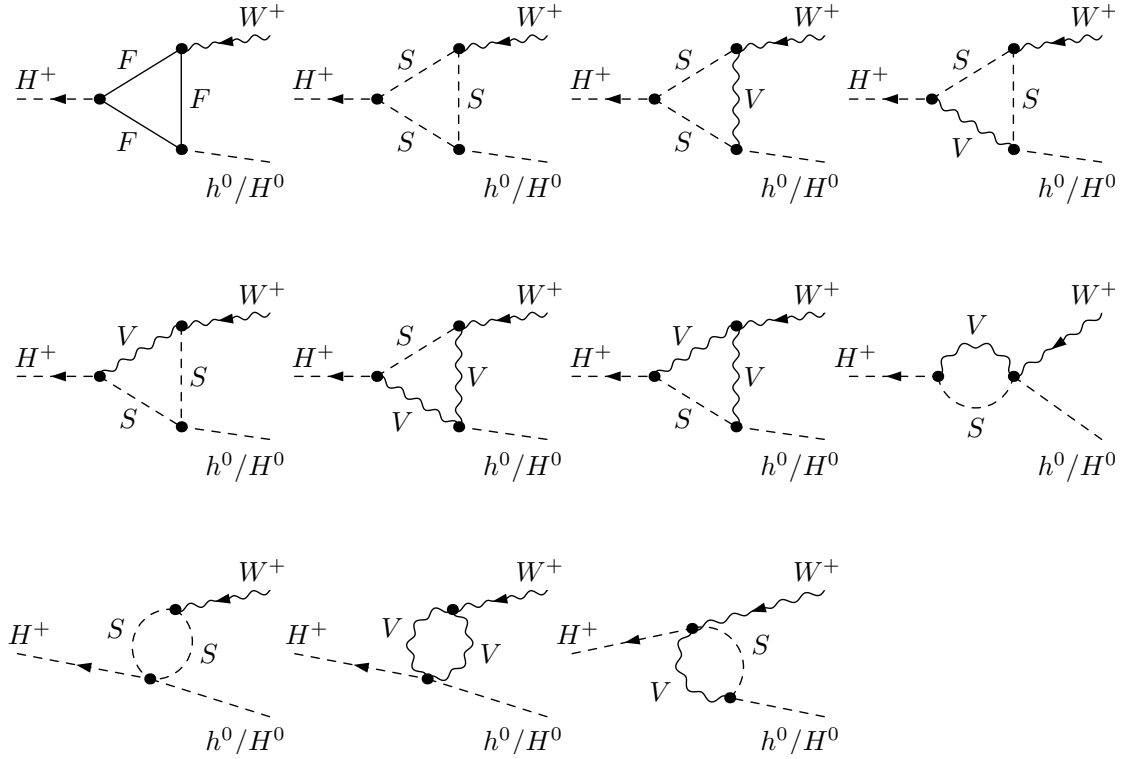


Figure 5.2.: All NLO vertex corrections to the decays $H^+ \rightarrow W^+ h^0/H^0$. All virtual vertex corrections $\mathcal{A}_{H^+W^+h^0/H^0}^{\text{VC}}$ are shown, grouped by their topological structure. The diagrams contain contributions from fermions F , scalar bosons S and gauge bosons V .

At the one-loop level, the vertex corrections consist of the sum of all diagrams shown in Fig. 5.2. In order to apply the gauge-independent renormalization schemes presented in Sec. 4.8 consistently and check for any residual gauge-dependence, the electroweak corrections were calculated in general R_ξ gauge. To this end, the amplitudes were automatically generated with `FeynArts 3.9` [55] and calculated with `FeynCalc 8.2.0` [118], enabling a reduction of the amplitudes to the well-known 't Hooft-Veltman scalar integrals [119]. It turns out that the LO amplitude, together with its Lorentz structure, factorizes from the sum of all vertex corrections,

$$\mathcal{A}_{H^+W^+h^0/H^0}^{\text{VC}} \equiv \mathcal{A}_{H^+W^+h^0/H^0}^{\text{LO}} \mathcal{F}_{H^+W^+h^0/H^0}^{\text{VC}} , \quad (5.7)$$

where $\mathcal{F}_{H^+W^+h^0/H^0}^{\text{VC}}$ is the form factor of the vertex corrections. Note that some of the diagrams in Fig. 5.2 contain photons as internal particles of the loops. As it was mentioned in Sec. 3.2, such diagrams give rise to IR divergences since the photon is a massless particle. Consequently, the one-loop integrals involved in calculating the amplitudes to the respective diagrams develop poles at vanishing loop momenta. In order to cancel these divergences, we have to include real corrections, which is described in detail in Sec. 5.3.

Apart from real corrections, the only missing ingredient for the NLO amplitude is the vertex counterterm. In both processes, the angle counterterms appear only in the form $s_{\beta-\alpha}$ or $c_{\beta-\alpha}$, resulting in the following NLO expansions:

$$\begin{aligned} \delta s_{\beta-\alpha} &\approx c_{\beta-\alpha} (\delta\beta - \delta\alpha) , \\ \delta c_{\beta-\alpha} &\approx -s_{\beta-\alpha} (\delta\beta - \delta\alpha) . \end{aligned} \quad (5.8)$$

The counterterms for both processes are given by

$$\begin{aligned} \mathcal{A}_{H^+W+h^0}^{\text{CT}} &= \mathcal{A}_{H^+W+h^0}^{\text{LO}} \left[\frac{\delta g}{g} + \frac{\delta Z_{WW}}{2} + \frac{\delta Z_{H^+H^+}}{2} + \frac{\delta Z_{h^0h^0}}{2} \right. \\ &\quad \left. + \frac{s_{\beta-\alpha}}{c_{\beta-\alpha}} \left(\frac{\delta Z_{G^+H^+}}{2} - \frac{\delta Z_{H^0h^0}}{2} + \delta\alpha - \delta\beta \right) \right] \\ &\equiv \mathcal{A}_{H^+W+h^0}^{\text{LO}} \mathcal{F}_{H^+W+h^0}^{\text{CT}} , \end{aligned} \quad (5.9)$$

$$\begin{aligned} \mathcal{A}_{H^+W+H^0}^{\text{CT}} &= \mathcal{A}_{H^+W+H^0}^{\text{LO}} \left[\frac{\delta g}{g} + \frac{\delta Z_{WW}}{2} + \frac{\delta Z_{H^+H^+}}{2} + \frac{\delta Z_{H^0H^0}}{2} \right. \\ &\quad \left. - \frac{c_{\beta-\alpha}}{s_{\beta-\alpha}} \left(\frac{\delta Z_{G^+H^+}}{2} + \frac{\delta Z_{h^0H^0}}{2} + \delta\alpha - \delta\beta \right) \right] \\ &\equiv \mathcal{A}_{H^+W+H^0}^{\text{LO}} \mathcal{F}_{H^+W+H^0}^{\text{CT}} , \end{aligned} \quad (5.10)$$

where the vertex counterterm form factors $\mathcal{F}_{H^+W+h^0/H^0}^{\text{CT}}$ have been introduced. Since the LO amplitude factorizes from both the counterterms and the vertex corrections, the resulting NLO width can be cast into a convenient form. By inserting Eq. (5.7) and the vertex counterterms into Eq. (3.12) and using the polarization sum in Eq. (5.3) for integrating out all degrees of freedom, we end up with the NLO partial decay width,

$$\Gamma_{H^+W+h^0/H^0}^{\text{NLO}} = \Gamma_{H^+W+h^0/H^0}^{\text{LO}} \left(1 + 2 \operatorname{Re} \left[\mathcal{F}_{H^+W+h^0/H^0}^{\text{VC}} + \mathcal{F}_{H^+W+h^0/H^0}^{\text{CT}} \right] \right) . \quad (5.11)$$

So far, we did not specify the tadpole scheme that is used for the renormalization of the processes. As it turns out, the decay $H^+ \rightarrow W^+ h^0/H^0$ is tadpole-invariant. We already discussed in Sec. 4.4.2 that the coupling constant $g_{h^0W-H^+}$ is unaffected by the shift of the vevs when turning from the standard to the alternative tadpole scheme. The same argument is valid for the other coupling constant $g_{H^0W-H^+}$ involving the heavy CP-even Higgs. Therefore, the form factors $\mathcal{F}_{H^+W+h^0/H^0}^{\text{VC}}$ of the vertex corrections are unaffected by a change of the tadpole scheme, since the shifts of the vevs do not induce additional tadpole diagrams.

On the other hand, the form factors $\mathcal{F}_{H^+W+h^0/H^0}^{\text{CT}}$ of the vertex counterterms depend on the tadpole scheme, since the individual counterterms contained in the second lines of Eqs. (5.9) and (5.10) are not tadpole-invariant. However, their combination in the counterterm form factors is such that all shifts in the counterterms precisely cancel, so that the form factors of the counterterms are tadpole-invariant, as well¹. Consequently, the virtual contributions to the NLO partial decay widths of Eq. (5.11) are tadpole-invariant.

On a technical side note, special care has to be taken when calculating amplitudes for diagrams containing internal photons if the calculation is performed in general R_ξ gauge. The longitudinal part of the photon propagator appearing in any gauge if $\xi_\gamma \neq 1$ is chosen, cf. Eq. (C.2), introduces additional poles in the vertex corrections, which, when using `FeynCalc`, lead to the appearance of scalar integrals

$$(1 - \xi_\gamma) C_0(0, m_W^2, m_W^2, 0, 0, \xi_W m_W^2) \quad (5.12)$$

which are numerically highly unstable². The fact that these integrals appear proportional to $(1 - \xi_\gamma)$ makes it clear that this numerical instability is introduced by choosing not to

¹This statement holds independently of the chosen renormalization scheme for the angle counterterms $\delta\alpha$ and $\delta\beta$. The shifts of the angle counterterms through the vev shifts is the same for all schemes presented in Sec. 4.8.

²It should be pointed out that this numerical instability is purely due to the structure of the scalar integral in Eq. (5.12) and not a consequence of using a numerically unstable renormalization scheme.

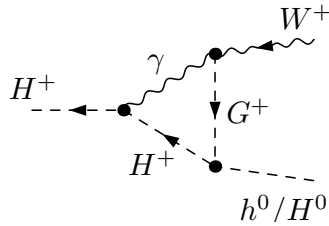


Figure 5.3.: Infrared divergent one-loop amplitude. Feynman diagram for an amplitude contributing to the processes $H^+ \rightarrow W^+ h^0/H^0$. Due to the internal massless photon, the one-loop amplitude contains an IR divergence.

perform the calculation in Feynman-’t Hooft gauge. In order to check if the appearance of these integrals is due to an undetected bug in `FeynCalc` or if it is an inevitable subtlety introduced by the R_ξ gauge itself, the vertex corrections were calculated independently by the use of `FormCalc` 9.1 [120]. Although both programs do not give the same analytic result for the diagrams involving internal photons, it turns out that `FormCalc` produces numerical instabilities for these amplitudes as well. The appearance of these instabilities threatens the success of performing calculations in R_ξ gauge. However, the same integrals appear when calculating the field strength renormalization constant δZ_{WW} in R_ξ gauge, and as it turns out, all integrals of the form of Eq. (5.12) cancel when summing up all vertex corrections and the counterterms. Thus, for numerically checking individual amplitudes in R_ξ gauge that contain internal photons, one might as well set the C_0 integrals in Eq. (5.12) to zero by hand without modifying the final NLO amplitude, avoiding the problem of these unstable integrals from the start.

5.3. IR Divergences and Real Corrections

The decay processes $H^+ \rightarrow W^+ h^0/H^0$ contain charged particles in the initial and final state. As it was mentioned at the end of Sec. 3.2, such processes introduce infrared divergences in the vertex corrections as well as in the corresponding counterterms of the charged particles at the one-loop level. The treatment of the IR divergences of the given processes has been carried out in great detail in [91], therefore, we give only a brief overview of the procedure of dealing with these divergences and adopt the result from the previous work, since it is needed for a correct numerical evaluation of the decay processes.

Shown in Fig. 5.3 is one exemplary amplitude out of all possible virtual vertex corrections in Fig. 5.2 that contain an internal photon. If we neglect the exact form of the amplitude and focus only on the propagator structure, then the one-loop integral has the form

$$\int \frac{d^4 l}{(2\pi)^4} \frac{1}{l^2 [(l+p_1)^2 - m_{H^\pm}^2] [(l+p_1-p_3)^2 - \xi_W m_W^2]}. \quad (5.13)$$

The photon is a massless particle, causing the one-loop amplitude to develop a pole at vanishing loop momentum, i.e. in the infrared regime. The photon is usually given a small but non-vanishing mass Λ as a regulator, so that the one-loop integral gets modified to

$$\xrightarrow{\text{regularized}} \int \frac{d^4 l}{(2\pi)^4} \frac{1}{[l^2 - \Lambda^2] [(l+p_1)^2 - m_{H^\pm}^2] [(l+p_1-p_3)^2 - \xi_W m_W^2]}. \quad (5.14)$$

The IR pole is now shifted towards $l^2 \rightarrow \Lambda^2$, enabling the calculation of the regularized one-loop amplitude. The result contains terms of the form $\ln(\Lambda^{-2})$, which, for vanishing photon mass $\Lambda \rightarrow 0$, are an analytic quantization of the divergence of the integral. However, after

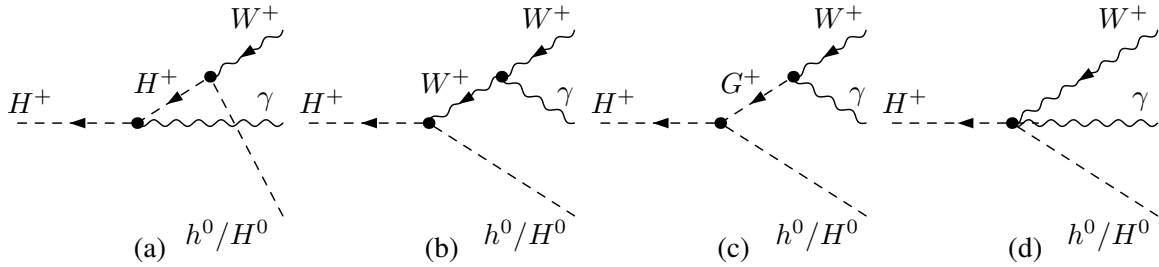


Figure 5.4.: Real corrections to the decays $H^+ \rightarrow W^+ h^0/H^0$ [91]. The real corrections needed for the cancellation of all IR divergences consist of Bremsstrahlung diagrams for the incoming H^+ (a) and outgoing W^+ (b), soft-photon emission from the $G^+W^+\gamma$ -vertex (c) and a soft-photon emission from a 2HDM-specific vertex (d).

carefully regularizing all IR divergences and combining them with the real corrections from diagrams containing the emission of one soft photon, it is ensured by the Kinoshita-Lee-Nauenberg (KLN) theorem [121, 122] that all divergences cancel against each other, so that in the end, the limit $\Lambda \rightarrow 0$ can be taken without running into singularities.

The appearance of IR divergences is a very general phenomenon of a quantum field theory [123] and not specific for the processes $H^+ \rightarrow W^+ h^0/H^0$ that were considered here. In fact, IR divergences can appear in every process that allows for the emission of additional photons through higher-order corrections. Since photons are massless, they can have an arbitrarily small energy, meaning that for any detector with an energy threshold ΔE , there will be an arbitrary amount of photons with energies smaller than ΔE that escape detection [124].

In order to account for the impossibility to detect photons with energies below the detector threshold, real corrections involving additional photons have to be taken into account, as well. The emitted photons of these additional corrections are considered to be soft, i.e. they have energies lower than ΔE . It is the sum of the virtual and real corrections that delivers an IR-finite result [5]. Note that for the cancellation of IR divergence to be consistent, only real corrections that correspond to the chosen order of perturbation theory are considered.

Applying this procedure to the processes $H^+ \rightarrow W^+ h^0/H^0$ gives additional contributions in the form of the Feynman diagrams shown in Fig. 5.4. The first three amplitudes, (a) to (c), are Bremsstrahlung and G^+W^+ vertex diagrams, while the fourth, (d), is a 2HDM-specific vertex that contributes at NLO to the partial decay width, as well. In order to calculate these contributions, the *soft-photon approximation* can be used, meaning that the dependence on the photon momentum in the real corrections can be neglected anywhere but in the regions where it dominates the amplitude due to forming an IR pole [91].

Calculating all relevant real corrections in Fig. 5.4 gives the soft-photon contribution to the partial decay width. In order to express the results in a closed form, we switch to the rest frame of the incoming H^+ boson, determining the energy E_2 and momentum $|\vec{p}_2|$ of the outgoing W^+ boson to be

$$|\vec{p}_2| = \frac{\lambda(m_{H^\pm}^2, m_W^2, p_3^2)}{2m_{H^+}}, \quad (5.15)$$

$$E_2 = \sqrt{m_W^2 + |\vec{p}_2|^2}. \quad (5.16)$$

The well-known integrals [119] involved when solving the real corrections can be brought into a convenient form [52, 91],

$$\begin{aligned}
I_{11} &= 2\pi \left[\ln \left(\frac{4\Delta E^2}{\Lambda^2} \right) - 2 \right] , \\
I_{22} &= 2\pi \left[\ln \left(\frac{4\Delta E^2}{\Lambda^2} \right) + \frac{E_2}{|\vec{p}_2|} \ln \left(\frac{E_2 - |\vec{p}_2|}{E_2 + |\vec{p}_2|} \right) \right] , \\
I_{12} &= \frac{\pi}{2} \frac{E_2}{|\vec{p}_2|} \left[2 \ln \left(\frac{(E_2 + |\vec{p}_2|)^2}{m_W^2} \right) \ln \left(\frac{4\Delta E^2}{\Lambda^2} \right) - \ln^2 \left(\frac{E_2 - |\vec{p}_2|}{E_2 + |\vec{p}_2|} \right) \right. \\
&\quad \left. - 4 \operatorname{Li}_2 \left(1 - \frac{E_2 - |\vec{p}_2|}{E_2 + |\vec{p}_2|} \right) \right] ,
\end{aligned} \tag{5.17}$$

where Li_2 denotes the Spence dilogarithm function [125]. With these results at hand, the full NLO soft-photon contributions to the partial decay widths are given by [91]:

$$\begin{aligned}
\Gamma_{H^+W+h^0}^{\text{real}} &= \frac{-e^2}{4\pi^2} \Gamma_{H^+W+h^0}^{\text{LO}} \left[\frac{\Delta E}{m_{H^\pm}} + \frac{1}{4\pi} (I_{11} + I_{22} - 2I_{12}) \right] \\
&\quad + \frac{3e^2 g^2 c_{\beta-\alpha}^2 \Delta E^2}{512\pi^3 m_{H^\pm}^3} \lambda(m_{H^\pm}^2, m_W^2, m_{h^0}^2) ,
\end{aligned} \tag{5.18}$$

$$\begin{aligned}
\Gamma_{H^+W+H^0}^{\text{real}} &= \frac{-e^2}{4\pi^2} \Gamma_{H^+W+H^0}^{\text{LO}} \left[\frac{\Delta E}{m_{H^\pm}} + \frac{1}{4\pi} (I_{11} + I_{22} - 2I_{12}) \right] \\
&\quad + \frac{3e^2 g^2 s_{\beta-\alpha}^2 \Delta E^2}{512\pi^3 m_{H^\pm}^3} \lambda(m_{H^\pm}^2, m_W^2, m_{H^0}^2) .
\end{aligned} \tag{5.19}$$

As it was noted in Eq. (3.13), the NLO partial decay widths of the decays $H^+ \rightarrow W^+ h^0/H^0$ are given by the sum of all virtual contributions in Eq. (5.11) and the soft-photon contributions in Eq. (5.18) or Eq. (5.19), depending on the chosen process.

Note the explicit appearance of the detector threshold ΔE in the soft-photon contributions, meaning that the calculated NLO partial decay widths depend on the chosen value of the energy threshold. However, if the soft photon approximation is valid, this dependence is in general weak [52], and especially for the processes $H^+ \rightarrow W^+ h^0/H^0$, it was shown [91] that a change of ΔE over a large range leads to changes in the total NLO partial decay width of only up to a few permille. Compared to the electroweak corrections that are one to two orders of magnitude higher, this dependence is negligible.

Through the integrals in Eq. (5.17), the soft-photon corrections explicitly depend on the photon mass Λ , regularizing the IR divergent behaviour of the amplitudes in the limit $\Lambda \rightarrow 0$. Combining these real corrections with the IR divergent virtual vertex corrections considered in Sec. 5.2 leads to the cancellation of all Λ dependent terms, enabling us to take the correct limit $\Lambda \rightarrow 0$ in the final result. The cancellation of these terms was checked numerically in [91].

5.4. Gauge-Dependence of the NLO Amplitude

Due to the fact that we calculated all components of the one-loop amplitude in general R_ξ gauge, we can analytically check for its gauge-dependence. We already mentioned in Sec. 5.2 that the NLO partial decay width in Eq. (5.11) is invariant under a change of the tadpole scheme. However, if we are interested in the gauge-dependence of the angle counterterms only, the two tadpole schemes differ.

Consider e.g. the process $H^+ \rightarrow W^+ h^0$ in the standard tadpole scheme³. If we calculate the complete virtual NLO amplitude, but set the angle counterterms $\delta\alpha$ and $\delta\beta$ in Eq. (5.9) to zero, then the gauge-dependence of the amplitude can be extracted as

$$\begin{aligned} \mathcal{A}_{H^+W^+h^0, \delta\alpha=\delta\beta=0}^{\text{NLO,sta}} &= \left[\mathcal{A}_{H^+W^+h^0, \delta\alpha=\delta\beta=0}^{\text{NLO,sta}} \right]_{\xi=1} - (1 - \xi_W) \frac{g\Lambda_5 m_W^2 c_{\beta-\alpha} s_{\beta-\alpha}^2 (p_1 \cdot \varepsilon_2^*)}{16\pi^2 (m_{H^0}^2 - m_{h^0}^2)} \alpha_W \\ &\quad - (1 - \xi_Z) \frac{g\Lambda_5 m_Z^2 c_{\beta-\alpha} s_{\beta-\alpha}^2 (p_1 \cdot \varepsilon_2^*)}{32\pi^2 (m_{H^0}^2 - m_{h^0}^2)} \alpha_Z, \end{aligned} \quad (5.20)$$

where we indicate the standard tadpole scheme with the superscript “sta” and used the definition of α_W and α_Z according to Eq. (C.8). Through the explicit appearance of the gauge-fixing-parameters ξ_W and ξ_Z , the amplitude without the angle counterterms in Eq. (5.20) is manifestly gauge-dependent. Additionally, the integrals α_W and α_Z are UV-divergent. Since the full NLO amplitude has to be gauge-independent and UV-finite, it is clear that the residual UV-divergent and gauge-dependent terms in Eq. (5.20) have to be absorbed by $\delta\alpha$ and $\delta\beta$. As a consequence, a gauge-independent definition of the angle counterterms is impossible within the standard tadpole scheme.

Within this standard tadpole scheme, we have discussed two possible choices of fixing the angle counterterms: Kanemura’s scheme in Sec. 4.8.2 and a process-dependent scheme in Sec. 4.8.4. Considering the latter scheme, we saw that the definition of $\delta\beta$ over the process $A^0 \rightarrow \tau^+ \tau^-$ leads to a manifestly gauge-independent angle counterterm $\delta\beta$. The definition of $\delta\alpha$ over the decay $H^0 \rightarrow \tau^+ \tau^-$ gives a gauge-dependent angle counterterm, however. If we insert the residual UV-divergent and gauge-dependent part of $\delta\alpha$ from Eq. (4.186) into the counterterm in Eq. (5.9), we see that the angle counterterm gives exactly the same gauge-dependent contributions as in Eq. (5.20), but with opposite signs, so that the gauge-dependences cancel against each other. Consequently, the process-dependent definition of the angle counterterms leads to a manifestly gauge-independent NLO decay amplitude of the process $H^+ \rightarrow W^+ h^0$.

If we consider Kanemura’s scheme, the gauge-dependences of the angle counterterms are more intricate. If we insert the explicit forms of Eqs. (4.155) and (4.156) into the counterterm in Eq. (5.9), we realize that the UV-divergent gauge-dependent terms in the second line of Eq. (4.156) cancel against the residual gauge-dependence in Eq. (5.20), as it was the case with the process-dependent scheme. However, all other UV-finite gauge-dependent terms in Eqs. (4.155) and (4.156) remain within the NLO amplitude and consequently in the partial decay width. Therefore, we have shown analytically that Kanemura’s scheme leads to an overall gauge-dependent partial decay width, breaking the gauge-independence of the decay amplitude at NLO. Additionally, a look at Eq. (5.20) makes it clear that a gauge-independent definition of the angle counterterms, as proposed in [85], is not possible, since the gauge-dependent terms proportional to the UV-divergent integrals α_W and α_Z in Eq. (4.156) are necessary for the cancellation of all UV divergences. Therefore, we conclude that Kanemura’s scheme is not a suitable scheme for the definition of the angle counterterms, since it violates the gauge-independence of the NLO partial decay width.

While the NLO decay amplitude is tadpole-invariant, a change from the standard to the alternative tadpole scheme affects the gauge-dependence of the amplitude if the angle counterterms $\delta\alpha$ and $\delta\beta$ are set to zero. In this case, the shift of the vevs introduces additional gauge-dependent terms in the amplitude which precisely cancel the residual gauge-dependence in Eq. (5.20). Explicitly, the amplitude without the angle counterterms reads

$$\mathcal{A}_{H^+W^+h^0, \delta\alpha=\delta\beta=0}^{\text{NLO,alt}} = \left[\mathcal{A}_{H^+W^+h^0, \delta\alpha=\delta\beta=0}^{\text{NLO,alt}} \right]_{\xi=1} \quad (5.21)$$

³The argumentation for the other process, $H^+ \rightarrow W^+ H^0$, is analogous and not stated in detail.

where the superscript “alt” now indicates the alternative tadpole scheme. Note that Eq. (5.21) holds for *all* gauge-fixing parameters $\xi \in \{\xi_W, \xi_Z, \xi_\gamma\}$, which means that the residual amplitude, with $\delta\alpha$ and $\delta\beta$ being set to zero, forms a gauge-independent subset by itself. As a consequence, the alternative tadpole scheme does not only allow for a gauge-independent definition of the angle counterterms, but it makes such a definition necessary in order to preserve the gauge-independence of the NLO decay amplitude.

The pinched scheme from Sec. 4.8.3 introduces angle counterterms which are manifestly gauge-independent by construction. Therefore, it is a suitable scheme for achieving an unambiguous gauge-independent NLO partial decay width. The same holds for the process-dependent scheme, where within the alternative tadpole scheme, the counterterms $\delta\alpha$ and $\delta\beta$ are manifestly gauge-independent, as shown in Eqs. (4.185) and (4.187). With respect to gauge-independence, the process-dependent scheme is a suitable renormalization scheme for the angle counterterms, as well.

On the other hand, the angle counterterms in Kanemura’s scheme are manifestly gauge-dependent within the alternative tadpole scheme. The gauge-dependence of $\delta\beta$ is independent of the chosen tadpole scheme and the same as before, explicitly stated in Eq. (4.155), while the gauge-dependence of $\delta\alpha$ in the alternative tadpole scheme is given by Eq. (4.157). It is exactly the gauge-dependence of these two terms that will remain in the NLO partial decay width. Therefore, Kanemura’s scheme breaks the gauge-independence of the NLO amplitude, independently of the chosen tadpole scheme. However, a gauge-independent definition of the angle counterterms in Kanemura’s scheme would in principle be possible within the alternative tadpole scheme, since the integrals in Eqs. (4.155) and (4.157) are UV-finite, but as it was mentioned in Sec. 4.8.2, the extraction of these gauge-dependent parts would not be unique.

 The Decay $H^0 \rightarrow Z^0 Z^0$ at Next-to-Leading Order

The second process to be considered is the decay of the heavy Higgs boson H^0 into a pair of Z^0 bosons. The partial decay width of the H^0 corresponding to this decay is proportional to $c_{\beta-\alpha}^2$. As such, the decay is expected to be highly suppressed, since experimental data gives a value of $s_{\beta-\alpha}$ very close to unity [32]. As a second restriction, the mass of the heavy Higgs has to be chosen such that the decay occurs on-shell. Nevertheless, it is still worth studying the process, since it is the only process of the scalar-vector-vector topology that contains physical particles and that could happen on-shell (together with $H^0 \rightarrow W^+ W^-$, which we do not consider here in order to avoid IR divergences).

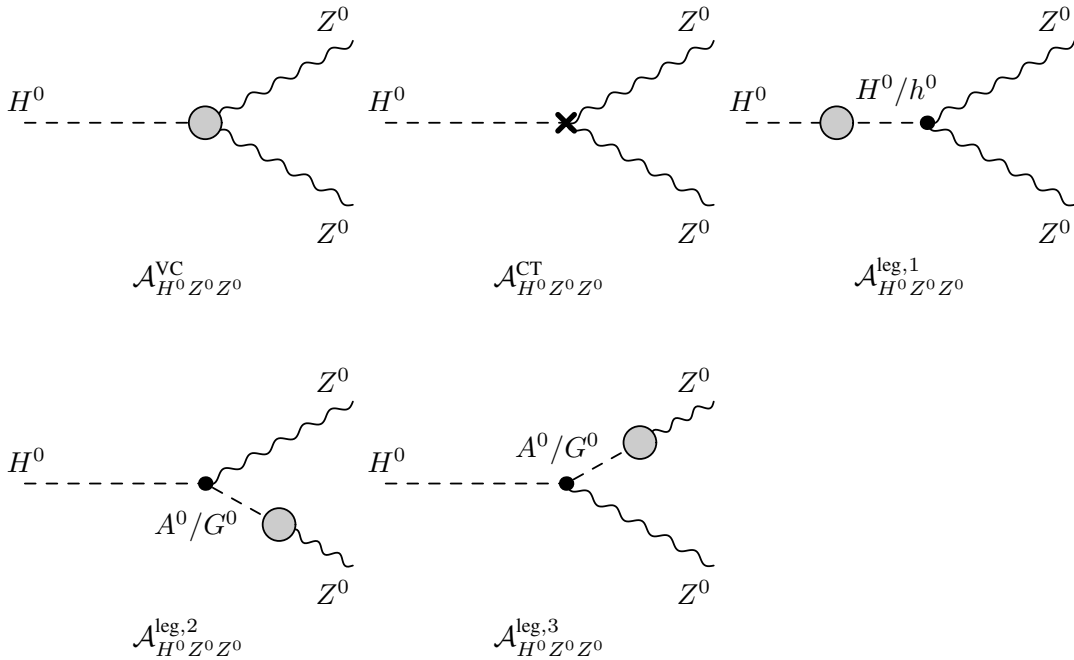


Figure 6.1.: NLO virtual corrections to the decays $H^0 \rightarrow Z^0 Z^0$. The one-loop amplitude $\mathcal{A}_{H^0 Z^0 Z^0}^{\text{1loop}}$ consists of all virtual vertex corrections $\mathcal{A}_{H^0 Z^0 Z^0}^{\text{VC}}$, the vertex counterterm $\mathcal{A}_{H^0 Z^0 Z^0}^{\text{CT}}$ as well as the external leg corrections $\mathcal{A}_{H^0 Z^0 Z^0}^{\text{leg},i}$ ($i = 1, 2, 3$).

6.1. The Partial Decay Width at LO

The LO partial decay width of the process is determined by the tree-level vertex $H^0 Z^0 Z^0$. With the generic notation of Sec. 3.1, the process describes the decay of the heavy Higgs boson H^0 with momentum p_1 into the two Z^0 bosons with momenta p_2, p_3 . The vector bosons have the polarizations λ_2 and λ_3 and their Lorentz structure is given by polarization vectors $\varepsilon_{2,\mu}^* := \varepsilon_{\lambda_2,\mu}^*(p_2)$ and $\varepsilon_{3,\nu}^* := \varepsilon_{\lambda_3,\nu}^*(p_3)$, respectively. The decay amplitude at LO explicitly reads

$$\begin{aligned} \mathcal{A}_{H^0 Z^0 Z^0}^{\text{LO}} &= \frac{g c_{\beta-\alpha} m_W}{c_W^2} g^{\mu\nu} \varepsilon_{2,\mu}^* \varepsilon_{3,\nu}^* \\ &= \frac{g c_{\beta-\alpha} m_W}{c_W^2} (\varepsilon_2^* \cdot \varepsilon_3^*) . \end{aligned} \quad (6.1)$$

In order to calculate the partial decay width, the absolute square of the amplitude has to be taken. Since we are not interested in the polarization states of the outgoing Z^0 bosons, we sum over all degrees of freedom by using the polarization sum

$$\begin{aligned} \sum_{\lambda_2, \lambda_3} (\varepsilon_2 \cdot \varepsilon_3) (\varepsilon_2^* \cdot \varepsilon_3^*) &= g^{\mu\nu} g^{\rho\sigma} \sum_{\lambda_2, \lambda_3} \varepsilon_{2,\mu} \varepsilon_{2,\rho}^* \varepsilon_{3,\nu} \varepsilon_{3,\sigma}^* \\ &= g_{\mu\nu} g_{\rho\sigma} \left(-g^{\mu\rho} + \frac{p_2^\mu p_2^\rho}{m_Z^2} \right) \left(-g^{\nu\sigma} + \frac{p_3^\nu p_3^\sigma}{m_Z^2} \right) \\ &= 3 + \frac{m_{H^0}^4}{4m_Z^4} - \frac{m_{H^0}^2}{m_Z^2} . \end{aligned} \quad (6.2)$$

The partial decay width at LO is gained by inserting Eq. (6.1) into the general formula in Eq. (3.7) and by using the polarization sum as stated above. The two Z^0 bosons in the final state are indistinguishable, therefore, the statistical factor $S = 1/2$ of the process has to be taken into account. Explicitly, the LO partial decay width reads:

$$\Gamma_{H^0 Z^0 Z^0}^{\text{LO}} = \frac{g^2 c_{\beta-\alpha}^2 m_W^2}{32\pi c_W^4 m_{H^0}^3} \lambda(m_{H^0}^2, m_Z^2, m_Z^2) \left(3 + \frac{m_{H^0}^4}{4m_Z^4} - \frac{m_{H^0}^2}{m_Z^2} \right) . \quad (6.3)$$

6.2. The Partial Decay Width at NLO

At NLO, from all possible contributions to the decay amplitude, as shown in Fig. 6.1, only a few are relevant. The external leg corrections $\mathcal{A}_{H^0 Z^0 Z^0}^{\text{leg},1}$ introduce a mixing between the H^0 and h^0 fields. This mixing vanishes due to the on-shell renormalization condition for the H^0 leg, as presented in Sec. 4.7. The other two external leg corrections, namely $\mathcal{A}_{H^0 Z^0 Z^0}^{\text{leg},2}$ and $\mathcal{A}_{H^0 Z^0 Z^0}^{\text{leg},3}$, vanish due to the transversality of the external on-shell Z^0 bosons. Hence, the only relevant terms for the process at one-loop level are the vertex corrections and the NLO counterterm:

$$\mathcal{A}_{H^0 Z^0 Z^0}^{\text{1loop}} = \mathcal{A}_{H^0 Z^0 Z^0}^{\text{VC}} + \mathcal{A}_{H^0 Z^0 Z^0}^{\text{CT}} . \quad (6.4)$$

For the one-loop vertex corrections $\mathcal{A}_{H^0 Z^0 Z^0}^{\text{VC}}$, all diagrams in Fig. 6.2 have been calculated with `FeynArts` and `FeynCalc` in general R_ξ gauge. Note that the $H^0 Z^0 Z^0$ vertex is not invariant under the shift of the vacuum expectation values when changing from the standard to the alternative tadpole scheme, as it was demonstrated in Eq. (4.80). Consequently, if one of the renormalization schemes defined by the different treatment of the tadpoles in Sec. 4.4.2 is chosen, the NLO vertex corrections of the process consist not only of all diagrams in Fig. 6.2, but additionally, the tadpole diagrams in Fig. 6.3 have to be calculated and added to $\mathcal{A}_{H^0 Z^0 Z^0}^{\text{VC}}$.

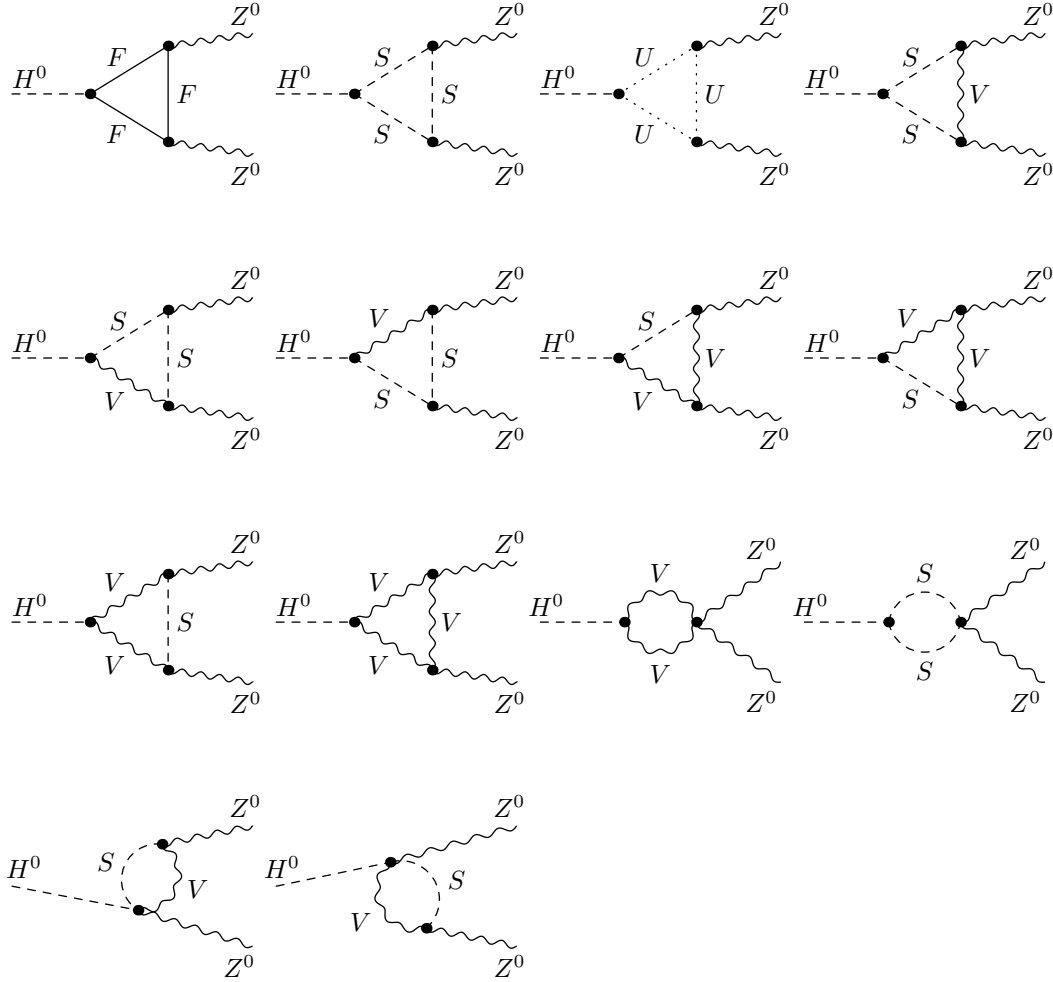


Figure 6.2.: All NLO vertex corrections to the decays $H^0 \rightarrow Z^0 Z^0$. All virtual vertex corrections $\mathcal{A}_{H^0 Z^0 Z^0}^{\text{VC}}$ are shown, grouped by their topological structure. The diagrams contain contributions from fermions F , scalar bosons S , ghosts U and gauge bosons V .

In contrast to the processes that were considered in Chapter 5, where the LO amplitudes factorized from the complete NLO vertex corrections, the process $H^0 \rightarrow Z^0 Z^0$ introduces an additional Lorentz structure through some of the loops in Fig. 6.2. To make these additional terms explicit, the one-loop vertex corrections may be split up according to their Lorentz structure,

$$\mathcal{A}_{H^0 Z^0 Z^0}^{\text{VC}} = \mathcal{A}_{H^0 Z^0 Z^0}^{\text{LO}} \mathcal{F}_{H^0 Z^0 Z^0}^{\text{VC},1} + \frac{g c_{\beta-\alpha} m_W (p_2 \cdot \varepsilon_3^*) (p_3 \cdot \varepsilon_2^*)}{c_W^2 m_{H^0}^2} \mathcal{F}_{H^0 Z^0 Z^0}^{\text{VC},2}, \quad (6.5)$$

with $\mathcal{F}_{H^0 Z^0 Z^0}^{\text{VC},1}$ being the form factor of the LO Lorentz structure and $\mathcal{F}_{H^0 Z^0 Z^0}^{\text{VC},2}$ being the form factor of the Lorentz structure that is induced by the one-loop corrections. Due to the appearance of this additional Lorentz structure, Eq. (6.2) is modified to account for the different contraction of four-momenta into the polarization sum:

$$\begin{aligned} \sum_{\lambda_2, \lambda_3} (\varepsilon_2 \cdot \varepsilon_3) (p_2 \cdot \varepsilon_3^*) (p_3 \cdot \varepsilon_2^*) &= g^{\mu\nu} p_2^\sigma p_3^\rho \sum_{\lambda_2, \lambda_3} \varepsilon_{2,\mu} \varepsilon_{2,\rho}^* \varepsilon_{3,\nu} \varepsilon_{3,\sigma}^* \\ &= g_{\mu\nu} p_{2,\sigma} p_{3,\rho} \left(-g^{\mu\rho} + \frac{p_2^\mu p_2^\rho}{m_Z^2} \right) \left(-g^{\nu\sigma} + \frac{p_3^\nu p_3^\sigma}{m_Z^2} \right) \\ &= m_{H^0}^2 + \frac{m_{H^0}^6}{8m_Z^4} - \frac{3m_{H^0}^4}{4m_Z^2}. \end{aligned} \quad (6.6)$$

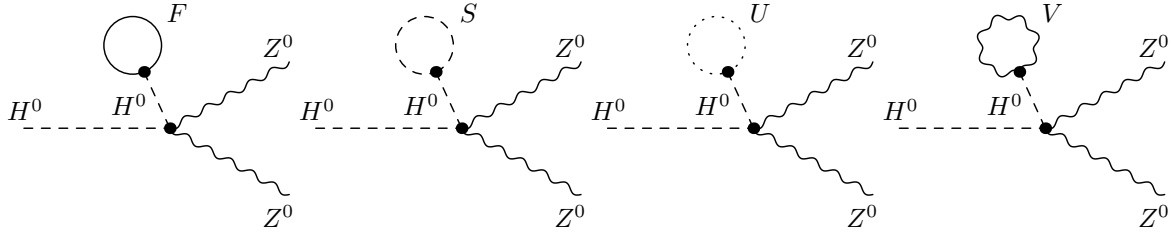


Figure 6.3.: NLO tadpole contributions to the process $H^0 \rightarrow Z^0 Z^0$. Shown are all tadpole diagrams which have to be added to the virtual vertex corrections $\mathcal{A}_{H^0 Z^0 Z^0}^{\text{VC}}$ if the alternative tadpole scheme is chosen. The particle content of the tadpole diagrams consist of fermions F , scalar bosons S , ghosts U and gauge bosons V .

In order to construct the counterterm, the same expansion as in Eq. (5.8) for the angle counterterm $\delta c_{\beta-\alpha}$ is used. With this expansion, the counterterm for the whole process reads [79]

$$\begin{aligned} \mathcal{A}_{H^0 Z^0 Z^0}^{\text{CT}} &= \mathcal{A}_{H^0 Z^0 Z^0}^{\text{LO}} \left[\frac{\delta g}{g} + \frac{\delta m_Z^2}{m_Z^2} - \frac{\delta m_W^2}{2m_W^2} + \frac{\delta Z_{H^0 H^0}}{2} + \delta Z_{ZZ} \right. \\ &\quad \left. + \frac{s_{\beta-\alpha}}{c_{\beta-\alpha}} \left(\frac{\delta Z_{h^0 H^0}}{2} + \delta\alpha - \delta\beta \right) \right] \\ &\equiv \mathcal{A}_{H^0 Z^0 Z^0}^{\text{LO}} \mathcal{F}_{H^0 Z^0 Z^0}^{\text{CT}}, \end{aligned} \quad (6.7)$$

where we split up the counterterm multiplicatively into the LO amplitude, together with its Lorentz structure, and the form factor $\mathcal{F}_{H^0 Z^0 Z^0}^{\text{CT}}$. With all ingredients for the NLO partial decay width at hand, we insert the vertex corrections and the counterterm – Eqs. (6.5) and (6.7), respectively – into the general formula for the partial decay width in Eq. (3.12) and use the two polarization sums in Eqs. (6.2) and (6.6). The process does not contain any charged particles in the initial or final state and the virtual vertex corrections and counterterms introduce no IR divergences at the one-loop level. Thus, the the full partial decay width for the process $H^0 \rightarrow Z^0 Z^0$ at NLO is given by:

$$\begin{aligned} \Gamma_{H^0 Z^0 Z^0}^{\text{NLO}} &= \Gamma_{H^0 Z^0 Z^0}^{\text{LO}} \left(1 + 2 \operatorname{Re} \left[\mathcal{F}_{H^0 Z^0 Z^0}^{\text{VC},1} + \mathcal{F}_{H^0 Z^0 Z^0}^{\text{CT}} \right] \right. \\ &\quad \left. + \frac{m_{H^0}^4 - 6m_{H^0}^2 m_Z^2 + 8m_Z^4}{m_{H^0}^4 - 4m_{H^0}^2 m_Z^2 + 12m_Z^4} \operatorname{Re} \left[\mathcal{F}_{H^0 Z^0 Z^0}^{\text{VC},2} \right] \right). \end{aligned} \quad (6.8)$$

Note that $\mathcal{F}_{H^0 Z^0 Z^0}^{\text{VC},2}$ is the form factor of a Lorentz structure that is purely induced through some of the loops in Fig. 6.2. This Lorentz structure is unique to those diagrams and is not present in the counterterm of the process, nor in any other part of the NLO amplitude. As such, this form factor must be UV-finite and gauge-fixing-parameter independent by itself, both of which has been checked numerically. Additionally, $\mathcal{F}_{H^0 Z^0 Z^0}^{\text{VC},2}$ is invariant under the shift of the vacuum expectation values, since the Lorentz structure of the tadpole diagrams in Fig. 6.3 gives contributions to $\mathcal{F}_{H^0 Z^0 Z^0}^{\text{VC},1}$, only.

The notation of the partial decay width in Eq. (6.8) is kept in a generic form, valid for any renormalization scheme that is chosen. The actual choice of renormalization scheme determines the content of the form factors $\mathcal{F}_{H^0 Z^0 Z^0}^{\text{VC},1}$ and $\mathcal{F}_{H^0 Z^0 Z^0}^{\text{CT}}$. Explicitly, the form factor of the vertex corrections, $\mathcal{F}_{H^0 Z^0 Z^0}^{\text{VC},1}$, is determined by all vertex corrections in Fig. 6.2 and, in case that the alternative tadpole scheme is applied, additionally on the tadpole diagrams in

Fig. 6.3. The form factors of both the vertex corrections and of the counterterm depend on the renormalization scheme of the tadpoles. However, the combination of both terms in the first line of Eq. (6.8) is such that all terms that are induced when changing from the standard to the alternative tadpole scheme precisely cancel against each other. Therefore, the full NLO partial decay width of the process $H^0 \rightarrow Z^0 Z^0$ is tadpole-invariant.

6.3. Gauge-Dependence of the NLO Amplitude

As it was done in Sec. 5.4, we analyze the NLO decay amplitude with $\delta\alpha$ and $\delta\beta$ being set to zero, allowing us to identify residual gauge-dependent parts which are introduced through an unsuitable renormalization scheme of the mixing angles. Considering the NLO decay amplitude in the standard (superscript “sta”) and in the alternative (superscript “alt”) tadpole scheme, the gauge-dependences of the residual amplitudes take the form

$$\begin{aligned} \mathcal{A}_{H^0 Z^0 Z^0, \delta\alpha=\delta\beta=0}^{\text{NLO,sta}} &= \left[\mathcal{A}_{H^0 Z^0 Z^0, \delta\alpha=\delta\beta=0}^{\text{NLO,sta}} \right]_{\xi=1} + (1 - \xi_W) \frac{g\Lambda_5 m_W m_Z^2 c_{\beta-\alpha} s_{\beta-\alpha}^2 (\varepsilon_2^* \cdot \varepsilon_3^*)}{16\pi^2 (m_{H^0}^2 - m_{h^0}^2)} \alpha_W \\ &\quad + (1 - \xi_Z) \frac{g\Lambda_5 m_W m_Z^2 c_{\beta-\alpha} s_{\beta-\alpha}^2 (\varepsilon_2^* \cdot \varepsilon_3^*)}{32\pi^2 c_W^2 (m_{H^0}^2 - m_{h^0}^2)} \alpha_Z, \end{aligned} \quad (6.9)$$

$$\mathcal{A}_{H^0 Z^0 Z^0, \delta\alpha=\delta\beta=0}^{\text{NLO,alt}} = \left[\mathcal{A}_{H^0 Z^0 Z^0, \delta\alpha=\delta\beta=0}^{\text{NLO,alt}} \right]_{\xi=1}, \quad (6.10)$$

for all $\xi \in \{\xi_W, \xi_Z, \xi_\gamma\}$, where we used the definition of α_W and α_Z from Eq. (C.8). The discussion is analogous to Sec. 5.4. In the standard tadpole scheme, the process-dependent definition of the mixing angles cancels the residual gauge-dependence in Eq. (6.9), while Kanemura’s scheme leads to a gauge-dependent NLO decay width. In the alternative tadpole scheme, $\delta\alpha$ and $\delta\beta$ have to be defined in a gauge-independent way, which is achieved by the pinched and the process-dependent scheme, but not by Kanemura’s scheme. With respect to the gauge-dependence, we have shown that also for the process $H^0 \rightarrow Z^0 Z^0$, the pinched and process-dependent schemes are suitable renormalization schemes for the mixing angles, while Kanemura’s scheme breaks gauge-independence.

 The Decay $H^0 \longrightarrow h^0 h^0$ at Next-to-Leading Order

The last considered process is the decay of a heavy Higgs H^0 into two lighter Higgses h^0 . Such Higgs-to-Higgs decays were rather scarcely found in literature for the 2HDM until recently, since they have not been observed so far and their observation at colliders is in general difficult. However, with the LHC now being operated at a center-of-mass energy of 13 TeV and with an increase of luminosity in the long run, the Higgs-to-Higgs decays begin to receive more attention. Despite the fact that the observed Higgs boson is in good agreement with the SM [25,26], the Higgs self-interactions serve as an indicator for BSM physics, since especially in the 2HDM, the NLO corrections to the self-interactions can become high and deviate considerably from the SM [56,126]. Additionally, the triple-scalar vertices of the 2HDM are the only trilinear vertices containing Λ_5 , which necessitates its renormalization at NLO.

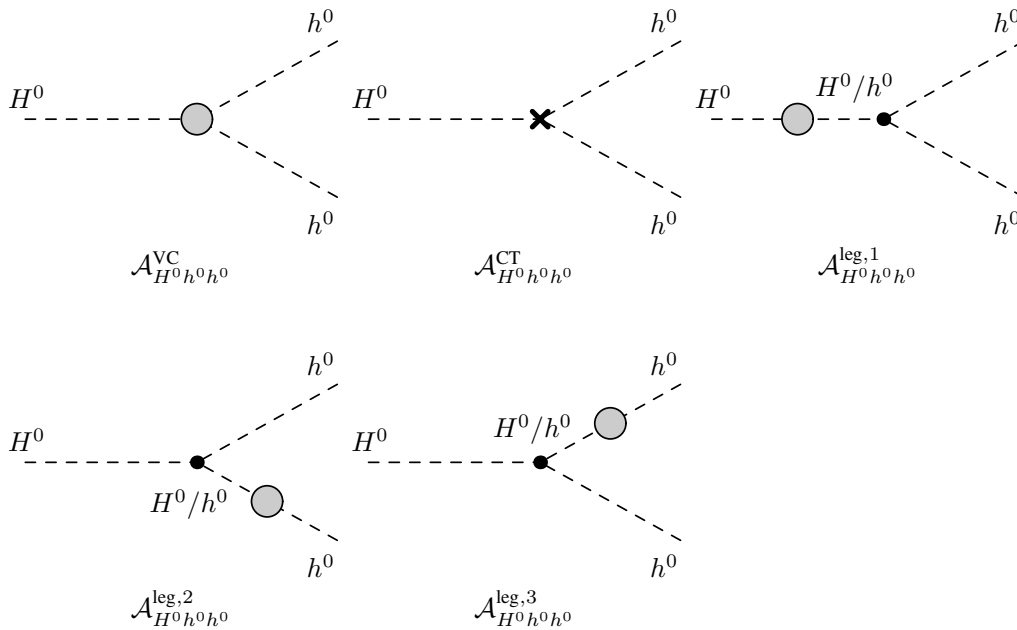


Figure 7.1.: NLO virtual corrections to the decay $H^0 \longrightarrow h^0 h^0$. The NLO amplitude $\mathcal{A}_{H^0 h^0 h^0}^{\text{loop}}$ consists of all virtual vertex corrections $\mathcal{A}_{H^0 h^0 h^0}^{\text{VC}}$, the vertex counterterm $\mathcal{A}_{H^0 h^0 h^0}^{\text{CT}}$ as well as the external leg corrections $\mathcal{A}_{H^0 h^0 h^0}^{\text{leg},i}$ ($i = 1, 2, 3$).

7.1. The Partial Decay Width at LO

The decay amplitude at LO equals the coupling constant $g_{H^0 h^0 h^0}$ for the $H^0 h^0 h^0$ tree-level vertex. Since all three particles are scalars, the vertex has the structure of a Lorentz scalar, and is therefore particularly simple. Explicitly, the LO decay amplitude reads

$$\begin{aligned} \mathcal{A}_{H^0 h^0 h^0}^{\text{LO}} &= g_{H^0 h^0 h^0} \\ &= \frac{-g c_{\beta-\alpha}}{2m_W s_{2\beta}} \left(s_{2\alpha} (2m_{h^0}^2 + m_{H^0}^2) - 2 \frac{m_W^2}{g^2} \Lambda_5 (3s_{2\alpha} - s_{2\beta}) \right). \end{aligned} \quad (7.1)$$

As spin 0 particles, the initial and final Higgses have no additional degrees of freedom. Therefore, the sum over all external degrees of freedom in Eq. (3.3) can be omitted. The statistical factor is $S = 1/2$, since the final states are indistinguishable. The partial decay width of the process at LO is directly given by inserting the absolute square of the amplitude into Eq. (3.7):

$$\Gamma_{H^0 h^0 h^0}^{\text{LO}} = \frac{g^2 c_{\beta-\alpha}^2 \lambda(m_{H^0}^2, m_{h^0}^2, m_{h^0}^2)}{128\pi m_W^2 m_{H^0}^3 s_{2\beta}^2} \left(s_{2\alpha} (2m_{h^0}^2 + m_{H^0}^2) - 2 \frac{m_W^2}{g^2} \Lambda_5 (3s_{2\alpha} - s_{2\beta}) \right)^2. \quad (7.2)$$

7.2. The Partial Decay Width at NLO

At NLO, we consider all one-loop contributions to the Higgs-to-Higgs decay given in Fig. 7.1. The external leg corrections consist of either off-diagonal or diagonal field mixing contributions $H^0 h^0$, $h^0 H^0$, $H^0 H^0$ or $h^0 h^0$, all of which vanish due to the on-shell renormalization conditions of the external fields, as introduced in Sec. 4.7. Hence, the full one-loop contribution to the decay amplitude is given by

$$\mathcal{A}_{H^0 h^0 h^0}^{\text{1loop}} = \mathcal{A}_{H^0 h^0 h^0}^{\text{VC}} + \mathcal{A}_{H^0 h^0 h^0}^{\text{CT}}. \quad (7.3)$$

All vertex corrections of the process are shown in Fig. 7.2, grouped by their topological structure. Just as it was the case for the process considered in the previous chapter, the vertex $H^0 h^0 h^0$ is not invariant under a shift of the vevs when changing from the standard to the alternative tadpole scheme. As a result, additional tadpole diagrams have to be taken into account if the alternative tadpole scheme is chosen. In that case, the relevant tadpole contributions, as shown in Fig. 7.3, have to be added to the vertex corrections $\mathcal{A}_{H^0 h^0 h^0}^{\text{VC}}$.

Since the process $H^0 \rightarrow h^0 h^0$ contains only external scalar particles, the LO amplitude factorizes from the one-loop vertex corrections. Calling the form factor of the vertex corrections $\mathcal{F}_{H^0 h^0 h^0}^{\text{VC}}$, the amplitude of the vertex corrections is decomposed as

$$\mathcal{A}_{H^0 h^0 h^0}^{\text{VC}} = \mathcal{A}_{H^0 h^0 h^0}^{\text{LO}} \mathcal{F}_{H^0 h^0 h^0}^{\text{VC}}. \quad (7.4)$$

In contrast to the other two processes, where the counterterms were adopted from the literature, the counterterm of the process $H^0 \rightarrow h^0 h^0$ shall be derived here. By doing so, we gain some insight on symmetry factors that play a role for constructing the whole counterterm, thus preventing a potential pitfall. To that end, it is useful to define the two triple-Higgs coupling constants [55]

$$g_{h^0 h^0 h^0} = \frac{3g}{2m_W s_{2\beta}} \left(4 \frac{m_W^2}{g^2} c_{\alpha+\beta} c_{\beta-\alpha}^2 \Lambda_5 - m_{h^0}^2 (2c_{\alpha+\beta} + s_{2\alpha} s_{\beta-\alpha}) \right), \quad (7.5)$$

$$g_{H^0 H^0 h^0} = \frac{g s_{\beta-\alpha}}{2m_W s_{2\beta}} \left(s_{2\alpha} (m_{h^0}^2 + 2m_{H^0}^2) - 2 \frac{m_W^2}{g^2} \Lambda_5 (3s_{2\alpha} + s_{2\beta}) \right). \quad (7.6)$$

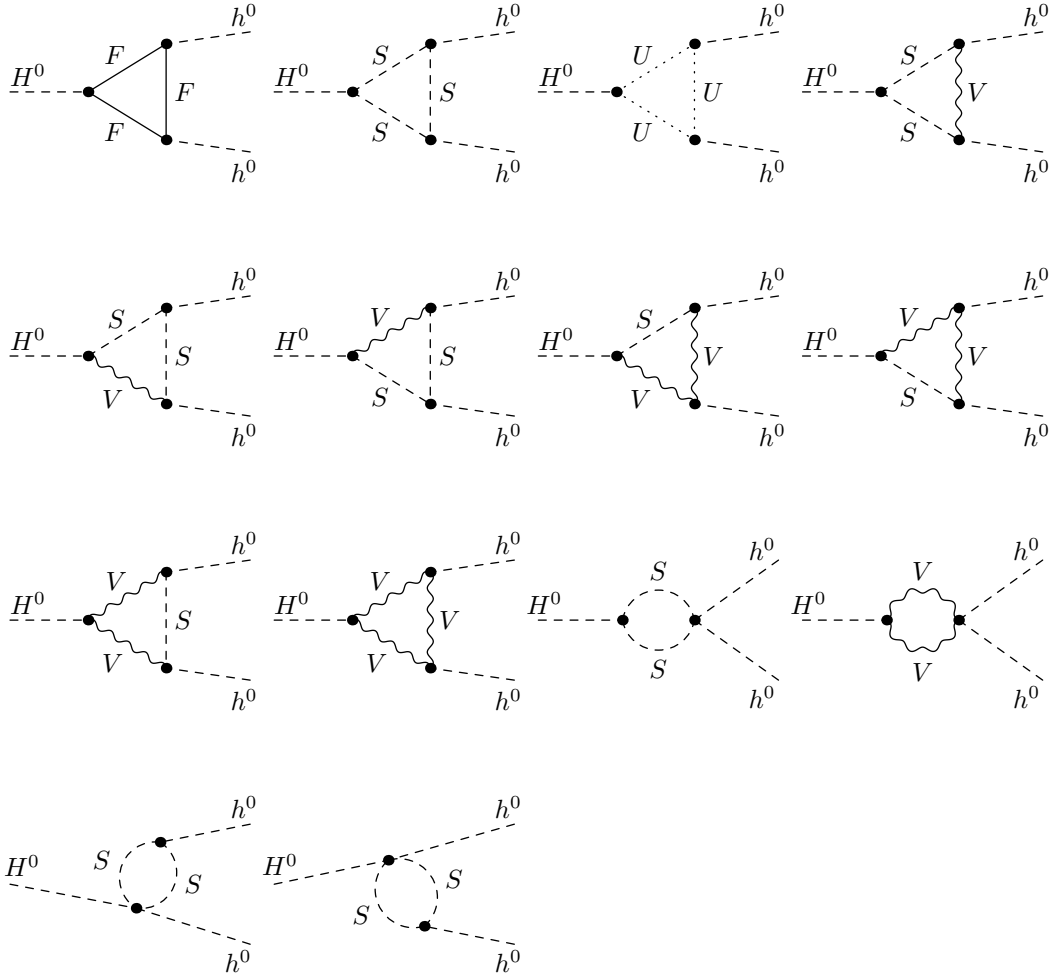


Figure 7.2.: All NLO vertex corrections to the decays $H^0 \rightarrow h^0 h^0$. All virtual vertex corrections $\mathcal{A}_{H^0 h^0 h^0}^{\text{VC}}$ are shown, grouped by their topological structure. The diagrams contain contributions from fermions F , scalar bosons S , ghosts U and gauge bosons V .

in addition to the already defined constant $g_{H^0 h^0 h^0}$ in Eq. (7.1). In order to derive the counterterm, the 2HDM potential in Eq. (A.2) is transformed to the mass basis via the inverse of the relations Eqs. (2.24) – (2.26). We consider only the parts of the bare interaction Lagrangian that contribute to the $H^0 h^0 h^0$ vertex counterterm, i.e. the parts which contain the bare CP-even Higgs fields that have to be renormalized according to Eq. (4.111). Omitting the tree-level coupling and all terms that are not proportional to the renormalized fields $H^0 h^0 h^0$, the relevant part of the interaction Lagrangian reads

$$\begin{aligned}
\mathcal{L}_{\text{int,rel}} &= \frac{-ig_{h^0 h^0 h^0}}{3!} h_0^0 h_0^0 h_0^0 + \frac{-ig_{H^0 h^0 h^0}}{2!} H_0^0 h_0^0 h_0^0 + \frac{-ig_{H^0 H^0 h^0}}{2!} H_0^0 H_0^0 h_0^0 \\
&\stackrel{\text{NLO}}{\approx} \left[\frac{-ig_{h^0 h^0 h^0}}{3!} \frac{3\delta Z_{h^0 H^0}}{2} + \frac{-ig_{H^0 h^0 h^0}}{2!} \left(\delta Z_{h^0 h^0} + \frac{\delta Z_{H^0 H^0}}{2} \right) \right. \\
&\quad \left. + \frac{-ig_{H^0 H^0 h^0}}{2!} \delta Z_{H^0 h^0} \right] H^0 h^0 h^0 .
\end{aligned} \tag{7.7}$$

The counterterm is derived through a functional derivative with respect to the three renormalized fields H^0 , h^0 and h^0 ,

$$\frac{\delta}{\delta H^0} \frac{\delta}{\delta h^0} \frac{\delta}{\delta h^0} (i\mathcal{L}_{\text{int,rel}}) , \tag{7.8}$$

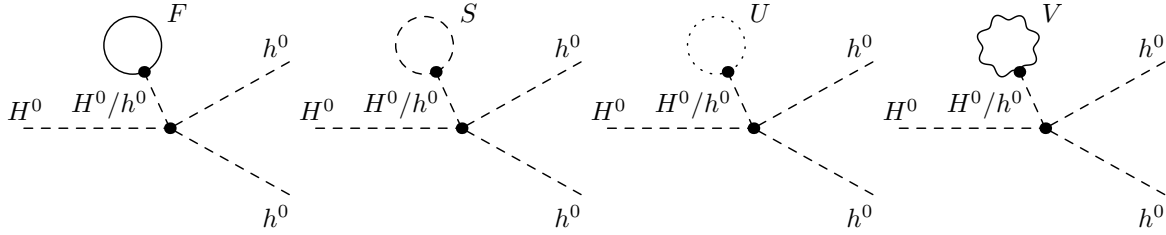


Figure 7.3.: NLO tadpole contributions to the process $H^0 \rightarrow h^0 h^0$. Shown are all tadpole diagrams which have to be added to the virtual vertex corrections $\mathcal{A}_{H^0 h^0 h^0}^{\text{VC}}$ if the alternative tadpole scheme is chosen. The particle content of the tadpole diagrams consist of fermions F , scalar bosons S , ghosts U and vector bosons V .

together with adding the renormalized tree-level vertex $\delta g_{H^0 h^0 h^0}$. Explicitly, the counterterm of the process reads

$$\begin{aligned} \mathcal{A}_{H^0 h^0 h^0}^{\text{CT}} &= g_{h^0 h^0 h^0} \frac{\delta Z_{h^0 H^0}}{2} + g_{H^0 h^0 h^0} \left(\delta Z_{h^0 h^0} + \frac{\delta Z_{H^0 H^0}}{2} \right) + g_{H^0 H^0 h^0} \delta Z_{H^0 h^0} \\ &+ \delta g_{H^0 h^0 h^0} , \end{aligned} \quad (7.9)$$

with the NLO expansion of the coupling constant $g_{H^0 h^0 h^0}$ given by

$$\begin{aligned} \delta g_{H^0 h^0 h^0} &= \left(g_{H^0 h^0 h^0} - \frac{2\Lambda_5 m_W c_{\beta-\alpha} (3s_{2\alpha} - s_{2\beta})}{g s_{2\beta}} \right) \left[\frac{\delta g}{g} - \frac{\delta m_W^2}{2m_W^2} \right] \\ &- \frac{g c_{\beta-\alpha}}{2m_W s_{2\beta}} \left[2s_{2\alpha} \delta m_{h^0}^2 + s_{2\alpha} \delta m_{H^0}^2 - \frac{2m_W^2 (3s_{2\alpha} - s_{2\beta})}{g^2} \delta \Lambda_5 \right] \\ &+ \left[\frac{g c_{\beta-\alpha} c_{2\alpha}}{m_W s_{2\beta}} \left(\frac{6m_W^2 \Lambda_5}{g^2} - 2m_{h^0}^2 - m_{H^0}^2 \right) - \frac{s_{\beta-\alpha}}{c_{\beta-\alpha}} g_{H^0 h^0 h^0} \right] \delta \alpha \\ &- \frac{2c_{2\beta}}{s_{2\beta}} \left(g_{H^0 h^0 h^0} + \frac{\Lambda_5 m_W c_{\beta-\alpha}}{g} \right) \delta \beta . \end{aligned} \quad (7.10)$$

Inserting this counterterm and the factorized vertex corrections from Eq. (7.4) into Eq. (3.12) results in the partial decay width for the process $H^0 \rightarrow h^0 h^0$ at NLO:

$$\begin{aligned} \Gamma_{H^0 h^0 h^0}^{\text{NLO}} &= \Gamma_{H^0 h^0 h^0}^{\text{LO}} \left(1 + 2 \text{Re} \left[\mathcal{F}_{H^0 h^0 h^0}^{\text{VC}} \right] \right) \\ &+ \frac{\lambda(m_{H^0}^2, m_{h^0}^2, m_{h^0}^2)}{16\pi m_{H^0}^3} \text{Re} \left[(\mathcal{A}_{H^0 h^0 h^0}^{\text{LO}})^* \mathcal{A}_{H^0 h^0 h^0}^{\text{CT}} \right] . \end{aligned} \quad (7.11)$$

We point out again that as with the previous processes, the generic form of the partial decay width in Eq. (7.11) is independent of the renormalization scheme. Choosing a scheme is equivalent to determining the content of the vertex corrections form factor $\mathcal{F}_{H^0 h^0 h^0}^{\text{VC}}$ as well as the counterterm $\mathcal{A}_{H^0 h^0 h^0}^{\text{CT}}$. In any case, the former will contain all diagrams shown in Fig. 7.2, and if the alternative tadpole scheme is chosen, the tadpole diagrams in Fig. 7.3 have to be taken into account, as well. As for the previous processes, the decay $H^0 \rightarrow h^0 h^0$ is invariant under the change from the standard to the alternative tadpole scheme if the counterterm $\delta \Lambda_5$ is renormalized either in a process-dependent or in the improved $\overline{\text{MS}}$ scheme.

7.3. Gauge-Dependence of the NLO Amplitude

Due to the intricate structure of the vertex corrections and the vertex counterterm of the process, we limit the discussion about gauge-dependence to a qualitative level, without stating the explicit form of the residual gauge-dependences.

If we calculate the complete NLO decay amplitude within the standard tadpole scheme, but set $\delta\alpha$, $\delta\beta$ and $\delta\Lambda_5$ to zero, we realize that this residual amplitude contains UV-divergent gauge-dependent parts. Renormalizing the angle counterterms either through Kanemura's or the process-dependent scheme leads to the cancellation of some of the UV-divergent gauge-dependent parts. The residual UV-divergent gauge-dependent parts are then cancelled by $\delta\Lambda_5$, defined either over the $\overline{\text{MS}}$ condition, cf. Sec. 4.9.1 and Sec. 4.9.2, or through the process $H^0 \rightarrow A^0 A^0$, as discussed in Sec. 4.9.3. However, the additional UV-finite gauge-dependent terms in Eqs. (4.155) and (4.156) present in Kanemura's scheme remain in the amplitude, leading to a gauge-dependent NLO decay width when using Kanemura's scheme.

Changing to the alternative tadpole scheme leads to the cancellation of the UV-divergent gauge-dependent parts within the residual amplitude, which allows for a gauge-independent definition of the angle counterterms $\delta\alpha$ and $\delta\beta$ and for the counterterm $\delta\Lambda_5$. The latter can be achieved by the improved $\overline{\text{MS}}$ condition of Sec. 4.9.2 and the process-dependent scheme of Sec. 4.9.3, while the unambiguous gauge-independent definition of the angle counterterms is accomplished through the pinched scheme of Sec. 4.8.3 or the process-dependent scheme of Sec. 4.8.4. Kanemura's scheme leads to a gauge-dependent NLO width through Eqs. (4.155) and (4.157) in the alternative tadpole scheme, as well.

From these discussions we conclude that with respect to gauge-independence for the process $H^0 \rightarrow h^0 h^0$, suitable renormalization schemes for the mixing angles $\delta\alpha$ and $\delta\beta$ are the pinched scheme and the process-dependent scheme, both leading to an overall gauge-independent NLO decay width. With these choices of the angle counterterms, the definitions of $\delta\Lambda_5$ through the usual or improved $\overline{\text{MS}}$ scheme or through a process-dependent scheme lead to a gauge-independent NLO decay width. We point out that if besides achieving a gauge-independent NLO decay width, we additionally require gauge-independent definitions of the counterterms $\delta\alpha$, $\delta\beta$ and $\delta\Lambda_5$, the alternative tadpole scheme has to be chosen, and Kanemura's scheme is ruled out. If additionally the counterterms shall be defined in a process-independent way, the only valid scheme for $\delta\alpha$ and $\delta\beta$ presented in this thesis is the pinched scheme, while for $\delta\Lambda_5$, the improved $\overline{\text{MS}}$ scheme has to be chosen.

In the previous three chapters, we considered distinct 2HDM-specific processes and calculated their NLO partial decay widths. In Chapter 4, we established several renormalization schemes for the mixing angles α and β and for the parameter Λ_5 , some of which are manifestly process- and gauge-independent. For the MSSM, a “no-go theorem” was proposed [36] which states that a renormalization scheme for the mixing angle β may not be simultaneously gauge-independent, process-independent and numerically stable. The question arises if such a “no-go theorem” is applicable to the 2HDM as well. In the following, we turn to the numerical evaluation of the partial decay widths of all processes considered in this thesis. This allows us to compare the size of the NLO corrections between the different renormalization schemes for $\delta\alpha$, $\delta\beta$ and Λ_5 and to propose a renormalization scheme for the 2HDM which is simultaneously process-independent, gauge-independent and numerically stable.

8.1. Used Software Packages

For the calculation of the NLO decay widths, the Python program `2HDMCalc` was developed. The program links the `Mathematica` [127] package `FeynArts 3.9` [55], which generates the LO and NLO decay amplitudes for all processes considered in this thesis in general R_ξ gauge and with enabled CKM mixing. We used the model file for a CP-conserving 2HDM which was already implemented in the package. Additionally, all tadpole and self-energy amplitudes needed for the definition of the counterterms and wave function renormalization constants were generated in general R_ξ gauge.

The calculation of all amplitudes is performed by linking the `Mathematica` package `FeynCalc 8.2.0` [118] which resolves the Lorentz structures of the amplitudes and reduces all one-loop integrals in the amplitudes down to the well-known 't Hooft-Veltman integrals [119]. Within `2HDMCalc`, the counterterms of the processes considered in this thesis are generated dynamically out of the 2HDM Lagrangian by calling a `Mathematica` script. The counterterms, one-loop corrections and LO terms are then combined to the full partial decay widths as presented in the previous chapters. In case of the decays of the charged Higgs H^+ , the real corrections to the partial decay widths were implemented by hand.

For the numerical evaluation of the partial decay widths, a C++ program is executed within `2HDMCalc`. The program links the C++ library `LoopTools 2.12` [120], which evaluates all

't Hooft-Veltman integrals by using the specific parameter sets described in the next section. The output of `2HDMCalc` consists of the partial decay widths at LO and NLO for every renormalization scheme of the mixing angles and of Λ_5 that are considered in this thesis.

For all renormalization schemes, UV-finiteness of the NLO partial decay widths was checked numerically by using the `LoopTools` function `setdelta(Δ)`, which allows to set the UV-divergent term Δ , as given in Eq. (4.4), to arbitrary values. Since the NLO decay width must not depend on the value of Δ when all UV divergences are cancelled, this serves as a numerical check for UV-finiteness. All renormalization schemes for the angle counterterms and Λ_5 used in this thesis were checked for UV-finiteness by varying the parameter Δ over ten orders of magnitude and it was found that all schemes lead to UV-finite NLO amplitudes¹. Therefore, we did not consider UV divergences any more in the following numerical evaluations and set the UV-divergent term Δ to zero in `LoopTools`, which is also its default value.

8.2. Input Parameter Sets

In order to evaluate the NLO partial decay widths numerically, we need to specify all input parameters. These consist of the physical parameters given in Eq. (2.58), together with the CKM matrix elements which show up in the NLO amplitude through internal quark loops. In the following, we specify all input parameters that are necessary for the numerical evaluation of the partial decay widths in `2HDMCalc`.

- **Masses of SM particles and the SM-like Higgs boson:**

The masses of all SM particles are extracted from [128]. Within the 2HDM, we consider the lighter CP-even Higgs boson h^0 as the SM-like Higgs boson for all processes considered in this thesis. The current value of the SM-like Higgs boson mass is adopted from [129]. The table below lists all masses of SM particles and the SM-like Higgs.

Mass	Value in GeV	Mass	Value in GeV
m_W	80.398	m_u	0.190
m_Z	91.1876	m_d	0.190
m_{h^0}	125.09	m_s	0.190
m_e	$5.10998910 \cdot 10^{-4}$	m_c	1.4
m_μ	0.105658367	m_b	4.75
m_τ	1.77684	m_t	172.5

- **The Weinberg angle:**

With our set of 2HDM input parameters in Eq. (2.58), the Weinberg angle is a derived parameter and can be calculated according to Eq. (2.46) by using the gauge boson masses m_W and m_Z stated in the table above. Since the 2HDM model file implemented in `FeynArts` uses the sine and cosine of the Weinberg angle per default, we nevertheless explicitly state their values for convenience:

$$c_W = 0.88168, \quad s_W = 0.47185. \quad (8.1)$$

¹In case of the $\overline{\text{MS}}$ scheme for Λ_5 , the UV-divergent part of the counterterm $\delta\Lambda_5$ was extracted by using the process $H^0 \rightarrow A^0 A^0$ and implemented as the counterterm by using the function `setdelta(Δ)`, thus allowing for a numerical check of UV-finiteness even when an $\overline{\text{MS}}$ scheme is chosen.

- **The elementary charge:**

For the purpose of evaluating decay widths at NLO, it is sufficient to consider the tree-level value of the electric charge. The most precise measurement is given by the value of Sommerfeld's fine-structure constant α_{em} in the Thomson limit, which currently reads [46]

$$\alpha_{\text{em}} = \frac{1}{137.035999074} . \quad (8.2)$$

The `FeynArts` model file uses the elementary charge e instead of the fine-structure constant as an input parameter. In natural units, the conversion, and hence the value of e , is given by

$$e = \sqrt{4\pi\alpha_{\text{em}}} = 0.30282212089 . \quad (8.3)$$

- **The CKM matrix elements:**

The CP-violating phase in the CKM matrix is considered to be zero for all calculations performed in this thesis. Consequently, we consider the matrix to be real. The values of all entries of the CKM matrix are given by [46]

$$V_{\text{CKM}} = \begin{pmatrix} V_{ud} & V_{us} & V_{ub} \\ V_{cd} & V_{cs} & V_{cb} \\ V_{td} & V_{ts} & V_{tb} \end{pmatrix} = \begin{pmatrix} 0.97427 & 0.22536 & 0.00355 \\ -0.22522 & 0.97343 & 0.0414 \\ 0.00886 & -0.0405 & 0.99914 \end{pmatrix} . \quad (8.4)$$

- **Yukawa coupling constants of the 2HDM:**

The couplings between the fermions and the Higgs bosons is parametrized in the 2HDM model file in `FeynArts` in the form of three Yukawa coupling constants Y_1 , Y_2 and Y_3 . The actual form of the constants is expressed through trigonometric combinations of the mixing angles α and β and depends on the chosen 2HDM type. For the two 2HDM types that we presented in Sec. 2.6, the coupling constants explicitly read [57]:

2HDM type	Y_1	Y_2	Y_3
I	$\frac{c_\alpha}{s_\beta}$	$\frac{s_\alpha}{s_\beta}$	$-\frac{1}{t_\beta}$
II	$-\frac{s_\alpha}{c_\beta}$	$\frac{c_\alpha}{c_\beta}$	t_β

- **Detector sensitivity ΔE :** For the processes $H^+ \rightarrow W^+ h^0/H^0$, we included real corrections into the NLO partial decay width in order to cancel all occurring IR divergences, cf. Sec. 5.3. As a consequence, we added the NLO soft-photon corrections in Eqs. (5.18) and (5.19) to the virtual NLO partial decay width. The former depend explicitly on the detector sensitivity ΔE . It was shown in [91] that this dependence is small. Within the scope of this thesis, we fix the value to

$$\Delta E = 10 \text{ GeV} . \quad (8.5)$$

The other parameters that have to be set are the missing masses of the extended scalar sector of the 2HDM, namely m_{H^0} , m_{A^0} and m_{H^\pm} , as well as the scalar mixing angles α and β and the parameter Λ_5 . We consider those as our *free* parameters. In principle, we could set

those parameters to arbitrary values, since we are only interested in an analysis of different renormalization schemes for α , β and Λ_5 with respect to numerical stability. However, an unphysical combination of input parameters can lead to the violation of perturbativity bounds, which results in the NLO corrections becoming very large independently of the renormalization scheme that is chosen. This effect has to be differed from numerical instability in the sense we are discussing it within the scope of this thesis, which is the result of choosing an unsuitable renormalization scheme which yields very large NLO corrections for almost all chosen input parameter set.

In order to isolate the two effects and analyze the different renormalization schemes only with respect to numerical stability as the term is used in this thesis, we choose to use only specific input parameter sets which are consistent with strict experimental and theoretical bounds. Therefore, we consider only input parameters which are still not excluded by theory and experiment. To that end, the tool **ScannerS** [130] was used. The program scans through the parameter space of the 2HDM and generates suitable input parameter sets, regarding several theoretical and experimental constraints that shall be briefly discussed in the following.

From the theoretical point of view, by fixing one CP-even minimum of the tree-level 2HDM potential, no additional charge-breaking or CP-violating vevs are allowed anymore [131–133]. This chosen CP-even minimum is required to be the global minimum of the potential [134]. Furthermore, tree-level unitarity has to be respected [135, 136] and the 2HDM potential has to be bounded from below [137].

Every parameter set generated by **ScannerS** has to obey all theoretical constraints mentioned above [138]. Additionally, the parameters have to be consistent with current experimental data. The 2HDM parameter sets generated by the program have to fulfill 95% consistency with the oblique S , T and U parameters, therefore satisfying electroweak precision measurements [19–21, 139–142]. Additionally, LEP results [143] and recent LHC results [144, 145] are included, which restrict the mass of the charged Higgs to be above $\mathcal{O}(100 \text{ GeV})$, depending on the type of 2HDM that is considered. For our scans, the current bound $m_{H^\pm} \geq 480 \text{ GeV}$ [116] for a type II 2HDM is used. Furthermore, the generated parameter sets have to be compatible with the LHC Higgs data. In order to check for compatibility, **ScannerS** is interfaced with **SusHi** [146] for the computation of the Higgs production cross sections through bottom quark and gluon fusion at NNLO QCD, while all other production cross sections are computed at NLO QCD [138]. Furthermore, the 2HDM decays are adopted from **HDECAY** [147, 148]. All electroweak corrections were neglected in the computation of these processes in order to be consistent, since they are not fully available for the 2HDM yet.

In addition to all constraints mentioned above, we further restrict the parameter sets to obey kinematic constraints dependent on the decay that is considered. Since we investigate a variety of different decay processes within this thesis, we use different parameter sets for each of the processes. In the following, we want to introduce these parameter sets and specify the additional kinematic constraints.

- **Parameter set C_2 :**

The first parameter set we want to specify was used in [91]. In order to prevent confusion, we adopt the notation and refer to this set as C_2 . The kinematic constraints for the parameters are given by

$$\begin{aligned} m_{H^\pm} &\geq m_{H^0} + m_W , \\ m_{H^\pm} &\geq m_{h^0} + m_W , \end{aligned} \tag{8.6}$$

thus allowing both processes $H^+ \rightarrow W^+ h^0/H^0$ from Chapter 5 to happen OS. The parameter set C_2 was generated for a type I 2HDM. The values of the parameters are stated in the following table.

m_{H^\pm} in GeV	m_{H^0} in GeV	m_{A^0} in GeV	β	α	Λ_5
[240, 310]	$m_{H^\pm} - 110$	$m_{H^\pm} - 50$	1.50423	0.25099	$\frac{2(m_{H^\pm} - 250)^2}{v^2 s_\beta c_\beta}$

The set C_2 allows for a variation of m_{H^\pm} , m_{H^0} , m_{A^0} and Λ_5 in arbitrarily small steps. We choose to vary m_{H^\pm} between 240 GeV and 310 GeV with a step size of 0.07 GeV. The set C_2 allows only the decay of the charged Higgs into the CP-even Higgses and the gauge boson W^+ to happen OS, but not all other processes that were considered within this thesis. We want to note that many of the parameter points contained in the set C_2 are actually excluded by **Scanners**. Nevertheless, we use the set in order to be able to compare our results from the ones presented in [91]. For a more detailed analysis, we will choose the other parameter sets described in the following, all of which are explicitly allowed by all theoretical and experimental constraints mentioned above.

- **Parameter sets S_1 to S_{60} :**

In order to allow all three decays considered in Chapters 5, 6 and 7 to happen OS simultaneously², we generated sixty parameter sets with the following kinematic constraints:

$$\begin{aligned} m_{H^\pm} &\geq m_{h^0} + m_W , \\ m_{H^0} &\geq 2m_{h^0} . \end{aligned} \tag{8.7}$$

Each of the sixty sets consists of 1 000 parameter points generated for a type II 2HDM. Within each set of 1 000 points, only one scalar mass is varied while all other 2HDM parameters are fixed. In the sets S_1 to S_{20} , the running mass is m_{H^0} , in the sets S_{21} to S_{40} we vary m_{H^\pm} and in the last twenty sets S_{41} to S_{60} , the variation is with respect to m_{A^0} . The parameters are generated within **ScannerS** by using a mass as a starting point from which the program moves away and searches for points that are still allowed considering all constraints mentioned above. Consequently, the sets S_1 to S_{60} have the advantage that we can consider the effects of different renormalization schemes with respect to the variation of only one running mass, but the disadvantage is that we only consider a narrow range of 2HDM parameters along certain “lines” in parameter space.

- **Parameter sets S_{61} to S_{70} :**

In order to compensate the narrow range of parameters given by the sets S_1 to S_{60} , we generated ten additional sets with a total of 10 000 points, each of which are randomly generated in the 2HDM parameter space. The kinematic constraints are the same as for the former sixty sets and the points were generated again for a type II 2HDM.

- **Parameter sets S_{71} to S_{90} :**

All sets mentioned so far have the insufficiency that the decay $H^0 \rightarrow A^0 A^0$ is prohibited to happen OS in almost all generated parameter points, since within them, the masses m_{H^0} and m_{A^0} are of the order of a few hundred GeV and rather close to each other. Since we use the OS decay of the heavy Higgs into two CP-odd Higgses for a process-dependent definition of $\delta\Lambda_5$, cf. Sec. 4.9.3, we generated twenty additional sets for a type II 2HDM with 1 000 points each and with the only kinematic constraints

$$\begin{aligned} m_{H^0} &\geq 2m_{h^0} , \\ m_{H^0} &\geq 2m_{A^0} . \end{aligned} \tag{8.8}$$

As it was already mentioned in Sec. 4.9.3, this imposes a strict kinematic limit on the scalar masses of the 2HDM.

²Note that within these parameter sets, we restrict ourselves to the process $H^+ \rightarrow W^+ h^0$, and the decay into the heavier Higgs H^0 is not necessarily allowed to happen OS in these parameter sets.

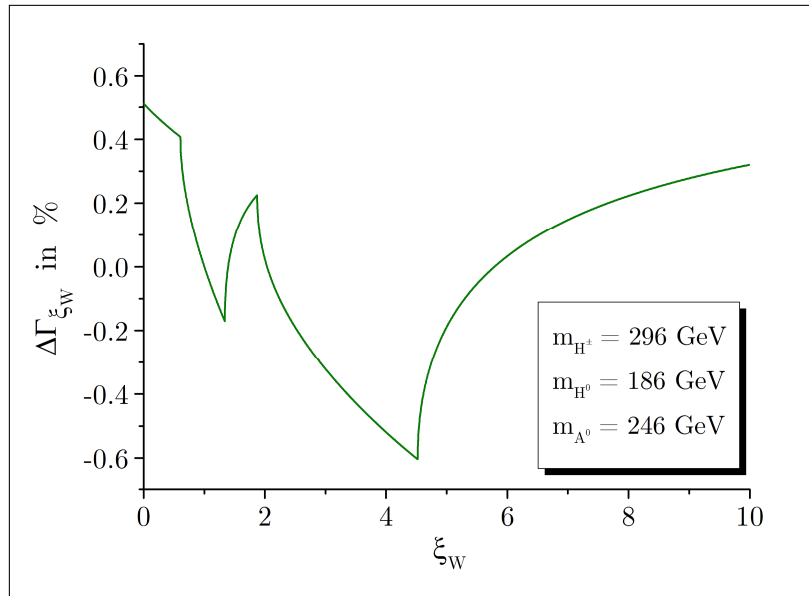


Figure 8.1.: Gauge-dependence of Kanemura's scheme. Shown is the normalized difference between the NLO partial decay width of the process $H^+ \rightarrow W^+ h^0$ for an arbitrary value of ξ_W and for the Feynman-'t Hooft gauge value $\xi_W = 1$, cf. Eq. (8.9), in Kanemura's scheme. The calculations were performed for one fixed point characterized by $m_{H^\pm} = 296$ GeV in the parameter set C_2 . The four kinks correspond to threshold effects of the loop integrals.

For a more detailed analysis, we consider specific parameter sets where only one scalar mass is varied. For completeness, we want to state the 2HDM parameters within these sets explicitly in the following table.

Set	m_{H^\pm} in GeV	m_{H^0} in GeV	m_{A^0} in GeV	β	α	Λ_5
S_6	700.354	[671, 804]	700.127	0.96978	-0.57038	14.18207
S_{13}	759.550	[598, 812]	720.501	0.80241	-0.80214	9.14651
S_{72}	617.936	607.461	[197, 208]	0.85304	-0.78038	1.02713

8.3. Numerical Results for the Decays $H^+ \rightarrow W^+ h^0/H^0$

Before we start to analyze the different renormalization schemes with respect to numerical stability, we want to investigate the gauge-dependence of the NLO partial decay width in one particular scheme for the scalar mixing angles α and β , namely in Kanemura's scheme from Sec. 4.8.2. For this investigation, we restrict ourselves to the process $H^+ \rightarrow W^+ h^0$. The results for the decay into the heavier Higgs H^0 are analogous.

We already worked out the analytic form of the gauge-dependence of $\delta\beta^{(2)}$ and $\delta\alpha$ in this scheme in Eqs. (4.155) and (4.157)³. This gauge-dependence is contained in the partial decay

³Note that we refer to Eq. (4.157) for the gauge-dependence of $\delta\alpha$ independently on the chosen tadpole scheme, since it was discussed in Sec. 5.4 that the second line of Eq. (4.156) is cancelled by the residual amplitude, leaving precisely the same form as in Eq. (4.157) of the residual gauge-dependence of $\delta\alpha$ in Kanemura's scheme.

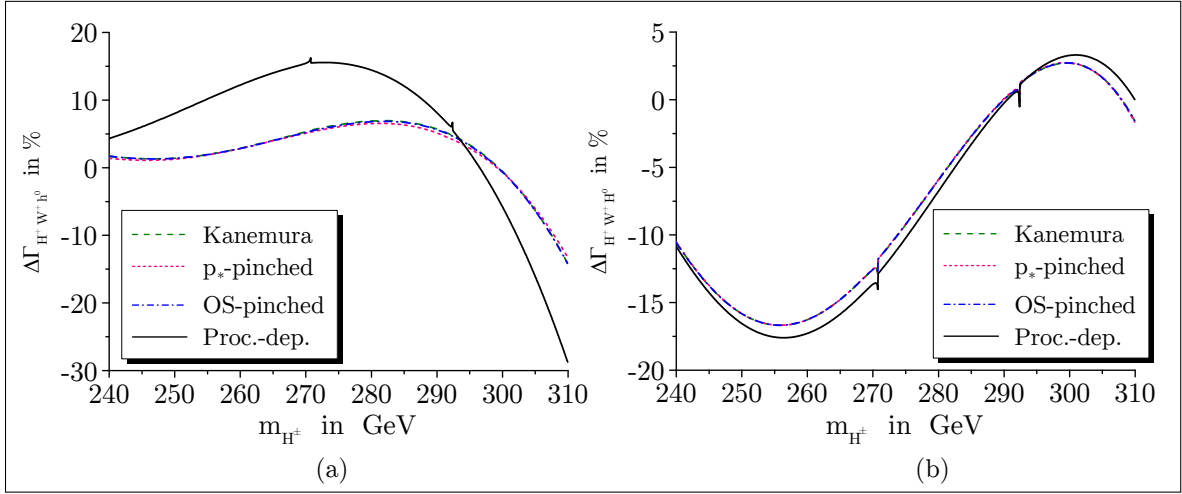


Figure 8.2.: NLO corrections for the parameter set C_2 . Shown is the normalized difference $\Delta\Gamma$ between the NLO and LO partial decay widths of the processes (a) $H^+ \rightarrow W^+ h^0$ and (b) $H^+ \rightarrow W^+ H^0$, as defined in Eq. (8.11), as a function of the charged Higgs mass. The calculations were performed for the full parameter set C_2 .

width through Eqs. (5.9) and (5.11). Now, we want to analyze the effect of the gauge-dependence numerically. To that end, we introduce the quantity

$$\Delta\Gamma_{\xi_W} := \frac{[\Gamma_{H^+W^+h^0}^{\text{NLO}}]_{\xi_W} - [\Gamma_{H^+W^+h^0}^{\text{NLO}}]_{\xi_W=1}}{[\Gamma_{H^+W^+h^0}^{\text{NLO}}]_{\xi_W=1}}, \quad (8.9)$$

where the subscript “ ξ_W ” indicates the evaluation of the NLO partial decay width for an arbitrary value of ξ_W . We analyze the gauge-dependence of the NLO partial decay width only with respect to a variation of the gauge-fixing-parameter ξ_W . The results for a variation of ξ_Z are analogous.

In Fig. 8.1, the NLO partial decay width of the process $H^+ \rightarrow W^+ h^0$ is shown for a variation of ξ_W for a fixed point in the parameter set C_2 , characterized by the charged Higgs mass $m_{H^\pm} = 296$ GeV. We focus on a small region of ξ_W , where the behavior of the decay width is particularly interesting.

The NLO partial decay width in Fig. 8.1 features four distinct kinks. Each of the kinks corresponds to threshold effects in the loop integrals given in Eqs. (4.155) and (4.157) or, to be more precise, in the corresponding gauge-dependent B_0 integrals through which the β integrals are defined. The integral $B_0(m_1^2; m_2^2, m_3^2)$ features an OS threshold effect at the kinematic point

$$m_1 = m_2 + m_3. \quad (8.10)$$

Through the optical theorem, such a threshold can be connected to a corresponding one-to-two process, with the invariant squared masses m_1^2 of the initial and m_2^2 and m_3^2 of the two final particles. The mass configuration in Eq. (8.10) corresponds precisely to the OS case of the decay, leading to a resonance in the loop integral.

In Fig. 8.1, each of the kinks can be traced back to one of the integrals contained in Eqs. (4.155) and (4.157) becoming OS and thus featuring a threshold effect:

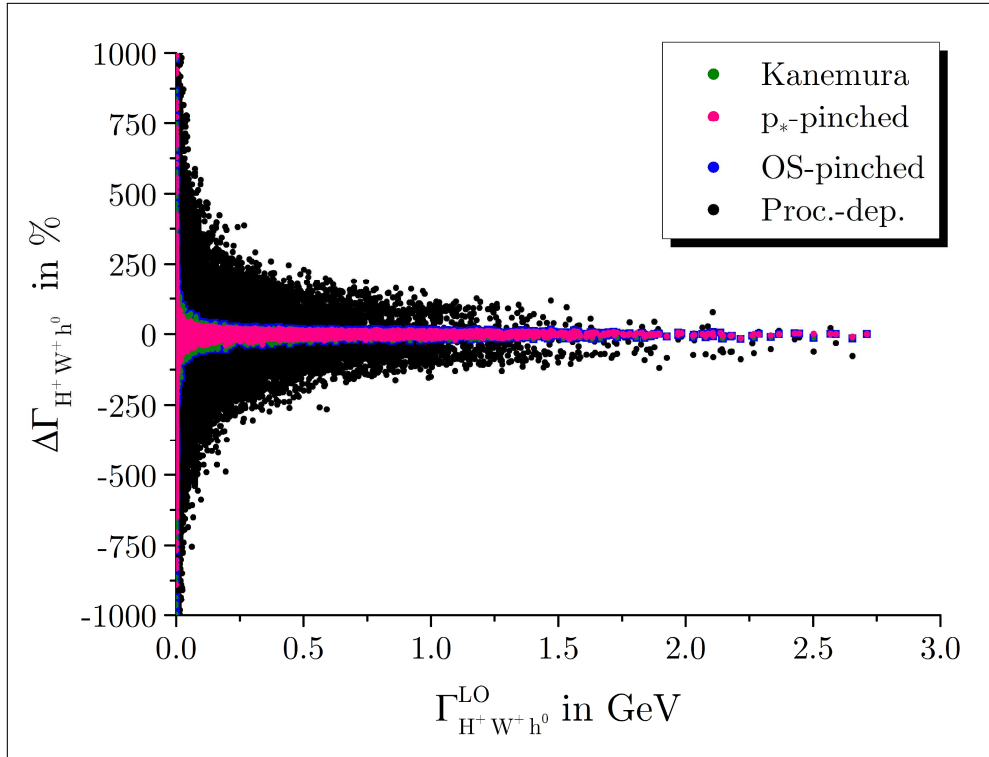


Figure 8.3.: Scatter plot for the process $H^+ \rightarrow W^+ h^0$. Shown is the normalized difference between the NLO and LO partial decay width of the process $H^+ \rightarrow W^+ h^0$ as a function of the LO partial decay width for all parameter sets S_1 to S_{70} . Kanemura’s and the pinched schemes yield NLO corrections of the same order of magnitude, while the process-dependent scheme leads to very large NLO corrections.

Kink	ξ_W	OS integral	Kinematic point	Origin
1	0.6052	$\beta_{W\xi W}(m_{h^0}^2)$	$m_{h^0} \approx \sqrt{\xi_W} m_W + \sqrt{\xi_W} m_W$	$\delta\alpha$
2	1.3881	$\beta_{W\xi W}(m_{H^0}^2)$	$m_{H^0} \approx \sqrt{\xi_W} m_W + \sqrt{\xi_W} m_W$	$\delta\alpha$
3	1.8718	$\beta_{WH^0}(m_{H^\pm}^2)$	$m_{H^\pm} \approx m_{H^0} + \sqrt{\xi_W} m_W$	$\delta\beta^{(2)}$
4	4.5190	$\beta_{Wh^0}(m_{H^\pm}^2)$	$m_{H^\pm} \approx m_{h^0} + \sqrt{\xi_W} m_W$	$\delta\beta^{(2)}$

The appearance of such kinks is a general feature of a perturbative calculation involving loop integrals and not a speciality of a certain renormalization scheme. In the following numerical results, we will therefore not analyze those kinks in detail, since they always correspond to some of the many one-loop integrals contained in the partial decay widths becoming OS.

With the numerical results presented in Fig. 8.1 and the analytic formula of the gauge-dependence of $\delta\alpha$ and $\delta\beta^{(2)}$ in Eqs. (4.155) and (4.157), our analysis of the gauge-dependence of Kanemura’s scheme is complete. The scheme inevitably leads to a gauge-dependent NLO partial decay width. Although it is shown in Fig. 8.1 that this gauge-dependence is of the order of a few permille and as such, the gauge-dependence might be considered negligible, the scheme nevertheless leads to a manifestly gauge-dependent NLO partial decay width, which is unacceptable. Furthermore, for other input parameter sets we observed that the gauge-dependence can become as high as a few tens of percents. Therefore, we conclude that Kanemura’s scheme is not a suitable scheme for the renormalization of the scalar mixing

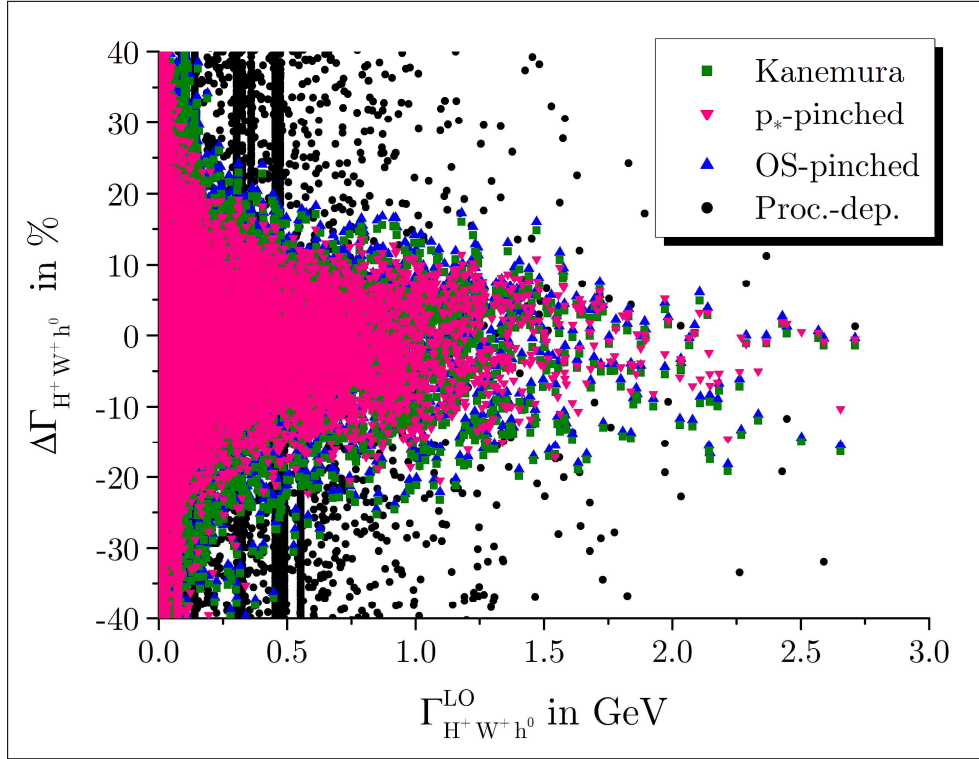


Figure 8.4.: Central region of the scatter plot. Shown is the central region of the scatter plot from Fig. 8.3, depicting the difference between the NLO and LO corrections to the partial decay width as a function of the LO partial decay width. Both pinched schemes and Kanemura’s scheme yield NLO corrections that are within the same order of magnitude.

angles. Interestingly, with respect to numerical stability, Kanemura’s scheme seems to be among the most stable schemes that were considered in this thesis. Therefore, we still include the scheme in the following numerical analyses, since it serves as a good benchmark for comparing the different schemes. Due to the gauge-dependence of Kanemura’s scheme, we have to choose a certain gauge for explicit calculations. For the rest of this chapter, we evaluated the NLO partial decay widths for Kanemura’s scheme in the Feynman-’t Hooft gauge.

In order to quantify the size of the NLO corrections compared to the LO partial decay widths, we define the quantity

$$\Delta\Gamma_{f_1 f_2 f_3} := \frac{\Gamma_{f_1 f_2 f_3}^{\text{NLO}} - \Gamma_{f_1 f_2 f_3}^{\text{LO}}}{\Gamma_{f_1 f_2 f_3}^{\text{LO}}}, \quad (8.11)$$

for any generic one-to-two process $f_1 \rightarrow f_2 f_3$. We start the numerical analysis by using the parameter set C_2 , which was used in [91] as well.

Shown in Fig. 8.2 is the normalized deviation of the NLO and LO partial decay widths, as defined by Eq. (8.11), as a function of the charged Higgs mass m_{H^\pm} , for the decay of the charged Higgs H^+ into the W^+ boson and into (a) the lighter Higgs h^0 and (b) the heavier Higgs H^0 . Each of the plots features four curves for the different renormalization schemes of the scalar mixing angles, indicated by “Kanemura” for the scheme presented in Sec. 4.8.2, “ p_* -pinched” and “OS-pinched” for the two pinched schemes⁴ of Sec. 4.8.3 and “Proc.-dep.” for the process-dependent scheme of Sec. 4.8.4.

⁴Analogous to Kanemura’s scheme, were we used $\delta\beta^{(2)}$ for all calculations, we use the definition of $\delta\beta$ through the charged sector from Eqs. (4.165) and (4.168) for the two pinched schemes here and in the following.

As it can be seen in Fig. 8.2, Kanemura’s scheme and the two pinched schemes lead to very similar NLO partial decay widths and their difference is only within a few permille to percent. For the decay into the heavier Higgs, the process-dependent scheme yields similar NLO corrections, as well. For the decay into the lighter Higgs however, the deviation of NLO and LO partial decay widths differ more strongly from the other three schemes⁵ and become as large as 30%. For the set C_2 , this is an indicator that the process-dependent scheme for the mixing angle counterterms $\delta\alpha$ and $\delta\beta$ introduces large NLO corrections to the partial decay width. On the other hand, the analysis within the parameter set C_2 shows that the two pinched schemes yield numerically stable NLO corrections.

In order to analyze the different renormalization schemes in a larger region of the parameter space, we calculated the NLO partial decay width for all renormalization schemes of $\delta\alpha$ and $\delta\beta$ for all 70 000 points contained in the parameter sets S_1 to S_{70} . Since we did not want to restrict the parameter space too strictly, we restricted ourselves to the process $H^+ \rightarrow W^+ h^0$ in the following analysis, although for the decay into the heavier Higgs, we would find analogous results.

In Fig. 8.3, we plotted the deviation $\Delta\Gamma_{H^+W^+h^0}$ as a function of the LO partial decay width $\Gamma_{H^+W^+h^0}$ for all parameter points of the sets S_1 to S_{70} . The plot features a central region for $\Delta\Gamma_{H^+W^+h^0}$ of $\pm 30\%$ within which most results for Kanemura’s scheme and the two pinched schemes are situated. Since the results for the OS-pinched and p_* -pinched schemes are very similar, we show in Fig. 8.4 the same plot with a different scale on the $\Delta\Gamma_{H^+W^+h^0}$ axis, showing that all three aforementioned schemes yield NLO corrections of the same order of magnitude. Note that $\Delta\Gamma_{H^+W^+h^0}$ becomes very large for $\Gamma_{H^+W^+h^0} \rightarrow 0$, since in this limit, the definition of Eq. (8.11) is ill-defined and diverges. Consequently, we restrict ourselves to regions where the LO partial decay width is not too small when we draw conclusions about numerical stability.

In contrast to that, it can be seen in Fig. 8.3 that the process-dependent scheme yields NLO corrections which are one to two orders of magnitude larger than in the other schemes. The NLO corrections in the process-dependent scheme are of the order of a few hundred percent, but electroweak corrections usually involve corrections of the order of a few up to tens of percents. Since we have considered a large variety of different parameter points of the 2HDM, we conclude that the process-dependent scheme is in general unsuitable for the renormalization of the scalar mixing angles, since it leads to numerical instability. On the other hand, by looking at Fig. 8.3, we realize that both Kanemura’s and the two pinched schemes lead to numerically stable results. Since the former is gauge-dependent, we conclude that the two pinched schemes are suitable renormalization schemes for the mixing angles, since they are process-independent, gauge-independent and numerically stable. Consequently, we conclude that the “no-go theorem” established in [36] for the MSSM is not applicable for the renormalization of the scalar mixing angles in the 2HDM. The size of the NLO corrections does not differ much between the p_* -pinched and OS-pinched scheme, therefore, it is an arbitrary choice which of the two pinched schemes is used in practice.

8.4. Numerical Results for the Decay $H^0 \rightarrow Z^0 Z^0$

The next process we want to analyze numerically is the decay $H^0 \rightarrow Z^0 Z^0$. We calculated the NLO partial decay widths for all four renormalization schemes of the scalar mixing angles as presented in Sec. 4.8 for the parameter sets S_1 to S_{70} . For a comparison between the NLO corrections and the LO partial decay widths, we use the quantity defined in Eq. (8.11).

⁵The reason behind this difference for the two decays is the proportionality factor in the counterterms in Eqs. (5.9) and (5.10). The counterterms $\delta\alpha$ and $\delta\beta$ become in general very large in the process-dependent scheme, but for the decay to the heavier Higgs, the angle counterterms in Eq. (5.10) are proportional to $c_{\beta-\alpha}$, which is suppressed compared to $s_{\beta-\alpha}$ in all parameter sets which we used in this thesis.

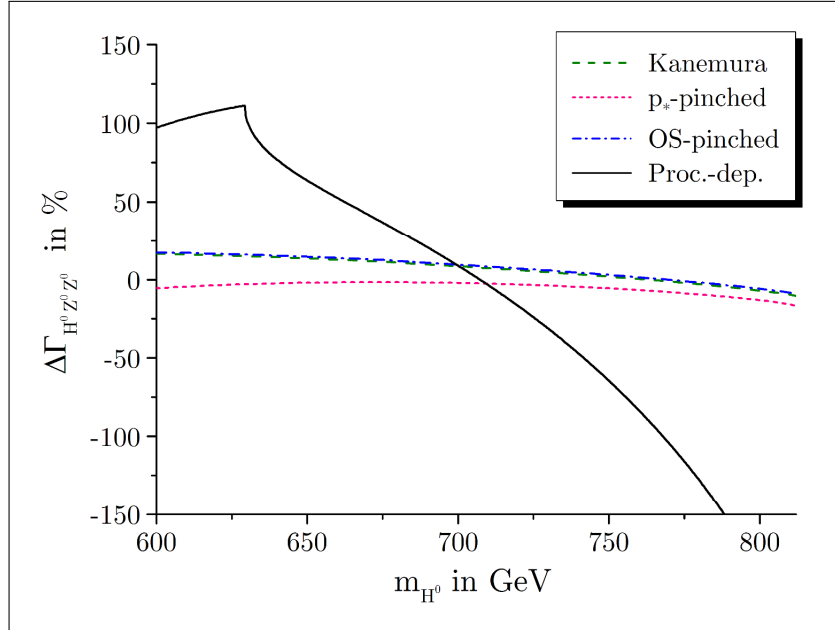


Figure 8.5.: NLO corrections for the parameter set S_{13} . Shown is the normalized difference $\Delta\Gamma$ between the NLO and LO partial decay widths of the processes $H^0 \rightarrow Z^0 Z^0$, as defined in Eq. (8.11), as a function of the heavy CP-even Higgs mass. The calculations were performed for the full parameter set S_{13} .

In order to compare the four schemes directly with each other, we first focus on the parameter set S_{13} which is specified at the end of Sec. 8.2. In Fig. 8.5, the normalized difference $\Delta\Gamma_{H^0 Z^0 Z^0}$ between the NLO and LO partial decay width is shown as a function of the CP-even Higgs mass m_{H^0} . The two pinched schemes as well as Kanemura’s scheme yield NLO corrections of up to $\pm 20\%$ which is still in the bounds which we consider as numerically stable. The process-dependent renormalization scheme for the mixing angles, however, yields NLO corrections that become up to one order of magnitude larger, as it was the case for the processes considered in the previous section. We note additionally that the NLO corrections for the OS-pinched scheme resembles the ones we get by using Kanemura’s scheme, while the corrections in the p_* -pinched scheme differ more significantly from Kanemura’s scheme. This is not only true for the parameter set S_{13} , but for almost all parameter sets which we considered in Sec. 8.2.

In order to increase the statistics, we considered all 70 000 points of the parameter sets S_1 to S_{70} . In the scatter plot in Fig. 8.6, we show the difference $\Delta\Gamma_{H^0 Z^0 Z^0}$ as a function of the LO partial decay width of the process $H^0 \rightarrow Z^0 Z^0$. The scatter plot is very similar to Fig. 8.3 from the previous section. In the central region of $\Delta\Gamma_{H^0 Z^0 Z^0}$ between $\pm 40\%$, most results for the two pinched schemes and Kanemura’s scheme are situated, while the process-dependent scheme yields NLO corrections that are approximately one order of magnitude higher. This indicates that the process-dependent scheme leads to numerical instability in general and not only for a few parameter sets and specific processes. This confirms our conclusion from the previous section, namely that we consider the process-dependent scheme as an unsuitable scheme for renormalizing α and β . Kanemura’s scheme and the two pinched schemes, on the other hand, yield NLO corrections which are considered to be numerically stable.

8.5. Numerical Results for the Decay $H^0 \rightarrow h^0 h^0$

The last process that we consider within the scope of this thesis is the Higgs-to-Higgs decay. Since it includes the counterterm $\delta\Lambda_5$ at NLO, we analyze the NLO partial decay width of the

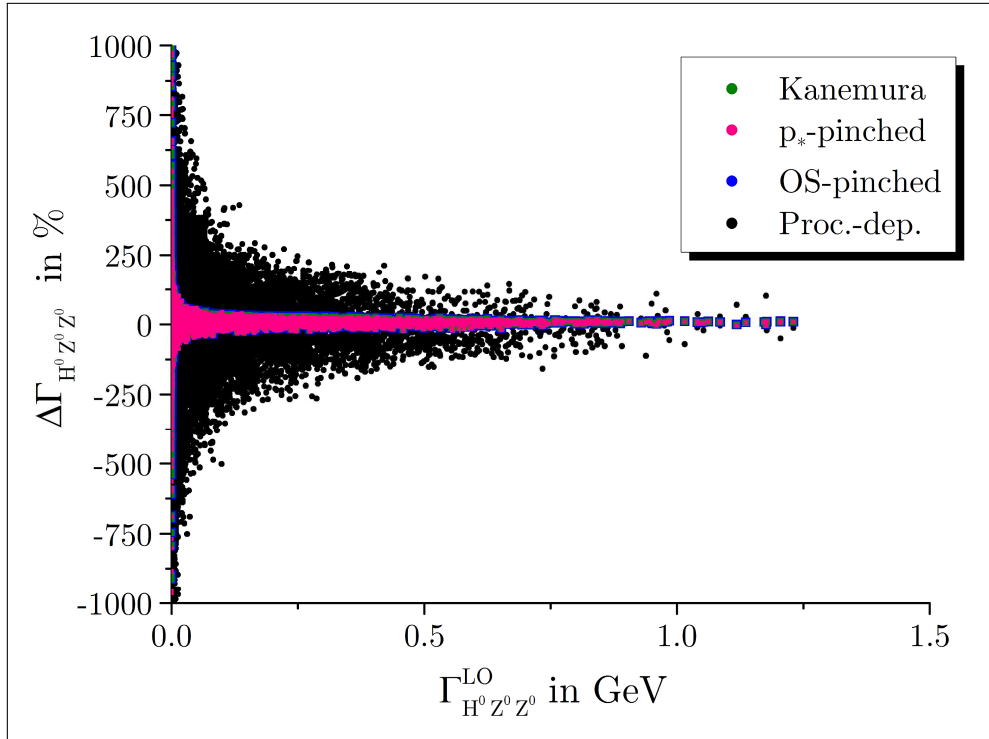


Figure 8.6.: Scatter plot for the process $H^0 \rightarrow Z^0 Z^0$. Shown is the normalized difference between the NLO and LO partial decay width of the process $H^0 \rightarrow Z^0 Z^0$ as a function of the LO partial decay width for all parameter sets S_1 to S_{70} . Kanemura’s and the pinched schemes yield NLO corrections of the same order of magnitude, while the process-dependent scheme leads to very large NLO corrections.

process with respect to different renormalization schemes for $\delta\Lambda_5$ and for the scalar mixing angles separately.

We start by considering the usual $\overline{\text{MS}}$ condition for $\delta\Lambda_5$ as introduced in Sec. 4.9.1. We calculated the NLO partial decay width of the process $H^0 \rightarrow h^0 h^0$ for all 70 000 parameter points included in the sets S_1 to S_{70} . In the scatter plot in Fig. 8.7, the normalized differences between the NLO and LO partial decay widths according to Eq. (8.11) are shown as a function of the LO partial decay width. We note that the $\Delta\Gamma_{H^0 h^0 h^0}$ axis is presented in a logarithmic scale. Since most of the differences $\Delta\Gamma_{H^0 h^0 h^0}$ of Kanemura’s and the process-dependent scheme were negative, we took the absolute of $\Delta\Gamma_{H^0 h^0 h^0}$ in order to present all results in the logarithmic scatter plot in Fig. 8.7. This does not change our interpretation with respect to numerical stability, since for this, we are only interested in the absolute value of Eq. (8.11).

The scatter plot in Fig. 8.7 shows two distinct results. First, in contrast to the previous two sections, the NLO corrections for Kanemura’s and the process-dependent scheme are now of the same order of magnitude and both are in general rather high. Second, the two pinched schemes differ from Kanemura’s and the process-dependent scheme by two to three orders of magnitude. We will discuss the former observation further below and consider first the implications of the latter.

It was already mentioned in Sec. 4.9.2 that the change from the standard to the alternative tadpole scheme might lead to numerical instability when using the usual $\overline{\text{MS}}$ condition. The change of the tadpole scheme introduces large UV-finite shifts in the NLO amplitude which would have to be compensated by corresponding shifts in $\delta\Lambda_5$. Since the counterterm is defined by an $\overline{\text{MS}}$ condition, those shifts are not present in $\delta\Lambda_5$, however, thus leading to

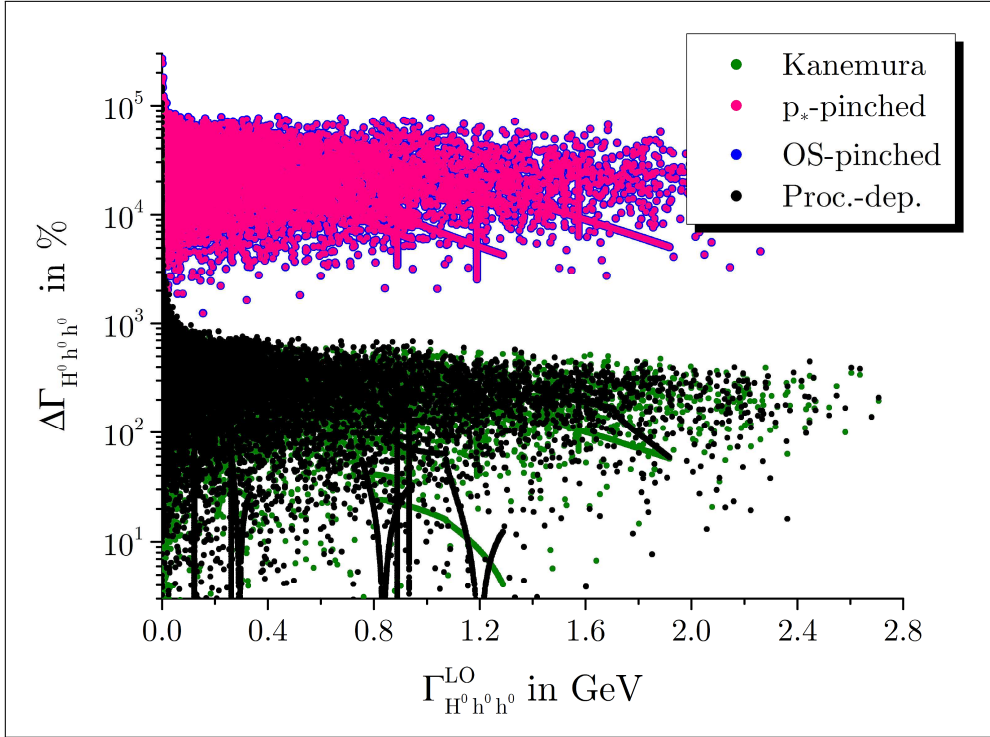


Figure 8.7.: Scatter plot for the usual $\overline{\text{MS}}$ condition. Shown is the normalized difference between the NLO and LO partial decay width of the process $H^0 \rightarrow h^0 h^0$ as a function of the LO partial decay width for all parameter sets S_1 to S_{70} . The counterterm $\delta\Lambda_5$ was renormalized by the usual $\overline{\text{MS}}$ condition. Note that the $\Delta\Gamma_{H^0 h^0 h^0}$ axis is depicted in logarithmic scale.

numerical instability in the NLO partial decay width. We discussed in Sec. 4.8.3 that for a process- and gauge-independent definition of the scalar mixing angles, the pinched scheme should be used, which requires the alternative treatment of the tadpoles. Consequently, the usual $\overline{\text{MS}}$ condition cannot be used as a renormalization scheme for $\delta\Lambda_5$ if we require a numerically stable NLO partial decay width.

Instead, we choose to use the improved $\overline{\text{MS}}$ scheme as introduced in Eq. (4.191), which contains additional shifts that compensate the effect of the vev shifts in the alternative tadpole scheme. Additionally, the improved $\overline{\text{MS}}$ scheme is manifestly gauge-independent. In Fig. 8.8, we show the scatter plot for all renormalization schemes of $\delta\alpha$ and $\delta\beta$ when using the improved $\overline{\text{MS}}$ condition for $\delta\Lambda_5$. It can be seen that now, all renormalization schemes lead to NLO corrections which are approximately of the same order of magnitude. Additionally, Kanemura's and the pinched schemes yield NLO corrections which are very similar, while for the process-dependent schemes, slight deviations can be observed.

We already mentioned that in contrast to the previous processes, the NLO corrections to the process $H^0 \rightarrow h^0 h^0$ can get as large as $\pm 400\%$ for most of the parameter points even in Kanemura's scheme, which seems to be unacceptable with respect to numerical stability. However, such large corrections were already previously observed in Higgs-to-Higgs decays within the 2HDM [56]. In the following, we present arguments that these large NLO corrections are not the results of choosing numerically unstable renormalization schemes. They are rather a speciality of the vertex corrections of the process $H^0 \rightarrow h^0 h^0$ following from freedom of the parameter choice within the 2HDM, which is not constrained by additional symmetries as it is the case in e.g. supersymmetric extensions of the SM.

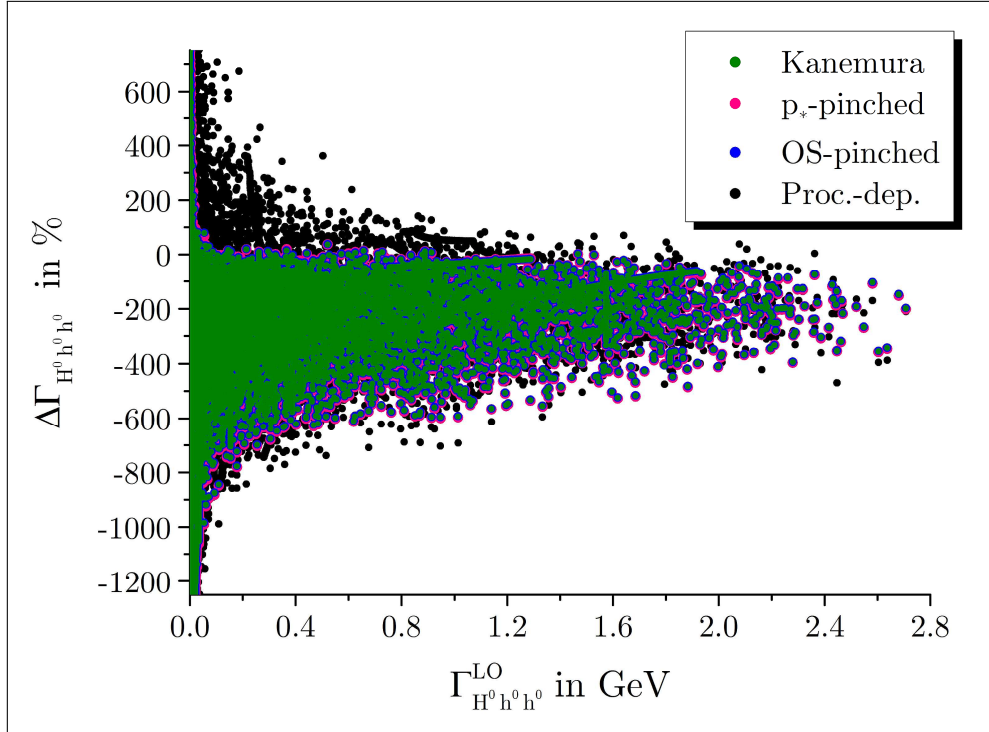


Figure 8.8.: Scatter plot for the improved $\overline{\text{MS}}$ condition. Shown is the normalized difference between the NLO and LO partial decay width of the process $H^0 \rightarrow h^0 h^0$ as a function of the LO partial decay width for all parameter sets S_1 to S_{70} . The counterterm $\delta\Lambda_5$ was renormalized by the improved $\overline{\text{MS}}$ condition.

If we consider the expressions for the scalar masses of the 2HDM given in Eqs. (2.29) – (2.34), we realize that the masses of the Higgses $\phi \in \{H^0, A^0, H^\pm\}$ can be written as [56]

$$m_\phi^2 = M^2 + \text{Lin}(\lambda_i v^2) + \mathcal{O}\left(\frac{v^4}{M^4}\right), \quad (8.12)$$

where we used the definition of M^2 given in Eq. (2.37). We refer to M^2 as the scale of the soft- \mathbb{Z}_2 -symmetry breaking. The expression “Lin” stands for linear combinations of the 2HDM potential parameters λ_i ($i = 1, \dots, 5$) of Eq. (2.7) corresponding to the respective scalar mass which is considered.

If our 2HDM input parameters, i.e. the scalar masses, the mixing angles and Λ_5 , are chosen such that $M^2 \gg \lambda_i v^2$ holds, then the scalar masses and the soft-breaking scale M^2 are of the same order of magnitude according to Eq. (8.12) and the former depend only weakly on the parameters λ_i . In this case, the 2HDM can be described by an effective theory with only one scalar doublet in the SM limit [56], and the NLO loop effects in the vertex corrections vanish in the limit of heavy masses m_ϕ due to the decoupling theorem [149]. In this regime, the corrections to the triple-Higgs couplings are within the boundaries of the processes we considered before. If we calculate the NLO corrections for the parameter set S_6 , which contains mass parameters which obey the limit $M^2 \gg \lambda_i v^2$, we observe in Fig. 8.9 that the normalized difference between the NLO and LO partial decay width is mostly below an absolute value of 30 % for Kanemura’s and the two pinched schemes, which we still consider as numerically stable. In contrast to that, we observe that the process-dependent scheme yields very large NLO corrections. Analogously to the previous processes, we conclude that the process-dependent scheme of the angle counterterms is an unsuitable renormalization scheme with respect to numerical stability, in general.

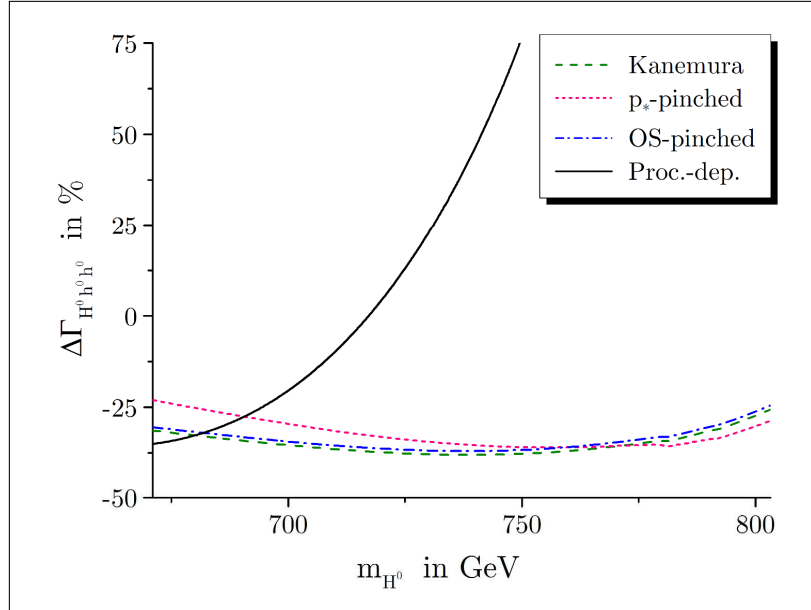


Figure 8.9.: NLO corrections for the parameter set S_6 . Shown is the normalized difference $\Delta\Gamma$ between the NLO and LO partial decay widths of the processes $H^0 \rightarrow h^0 h^0$, as defined in Eq. (8.11), as a function of the heavy CP-even Higgs mass. The counterterm $\delta\Lambda_5$ is renormalized by the improved $\overline{\text{MS}}$ condition. The calculations were performed for the full parameter set S_6 .

If the input parameter set corresponds to the other limit, namely $M^2 \lesssim \lambda_i v^2$, and simultaneously large scalar masses are chosen, then the coupling constants λ_i have to adopt large values according to Eq. (8.12). This corresponds to the strong coupling limit where the decoupling theorem does not apply. In this limit, the loop contributions in the scalar sector are in general given by a power law in the scalar masses m_ϕ [56]. For the vertex corrections of the process $H^0 \rightarrow h^0 h^0$, the size of the corrections is a function of $m_{H^0}^4$, which has been checked explicitly for several parameter sets. Since we choose parameter sets with high Higgs masses, the NLO corrections are very high in this regime. Most of the parameter sets S_1 to S_{70} correspond to this case. Consequently, the deviations between the LO and NLO partial decay width that we observe in Fig. 8.8 are very high.

We note that the Higgs sector of the MSSM corresponds to the decoupling limit $M^2 \gg \lambda_i v^2$, since the coupling constants λ_i are fixed at $\mathcal{O}(g^2)$ and consequently, large Higgs masses can only be generated by choosing M^2 to be large [56]. Therefore, the parameters of the MSSM Higgs sector are protected by supersymmetric relations and automatically do not depend strongly on large Higgs masses. In the 2HDM however, there is no corresponding symmetry which restricts the parameter choice of the scalar sector.

We conclude from this that the large deviations between the LO and NLO partial decay widths which we observed in Fig. 8.8 are not due to numerical instability of our chosen renormalization schemes, but rather due to the freedom of the parameter choice within the 2HDM. In Fig. 8.9, we observe that parameters exist within current theoretical and experimental bounds which yield moderate NLO corrections for Kanemura's and the two pinched schemes. Therefore, we suggest the renormalization of $\delta\Lambda_5$ in the improved $\overline{\text{MS}}$ scheme together with one of the two pinched schemes for $\delta\alpha$ and $\delta\beta$ as a process-independent, gauge-independent and numerically stable renormalization scheme for the 2HDM.

As the last analysis for the process $H^0 \rightarrow h^0 h^0$, we consider the numerical results for the process-dependent definition of $\delta\Lambda_5$. Since the counterterm is defined over the OS decay of

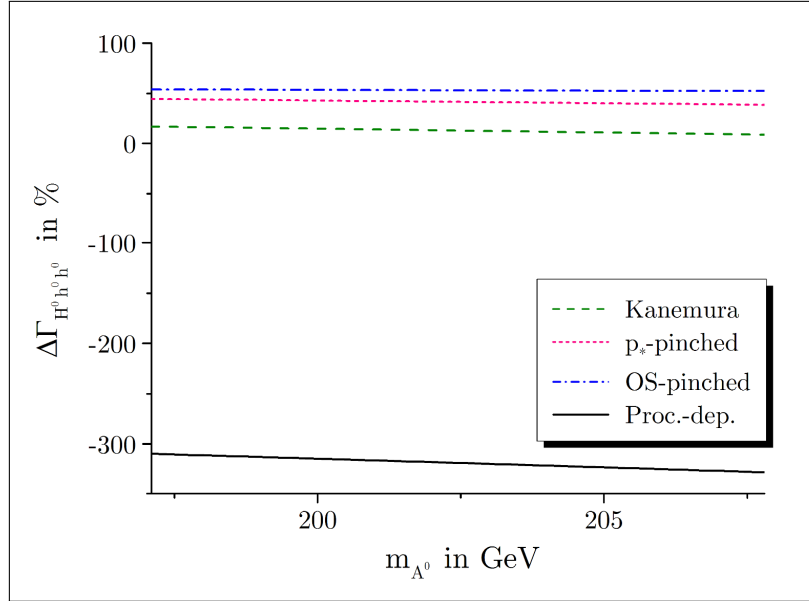


Figure 8.10.: NLO corrections for the parameter set S_{72} . Shown is the normalized difference $\Delta\Gamma$ between the NLO and LO partial decay widths of the processes $H^0 \rightarrow h^0 h^0$, as defined in Eq. (8.11), as a function of the heavy CP-even Higgs mass. The counterterm $\delta\Lambda_5$ is renormalized in the process-dependent scheme. The calculations were performed for the full parameter set S_{72} .

the heavy Higgs into two CP-odd Higgses A^0 , we only used the parameter sets S_{71} to S_{90} which were generated with the appropriate kinematic constraints. However, it turned out in the numerical evaluation that the parameter sets are not suitable for a detailed analysis in the form of a scatter plot, since almost all parameter sets lead to NLO partial decay widths which are negative for the process-dependent scheme of $\delta\Lambda_5$. We note that these negative results are not due to a bug in the used software, but rather the consequence of very large negative NLO contributions which lead to an overall negative NLO partial decay width, since at NLO, we consider in Eq. (3.12) only the interference term of the LO and NLO amplitude, but not the absolute square of the NLO amplitude.

The parameter set S_{72} is one of the few sets which contains enough parameters that lead to a positive NLO partial decay width for the process-dependent scheme for $\delta\Lambda_5$. Shown in Fig. 8.10 is the normalized difference between the LO and NLO partial decay width as a function of the CP-odd mass. As it can be seen in the plot, the process-dependent scheme of the scalar mixing angles leads to very large NLO corrections, while the corrections for Kanemura’s scheme are moderate. The results for the two pinched schemes are numerically more stable than for the process-dependent scheme, but with a deviation of 50% still in a region where they are rather high.

Since the parameter set S_{72} features only a small variation of m_{A^0} , we present only a preliminary conclusion due to the lack of statistics. The fact that most parameter sets yield negative NLO partial decay widths for the process-dependent scheme of $\delta\Lambda_5$ can be considered as an indicator that the scheme itself might be unsuitable. However, this has to be investigated further in future work. For the parameters which yield positive NLO partial decay widths, it can be seen that only Kanemura’s scheme is in the region of numerical stability, but this scheme is explicitly gauge-dependent. This result, together with the fact that the process-dependent definition of $\delta\Lambda_5$ leads to very strict kinematic bounds on the 2HDM input parameters, leads us to the preliminary conclusion that the process-dependent scheme is an unsuitable renormalization scheme for the 2HDM parameter Λ_5 .

Conclusion and Outlook

This thesis has dealt with the complete renormalization of the CP-conserving 2HDM in the electroweak sector. Despite its enormous success, the SM of particle physics does not explain several observed phenomena, such as the dominance of matter over antimatter [27] and the abundance of dark matter compared to baryonic matter in our universe [28]. The 2HDM, as one of the simplest extensions of the SM, provides an extended scalar sector with an enriched phenomenology, a possible dark matter candidate for a special type of 2HDM [29, 30] and mechanisms of CP-violation necessary for the explanation of the matter-antimatter asymmetry [31].

We presented the electroweak Lagrangian of the 2HDM. In comparison to the SM with only one scalar $SU(2)_L$ doublet, the scalar Lagrangian of the 2HDM contains two scalar $SU(2)_L$ doublets with non-vanishing vevs v_1 and v_2 [32]. Through the mechanism of spontaneous symmetry breaking, the particles of the 2HDM gain mass, and the fields of the two scalar doublets can be rotated with the two scalar mixing angles α and β from the gauge basis to the mass basis. Through this rotation, five physical Higgs bosons arise: two CP-even Higgses H^0 and h^0 , one CP-odd Higgs A^0 and two charged Higgs bosons H^\pm . Furthermore, the scalar potential features a rich vacuum structure, parametrized by two tadpole parameters whose vanishing represents the minimum states of the potential [33]. These tadpole parameters, together with the masses of the 2HDM, the two scalar mixing angles and the scalar potential parameter Λ_5 , are contained in our set of independent parameters of the 2HDM.

The first run of the LHC unveiled the existence of a scalar SM-like Higgs boson [17, 18]. Due to the current run II at a center-of-mass energy of 13 TeV, it is expected that the scalar sector will be explored in even more detail. For a comparison of experimental data with BSM theories like the 2HDM, precise predictions are needed. In order to refine these predictions by calculating several decay modes at NLO, we need to specify the renormalization program for the 2HDM. We presented a generic OS renormalization approach through which all mass counterterms and wave function renormalization constants of the 2HDM were fixed. For the renormalization of the vacuum conditions, namely that the vevs represent the true minimum states of the two scalar doublets even at NLO, we presented two distinct approaches, the standard and the alternative tadpole scheme. While the former is the scheme which is most prevalent in literature [52, 56, 85], we emphasized the advantages of using the latter scheme [84], namely that it allows for a manifestly gauge-independent definition of all counterterms of the masses,

the scalar mixing angles and of Λ_5 . Additionally, we presented in detail the implications of the alternative tadpole scheme on the explicit form of all renormalization constants. Within this alternative scheme, the tadpole counterterms appearing in the mass counterterms and wave function renormalization constants of the scalar sector vanish, while all amplitudes associated with NLO calculations, i.e. vertex corrections and self-energies involved in the definitions of counterterms, must include contributions from tadpole diagrams wherever they can appear in the 2HDM.

Within the MSSM, a “no-go theorem” was established [36] which states that renormalization schemes for the mixing angle β are not simultaneously gauge-independent, process-independent and numerically stable. For the renormalization of the two scalar mixing angles α and β in the 2HDM, we presented several distinct renormalization schemes and analyzed them with respect to gauge-dependence. One of the renormalization schemes of the scalar mixing angles is Kanemura’s scheme [56, 85] which connects the definition of the counterterms $\delta\alpha$ and $\delta\beta$ with the off-diagonal wave function renormalization constants of the scalar sector. We have shown analytically that this approach leads to a manifestly gauge-dependent definition of the two counterterms. By using the alternative tadpole scheme and the modified versions of the CP-even, CP-odd and charged scalar self-energies gained by the application of the pinch technique [92–97], we introduced the pinched scheme as a manifestly gauge-independent renormalization scheme for $\delta\alpha$ and $\delta\beta$. Additionally, we presented a process-dependent scheme [36] for comparison with the other schemes, where the scalar mixing angle counterterms are fixed through the OS processes $A^0 \rightarrow \tau^+ \tau^-$ and $H^0 \rightarrow \tau^+ \tau^-$. We have shown analytically that within the process-dependent scheme, the counterterms of the scalar mixing angles are gauge-dependent when using the standard tadpole scheme and manifestly gauge-independent when the alternative tadpole scheme is used.

For the renormalization of the 2HDM parameter Λ_5 , we presented an $\overline{\text{MS}}$ scheme [56]. When using the alternative tadpole scheme instead of the standard one, we have shown numerically that the counterterm $\delta\Lambda_5$ is manifestly gauge-independent. Furthermore, we discussed that within the alternative tadpole scheme, the $\overline{\text{MS}}$ condition for $\delta\Lambda_5$ has to be modified consistently within the internal parameter relations of the 2HDM in order to yield a numerically stable NLO partial decay width. As a comparison to the $\overline{\text{MS}}$ scheme, we additionally presented a process-dependent scheme for $\delta\Lambda_5$, where the counterterm is fixed through the OS process $H^0 \rightarrow A^0 A^0$.

For the application of the different renormalization schemes presented in this thesis, we considered several 2HDM-specific decays as exemplary processes. We introduced a generic formalism for the calculation of partial decay widths of one-to-two decay processes at LO and NLO. This formalism was applied to the decays $H^+ \rightarrow W^+ h^0/H^0$, $H^0 \rightarrow Z^0 Z^0$ and $H^0 \rightarrow h^0 h^0$. We calculated the full electroweak NLO corrections to all decays in general R_ξ gauge by use of the automatization tools **FeynArts** 3.9 [55] and **FeynCalc** 8.2.0 [118]. In case of the decays of the charged Higgs H^+ , we included real corrections to render the NLO amplitude IR-finite [91]. By use of the tool **LoopTools** 2.12 [120], we verified the UV-finiteness of the NLO partial decay widths for every process and all renormalization schemes numerically. Additionally, we analyzed the full NLO decay amplitudes of all processes analytically and numerically with respect to gauge-dependence. We showed that for the renormalization of the scalar mixing angles, Kanemura’s scheme inevitably leads to a gauge-dependent NLO partial decay width, while the process-dependent and the two pinched schemes yield manifestly gauge-independent NLO partial decay widths independently on the chosen tadpole scheme. For the potential parameter Λ_5 , we have checked numerically that all renormalization schemes for $\delta\Lambda_5$ lead to an overall gauge-independent partial decay width at NLO if the angle counterterms are defined by a gauge-independent scheme.

In order to check for numerical stability, we implemented the SM input parameters [46, 128, 129] and generated several input files for the 2HDM-specific input parameters with the help of the tool `ScannerS` [130]. All generated scalar masses, mixing angles and Λ_5 are points in the 2HDM parameter space which are still allowed after the experimental and theoretical constraints have been applied [138]. The generated parameter points were used for a numerical evaluation of the NLO partial decay widths of the processes $H^+ \rightarrow W^+ h^0/H^0$ and $H^0 \rightarrow Z^0 Z^0$. It was verified numerically that Kanemura’s scheme yields a gauge-dependent NLO partial decay width. Furthermore, it was shown that the process-dependent scheme for renormalizing the scalar mixing angles leads to numerical instability for almost all parameter sets and processes that we considered. Therefore, both Kanemura’s and the process-dependent scheme are considered to be unsuitable renormalization schemes. The renormalization of the scalar mixing angles in the two pinched schemes yields moderate NLO corrections to the partial decay widths for almost all parameter sets for the decays that we considered in the thesis. In summary, it was shown that the two pinched schemes are manifestly gauge-independent, process-independent and numerically stable renormalization schemes for $\delta\alpha$ and $\delta\beta$, and a “no-go theorem” analogous to the MSSM is not established for the 2HDM.

For the decay $H^0 \rightarrow h^0 h^0$, we have shown that within the alternative tadpole scheme, the $\overline{\text{MS}}$ scheme for $\delta\Lambda_5$ leads to numerically highly unstable NLO corrections, but the application of the improved $\overline{\text{MS}}$ scheme leads to NLO corrections which are in the same order of magnitude as for the $\overline{\text{MS}}$ condition in the standard tadpole scheme and for the process-dependent definition of Λ_5 . The numerical analysis showed that the NLO corrections are in general large for all renormalization schemes of the scalar mixing angles, which was explained as being a general phenomenon of the freedom of parameter choice within the 2HDM instead of being an indicator of numerical instability. Some of our generated parameter sets were in the region of the strong coupling limit, in which large scalar masses contribute in the form of a power law to the NLO virtual vertex corrections, consequently leading to numerical instability. We have shown that for other parameter sets, the decoupling limit can be applied, where the NLO corrections are only weakly dependent on large scalar masses, leading to moderate and numerically stable NLO corrections for the improved $\overline{\text{MS}}$ scheme. The process-dependent scheme for $\delta\Lambda_5$ yielded larger NLO corrections. However, only a few generated 2HDM input parameter sets were suitable for an analysis of the scheme. Therefore, we did not conclude a strong statement on numerical stability for this scheme.

In future work, it would be interesting to increase the statistics of the numerical analysis in general and especially for the Higgs-to-Higgs decays by generating a larger amount of 2HDM parameter sets. By separating the parameters of these sets according to their affiliations to the strong coupling or decoupling limits or by a more systematic variation of the 2HDM parameters, it would be possible to draw a stronger conclusion of the effects of the chosen input parameter sets on the size of the NLO corrections. Additionally, the generation of more suitable parameter sets for the process-dependent scheme for $\delta\Lambda_5$ would allow for a stronger statement on the numerical stability of this scheme. Furthermore, the pinched scheme for $\delta\alpha$ and $\delta\beta$ as well as the improved $\overline{\text{MS}}$ scheme for $\delta\Lambda_5$ should be applied to all possible decays of the 2HDM at NLO. A numerical evaluation of all processes would show if these schemes fulfill the criterion of numerical stability in general, additionally to being manifestly gauge-independent and process-independent. If this was shown for all processes, the pinched schemes for $\delta\alpha$ and $\delta\beta$ and the improved $\overline{\text{MS}}$ scheme for $\delta\Lambda_5$ could be established as the preferred renormalization schemes for the 2HDM.

Alternative Parametrization of the 2HDM Potential

The form of the 2HDM potential introduced in Eq. (2.7) is one of the most commonly used ones in the literature [33, 150], although, it is not the only way to parametrize the scalar sector. Another form of parametrization is the one introduced in the *Higgs Hunter's Guide* [32], which is implemented in the `FeynArts` [55] model file. Therefore, it is convenient to state this form of the potential explicitly, as well.

The most general form of the 2HDM potential in the *Higgs Hunter's Guide* parametrization, restricted by a discrete \mathbb{Z}_2 symmetry $\Phi_1 \rightarrow -\Phi_1$ that is only softly violated, contains seven real parameters Λ_i ($i = 1, \dots, 7$), two real vacuum expectation values V_1 , V_2 and one real CP-violating phase ξ . Note that we use an upper case notation for the vevs in order to distinguish them from those of the potential in Sec. 2.4. The vevs for the two different parametrizations of the potentials are connected through the relations

$$V_1 = \frac{v_1}{\sqrt{2}}, \quad V_2 = \frac{v_2}{\sqrt{2}}, \quad v^2 = \frac{2V_1V_2}{s_\beta c_\beta}. \quad (\text{A.1})$$

The minimum conditions are automatically fulfilled by the parametrization. In the CP-conserving case, i.e. for $\Lambda_7 = 0$ and $\xi = 0$, the 2HDM potential is given by [150]

$$\begin{aligned} V = & \Lambda_1 \left(\Phi_1^\dagger \Phi_1 - V_1^2 \right)^2 + \Lambda_2 \left(\Phi_2^\dagger \Phi_2 - V_2^2 \right)^2 + \Lambda_3 \left[\left(\Phi_1^\dagger \Phi_1 - V_1^2 \right) + \left(\Phi_2^\dagger \Phi_2 - V_2^2 \right) \right]^2 \\ & + \Lambda_4 \left[\left(\Phi_1^\dagger \Phi_1 \right) \left(\Phi_2^\dagger \Phi_2 \right) - \left(\Phi_1^\dagger \Phi_2 \right) \left(\Phi_2^\dagger \Phi_1 \right) \right] + \Lambda_5 \left[\text{Re} \left(\Phi_1^\dagger \Phi_2 \right) - V_1 V_2 \right]^2 \\ & + \Lambda_6 \left[\text{Im} \left(\Phi_1^\dagger \Phi_2 \right) \right]^2. \end{aligned} \quad (\text{A.2})$$

In the CP-conserving case, the parameters of the potential in Eq. (2.7) can be converted into those of the potential in Eq. (A.2) through the relations [150]

$$\begin{aligned}
\lambda_1 &= 2(\Lambda_1 + \Lambda_3) , \\
\lambda_2 &= 2(\Lambda_2 + \Lambda_3) , \\
\lambda_3 &= 2\Lambda_3 + \Lambda_4 , \\
\lambda_4 &= -\Lambda_4 + \frac{\Lambda_5 + \Lambda_6}{2} , \\
\lambda_5 &= \frac{\Lambda_5 - \Lambda_6}{2} , \\
m_{11}^2 &= -2V_1^2\Lambda_1 - 2(V_1^2 + V_2^2)\Lambda_3 , \\
m_{22}^2 &= -2V_2^2\Lambda_2 - 2(V_1^2 + V_2^2)\Lambda_3 , \\
m_{12}^2 &= V_1V_2\Lambda_5 ,
\end{aligned} \tag{A.3}$$

and vice versa through [150]

$$\begin{aligned}
\Lambda_1 &= \frac{\lambda_1 - \lambda_{345}}{2} + \frac{m_{12}^2}{v^2 s_\beta c_\beta} , \\
\Lambda_2 &= \frac{\lambda_2 - \lambda_{345}}{2} + \frac{m_{12}^2}{v^2 s_\beta c_\beta} , \\
\Lambda_3 &= \frac{\lambda_{345}}{2} - \frac{m_{12}^2}{v^2 s_\beta c_\beta} , \\
\Lambda_4 &= \frac{2m_{12}^2}{v^2 s_\beta c_\beta} - \lambda_4 - \lambda_5 , \\
\Lambda_5 &= \frac{2m_{12}^2}{v^2 s_\beta c_\beta} , \\
\Lambda_6 &= \frac{2m_{12}^2}{v^2 s_\beta c_\beta} - 2\lambda_5 .
\end{aligned} \tag{A.4}$$

Note that m_{11}^2 and m_{22}^2 are absent in Eq. (A.4), since both parameters can be eliminated from the 2HDM potential by using the tadpole conditions, as shown in Eq. (2.14).

Introduction to the Pinch Technique

In the following, we want to present a detailed introduction to the pinch technique. The main focus of the introduction lies on the presentation of the principles of the pinch technique as well as on the performance of actual calculations. Most of this introduction is adopted from D. Binosi and J. Papavassiliou [93] and can be seen as a brief review of some parts of their work.

B.1. Motivation

The quantization of vector fields in quantum field theories gives rise to gauge-freedom. Such a freedom is inherently unphysical in the sense that it introduces a gauge-dependence in the results of many calculations within the field-theoretical framework. Since gauge-freedom is purely unphysical, it is clear that all calculated physical predictions, e.g. partial decay widths as observables, must be manifestly gauge-independent. However, it may happen that intermediate parts of the calculations, e.g. self-energies or mass counterterms, turn out to be gauge-dependent. It is then only the coherent sum of all these contributions that gives manifestly gauge-independent results.

With the help of the pinch technique, it is possible to extract these gauge-dependences in an unambiguous way. It turns out that the gauge-dependences are similar in structure, no matter of their origins. In the language of Feynman diagrams, it can be shown that all gauge-dependences of a certain process have structures like e.g. self-energies. The pinch technique allows to isolate and extract these gauge-dependences in a unique way. It is then possible to construct e.g. self-energies and mass counterterms which are manifestly gauge-independent by themselves.

The main motivation for using the pinch technique within the scope of this thesis is the gauge-independent construction of scalar mixing angle counterterms in the 2HDM. The concept of the technique itself is independent of the considered model, however. For the introduction of the pinch technique we will restrict ourselves to QCD since in this theory, many calculations are simplified considerably.

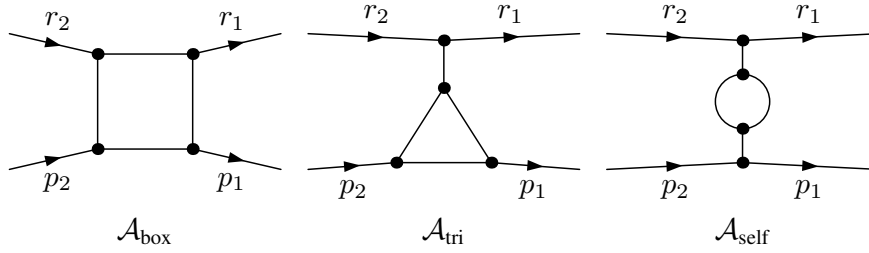


Figure B.1.: Topological contributions to the one-loop scattering amplitude. The one-loop amplitude of the fermion-fermion scattering process consists of all box diagrams \mathcal{A}_{box} , triangle diagrams \mathcal{A}_{tri} and self-energy diagrams $\mathcal{A}_{\text{self}}$. The diagrams represent only the respective topologies and have to be replaced by the actual QCD diagrams for performing the calculations.

B.2. Basic Principles of the Pinch Technique

B.2.1. Cancellation of Gauge-Dependences within One-Loop Amplitudes

We consider an elastic two-to-two scattering process of two fermions with masses m_1 and m_2 as an exemplary scattering process. At the one-loop level, the scattering amplitude contains contributions¹ from box diagrams \mathcal{A}_{box} , triangle diagrams \mathcal{A}_{tri} and self-energy diagrams $\mathcal{A}_{\text{self}}$. The topological contributions as well as the momenta of the fermions are depicted in Fig. B.1. For convenience, we introduce the Mandelstam variables

$$s := (r_1 + p_1)^2 = (r_2 + p_2)^2, \quad (\text{B.1})$$

$$t := (r_1 - r_2)^2 = (p_1 - p_2)^2, \quad (\text{B.2})$$

$$u := (r_1 - p_2)^2 = (p_1 - r_2)^2. \quad (\text{B.3})$$

Each of the amplitudes shown in Fig. B.1 contains internal gluons. If we perform the gauge-fixing of our theory in general R_ξ gauge, then the gauge-dependence in these amplitudes appears through longitudinal components in the gluon propagators, parametrized by the gauge-fixing parameter ξ of the gluons. The full one-loop contribution to the fermion-fermion scattering amplitude is simply the sum of all topological contributions,

$$\mathcal{A}_{\text{1loop}}(s, t, m_1, m_2) := \mathcal{A}_{\text{box}}(s, t, m_1, m_2; \xi) + \mathcal{A}_{\text{tri}}(t, m_1, m_2; \xi) + \mathcal{A}_{\text{self}}(t; \xi), \quad (\text{B.4})$$

where in brackets, we stated the explicit dependence of the respective amplitudes on the Mandelstam variables, the fermion masses and on the gauge-fixing parameter ξ . On the left-hand side of Eq. (B.4), we made explicit that the full one-loop contribution $\mathcal{A}_{\text{1loop}}$ is manifestly gauge-independent².

Due to the fact that the left-hand side of Eq. (B.4) does not depend on ξ , it is clear that the gauge-dependences of the box, triangle and self-energy diagrams in the right-hand side of Eq. (B.4) must cancel against each other. The main idea of the pinch technique is to isolate the gauge-dependent parts of each topology and rearrange the amplitudes in such a way that each amplitude in Eq. (B.4) is manifestly gauge-independent *by itself*. That such a rearrangement is in principle possible shall be outlined in the following.

Differentiating Eq. (B.4) with respect to s and ξ immediately yields

$$\frac{d^2 \mathcal{A}_{\text{box}}(s, t, m_1, m_2; \xi)}{ds d\xi} = 0. \quad (\text{B.5})$$

¹For better readability, we omit a global factor of i in all amplitudes in this section.

²The full scattering amplitude, i.e. the S -matrix element of the corresponding process, is gauge-independent order-by-order in perturbation theory [5].

Consequently, the sum of all box diagrams of the scattering process can be brought into the form

$$\mathcal{A}_{\text{box}}(s, t, m_1, m_2; \xi) \equiv \widehat{\mathcal{A}}_{\text{box}}(s, t, m_1, m_2) + f_{\text{box}}(t, m_1, m_2; \xi) , \quad (\text{B.6})$$

where the term f_{box} contains all gauge-dependent parts which originate from the box diagrams, while $\widehat{\mathcal{A}}_{\text{box}}$ is manifestly gauge-independent. Since the contributions in f_{box} have the same dependence on the Mandelstam variables and masses as the triangle diagrams, we can add the former to the triangle diagrams in Eq. (B.4) by defining

$$\widetilde{\mathcal{A}}_{\text{tri}}(t, m_1, m_2; \xi) := \mathcal{A}_{\text{tri}}(t, m_1, m_2; \xi) + f_{\text{box}}(t, m_1, m_2; \xi) . \quad (\text{B.7})$$

Next, we differentiate Eq. (B.4) with respect to ξ and the masses m_1, m_2 , which yields

$$\frac{d^3 \widetilde{\mathcal{A}}_{\text{tri}}(t, m_1, m_2; \xi)}{dm_1 dm_2 d\xi} = 0 . \quad (\text{B.8})$$

This allows us to cast the triangle diagrams into the form

$$\widetilde{\mathcal{A}}_{\text{tri}}(t, m_1, m_2; \xi) \equiv \widehat{\mathcal{A}}_{\text{tri}}(t, m_1, m_2) + f_{\text{tri}}(t; \xi) , \quad (\text{B.9})$$

where the quantity $\widehat{\mathcal{A}}_{\text{tri}}$ is manifestly gauge-independent and all gauge-dependent parts of the triangle diagrams were shifted into the term f_{tri} . The latter has the same structure as the self-energy contributions in Eq. (B.4), therefore, we combine both to create the modified self-energy contributions

$$\widetilde{\mathcal{A}}_{\text{self}}(t; \xi) := \mathcal{A}_{\text{self}}(t; \xi) + f_{\text{tri}}(t; \xi) . \quad (\text{B.10})$$

As a last step, we differentiate Eq. (B.4) again, now with respect to ξ only, which yields

$$\frac{d \widetilde{\mathcal{A}}_{\text{self}}(t; \xi)}{d\xi} = 0 . \quad (\text{B.11})$$

This identity makes it clear that the modified self-energies are manifestly gauge-independent by themselves:

$$\widetilde{\mathcal{A}}_{\text{self}}(t; \xi) \equiv \widehat{\mathcal{A}}_{\text{self}}(t) . \quad (\text{B.12})$$

The rearrangement of the gauge-dependent parts through Eqs. (B.6), (B.9) and (B.12) shows that Eq. (B.4) can be written in an alternative, though completely analogous form as

$$\mathcal{A}_{\text{1loop}}(s, t, m_1, m_2) = \widehat{\mathcal{A}}_{\text{box}}(s, t, m_1, m_2) + \widehat{\mathcal{A}}_{\text{tri}}(t, m_1, m_2) + \widehat{\mathcal{A}}_{\text{self}}(t) . \quad (\text{B.13})$$

However, in contrast to Eq. (B.4), this form of the one-loop scattering amplitude makes it clear that all *modified contributions* from box, triangle and self-energy diagrams in Eq. (B.13) form manifestly gauge-independent subsets by themselves.

We have demonstrated that the gauge-dependences of the box, triangle and self-energy diagrams cancel against each other in order to create the overall gauge-independent one-loop amplitude. On the other hand, we also have shown that the gauge-dependences of each topology can be extracted in the form of the terms f_{box} and f_{tri} . The combination of these terms with the topological contributions of the amplitude allows for the creation of gauge-independent subsets for each topology. The pinch technique is a computational tool which allows us to determine precisely these terms f_{box} and f_{tri} in an unambiguous way. As a consequence, the cancellation of the gauge-dependences within a one-loop amplitude is made explicit. Furthermore, the pinch technique allows for the creation of a manifestly gauge-independent *pinched self-energy*, which will be demonstrated in App. B.3.9.

B.2.2. The Pinch Technique in Practice

In order to apply the pinch technique, we have to specify a toy scattering process involving external fermions. We consider any external fermion with momentum p and mass m to be OS, so that the Dirac equation holds:

$$\begin{aligned}\bar{u}(p) (\not{p} - m) &= 0 , \\ (\not{p} - m) u(p) &= 0 .\end{aligned}\tag{B.14}$$

If our goal is not only the analysis of the cancellation of all gauge-dependences within the one-loop scattering amplitude, but furthermore the creation of a manifestly gauge-independent pinched self-energy, we have to choose a process which contains the unpinched version of this self-energy in the LO scattering amplitude in the form of a LO propagator.

We define the propagator for a fermion with momentum p ,

$$iS(p) := \frac{i(\not{p} + m)}{p^2 - m^2} \equiv \frac{i}{\not{p} - m} ,\tag{B.15}$$

where the momentum is pointing in the direction of fermion number flow. Up to a factor of i , the inverse of the propagator is given by

$$S^{-1}(p) = \not{p} - m .\tag{B.16}$$

Many of the box, triangle and self-energy contributions in Fig. B.1 contain internal fermions with momenta $k + p$ inside loops, with k being the loop momentum, which appear in the form of a fermion propagator $S(k + p)$. The main idea of the pinch technique is to trigger the elementary Ward identity

$$\begin{aligned}\not{k} &= (\not{k} + \not{p} - m) - (\not{p} - m) \\ &= S^{-1}(k + p) - S^{-1}(p)\end{aligned}\tag{B.17}$$

for any of these internal fermions inside the loop. If p is an external fermion momentum, then the second part of Eq. (B.17) vanishes OS due to Eq. (B.14),

$$\bar{u}(p)S^{-1}(p) = S^{-1}(p)u(p) = 0 ,\tag{B.18}$$

while the first part of Eq. (B.17) has the structure to cancel the internal fermion propagator, i.e. the internal fermion is *pinched out*:

$$S(k + p)S^{-1}(k + p) = S^{-1}(k + p)S(k + p) = \mathbb{1} .\tag{B.19}$$

In the language of Feynman diagrams, this means that diagrams with internal fermion propagators are reduced to diagrams with effective, unphysical vertices (i.e. vertices that are not contained in the Lagrangian) in order to make the gauge-dependence explicit. In the end, all gauge-dependent contributions of these diagrams cancel precisely when calculating the full one-loop scattering amplitude.

In order to demonstrate this procedure, we will calculate the full one-loop contributions to the quark-quark scattering amplitude in QCD and show how the pinch technique is applied in order to unambiguously isolate the gauge-dependent parts.

B.3. Gauge-Independent Quark-Quark Scattering Amplitude

B.3.1. Preliminary Remarks

Throughout our calculations, we need several identities of the color algebra as listed below. We follow Einstein's sum convention, meaning that we sum over repeated indices. The useful relations are [5]

$$[t^a, t^b] = i f^{abc} t^c, \quad (\text{B.20})$$

$$i f^{abc} t^a t^b = -\frac{1}{2} C_A t^c, \quad (\text{B.21})$$

$$t^a t^b t^a = \left(C_f - \frac{1}{2} C_A \right) t^b, \quad (\text{B.22})$$

$$f^{abc} f^{abd} = C_A \delta^{cd}, \quad (\text{B.23})$$

where $t^a \equiv t_f^a$ ($a = 1, 2, \dots, 8$) are the generators in the fundamental representation, f^{abc} are the structure constants and C_r are the Casimir eigenvalues of the $SU(3)_C$, i.e. the invariants of the representation r as defined by

$$t_r^a t_r^a = C_r \mathbb{1} \quad (\text{B.24})$$

for both the adjoint ($r = A$) and fundamental ($r = f$) representation.

For the calculation of the pinch contributions beyond LO, we define the short-hand notation

$$\int_k := \int \frac{d^4 k}{(2\pi)^4} \quad (\text{B.25})$$

for the integral operator appearing in the one-loop amplitudes. We want to emphasize that the application of the pinch technique is independent of the regularization of the UV-divergent one-loop integrals. Consequently, the cancellation of all gauge-dependent pinched parts within the one-loop amplitude takes place before any UV divergences are regularized and renormalized. For the purpose of demonstrating the cancellation of all gauge-dependences, we will not solve any one-loop diagram. We will, however, make use of the following integral [5]:

$$\int_k \frac{k_\mu}{k^4} = 0. \quad (\text{B.26})$$

B.3.2. The Scattering Amplitude at LO

We choose the scattering of two quarks with equal masses m as depicted in Fig. B.2 as our toy process. In order to perform the calculations by hand, we need the gluon propagator for a gluon with momentum q in general R_ξ gauge, which reads [5]

$$i\Delta_{\mu\nu}(q) = -\frac{i}{q^2} \left[g_{\mu\nu} - (1 - \xi) \frac{q_\mu q_\nu}{q^2} \right] \equiv -\frac{i}{q^2} \left[g_{\mu\nu} - \lambda \frac{q_\mu q_\nu}{q^2} \right], \quad (\text{B.27})$$

where we introduced the shorthand notation

$$\lambda := 1 - \xi. \quad (\text{B.28})$$

Since our toy process in Fig. B.2 is a t -channel scattering diagram, the kinematics of the process is determined by

$$q = r_2 - r_1 = p_1 - p_2 = \sqrt{t}. \quad (\text{B.29})$$

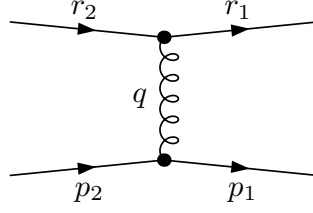


Figure B.2.: Quark-quark scattering at LO. The scattering of two quarks, here depicted at LO, serves as our toy process for introducing the pinch technique. Note that we are only interested in the QCD-part of the scattering, i.e. the diagram that contains a gluon.

At LO, the scattering amplitude is given by

$$i\mathcal{A}_{\text{LO}} = i\Gamma_{(r_1, r_2)}^{a\mu} i\Delta_{\mu\nu}(q) i\Gamma_{(p_1, p_2)}^{a\nu}, \quad (\text{B.30})$$

where we defined the quark-quark-gluon vertex together with the contracted external spinor structure [5],

$$i\Gamma_{(p_1, p_2)}^{a\nu} := i\bar{u}(p_1)g_s t^a \gamma^\nu u(p_2), \quad (\text{B.31})$$

with γ^ν being the Dirac matrices, g_s the strong coupling constant and $\bar{u}(p_1)$ and $u(p_2)$ the (adjoint) spinors of the external quarks with momenta p_1 and p_2 , respectively. The form of the other quark-quark-gluon vertex appearing in Fig. B.2 is analogous to Eq. (B.31).

Due to the appearance of the gauge-fixing parameter ξ in Eq. (B.27), we would expect that the scattering amplitude in Eq. (B.30) is manifestly gauge-dependent even at LO. When inserting Eqs. (B.27) and (B.29) into Eq. (B.30) however, we realize that due to the Dirac equation in Eq. (B.14), the gauge-dependent part of the propagator is removed and the scattering amplitude reduces to

$$i\mathcal{M}_{\text{tree}} = i\Gamma_{(r_1, r_2)}^{a\mu} \frac{-ig_{\mu\nu}}{q^2} i\Gamma_{(p_1, p_2)}^{a\nu}, \quad (\text{B.32})$$

which is manifestly gauge-independent as expected.

In the following, we want to apply the pinching procedure to the one-loop level. In order to simplify the bookkeeping, we will investigate the distinct topological contributions from Fig. B.1 of the one-loop amplitude separately.

B.3.3. Pinch Contributions from the Box Diagrams

We first consider the two NLO box diagrams shown in Fig. B.3. With the kinematics stated in the Feynman diagrams, the sum of the two contributions reads

$$i\mathcal{A}_{\text{box}} = \int_k g_s^2 \bar{u}(r_1) \gamma^\alpha t^a S(r_2 - k) \gamma^\rho t^b u(r_2) \Delta_{\alpha\beta}(k - q) \Delta_{\rho\sigma}(k) \cdot g_s^2 \bar{u}(p_1) \left[\gamma^\beta t^a S(p_2 + k) \gamma^\sigma t^b + \gamma^\sigma t^b S(p_1 - k) \gamma^\beta t^a \right] u(p_2). \quad (\text{B.33})$$

Inserting the product of the two gluon propagators,

$$\Delta_{\alpha\beta}(k - q) \Delta_{\rho\sigma}(k) = \frac{1}{k^2(k - q)^2} \left[g_{\alpha\beta} g_{\rho\sigma} - \lambda \left(\frac{(k - q)_\alpha (k - q)_\beta}{(k - q)^2} g_{\rho\sigma} + \frac{k_\rho k_\sigma}{k^2} g_{\alpha\beta} \right) + \lambda^2 \frac{(k - q)_\alpha (k - q)_\beta k_\rho k_\sigma}{k^2(k - q)^2} \right], \quad (\text{B.34})$$

into Eq. (B.33) allows for the separation of the box diagrams into three distinct contributions,

$$i\mathcal{A}_{\text{box}} = [i\mathcal{A}_{\text{box}}]_{\xi=1} + [i\mathcal{A}_{\text{box}}]_\lambda + [i\mathcal{A}_{\text{box}}]_{\lambda^2}, \quad (\text{B.35})$$

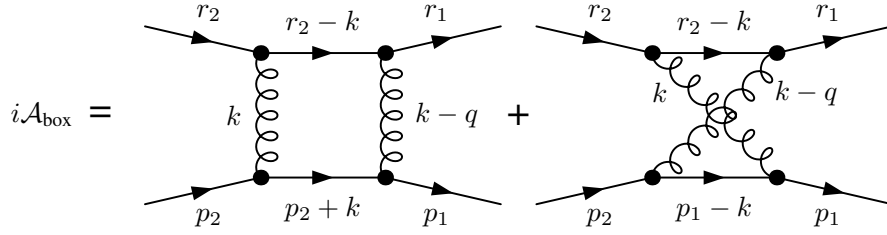


Figure B.3.: One-loop box contributions. The one-loop box diagrams introduce several pinching terms which contain the gauge-dependence. The kinematics is given in the diagram. For the quarks, the direction of momentum flow is equivalent to the direction of fermion number flow.

where we defined

$$[i\mathcal{A}_{\text{box}}]_{\xi=1} := \int_k g_s^2 \bar{u}(r_1) \gamma^\alpha t^a S(r_2 - k) \gamma^\rho t^b u(r_2) \frac{g_{\alpha\beta} g_{\rho\sigma}}{k^2 (k - q)^2} \cdot g_s^2 \bar{u}(p_1) \left[\gamma^\beta t^a S(p_2 + k) \gamma^\sigma t^b + \gamma^\sigma t^b S(p_1 - k) \gamma^\beta t^a \right] u(p_2), \quad (\text{B.36})$$

$$[i\mathcal{A}_{\text{box}}]_\lambda := -\lambda \int_k g_s^2 \bar{u}(r_1) \gamma^\alpha t^a S(r_2 - k) \gamma^\rho t^b u(r_2) \left(\frac{(k - q)_\alpha (k - q)_\beta}{k^2 (k - q)^4} g_{\rho\sigma} + \frac{k_\rho k_\sigma}{k^4 (k - q)^2} g_{\alpha\beta} \right) \cdot g_s^2 \bar{u}(p_1) \left[\gamma^\beta t^a S(p_2 + k) \gamma^\sigma t^b + \gamma^\sigma t^b S(p_1 - k) \gamma^\beta t^a \right] u(p_2), \quad (\text{B.37})$$

$$[i\mathcal{A}_{\text{box}}]_{\lambda^2} := \lambda^2 \int_k g_s^2 \bar{u}(r_1) \gamma^\alpha t^a S(r_2 - k) \gamma^\rho t^b u(r_2) \frac{(k - q)_\alpha (k - q)_\beta k_\rho k_\sigma}{k^4 (k - q)^4} \cdot g_s^2 \bar{u}(p_1) \left[\gamma^\beta t^a S(p_2 + k) \gamma^\sigma t^b + \gamma^\sigma t^b S(p_1 - k) \gamma^\beta t^a \right] u(p_2). \quad (\text{B.38})$$

The pinch technique is always applied if a contracted loop momentum \not{k} (or other combinations $\not{k} \pm \not{q}$ containing the loop momentum) appears next to an internal fermion propagator. To illustrate the procedure, we first focus on Eq. (B.37) and take a look at the effect of the loop momentum k_σ being contracted with the Dirac matrices in the second line of Eq. (B.37):

$$\begin{aligned} & k_\sigma g_s^2 \bar{u}(p_1) \left[\gamma^\beta t^a S(p_2 + k) \gamma^\sigma t^b + \gamma^\sigma t^b S(p_1 - k) \gamma^\beta t^a \right] u(p_2) \\ &= g_s^2 \bar{u}(p_1) \left[\gamma^\beta t^a S(p_2 + k) \not{k} t^b + \not{k} t^b S(p_1 - k) \gamma^\beta t^a \right] u(p_2) \\ &\stackrel{(\text{B.17})}{=} g_s^2 \bar{u}(p_1) \left[\gamma^\beta t^a S(p_2 + k) (S^{-1}(p_2 + k) - S^{-1}(p_2)) t^b \right. \\ &\quad \left. - (S^{-1}(p_1 - k) - S^{-1}(p_1)) t^b S(p_1 - k) \gamma^\beta t^a \right] u(p_2) \\ &\stackrel{(\text{B.18})}{=} g_s^2 \bar{u}(p_1) \left[\gamma^\beta t^a S(p_2 + k) S^{-1}(p_2 + k) t^b \right. \\ &\quad \left. - S^{-1}(p_1 - k) t^b S(p_1 - k) \gamma^\beta t^a \right] u(p_2) \\ &\stackrel{(\text{B.19})}{=} g_s^2 \bar{u}(p_1) \gamma^\beta \left[t^a, t^b \right] u(p_2) \\ &\stackrel{(\text{B.20})}{=} i g_s^2 \bar{u}(p_1) \gamma^\beta f^{abc} t^c u(p_2) \\ &\stackrel{(\text{B.31})}{=} g_s f^{abc} i \Gamma_{(p_1, p_2)}^{c\beta} \end{aligned} \quad (\text{B.39})$$

Using Eqs. (B.17) and (B.19) is precisely the application of the pinch technique. The intermediate result in Eq. (B.39) has the form of a new effective vertex of two quarks and two gluons, since the lower internal fermions in the two loops in Fig. B.3 are pinched out.

In order to consistently apply the pinch technique, we have to pinch again, since the other momentum k_ρ can also be contracted with the Dirac matrix in the first line of Eq. (B.37):

$$\begin{aligned}
& k_\rho g_s^2 \bar{u}(r_1) \gamma^\alpha t^a S(r_2 - k) \gamma^\rho t^b u(r_2) \\
&= g_s^2 \bar{u}(r_1) \gamma^\alpha t^a S(r_2 - k) \not{k} t^b u(r_2) \\
&= -g_s^2 \bar{u}(r_1) \gamma^\alpha t^a S(r_2 - k) (S^{-1}(r_2 - k) - S^{-1}(r_2)) t^b u(r_2) \\
&= -g_s^2 \bar{u}(r_1) \gamma^\alpha t^a t^b u(r_2) .
\end{aligned} \tag{B.40}$$

Combining both results gives the first part of the contribution to $[i\mathcal{A}_{\text{box}}]_\lambda$:

$$\begin{aligned}
& -\lambda \int_k g_s^2 \bar{u}(r_1) \gamma^\alpha t^a S(r_2 - k) \gamma^\rho t^b u(r_2) \frac{k_\rho k_\sigma}{k^4(k-q)^2} g_{\alpha\beta} \\
& \quad \cdot g_s^2 \bar{u}(p_1) \left[\gamma^\beta t^a S(p_2 + k) \gamma^\sigma t^b + \gamma^\sigma t^b S(p_1 - k) \gamma^\beta t^a \right] u(p_2) \\
&= \lambda \int_k \frac{g_{\alpha\beta}}{k^4(k-q)^2} g_s^3 \bar{u}(r_1) \gamma^\alpha f^{abc} t^a t^b u(r_2) i\Gamma_{(p_1, p_2)}^{c\beta} \\
&\stackrel{\text{(B.21)}}{=} \frac{1}{2} \lambda g_s^2 C_A \int_k \frac{g_{\alpha\beta}}{k^4(k-q)^2} i\bar{u}(r_1) g_s t^c \gamma^\alpha u(r_2) i\Gamma_{(p_1, p_2)}^{c\beta} \\
&= \frac{1}{2} \lambda g_s^2 C_A \int_k \frac{g_{\alpha\beta}}{k^4(k-q)^2} i\Gamma_{(r_1, r_2)}^{c\alpha} i\Gamma_{(p_1, p_2)}^{c\beta} \\
&= \frac{1}{2} \lambda g_s^2 C_A \int_k \frac{g_{\alpha\beta}}{k^2(k+q)^4} i\Gamma_{(r_1, r_2)}^{c\alpha} i\Gamma_{(p_1, p_2)}^{c\beta} .
\end{aligned} \tag{B.41}$$

In the last step, a shift of the loop momentum has been performed. The calculations of the second contribution to $[i\mathcal{A}_{\text{box}}]_\lambda$ as well as of the contribution $[i\mathcal{A}_{\text{box}}]_{\lambda^2}$ proportional to λ^2 are completely analogous. In total, the contributions read

$$[i\mathcal{A}_{\text{box}}]_\lambda = \lambda g_s^2 C_A \int_k \frac{g_{\alpha\beta}}{k^2(k+q)^4} i\Gamma_{(r_1, r_2)}^{c\alpha} i\Gamma_{(p_1, p_2)}^{c\beta} , \tag{B.42}$$

$$[i\mathcal{A}_{\text{box}}]_{\lambda^2} = -\lambda^2 g_s^2 \frac{C_A}{2} \int_k \frac{k_\alpha k_\beta}{k^4(k+q)^4} i\Gamma_{(r_1, r_2)}^{c\alpha} i\Gamma_{(p_1, p_2)}^{c\beta} . \tag{B.43}$$

With these results at hand, the full box contributions from Eq. (B.35) can be cast into a convenient form:

$$\begin{aligned}
i\mathcal{A}_{\text{box}} &= [i\mathcal{A}_{\text{box}}]_{\xi=1} + \lambda g_s^2 C_A \int_k \frac{g_{\alpha\beta}}{k^2(k+q)^4} i\Gamma_{(r_1, r_2)}^{c\alpha} i\Gamma_{(p_1, p_2)}^{c\beta} \\
& \quad - \lambda^2 g_s^2 \frac{C_A}{2} \int_k \frac{k_\alpha k_\beta}{k^4(k+q)^4} i\Gamma_{(r_1, r_2)}^{c\alpha} i\Gamma_{(p_1, p_2)}^{c\beta} \\
&= [i\mathcal{A}_{\text{box}}]_{\xi=1} \\
& \quad + i\Gamma_{(r_1, r_2)}^{c\alpha} \frac{-i}{q^2} g_s^2 q^2 \left[\lambda^2 q^2 \frac{C_A}{2} \int_k \frac{k_\alpha k_\beta}{k^4(k+q)^4} - \lambda q^2 C_A \int_k \frac{g_{\alpha\beta}}{k^2(k+q)^4} \right] \frac{-i}{q^2} i\Gamma_{(p_1, p_2)}^{c\beta} \\
&\equiv [i\mathcal{A}_{\text{box}}]_{\xi=1} + i\Gamma_{(r_1, r_2)}^{c\alpha} \frac{-i g_{\alpha\mu}}{q^2} i\Sigma_{\text{box}}^{\mu\nu}(q^2) \frac{-i g_{\beta\nu}}{q^2} i\Gamma_{(p_1, p_2)}^{c\beta} .
\end{aligned} \tag{B.44}$$

The gauge-dependence is completely shifted into the factor

$$i\Sigma_{\text{box}}^{\mu\nu}(q^2) = g_s^2 q^2 \left[\lambda^2 q^2 \frac{C_A}{2} \int_k \frac{k^\mu k^\nu}{k^4(k+q)^4} - \lambda q^2 C_A \int_k \frac{g^{\mu\nu}}{k^2(k+q)^4} \right] , \tag{B.45}$$

which has the structure of a self-energy, i.e. the factor depends only on $q = \sqrt{t}$, but not on any other Mandelstam variables nor on any external masses m . This is exactly the achievement of the pinch technique. We started with gauge-dependent contributions originating from box diagrams, but as it turns out, these gauge-dependent contributions have the structure of self-energies.

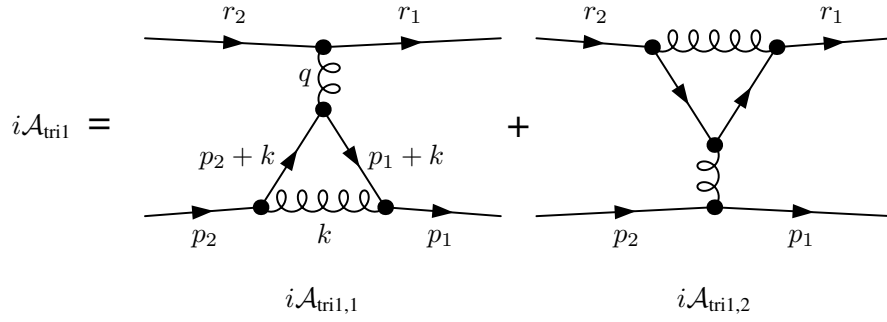


Figure B.4.: First part of one-loop triangle contributions. The first part of the one-loop triangle contributions consisting of two triangle diagrams. Since both diagrams yield equal pinch contributions, we calculate only the first diagram $i\mathcal{A}_{\text{tri1},1}$ explicitly.

B.3.4. Pinch Contributions from the Triangle Diagrams

The next pinch contributions originate from the triangle diagrams depicted in Figs. B.4 and B.5. We start with the calculation of the former two diagrams. The full amplitude of these triangle contributions is given by

$$i\mathcal{A}_{\text{tri1}} := i\mathcal{A}_{\text{tri1},1} + i\mathcal{A}_{\text{tri1},2} , \quad (\text{B.46})$$

where the amplitudes corresponding to the two diagrams, $i\mathcal{A}_{\text{tri1},1}$ and $i\mathcal{A}_{\text{tri1},2}$, are defined in Fig. B.4. The first of the two explicitly reads

$$\begin{aligned} i\mathcal{A}_{\text{tri1},1} &= \int_k \bar{u}(r_1) g_s^4 \gamma^\alpha t^a u(r_2) \Delta_{\alpha\beta}(q) \Delta_{\rho\sigma}(k) \bar{u}(p_1) \gamma^\rho t^b S(p_1+k) \gamma^\beta t^a S(p_2+k) \gamma^\sigma t^b u(p_2) \\ &= \frac{-i}{q^2} i\Gamma_{(r_1, r_2)}^{a\alpha} g_s^3 \int_k g_{\alpha\beta} \frac{1}{k^2} \left(g_{\rho\sigma} - \lambda \frac{k_\rho k_\sigma}{k^2} \right) \bar{u}(p_1) \gamma^\rho t^b S(p_1+k) \gamma^\beta t^a S(p_2+k) \gamma^\sigma t^b u(p_2) \\ &\equiv [i\mathcal{A}_{\text{tri1},1}]_{\xi=1} + [i\mathcal{A}_{\text{tri1},1}]_\lambda , \end{aligned} \quad (\text{B.47})$$

where we have split up the amplitude by defining

$$[i\mathcal{A}_{\text{tri1},1}]_{\xi=1} := \frac{-i}{q^2} i\Gamma_{(r_1, r_2)}^{a\alpha} g_s^3 \int_k \frac{g_{\alpha\beta} g_{\rho\sigma}}{k^2} \bar{u}(p_1) \gamma^\rho t^b S(p_1+k) \gamma^\beta t^a S(p_2+k) \gamma^\sigma t^b u(p_2) , \quad (\text{B.48})$$

$$[i\mathcal{A}_{\text{tri1},1}]_\lambda := \lambda \frac{i}{q^2} i\Gamma_{(r_1, r_2)}^{a\alpha} g_s^3 \int_k \frac{g_{\alpha\beta} k_\rho k_\sigma}{k^4} \bar{u}(p_1) \gamma^\rho t^b S(p_1+k) \gamma^\beta t^a S(p_2+k) \gamma^\sigma t^b u(p_2). \quad (\text{B.49})$$

The calculation of the gauge-dependent part $[i\mathcal{A}_{\text{tri1},1}]_\lambda$ is analogous to the calculations of the box diagrams:

$$\begin{aligned} [i\mathcal{A}_{\text{tri1},1}]_\lambda &= \lambda \frac{i}{q^2} i\Gamma_{(r_1, r_2)}^{a\alpha} g_s^3 \int_k \frac{g_{\alpha\beta}}{k^4} \bar{u}(p_1) \not{k} t^b S(p_1+k) \gamma^\beta t^a S(p_2+k) \not{k} t^b u(p_2) \\ &\stackrel{(\text{B.17})}{=} \lambda \frac{i}{q^2} i\Gamma_{(r_1, r_2)}^{a\alpha} g_s^3 \int_k \frac{g_{\alpha\beta}}{k^4} \bar{u}(p_1) (S^{-1}(p_1+k) - S^{-1}(p_1)) t^b S(p_1+k) \\ &\quad \cdot \gamma^\beta t^a S(p_2+k) (S^{-1}(p_2+k) - S^{-1}(p_2)) t^b u(p_2) \quad (\text{B.50}) \\ &\stackrel{(\text{B.18})}{=} \lambda \frac{i}{q^2} i\Gamma_{(r_1, r_2)}^{a\alpha} g_s^3 \int_k \frac{g_{\alpha\beta}}{k^4} \bar{u}(p_1) \gamma^\beta t^b t^a t^b u(p_2) \\ &\stackrel{(\text{B.22})}{=} i\Gamma_{(r_1, r_2)}^{a\alpha} \lambda \frac{1}{q^2} g_s^2 \left(C_f - \frac{C_A}{2} \right) \int_k \frac{g_{\alpha\beta}}{k^4} i\Gamma_{(p_1, p_2)}^{a\beta} . \end{aligned}$$

If we repeat this procedure for the second diagram in Fig. B.4 by splitting the amplitude into two parts,

$$i\mathcal{A}_{\text{tri1},2} \equiv [i\mathcal{A}_{\text{tri1},2}]_{\xi=1} + [i\mathcal{A}_{\text{tri1},2}]_\lambda , \quad (\text{B.51})$$

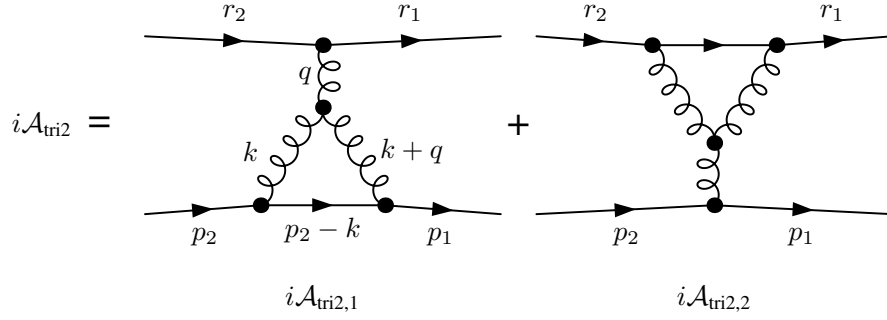


Figure B.5.: Second part of one-loop triangle contributions. The second part of the one-loop triangle contributions consists of two diagrams. Since these diagrams contain the three-gluon vertex, they yield pinch contributions not only through internal gluons in the loop, but additionally, through the three-gluon vertex itself.

we realize after a short calculation that the gauge-dependent part equals the one from the first diagram:

$$[i\mathcal{A}_{\text{tri1},2}]_{\lambda} = [i\mathcal{A}_{\text{tri1},1}]_{\lambda} = (\text{B.50}) . \quad (\text{B.52})$$

With these results at hand, the full contribution of the first two triangle diagrams in Fig. B.4 is given by

$$\begin{aligned} i\mathcal{A}_{\text{tri1}} &= [i\mathcal{A}_{\text{tri1},1}]_{\xi=1} + [i\mathcal{A}_{\text{tri1},1}]_{\lambda} + [i\mathcal{A}_{\text{tri1},2}]_{\xi=1} + [i\mathcal{A}_{\text{tri1},2}]_{\lambda} \\ &\stackrel{(\text{B.52})}{=} [i\mathcal{A}_{\text{tri1}}]_{\xi=1} + 2 \cdot [i\mathcal{A}_{\text{tri1},1}]_{\lambda} \\ &\stackrel{(\text{B.50})}{=} [i\mathcal{A}_{\text{tri1}}]_{\xi=1} + i\Gamma_{(r_1, r_2)}^{a\alpha} \frac{-i}{q^2} g_s^2 q^2 \left[\lambda (C_A - 2 C_f) \int_k \frac{g_{\alpha\beta}}{k^4} \right] \frac{-i}{q^2} i\Gamma_{(p_1, p_2)}^{a\beta} \\ &\equiv [i\mathcal{A}_{\text{tri1}}]_{\xi=1} + i\Gamma_{(r_1, r_2)}^{a\alpha} \frac{-ig_{\alpha\mu}}{q^2} i\Sigma_{\text{tri1}}^{\mu\nu}(q^2) \frac{-ig_{\beta\nu}}{q^2} i\Gamma_{(p_1, p_2)}^{a\beta} . \end{aligned} \quad (\text{B.53})$$

We have shifted the full gauge-dependence into the factor

$$i\Sigma_{\text{tri1}}^{\mu\nu}(q^2) = g_s^2 q^2 \left[\lambda (C_A - 2 C_f) \int_k \frac{g^{\mu\nu}}{k^4} \right] , \quad (\text{B.54})$$

which again has the structure of a self-energy, even though the gauge-dependent parts originated from triangle diagrams.

We turn to the second class of triangle diagrams shown in Fig. B.5. We calculate both diagrams separately again by splitting up the amplitude according to

$$i\mathcal{A}_{\text{tri2}} := i\mathcal{A}_{\text{tri2},1} + i\mathcal{A}_{\text{tri2},2} , \quad (\text{B.55})$$

and begin by calculating the former:

$$\begin{aligned} i\mathcal{A}_{\text{tri2},1} &= -ig_s^4 f^{amnn} \int_k \bar{u}(r_1) \gamma^{\alpha} t^a u(r_2) \bar{u}(p_1) \gamma^{\nu} t^n S(p_2 - k) \gamma^{\mu} t^m u(p_2) \Delta_{\alpha\beta}(q) \Delta_{\mu\mu'}(k) \\ &\quad \cdot \Delta_{\nu\nu'}(-q - k) \left[g^{\beta\mu'} (q - k)^{\nu'} + g^{\mu'\nu'} (2k + q)^{\beta} - g^{\nu'\beta} (2q + k)^{\mu'} \right] \\ &\stackrel{(\text{B.34})}{=} ig_s^4 \frac{1}{q^2} f^{amnn} \int_k \frac{1}{k^2(k+q)^2} \bar{u}(r_1) \gamma^{\alpha} t^a u(r_2) \bar{u}(p_1) \gamma^{\nu} t^n S(p_2 - k) \gamma^{\mu} t^m u(p_2) g_{\alpha\beta} \\ &\quad \cdot \left[g_{\mu\mu'} g_{\nu\nu'} - \lambda \left(\frac{k_{\mu} k_{\mu'}}{k^2} g_{\nu\nu'} + \frac{(k+q)_{\nu} (k+q)_{\nu'}}{(k+q)^2} g_{\mu\mu'} \right) + \lambda^2 \frac{k_{\mu} k_{\mu'} (k+q)_{\nu} (k+q)_{\nu'}}{k^2 (k+q)^2} \right] \\ &\quad \cdot \left[g^{\beta\mu'} (q - k)^{\nu'} + g^{\mu'\nu'} (2k + q)^{\beta} - g^{\nu'\beta} (2q + k)^{\mu'} \right] \\ &\equiv [i\mathcal{A}_{\text{tri2},1}]_{\xi=1} + [i\mathcal{A}_{\text{tri2},1}]_{\lambda} + [i\mathcal{A}_{\text{tri2},1}]_{\lambda^2} . \end{aligned} \quad (\text{B.56})$$

In the last step, we split the amplitude into three different parts:

$$[i\mathcal{A}_{\text{tri2},1}]_{\xi=1} := ig_s^4 \frac{1}{q^2} f^{amn} \int_k \frac{1}{k^2(k+q)^2} \bar{u}(r_1) \gamma^\alpha t^a u(r_2) \bar{u}(p_1) \gamma^\nu t^n S(p_2 - k) \gamma^\mu t^m u(p_2) \\ \cdot g_{\alpha\beta} g_{\mu\mu'} g_{\nu\nu'} \left[g^{\beta\mu'} (q-k)^{\nu'} + g^{\mu'\nu'} (2k+q)^\beta - g^{\nu'\beta} (2q+k)^{\mu'} \right], \quad (\text{B.57})$$

$$[i\mathcal{A}_{\text{tri2},1}]_\lambda := -\lambda ig_s^4 \frac{1}{q^2} f^{amn} \int_k \frac{1}{k^2(k+q)^2} \bar{u}(r_1) \gamma^\alpha t^a u(r_2) \bar{u}(p_1) \gamma^\nu t^n S(p_2 - k) \gamma^\mu t^m u(p_2) \\ \cdot \left[g^{\beta\mu'} (q-k)^{\nu'} + g^{\mu'\nu'} (2k+q)^\beta - g^{\nu'\beta} (2q+k)^{\mu'} \right] \quad (\text{B.58}) \\ \cdot g_{\alpha\beta} \left(\frac{k_\mu k_{\mu'}}{k^2} g_{\nu\nu'} + \frac{(k+q)_\nu (k+q)_{\nu'}}{(k+q)^2} g_{\mu\mu'} \right),$$

$$[i\mathcal{A}_{\text{tri2},1}]_{\lambda^2} := \lambda^2 ig_s^4 \frac{1}{q^2} f^{amn} \int_k \frac{1}{k^2(k+q)^2} \bar{u}(r_1) \gamma^\alpha t^a u(r_2) \bar{u}(p_1) \gamma^\nu t^n S(p_2 - k) \gamma^\mu t^m u(p_2) \\ \cdot \left[g^{\beta\mu'} (q-k)^{\nu'} + g^{\mu'\nu'} (2k+q)^\beta - g^{\nu'\beta} (2q+k)^{\mu'} \right] \quad (\text{B.59}) \\ \cdot g_{\alpha\beta} \frac{k_\mu k_{\mu'} (k+q)_\nu (k+q)_{\nu'}}{k^2 (k+q)^2}.$$

With regard to the pinch technique, this triangle diagram provides a special case which we did not encounter so far, since it contains a three-gluon vertex. We observe that it is not only the parts proportional to λ or λ^2 that contain pinch parts through the application of the Ward identity in Eq. (B.17). The term in Eq. (B.57) which is proportional to λ^0 , i.e. the term which remains in the amplitude if the calculation is performed in the Feynman-'t Hooft gauge, contains loop momenta originating from the three-gluon vertex. Contracting these loop momenta with the Dirac matrices in Eq. (B.57) yields additional pinch contributions by applying Eq. (B.17). For the moment, we will neglect these contributions, since we focus on the gauge-dependent parts only. In App. B.3.8, we consider these contributions in detail and present arguments for the inclusion of these additional gauge-independent terms in order to make the pinch technique consistent.

The calculation of the parts proportional to λ and λ^2 in Eqs. (B.58) and (B.59) is completely analogous to all calculations performed before. Therefore, we will directly state the results:

$$[i\mathcal{A}_{\text{tri2},1}]_\lambda = i\Gamma_{(r_1,r_2)}^{a\alpha} \lambda g_s^2 \frac{-1}{q^2} C_A \int_k \left(\frac{k_\alpha k_\beta}{k^4 (k+q)^2} + q^2 \frac{g_{\alpha\beta}}{k^2 (k+q)^4} - \frac{g_{\alpha\beta}}{k^4} \right) i\Gamma_{(p_1,p_2)}^{a\beta}, \quad (\text{B.60})$$

$$[i\mathcal{A}_{\text{tri2},1}]_{\lambda^2} = i\Gamma_{(r_1,r_2)}^{a\alpha} \frac{\lambda^2}{2} g_s^2 C_A \int_k \frac{k_\alpha k_\beta}{k^4 (k+q)^4} i\Gamma_{(p_1,p_2)}^{b\beta}. \quad (\text{B.61})$$

In order to get the full result, we need to calculate the second diagram of Fig. B.5 as well. The pinch contributions given by this diagram are exactly the same as the ones we calculated before, so the full gauge-dependent part is easily obtained:

$$i\mathcal{A}_{\text{tri2}} = [i\mathcal{A}_{\text{tri2}}]_{\xi=1} + i\Gamma_{(r_1,r_2)}^{a\alpha} \frac{-ig_{\alpha\mu}}{q^2} i\Sigma_{(\text{tri2})}^{\mu\nu}(q^2) \frac{-ig_{\beta\nu}}{q^2} i\Gamma_{(p_1,p_2)}^{a\beta}, \quad (\text{B.62})$$

where we defined

$$i\Sigma_{\text{tri2}}^{\mu\nu}(q^2) = g_s^2 q^2 \left[\lambda \left(2q^2 C_A \int_k \frac{g^{\mu\nu}}{k^2 (k+q)^4} + 2C_A \int_k \frac{k^\mu k^\nu}{k^4 (k+q)^2} - 2C_A \int_k \frac{g^{\mu\nu}}{k^4} \right) \right. \\ \left. - \lambda^2 q^2 C_A \int_k \frac{k^\mu k^\nu}{k^4 (k+q)^4} \right], \quad (\text{B.63})$$

which again has the structure of a self-energy.

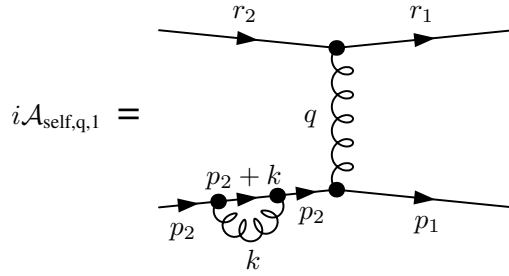


Figure B.6.: One-loop correction to the quark self-energies. For a consistent calculation of the one-loop scattering amplitude, the one-loop corrections of the external quark legs have to be considered as well. The pinch contributions are the same for all four external leg corrections, therefore, we depict only the correction to one external leg.

B.3.5. Pinch Contributions from the Quark Self-Energy Diagrams

So far, we calculated all NLO box and triangle contributions to the quark-quark-scattering. Next, we focus on self-energy contributions. In order to consistently apply the pinch technique, we need to include one-loop corrections to the external quark legs as depicted in Fig. B.6. Note that all four diagrams carry a factor of $1/2$ which originates from the correct application of the LSZ reduction formula for the external leg corrections. The correction to one external quark in Fig. B.6 is given by

$$\begin{aligned}
i\mathcal{A}_{\text{self},q,1} &= \frac{1}{2}g_s^4 \int_k \bar{u}(r_1)\gamma^\alpha t^a u(r_2)\bar{u}(p_1)\gamma^\beta t^a S(p_2)\gamma^\rho t^b S(p_2+k)\gamma^\sigma t^b u(p_2)\Delta_{\alpha\beta}(q)\Delta_{\rho\sigma} \\
&\stackrel{\text{(B.24)}}{=} [i\mathcal{A}_{\text{self},q,1}]_{\xi=1} + i\lambda\frac{g_s^3}{2}C_f g_{\alpha\beta}\frac{1}{q^2}i\Gamma_{(r_1,r_2)}^{a\alpha} \int_k \frac{1}{k^4}\bar{u}(p_1)\gamma^\beta t^a S(p_2)\not{k}S(p_2+k)\not{k}u(p_2) \\
&\stackrel{\text{(B.17)}}{=} [i\mathcal{A}_{\text{self},q,1}]_{\xi=1} + i\lambda\frac{g_s^3}{2}C_f g_{\alpha\beta}\frac{1}{q^2}i\Gamma_{(r_1,r_2)}^{a\alpha} \int_k \frac{1}{k^4}\bar{u}(p_1)\gamma^\beta t^a S(p_2)u(p_2) \\
&\quad \cdot [S^{-1}(p_2+k) - 2S^{-1}(p_2) + S^{-1}(p_2)S(p_2+k)S^{-1}(p_2)] \\
&\stackrel{\text{(B.26)}}{=} [i\mathcal{A}_{\text{self},q,1}]_{\xi=1} - i\lambda\frac{g_s^3}{2}C_f g_{\alpha\beta}\frac{1}{q^2}i\Gamma_{(r_1,r_2)}^{a\alpha} \int_k \bar{u}(p_1)\gamma^\beta t^a S(p_2)S^{-1}(p_2) \\
&\quad \cdot \left(\frac{1}{k^4} - S(p_2+k)S^{-1}(p_2)\right) u(p_2) \\
&= [i\mathcal{A}_{\text{self},q,1}]_{\xi=1} + i\Gamma_{(r_1,r_2)}^{a\alpha}\frac{-ig_{\alpha\mu}}{q^2}\left[\frac{\lambda}{2}g_s^2C_f q^2 \int_k \frac{g^{\mu\nu}}{k^4}\right]\frac{-ig_{\beta\nu}}{q^2}i\Gamma_{(p_1,p_2)}^{a\beta}.
\end{aligned} \tag{B.64}$$

Repeating the calculation for the other three external quark legs reveals that they all give the same result with respect to the pinch technique. In total, the full one-loop quark self-energy contributions, given as the sum of the four external leg corrections, reads

$$i\mathcal{A}_{\text{self},q} = [i\mathcal{A}_{\text{self},q}]_{\xi=1} + i\Gamma_{(r_1,r_2)}^{a\alpha}\frac{-ig_{\alpha\mu}}{q^2}i\Sigma_{(\text{self},q)}^{\mu\nu}(q^2)\frac{-ig_{\beta\nu}}{q^2}i\Gamma_{(p_1,p_2)}^{a\beta}, \tag{B.65}$$

where we defined

$$i\Sigma_{\text{self},q}^{\mu\nu}(q^2) = g_s^2 q^2 \left[2\lambda C_f \int_k \frac{g^{\mu\nu}}{k^4} \right]. \tag{B.66}$$

B.3.6. Pinch Contributions from the Gluon Self-Energy Diagrams

The only missing ingredients to the full one-loop amplitude of the quark-quark scattering are the Feynman diagrams containing the gluon self-energy corrections, depicted in Fig. B.7. The fermion loops do not introduce gauge-dependences and since gluons are massless particles,

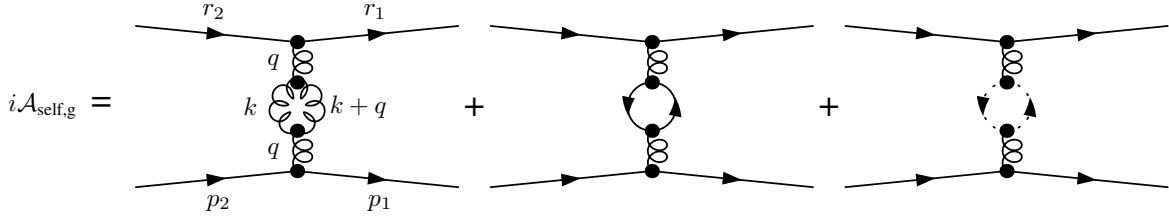


Figure B.7.: One-loop corrections to the gluon self-energy. The quark-quark scattering amplitude contains contributions consisting of one-loop corrections to the gluon self-energy. The corrections include loops with gluons, fermions and ghosts. Neither the fermion nor the ghost loops introduce pinching parts.

the ghost loops introduce no gauge-dependent parts either. Thus, the only diagram we need to pinch is the one with the gluon loop. The calculation is exactly analogous as the previous calculations, thus, we shorten the presentation of the calculation and directly state the result. Taking into account the symmetry factor of $1/2$ for the gluon loop, the sum of all contributions from Fig. B.7 reads

$$\begin{aligned}
i\mathcal{A}_{\text{self,g}} &= -\frac{1}{2}g_s^4 \int_k \bar{u}(r_1)\gamma^\alpha t^a u(r_2)\bar{u}(p_1)\gamma^\beta t^b u(p_2)\Delta_{\alpha\alpha'}(q)\Delta_{\beta\beta'}(q)\Delta_{\mu\mu'}(k)\Delta_{\nu\nu'}(k+q) \\
&\quad \cdot f^{mbn} f^{man} \left[g^{\mu\beta'}(k-q)^\nu + g^{\beta'\nu}(2q+k)^\mu + g^{\nu\mu}(-2k-q)^{\beta'} \right] \\
&\quad \cdot \left[g^{\mu'\alpha'}(q-k)^{\nu'} + g^{\alpha'\nu'}(-2q-k)^{\mu'} + g^{\nu'\mu'}(2k+q)^{\alpha'} \right] \\
&\quad + [i\mathcal{A}_{\text{self,g}}]_{\text{fermion}} + [i\mathcal{A}_{\text{self,g}}]_{\text{ghost}} \\
&\stackrel{(B.23)}{=} g_s^2 \frac{1}{q^4} \frac{C_A}{2} i\Gamma_{(r_1,r_2)}^{a\alpha} i\Gamma_{(p_1,p_2)}^{a\beta} \int_k \frac{g_{\alpha\alpha'}g_{\beta\beta'}}{k^2(k+q)^2} \left[g_{\mu\mu'}g_{\nu\nu'} + \lambda^2 \frac{k_\mu k_{\mu'}(k+q)_\nu(k+q)_{\nu'}}{k^2(k+q)^2} \right. \\
&\quad \left. - \lambda \left(\frac{k_\mu k_{\mu'}g_{\nu\nu'}}{k^2} + \frac{(k+q)_\nu(k+q)_{\nu'}g_{\mu\mu'}}{(k+q)^2} \right) \right] \quad (B.67) \\
&\quad \cdot \left[g^{\mu\beta'}(k-q)^\nu + g^{\beta'\nu}(2q+k)^\mu + g^{\nu\mu}(-2k-q)^{\beta'} \right] \\
&\quad \cdot \left[g^{\mu'\alpha'}(q-k)^{\nu'} + g^{\alpha'\nu'}(-2q-k)^{\mu'} + g^{\nu'\mu'}(2k+q)^{\alpha'} \right] \\
&\quad + [i\mathcal{A}_{\text{self,g}}]_{\text{fermion}} + [i\mathcal{A}_{\text{self,g}}]_{\text{ghost}} \\
&\equiv [i\mathcal{A}_{\text{self,g}}]_{\xi=1} + i\Gamma_{(r_1,r_2)}^{a\alpha} \frac{-ig_{\alpha\mu}}{q^2} i\Sigma_{\text{self,g}}^{\mu\nu}(q^2) \frac{-ig_{\beta\nu}}{q^2} i\Gamma_{(p_1,p_2)}^{a\beta},
\end{aligned}$$

where we defined

$$i\Sigma_{\text{self,g}}^{\mu\nu}(q^2) = g_s^2 q^2 \left[\lambda^2 \frac{C_A}{2} q^2 \int_k \frac{k^\mu k^\nu}{k^4(k+q)^4} - \lambda C_A \int_k \left(q^2 \frac{g^{\mu\nu}}{k^2(k+q)^4} + 2 \frac{k^\mu k^\nu}{k^4(k+q)^2} - \frac{g^{\mu\nu}}{k^4} \right) \right] \quad (B.68)$$

which has the structure of a self-energy, as well. Analogous to the second class of triangle diagrams, cf. Fig. B.5, the presence of the three-gluon vertex introduces pinching which does not remove an internal fermion line but one or two internal gluon propagators, depending if the separate terms in the pinch contribution in Eq. (B.68) are proportional to q^2 or q^4 , respectively.

B.3.7. The Full One-Loop Scattering Amplitude

With every gauge-dependent one-loop contribution to the quark-quark scattering being calculated, we are now ready to calculate the full one-loop contribution to the scattering process.

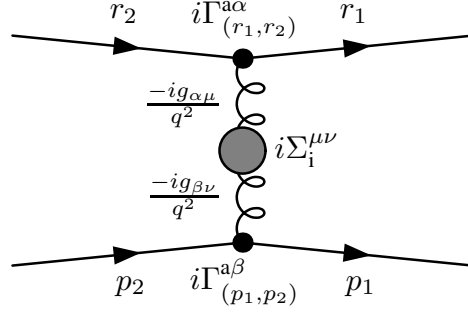


Figure B.8.: Generic result of the pinch technique. The application of the pinch technique allows for the extraction of all gauge-dependent parts originating from boxes, triangles and self-energies. The extracted pinched parts always have the structure of self-energies $i\Sigma_i^{\mu\nu}$ embedded into a generic tensor structure which consists of two gluon propagators and two quark-quark-gluon vertices.

First, we observe that the application of the pinch technique to all box, triangle and self-energy diagrams allowed us to split every amplitude into two parts,

$$i\mathcal{A}_i = [i\mathcal{A}_i]_{\xi=1} + i\Gamma_{(r_1,r_2)}^{a\alpha} \frac{-ig_{\alpha\mu}}{q^2} i\Sigma_i^{\mu\nu}(q^2) \frac{-ig_{\beta\nu}}{q^2} i\Gamma_{(p_1,p_2)}^{a\beta}, \quad (\text{B.69})$$

where the subscript “i” is a generic notation for all the amplitudes that we calculated in the previous subsections. The terms containing the gauge-dependent parts, $i\Sigma_i^{\mu\nu}(q^2)$, are purely self-energy-like, i.e. they depend only on the momentum transfer q , but not on any additional momenta or external masses m . This result is depicted diagrammatically in Fig. B.8.

For the calculation of the full one-loop amplitude of the quark-quark scattering process, we add up all diagrammatic contributions:

$$i\mathcal{A}_{\text{NLO}} := i\mathcal{A}_{\text{box}} + i\mathcal{A}_{\text{tri1}} + i\mathcal{A}_{\text{tri2}} + i\mathcal{A}_{\text{self,q}} + i\mathcal{A}_{\text{self,g}}. \quad (\text{B.70})$$

Since we calculated all parts of the one-loop amplitude explicitly in the previous subsections, we insert our results from Eqs. (B.44), (B.53), (B.62), (B.65) and (B.67), which yields

$$\begin{aligned} i\mathcal{A}_{\text{NLO}} &= [i\mathcal{A}_{\text{box}}]_{\xi=1} + [i\mathcal{A}_{\text{tri1}}]_{\xi=1} + [i\mathcal{A}_{\text{tri2}}]_{\xi=1} + [i\mathcal{A}_{\text{self,q}}]_{\xi=1} + [i\mathcal{A}_{\text{self,g}}]_{\xi=1} \\ &+ i\Gamma_{(r_1,r_2)}^{a\alpha} \frac{-ig_{\alpha\mu}}{q^2} \left[i\Sigma_{\text{box}}^{\mu\nu}(q^2) + i\Sigma_{\text{tri1}}^{\mu\nu}(q^2) + i\Sigma_{\text{tri2}}^{\mu\nu}(q^2) + i\Sigma_{\text{self,g}}^{\mu\nu}(q^2) + i\Sigma_{\text{self,q}}^{\mu\nu}(q^2) \right] \\ &\cdot \frac{-ig_{\beta\nu}}{q^2} i\Gamma_{(p_1,p_2)}^{a\beta} \\ &\equiv [i\mathcal{A}_{\text{NLO}}]_{\xi=1} + i\Gamma_{(r_1,r_2)}^{a\alpha} \frac{-ig_{\alpha\mu}}{q^2} i\Sigma_{\text{g.d.}}^{\mu\nu}(q^2) \frac{-ig_{\beta\nu}}{q^2} i\Gamma_{(p_1,p_2)}^{a\beta}. \end{aligned} \quad (\text{B.71})$$

In the last line, we combined all gauge-dependent parts into a single term

$$i\Sigma_{\text{g.d.}}^{\mu\nu}(q^2) := i\Sigma_{\text{box}}^{\mu\nu}(q^2) + i\Sigma_{\text{tri1}}^{\mu\nu}(q^2) + i\Sigma_{\text{tri2}}^{\mu\nu}(q^2) + i\Sigma_{\text{qself}}^{\mu\nu}(q^2) + i\Sigma_{\text{gself}}^{\mu\nu}(q^2), \quad (\text{B.72})$$

which, when inserting the expressions for the gauge-dependent parts, namely Eqs. (B.45), (B.54), (B.63), (B.66) and (B.68), vanishes:

$$i\Sigma_{\text{g.d.}}^{\mu\nu}(q^2) = 0. \quad (\text{B.73})$$

In order to illustrate the intricate cancellations of the gauge-dependent parts originating from the boxes, triangles and self-energies more clearly, we list in Table B.1 all gauge-dependent

	$g_s^2 q^2 \lambda^2 \int_k \frac{k^\mu k^\nu}{k^4 (k+q)^4}$	$g_s^2 q^2 \lambda \int_k \frac{k^\mu k^\nu}{k^4 (k+q)^2}$	$g_s^2 q^2 \lambda \int_k \frac{g^{\mu\nu}}{k^2 (k+q)^4}$	$g_s^2 q^2 \lambda \int_k \frac{g^{\mu\nu}}{k^4}$
$i\Sigma_{\text{box}}^{\mu\nu}$	$q^2 \frac{C_A}{2}$	0	$-q^2 C_A$	0
$i\Sigma_{\text{tri1}}^{\mu\nu}$	0	0	0	$C_A - 2C_f$
$i\Sigma_{\text{tri2}}^{\mu\nu}$	$-q^2 C_A$	$2C_A$	$2q^2 C_A$	$-2C_A$
$i\Sigma_{\text{self,q}}^{\mu\nu}$	0	0	0	$2C_f$
$i\Sigma_{\text{self,g}}^{\mu\nu}$	$q^2 \frac{C_A}{2}$	$-2C_A$	$-q^2 C_A$	C_A
Sum	0	0	0	0

Table B.1.: Cancellation of all gauge-dependent parts (adopted from [93]). The gauge-dependent parts originating from different topologies, i.e. boxes, triangles and self-energies, cancel against each other in order to yield a manifestly gauge-independent one-loop scattering amplitude.

parts and their cancellations against each other. With that result at hand, the full one-loop amplitude reduces to

$$i\mathcal{A}_{\text{NLO}} = [i\mathcal{A}_{\text{NLO}}]_{\xi=1} . \quad (\text{B.74})$$

We want to emphasize that – while this result creates the impression that we have chosen a specific gauge, namely the Feynman-’t Hooft gauge – Eq. (B.74) is valid for *any arbitrary value* of the gauge-fixing parameter ξ . If we would have chosen e.g. Landau gauge with $\xi = 0$ and calculated all box, triangle and self-energy diagrams, then the full one-loop result would nevertheless have been equivalent to Eq. (B.74). The one-loop scattering amplitude *coincides* with the amplitude being calculated in Feynman-’t Hooft gauge *after* all gauge-dependent parts cancelled against each other. This makes the gauge-independence of the amplitude manifest.

Through the application of the pinch technique, we were able to extract all gauge-dependent parts originating from box, triangle and self-energy diagrams, all of which have the kinematic structure of self-energies. We have shown that all gauge-dependent parts precisely cancel against each other, yielding a manifestly gauge-independent one-loop amplitude.

B.3.8. Additional Pinch Contributions from the Three-Gluon Vertex

With the cancellation of all gauge-dependent parts within our one-loop scattering amplitude having taken place, we might consider our investigation of the pinch technique to be complete. However, in App. B.3.4 we already mentioned that there is another source of pinch contributions originating from the three-gluon vertex. In Eq. (B.57), the momenta of the three-gluon vertex can be contracted with Dirac matrices appearing next to internal fermion propagators, which creates additional sources of pinch contributions. In the following, we want to investigate these additional pinch contributions. Note that since the gauge-dependent parts already cancelled against each other completely, we expect these additional pinch contributions to be manifestly gauge-independent by themselves.

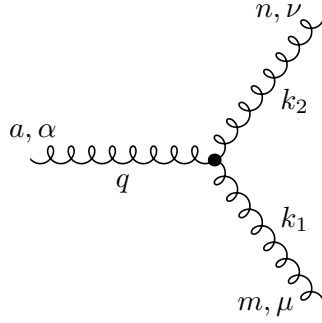


Figure B.9.: Three-gluon vertex. Depiction of a generic three-gluon vertex with external color indices a , m and n and Lorentz indices α , μ and ν . All momenta are defined to point into the vertex, so that $q + k_1 + k_2 = 0$ holds.

In order to generalize the procedure of the additional pinching, we consider a general three-gluon vertex as depicted in Fig. B.9. The Feynman rule of the three-gluon vertex reads

$$\Gamma_{\alpha\mu\nu}^{amn}(q, k_1, k_2) = g_s f^{amn} \Gamma_{\alpha\mu\nu}(q, k_1, k_2) , \quad (\text{B.75})$$

where we defined the short-hand notation

$$\Gamma_{\alpha\mu\nu}(q, k_1, k_2) := g_{\mu\nu} (k_1 - k_2)_\alpha + g_{\alpha\nu} (k_2 - q)_\mu + g_{\alpha\mu} (q - k_1)_\nu . \quad (\text{B.76})$$

Note that we define all momenta to point into the vertex so that

$$q + k_1 + k_2 = 0 \quad (\text{B.77})$$

holds. If the three-gluon vertex appears inside a one-loop amplitude as e.g. in Fig. B.10, then two of the gluons are connected via quark-quark-gluon vertices with a quark propagator inside the loop. Exactly this quark propagator can be pinched out with the loop momenta appearing in Eq. (B.76) by applying the Ward identity from Eq. (B.17). If we let the two gluons with momenta k_1 and k_2 be connected with a quark propagator, then we can split the three-gluon vertex into two parts,

$$\Gamma_{\alpha\mu\nu}(q, k_1, k_2) = \Gamma_{\alpha\mu\nu}^{\text{np}}(q, k_1, k_2) + \Gamma_{\alpha\mu\nu}^{\text{p}}(q, k_1, k_2) , \quad (\text{B.78})$$

where we defined

$$\Gamma_{\alpha\mu\nu}^{\text{np}}(q, k_1, k_2) = (k_1 - k_2)_\alpha g_{\mu\nu} + 2q_\nu g_{\alpha\mu} - 2q_\mu g_{\alpha\nu} , \quad (\text{B.79})$$

$$\Gamma_{\alpha\mu\nu}^{\text{p}}(q, k_1, k_2) = k_{2,\nu} g_{\alpha\mu} - k_{1,\mu} g_{\alpha\nu} . \quad (\text{B.80})$$

The superscripts “np” and “p” indicate the non-pinching and pinching parts, respectively. Only $\Gamma_{\alpha\mu\nu}^{\text{p}}$ will pinch, since only this term contains the two momenta k_1 and k_2 with Lorentz indices μ and ν . Exactly these two loop momenta $k_{1,\mu}$ and $k_{2,\nu}$ are contracted with Dirac matrices from the quark-quark-gluon vertices inside the spinor chain which also contains the to-be pinched internal fermion inside the loop, cf. Fig. B.10. On the other hand, the term $\Gamma_{\alpha\mu\nu}^{\text{np}}$ contains the loop momenta $(k_1 - k_2)_\alpha$ which are contracted with a Dirac matrix inside the upper quark-quark-gluon propagator in Fig. B.10. Since the spinor chain which contains this vertex does not contain any additional internal fermion propagators, there are no additional pinch terms induced by $\Gamma_{\alpha\mu\nu}^{\text{np}}$.

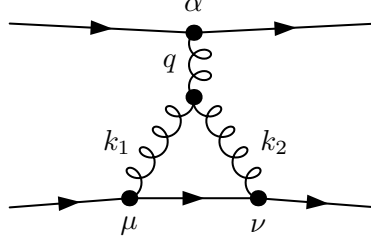


Figure B.10.: Three-gluon vertex inside a triangle diagram. The loop momenta $k_{1,\mu}$ and $k_{2,\nu}$ appearing in $\Gamma_{\alpha\mu\nu}^{\text{p}}$ are contracted with Dirac matrices from the quark-quark-gluon vertex which appear next to the internal fermion propagator, thus yielding pinch contributions. The loop momenta $(k_1 - k_2)_\alpha$ contained in $\Gamma_{\alpha\mu\nu}^{\text{np}}$ are contracted with the quark-quark-gluon vertex which contains no additional internal fermions in a loop, thus, they yield no pinch contributions.

With this general result at hand, we consider again the first of the two Feynman diagrams shown in Fig. B.5. We rewrite the so-far unpinched amplitude given Eq. (B.57) in such a form that it contains the general form of the three-gluon vertex in Eq. (B.76),

$$\begin{aligned}
[i\mathcal{A}_{\text{tri2},1}]_{\xi=1} &= ig_s^4 \frac{1}{q^2} f^{amn} \int_k \frac{1}{k^2(k+q)^2} \bar{u}(r_1) \gamma^\alpha t^a u(r_2) \bar{u}(p_1) \gamma^\nu t^n S(p_2 - k) \gamma^\mu t^m u(p_2) \\
&\quad \cdot g_{\alpha\beta} g_{\mu\mu'} g_{\nu\nu'} \Gamma^{\beta\mu'\nu'}(q, k, -k - q) \\
&\stackrel{\text{(B.78)}}{=} ig_s^4 \frac{1}{q^2} f^{amn} \int_k \frac{1}{k^2(k+q)^2} \bar{u}(r_1) \gamma^\alpha t^a u(r_2) \bar{u}(p_1) \gamma^\nu t^n S(p_2 - k) \gamma^\mu t^m u(p_2) \\
&\quad \cdot g_{\alpha\beta} g_{\mu\mu'} g_{\nu\nu'} \left[\Gamma_{\text{np}}^{\beta\mu'\nu'}(q, k, -k - q) + \Gamma_{\text{p}}^{\beta\mu'\nu'}(q, k, -k - q) \right] \\
&\equiv [i\mathcal{A}_{\text{tri2},1}^{\text{np}}]_{\xi=1} + [i\mathcal{A}_{\text{tri2},1}^{\text{p}}]_{\xi=1} , \tag{B.81}
\end{aligned}$$

where in the last line, we defined

$$\begin{aligned}
[i\mathcal{A}_{\text{tri2},1}^{\text{np}}]_{\xi=1} &:= ig_s^4 \frac{1}{q^2} f^{amn} \int_k \frac{1}{k^2(k+q)^2} \bar{u}(r_1) \gamma^\alpha t^a u(r_2) \bar{u}(p_1) \gamma^\nu t^n S(p_2 - k) \gamma^\mu t^m u(p_2) \\
&\quad \cdot g_{\alpha\beta} g_{\mu\mu'} g_{\nu\nu'} \Gamma_{\text{np}}^{\beta\mu'\nu'}(q, k, -k - q) , \tag{B.82}
\end{aligned}$$

$$\begin{aligned}
[i\mathcal{A}_{\text{tri2},1}^{\text{p}}]_{\xi=1} &:= ig_s^4 \frac{1}{q^2} f^{amn} \int_k \frac{1}{k^2(k+q)^2} \bar{u}(r_1) \gamma^\alpha t^a u(r_2) \bar{u}(p_1) \gamma^\nu t^n S(p_2 - k) \gamma^\mu t^m u(p_2) \\
&\quad \cdot g_{\alpha\beta} g_{\mu\mu'} g_{\nu\nu'} \Gamma_{\text{p}}^{\beta\mu'\nu'}(q, k, -k - q) . \tag{B.83}
\end{aligned}$$

It is only Eq. (B.83) that contains additional pinch contributions. The rest of the calculation is analogous to the previous subsections. We insert the definition of the three-gluon vertex, Eq. (B.80), into Eq. (B.83) and make use of the Ward identity in Eq. (B.17) in order to pinch out the internal fermion propagator. In the end, this yields

$$[i\mathcal{A}_{\text{tri2},1}^{\text{p}}]_{\xi=1} = -i\Gamma_{(r_1,r_2)}^{a\alpha} g_s^2 \frac{1}{q^2} C_A \int_k \frac{g_{\alpha\beta}}{k^2(k+q)^2} i\Gamma_{(p_1,p_2)}^{a\beta} . \tag{B.84}$$

The second Feynman diagram in Fig. B.5 gives exactly the same pinch contribution. Therefore, the complete additional contributions from the triangle diagrams containing the three-gluon vertex read

$$[i\mathcal{A}_{\text{tri2}}]_{\xi=1} = [i\mathcal{A}_{\text{tri2}}^{\text{np}}]_{\xi=1} + i\Gamma_{(r_1,r_2)}^{a\alpha} \frac{-ig_{\alpha\mu}}{q^2} i\Sigma_{\text{add}}^{\mu\nu}(q^2) \frac{-ig_{\beta\nu}}{q^2} i\Sigma_{(p_1,p_2)}^{a\beta} , \tag{B.85}$$

where we defined

$$i\Sigma_{\text{add}}^{\mu\nu}(q^2) = g_s^2 q^2 \left[2C_A \int_k \frac{g^{\mu\nu}}{k^2(k+q)^2} \right]. \quad (\text{B.86})$$

The remaining unpinched part of the amplitude, $[i\mathcal{A}_{\text{tri}2}^{\text{np}}]_{\xi=1}$, is the sum of the unpinched part of the first Feynman diagram in Eq. (B.82) and the contribution from the second diagram, which we did not write down explicitly. As it was the case in the previous subsections, the additional pinch contribution originating from the three-gluon vertex in Eq. (B.86) has the structure of a self-energy. In contrast to the other terms however, this additional term is manifestly gauge-independent by itself, as we expected it.

The question remains why we should make the effort to investigate the effects of this additional pinching of the three-gluon vertex in the first place, since we already demonstrated the gauge-independence of the one-loop scattering amplitude in Sec. B.3.7. However, the demonstration of the cancellation of these gauge-dependences is not the only application of the pinch technique. Furthermore, the technique can be used to create pinched vertices and self-energies which satisfy additional useful relations, e.g. tree-level Ward identities.

We have seen in Eq. (B.86) that the pinch term originating from $[i\mathcal{A}_{\text{tri}2}^{\text{p}}]_{\xi=1}$ has the structure of a self-energy. In order to construct a pinched vertex, this self-energy-like term has to be excluded, since the proper pinched vertex should contain vertex-like parts, only. We consider the term $[i\mathcal{A}_{\text{tri}2}^{\text{p}}]_{\xi=1}$ again in App. B.3.9 as soon as we create a pinched self-energy.

For the creation of the pinched quark-quark-gluon vertex, we combine the terms $[i\mathcal{A}_{\text{tri}2}^{\text{np}}]_{\xi=1}$ as well as the complete triangle contributions $[i\mathcal{A}_{\text{tri}1}]_{\xi=1}$, since the latter contain no self-energy-like parts either. The pinched vertex itself can be extracted from the sum of these terms by truncating the diagram, i.e. by removing the internal gluon propagator and the quark-quark-gluon vertex which is not connected to the loop, cf. Fig. B.10. In contrast to the ordinary quark-quark-gluon vertex, the hereby created pinched quark-quark-gluon vertex has a remarkable property. If we denote with Z_1 and Z_2 the renormalization constants of the pinched quark-quark-gluon vertex and the quark self-energy following from the external leg corrections, respectively, then it can be shown [93] that

$$Z_1 = Z_2 \quad (\text{B.87})$$

holds at the one-loop level. Of course, Eq. (B.87) has exactly the same form as the famous identity between the renormalization constants of the electron-electron-photon vertex and the electron self-energy which can be derived in the framework of QED [5], which is an abelian gauge theory. If we would have chosen to use the ordinary quark-quark-gluon vertex, Eq. (B.87) would not hold, but instead, the vertex and the quark self-energies would be connected by a more intricate Slavnov-Taylor identity [93]. However, by using the pinched quark-quark-gluon vertex, we find with Eq. (B.87) an identity for QCD, which is a non-abelian gauge theory, that is completely analogous to QED, i.e. the pinched quark-quark-gluon vertex satisfies a tree-level-like Ward identity.

B.3.9. Creation of a Pinched Gluon Self-Energy

In the last subsection of this introduction, we want to present another major achievement of the pinch technique, namely the creation of a manifestly gauge-independent pinched gluon self-energy. In the previous subsection, we have shown that the three-gluon vertex gets modified when using this pinch technique and the pinched three-gluon vertex does not contain the term $[i\mathcal{A}_{\text{tri}2}^{\text{p}}]_{\xi=1}$ any more. For the pinch technique to be consistent, these terms have to be absorbed somewhere else in the one-loop amplitude. As we will see in the following, this is achieved by the creation of the pinched self-energy.

$$i\Sigma_{gg}^{\mu\nu}(q^2) = \text{diagram 1} + \text{diagram 2} + \text{diagram 3}$$

Figure B.11.: Truncated gluon self-energy. One-loop contributions to the gluon self-energy. The corrections include loops with gluons, fermions and ghosts. The fermion and ghost loops are gauge-independent, while the gluon loop introduces a gauge-dependence to the self-energy. Note that all diagrams are truncated, i.e. the polarization vectors of the external gluons are omitted.

The ordinary gluon self-energy $i\Sigma_{gg}^{\mu\nu}(q^2)$ is given as the sum of the three contributions depicted in Fig. B.11. Since we already considered the gluon self-energy diagrams contributing to the quark-quark scattering in App. B.3.6, we can directly present the gauge-dependence of the ordinary gluon self-energy. By truncating the diagrams in Fig. B.7, i.e. by removing the external fermions, the quark-quark-gluon vertices and the internal gluon propagators carrying the momentum transfer q , we end up with the truncated gluon self-energy shown in Fig. B.11. This allows us to identify the gauge-dependence of the self-energy with the already calculated term in Eq. (B.68). Thus, the gluon self-energy takes the form

$$i\Sigma_{gg}^{\mu\nu}(q^2) = [i\Sigma_{gg}^{\mu\nu}(q^2)]_{\xi=1} + i\Sigma_{\text{self,g}}^{\mu\nu}(q^2). \quad (\text{B.88})$$

In the previous subsections, we observed that all pinch contributions are self-energy-like. Consequently, we create the pinched self-energy by adding to Eq. (B.88) all pinch contributions³. Hence, the pinched gluon self-energy is given by

$$\begin{aligned} i\Sigma_{gg}^{\text{pinched},\mu\nu}(q^2) &:= i\Sigma_{gg}^{\mu\nu}(q^2) + i\Sigma_{\text{box}}^{\mu\nu}(q^2) + i\Sigma_{\text{tri1}}^{\mu\nu}(q^2) + i\Sigma_{\text{tri2}}^{\mu\nu}(q^2) + i\Sigma_{\text{self,q}}^{\mu\nu}(q^2) + i\Sigma_{\text{add}}^{\mu\nu}(q^2) \\ &\stackrel{(\text{B.88})}{=} [i\Sigma_{gg}^{\mu\nu}(q^2)]_{\xi=1} + i\Sigma_{\text{box}}^{\mu\nu}(q^2) + i\Sigma_{\text{tri1}}^{\mu\nu}(q^2) + i\Sigma_{\text{tri2}}^{\mu\nu}(q^2) + i\Sigma_{\text{self,q}}^{\mu\nu}(q^2) \\ &\quad + i\Sigma_{\text{self,g}}^{\mu\nu}(q^2) + i\Sigma_{\text{add}}^{\mu\nu}(q^2) \\ &\stackrel{(\text{B.72})}{=} [i\Sigma_{gg}^{\mu\nu}(q^2)]_{\xi=1} + i\Sigma_{\text{g.d.}}^{\mu\nu}(q^2) + i\Sigma_{\text{add}}^{\mu\nu}(q^2) \\ &\stackrel{(\text{B.73})}{=} [i\Sigma_{gg}^{\mu\nu}(q^2)]_{\xi=1} + i\Sigma_{\text{add}}^{\mu\nu}(q^2). \end{aligned} \quad (\text{B.89})$$

Analogous to our discussion after the cancellation of all gauge-dependent parts within the one-loop amplitude, cf. Sec. B.3.7, we want to emphasize that the form of the pinched self-energy is valid for *all* gauge-fixing parameters ξ , despite Eq. (B.89) has a form that might suggest that a specific gauge was chosen. Consequently, this pinched gluon self-energy is manifestly gauge-independent and equivalent with the sum of the ordinary self-energy calculated in Feynman-'t Hooft gauge and the additional terms originating from the three-gluon vertex derived in Sec. B.3.8.

As it was the case for the pinched three-gluon vertex, the pinched gluon self-energy yields an analogy to QED. If we denote with Z_{g_s} the renormalization constant of the strong coupling constant and with Z_{gg} the wave function renormalization constant of the gluon field as defined over the pinched self-energy, then it can be shown [93] that

$$Z_{g_s} = Z_{gg}^{-1/2} \quad (\text{B.90})$$

holds at the one-loop level. This is nothing else than the QCD-analogue to the QED relation between the renormalization constant of the elementary charge e and the wave function renormalization constant of the photon [5].

³Apart from the pinch contributions originating from the self-energy diagram in Fig. B.7 to avoid double-counting.

As a final remark, we want to point out that the pinched self-energy in Eq. (B.89) can be derived not only by use of the pinch technique. As an alternative, we could have chosen to formulate QCD in the framework of the *background field method* [101–104]. The Green's functions derived within this framework have numerous desirable properties, e.g. they fulfill tree-level-like Ward identities to all orders of perturbation theory and for every background-gauge-fixing-parameter. By calculating the gluon self-energy within the background field method, it can be shown [93] that the self-energy coincides with Eq. (B.89) if the Feynman-'t Hooft gauge for the background-gauge-fixing-parameter is chosen. Consequently, the Green's function derived by means of the pinch technique adopts all desirable properties from the one derived with the background field method.

The Pinch Technique in the 2HDM

In this thesis, we used the pinched self-energies of the scalar sector of the 2HDM in order to define manifestly gauge-independent scalar mixing angle counterterms $\delta\alpha$ and $\delta\beta$. In the following, we want to give a brief presentation of the derivation of these pinched scalar self-energies. For the CP-even Higgs self-energies, the application of the pinch technique within the MSSM was discussed in [100]. We want to present the analogous calculation within the 2HDM and compare it with the results for the MSSM. Additionally, we apply the pinch technique to the CP-odd and charged Higgs sector.

C.1. The Pinch Technique in the 2HDM in Practice

In App. B, we presented the application of the pinch technique in QCD. For the calculation of the pinched self-energies, we will apply the pinch technique to the electroweak sector of the 2HDM, since all pinch contributions for the scalar self-energies stem from electroweak one-loop corrections. In order to apply the pinch technique, we have to choose a toy scattering process which contains the to-be pinched self-energies in the form of tree-level propagators.

The toy processes that we consider for the derivation of the pinched self-energies in the 2HDM are processes with non-conserved fermion currents. The application of the pinch technique within such a theory is significantly more involved than within QCD. If we wish to create the pinched self-energy of e.g. the charged Higgs, we observe that the particle couples to external fermions with different masses m_1 and m_2 . In practice, this means that the fundamental Ward identity from Eq. (B.17), which is applied every time we want to pinch out an external fermion, has to be modified to [93, 96]

$$\begin{aligned} \not{k}\omega_{\mp} &= S_1^{-1}(p+k)\omega_{\mp} - \omega_{\pm}S_2^{-1}(p) + m_1\omega_{\mp} - m_2\omega_{\pm} , \\ \omega_{\mp}\not{k} &= \omega_{\mp}S_1^{-1}(p+k) - S_2^{-1}(p)\omega_{\pm} + m_1\omega_{\mp} - m_2\omega_{\pm} , \end{aligned} \tag{C.1}$$

with iS_1 and iS_2 being the propagators of the fermions with masses m_1 and m_2 , respectively, and with the definition of the chiral projection operators given in Eq. (2.49). The additional terms on the right-hand sides of Eq. (C.1) give rise to additional pinch contributions.

In contrast to QCD, where the gluon self-energy was the only available self-energy to be pinched, the electroweak sector of the 2HDM offers a variety of self-energies that can be

modified by use of the pinch technique. If we want to apply the pinch technique e.g. to the charged sector for the derivation of a pinched self-energy of the charged Higgs H^\pm , we have to allot the pinching parts for the charged sector between the self-energies of the H^\pm , G^\pm and W^\pm bosons as well as between the mixing self-energies of these particles. In this chapter, we present the application only to a small subset of all possible self-energies of the 2HDM. For more details on the subtleties that arise when applying the pinch technique to a theory with non-conserved fermion currents, we refer to [93, 96].

In order to perform the calculations by hand, we introduce the propagator for a gauge boson $V \in \{Z^0, W^\pm, \gamma\}$ with momentum q in general R_ξ gauge,

$$i\Delta_{\mu\nu}(q) = \frac{-i}{q^2 - m_V^2} \left[g_{\mu\nu} - \lambda_V \frac{q_\mu q_\nu}{q^2 - \xi_V m_V^2} \right], \quad (\text{C.2})$$

where we defined the short-hand notation

$$\lambda_V := 1 - \xi_V \quad (\text{C.3})$$

for the gauge-fixing parameter ξ_V of the gauge boson V . In the case of massive gauge bosons, additional gauge-dependences are introduced to the one-loop amplitude through the ghost and Goldstone propagators

$$\frac{i}{q^2 - \xi_V m_V^2}. \quad (\text{C.4})$$

Additionally, we introduce the parameters

$$\mathcal{O}_{h_i h_j}^{(1)} = \begin{cases} s_{\beta-\alpha}^2 & , \text{ if } h_i = h_j = H^0 \\ -s_{\beta-\alpha} c_{\beta-\alpha} & , \text{ if } h_i \neq h_j \\ c_{\beta-\alpha}^2 & , \text{ if } h_i = h_j = h^0 \end{cases}, \quad \mathcal{O}_{h_i h_j}^{(2)} = \begin{cases} c_{\beta-\alpha}^2 & , \text{ if } h_i = h_j = H^0 \\ s_{\beta-\alpha} c_{\beta-\alpha} & , \text{ if } h_i \neq h_j \\ s_{\beta-\alpha}^2 & , \text{ if } h_i = h_j = h^0 \end{cases} \quad (\text{C.5})$$

which account for the coupling structure of the Higgs particles within the 2HDM.

For a convenient presentation of the results of our calculations, we introduce the scalar integrals defined by 't Hooft and Veltman [119],

$$\frac{i}{16\pi^2} A_0(m^2) := \int_k \frac{1}{[k^2 - m^2]}, \quad (\text{C.6})$$

$$\frac{i}{16\pi^2} B_0(p^2; m_1^2, m_2^2) := \int_k \frac{1}{[k^2 - m_1^2] [(k+p)^2 - m_2^2]}, \quad (\text{C.7})$$

where we used the definition of the integral operator presented in Eq. (B.25). Furthermore, we introduce the two additional integrals [100]

$$\frac{i}{16\pi^2} \alpha_V := \int_k \frac{1}{[k^2 - m_V^2] [k^2 - \xi_V m_V^2]}, \quad (\text{C.8})$$

$$\frac{i}{16\pi^2} \beta_{Vj}(p^2) := \int_k \frac{1}{[k^2 - m_V^2] [k^2 - \xi_V m_V^2] [(k+p)^2 - m_j^2]}, \quad (\text{C.9})$$

where m_j is the mass of an arbitrary particle. Note that these integrals are closely related to the usual scalar integrals defined in Eqs. (C.6) and (C.7). If the A_0 or B_0 integrals contain the gauge-fixing parameter ξ_V , they may be converted to the α_V and β_{Vj} integrals according to

$$A_0(\xi_V m_V^2) = A_0(m_V^2) - \lambda_V m_V^2 \alpha_V, \quad (\text{C.10})$$

$$B_0(p^2; \xi_V m_V^2, m_j^2) = B_0(p^2; m_V^2, m_j^2) - \lambda_V m_V^2 \beta_{Vj}(p^2), \quad (\text{C.11})$$

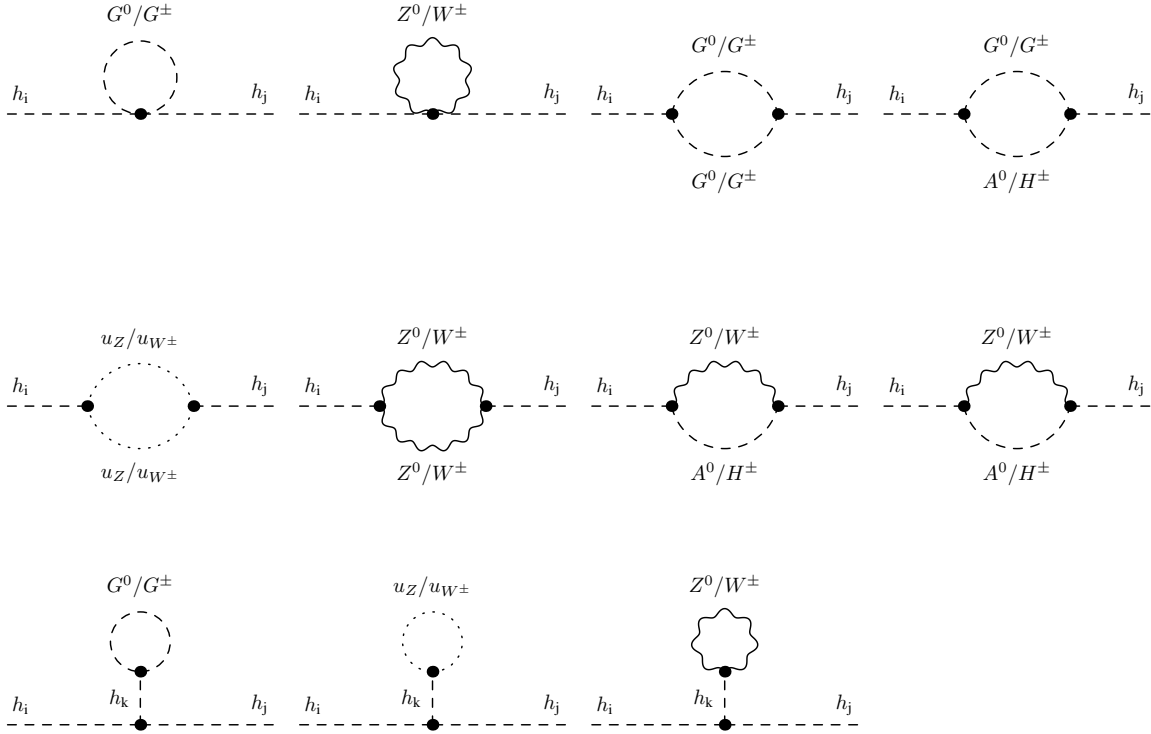


Figure C.1.: Gauge-dependent CP-even self-energy contributions. The figure shows all CP-even self-energies for the Higgses $h_i, h_j \in \{H^0, h^0\}$ that introduce a gauge-dependence in the CP-even sector. The tadpole diagrams are the sum over both Higgses $h_k \in \{H^0, h^0\}$ and only have to be included if the alternative tadpole scheme is chosen. Note the absence of diagrams for the gauge-fixing parameter λ_γ , since the CP-even Higgs bosons do not couple to the massless photon.

C.2. The Pinch Technique in the CP-Even Sector

We start our analysis by pinching the self-energies of the scalar CP-even sector, i.e. the self-energies $i\Sigma_{h_i h_j}$ for $h_i, h_j \in \{H^0, h^0\}$. In [100], the pinched versions of these self-energies were calculated within the MSSM. The goal of this section is to redo the calculation for the 2HDM in order to compare our results with the ones derived in the MSSM¹.

C.2.1. Gauge-Dependence of the CP-Even Self-Energies

Before extracting the pinch contributions of the CP-even sector, we work out the gauge-dependence of the CP-even self-energies explicitly by calculating all diagrams in Fig. C.1 that introduce gauge-dependent terms to the self-energies. In order to extract the gauge-dependences, we calculate each diagram in general R_ξ gauge and extract from it the same diagram calculated in Feynman-t'Hooft gauge, i.e. we calculate the quantity

$$[i\mathcal{A}]_{\text{g.d.}} := [i\mathcal{A}]_\xi - [i\mathcal{A}]_{\xi=1} \quad (\text{C.12})$$

for each diagram and for each gauge-fixing parameter $\xi \in \{\xi_Z, \xi_W, \xi_\gamma\}$. It is precisely Eq. (C.12) which we call the gauge-dependent part of the self-energy. Note that this definition is *a priori* not clear. In Eq. (C.12), we emphasize the Feynman-t'Hooft gauge as an

¹Since the MSSM and the 2HDM do not differ with respect to gauge-dependent contributions to one-loop amplitudes, we expect to get the same result as in [100] from the start.

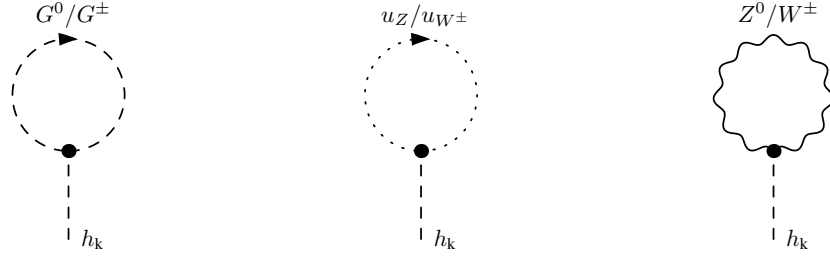


Figure C.2.: Gauge-dependent contributions to the CP-even Higgs tadpoles. The three diagrams are the only contributions to the CP-even tadpoles iT_{h_k} with $h_k \in \{H^0, h^0\}$ that introduce gauge-dependent terms. The gauge-dependences of the ghost loops precisely cancel the ones originating from the gauge boson loops.

outstanding gauge amongst all possible R_ξ gauges, since it is exactly this gauge with which we define the gauge-dependent part. We might as well could have chosen to use the Landau gauge with $\xi_V = 0$ or any other gauge to define the gauge-dependent parts. However, as we already have seen in App. B and as we will see in App. C.2.2 again, it turns out that all gauge-dependent pinch contributions are proportional to λ_V , which makes it clear that the Feynman-'t Hooft gauge indeed takes a special role in defining the gauge-dependent parts. *A posteriori*, the choice of Eq. (C.12) is justified and will lead to a structure of the CP-even self-energies of the form

$$i\Sigma_{h_i h_j}(q^2) = [i\Sigma_{h_i h_j}(q^2)]_{\xi=1} + [i\Sigma_{h_i h_j}(q^2)]_{\text{g.d.}} \quad (\text{C.13})$$

for the standard tadpole scheme and

$$i\Sigma_{h_i h_j}^{\text{tad}}(q^2) = [i\Sigma_{h_i h_j}^{\text{tad}}(q^2)]_{\xi=1} + [i\Sigma_{h_i h_j}^{\text{tad}}(q^2)]_{\text{g.d.}} \quad (\text{C.14})$$

for the alternative tadpole scheme, with the last terms being the sums of all gauge-dependent contributions determined by Eq. (C.12) and q being the momentum transfer of the self-energy.

We first consider all gauge-dependent contributions in Fig. C.1 which contain no tadpole diagrams, since this is the usual form of the self-energy within the standard tadpole scheme which is widely used in literature, cf. Sec. 4.4.1. The full gauge-dependence of the CP-even self-energies reads²:

$$\begin{aligned} [i\Sigma_{h_i h_j}(q^2)]_{\text{g.d.}} = & \lambda_Z \frac{ig^2}{64\pi^2 c_W^2} \left[\mathcal{O}_{h_i h_j}^{(1)} \left(q^4 - 2q^2 m_{A^0}^2 + m_{A^0}^2 (m_{h_i}^2 + m_{h_j}^2) - m_{h_i}^2 m_{h_j}^2 \right) \beta_{ZA^0}(q^2) \right. \\ & \left. - \delta_{h_i h_j} \left(q^2 - \frac{m_{h_i}^2 + m_{h_j}^2}{2} \right) \alpha_Z + \mathcal{O}_{h_i h_j}^{(2)} \frac{1}{2} \left(q^4 - m_{h_i}^2 m_{h_j}^2 \right) (\beta_{ZZ}(q^2) + \beta_{Z\xi Z}(q^2)) \right] \\ & + \lambda_W \frac{ig^2}{32\pi^2} \left[\mathcal{O}_{h_i h_j}^{(1)} \left(q^4 - 2q^2 m_{H^\pm}^2 + m_{H^\pm}^2 (m_{h_i}^2 + m_{h_j}^2) - m_{h_i}^2 m_{h_j}^2 \right) \beta_{WH^\pm}(q^2) \right. \\ & \left. - \delta_{h_i h_j} \left(q^2 - \frac{m_{h_i}^2 + m_{h_j}^2}{2} \right) \alpha_W + \mathcal{O}_{h_i h_j}^{(2)} \frac{1}{2} \left(q^4 - m_{h_i}^2 m_{h_j}^2 \right) (\beta_{WW}(q^2) + \beta_{W\xi W}(q^2)) \right] \\ & + \lambda_Z \frac{ig^2}{128\pi^2 c_W^2} \left[\left(\frac{4m_W^2 \Lambda_5}{g^2} - \frac{s_{2\alpha}}{s_{2\beta}} (m_{H^0}^2 - m_{h^0}^2) \right) \mathcal{O}_{h_i h_j}^{(1)} - 3 \frac{m_{h_i}^2 + m_{h_j}^2}{2} \delta_{h_i h_j} \right] \alpha_Z \\ & + \lambda_W \frac{ig^2}{64\pi^2} \left[\left(\frac{4m_W^2 \Lambda_5}{g^2} - \frac{s_{2\alpha}}{s_{2\beta}} (m_{H^0}^2 - m_{h^0}^2) \right) \mathcal{O}_{h_i h_j}^{(1)} - 3 \frac{m_{h_i}^2 + m_{h_j}^2}{2} \delta_{h_i h_j} \right] \alpha_W . \end{aligned} \quad (\text{C.15})$$

²Note that we denote with $\beta_{Z\xi Z}$ a modification of our notation in Eq. (C.9), meaning that in this case, $m_V^2 = m_Z^2$ and $m_j^2 = \xi_Z m_Z^2$ should be inserted. For $\beta_{W\xi W}$, the modification of Eq. (C.9) is analogous.

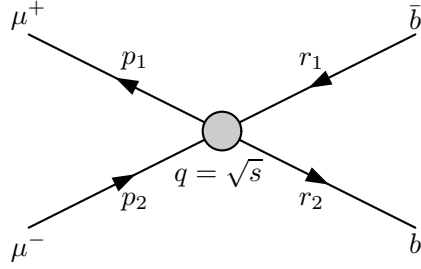


Figure C.3.: Toy process for the CP-even sector. We use the process $\mu^+ \mu^- \rightarrow \bar{b} b$ as a toy process for the extraction of all pinch contributions to the CP-even Higgs self-energies. The grey dot represents all electroweak one-loop corrections that introduce pinch terms. The momentum transfer q is characterized by the Mandelstam variable s as the square of center-of-mass energy.

All CP-even Higgs self-energies for any combination of Higgses $h_i, h_j \in \{H^0, h^0\}$ are manifestly gauge-dependent.

If we want to calculate the self-energies in the alternative tadpole scheme, we have to include the tadpole contributions from Fig. C.1. To this end, it is useful to consider the gauge-dependence of the truncated tadpole diagrams first. Figure C.2 depicts all contributions to the CP-even tadpole diagrams which introduce gauge-dependent parts. The gauge-dependence of the ghost loops and of the gauge boson loops precisely cancel. Consequently, the gauge-dependence of the tadpoles is determined by the Goldstone loops. Explicitly, the gauge-dependence reads

$$[iT_{h^0}]_{\text{g.d.}} = -\lambda_Z \frac{igm_Z s_{\beta-\alpha} m_{h^0}^2}{64\pi^2 c_W} \alpha_Z - \lambda_W \frac{igm_W s_{\beta-\alpha} m_{h^0}^2}{32\pi^2} \alpha_W, \quad (\text{C.16})$$

$$[iT_{H^0}]_{\text{g.d.}} = -\lambda_Z \frac{igm_Z c_{\beta-\alpha} m_{H^0}^2}{64\pi^2 c_W} \alpha_Z - \lambda_W \frac{igm_W c_{\beta-\alpha} m_{H^0}^2}{32\pi^2} \alpha_W. \quad (\text{C.17})$$

We denote with $g_{h_i h_j h_k}$ the trilinear Higgs couplings between three CP-even Higgses h_i, h_j and h_k . The explicit form of the couplings is given by

$$g_{H^0 H^0 H^0} = \frac{3g}{2m_W s_{2\beta}} \left(4 \frac{m_W^2}{g^2} s_{\alpha+\beta} s_{\beta-\alpha}^2 \Lambda_5 - m_{H^0}^2 (2s_{\alpha+\beta} - s_{2\alpha} c_{\beta-\alpha}) \right). \quad (\text{C.18})$$

as well as by Eqs. (7.1), (7.5) and (7.6). With the explicit form of the gauge-dependence of the tadpoles in Eqs. (C.16) and (C.17), the gauge-dependence of the tadpole diagrams of the CP-even self-energies can be calculated:

$$\begin{aligned} & \left[\left(\begin{array}{c} \text{---} h_i \text{---} \\ | \\ \bullet \\ | \\ H^0 \\ | \\ \bullet \\ | \\ \text{---} h_j \text{---} \end{array} \right) + \left(\begin{array}{c} \text{---} h_i \text{---} \\ | \\ \bullet \\ | \\ h^0 \\ | \\ \bullet \\ | \\ \text{---} h_j \text{---} \end{array} \right) \right]_{\text{g.d.}} \\ &= ig_{h_i h_j H^0} \frac{i}{-m_{H^0}^2} [iT_{H^0}]_{\text{g.d.}} + ig_{h_i h_j h^0} \frac{i}{-m_{h^0}^2} [iT_{h^0}]_{\text{g.d.}} \\ &= -\lambda_Z \frac{ig^2}{128\pi^2 c_W^2} \left[\left(\frac{4m_W^2 \Lambda_5}{g^2} - \frac{s_{2\alpha}}{s_{2\beta}} (m_{H^0}^2 - m_{h^0}^2) \right) \mathcal{O}_{h_i h_j}^{(1)} - 3 \frac{m_{h_i}^2 + m_{h_j}^2}{2} \delta_{h_i h_j} \right] \alpha_Z \\ &\quad - \lambda_W \frac{ig^2}{64\pi^2} \left[\left(\frac{4m_W^2 \Lambda_5}{g^2} - \frac{s_{2\alpha}}{s_{2\beta}} (m_{H^0}^2 - m_{h^0}^2) \right) \mathcal{O}_{h_i h_j}^{(1)} - 3 \frac{m_{h_i}^2 + m_{h_j}^2}{2} \delta_{h_i h_j} \right] \alpha_W. \end{aligned} \quad (\text{C.19})$$

We note that these additional tadpole terms have exactly the same form as the last two lines of Eq. (C.15), but with opposite signs. Consequently, these last two lines are cancelled

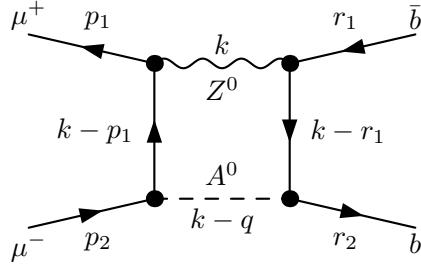


Figure C.4.: Detailed CP-even box contribution. The Feynman diagram represents one amplitude that will contribute to the λ_Z pinch part. The kinematics necessary for the calculation of the pinch part is defined in the diagram. All fermion momenta follow the flow of fermion number, except for the external particles, where the momenta are purely ingoing and outgoing, respectively.

when we consider the CP-even self-energies in the alternative tadpole scheme, whose gauge-dependences are given as the sum of Eqs. (C.15) and (C.19):

$$\begin{aligned}
\left[i\Sigma_{h_i h_j}^{\text{tad}}(q^2) \right]_{\text{g.d.}} &= \lambda_Z \frac{ig^2}{64\pi^2 c_W^2} \left[\mathcal{O}_{h_i h_j}^{(1)} \left(q^4 - 2q^2 m_{A^0}^2 + m_{A^0}^2 \left(m_{h_i}^2 + m_{h_j}^2 \right) - m_{h_i}^2 m_{h_j}^2 \right) \beta_{ZA^0}(q^2) \right. \\
&\quad \left. - \delta_{h_i h_j} \left(q^2 - \frac{m_{h_i}^2 + m_{h_j}^2}{2} \right) \alpha_Z + \mathcal{O}_{h_i h_j}^{(2)} \frac{1}{2} \left(q^4 - m_{h_i}^2 m_{h_j}^2 \right) \left(\beta_{ZZ}(q^2) + \beta_{Z\xi Z}(q^2) \right) \right] \\
&+ \lambda_W \frac{ig^2}{32\pi^2} \left[\mathcal{O}_{h_i h_j}^{(1)} \left(q^4 - 2q^2 m_{H^\pm}^2 + m_{H^\pm}^2 \left(m_{h_i}^2 + m_{h_j}^2 \right) - m_{h_i}^2 m_{h_j}^2 \right) \beta_{WH^\pm}(q^2) \quad (\text{C.20}) \right. \\
&\quad \left. - \delta_{h_i h_j} \left(q^2 - \frac{m_{h_i}^2 + m_{h_j}^2}{2} \right) \alpha_W + \mathcal{O}_{h_i h_j}^{(2)} \frac{1}{2} \left(q^4 - m_{h_i}^2 m_{h_j}^2 \right) \left(\beta_{WW}(q^2) + \beta_{W\xi W}(q^2) \right) \right].
\end{aligned}$$

We observe that the CP-even self-energies in the alternative tadpole scheme are still gauge-dependent. However, the gauge-dependences of the diagonal self-energies vanish on their respective mass-shells:

$$\left[i\Sigma_{H^0 H^0}^{\text{tad}}(m_{H^0}^2) \right]_{\text{g.d.}} = 0, \quad (\text{C.21})$$

$$\left[i\Sigma_{h^0 h^0}^{\text{tad}}(m_{h^0}^2) \right]_{\text{g.d.}} = 0. \quad (\text{C.22})$$

As a consequence, the counterterms of the CP-even Higgs masses m_{H^0} and m_{h^0} , as defined over the diagonal OS CP-even self-energies in Eqs. (4.130) and (4.131), are manifestly gauge-independent.

C.2.2. Derivation of the CP-Even Pinched Self-Energies

Our toy process for extracting the pinch contributions for the CP-even self-energies is the process $\mu^+ \mu^- \rightarrow \bar{b} b$ as depicted in Fig. C.3. The kinematics of the process is shown in the Feynman diagram. Explicitly, we denote with p_1 and p_2 the momenta of the external (anti) muons and with r_1 and r_2 the momenta of the external (anti) bottom quarks. For those, the four-momentum conservation

$$q^2 \equiv s := (p_1 + p_2)^2 = (r_1 + r_2)^2 \quad (\text{C.23})$$

holds, with s being the Mandelstam variable as the center-of-mass energy. Note that in contrast to App. B, we now consider a process which is determined over the s channel and

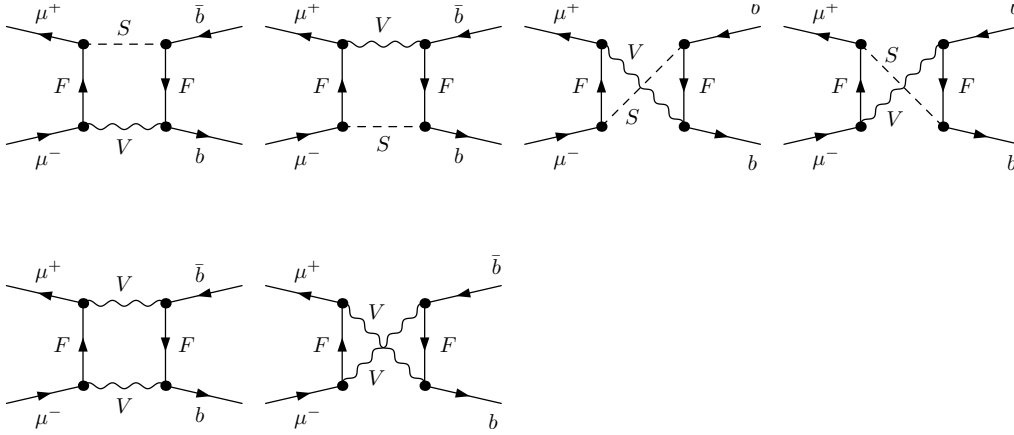


Figure C.5.: CP-even box contributions. Full set of one-loop box diagrams for our toy process that contain pinch contributions to the CP-even Higgs sector. The diagrams consist of contributions from fermions F , gauge bosons V and scalar bosons S .

not the t channel, with t being the Mandelstam variable as the square of four-momentum transfer. This makes no difference in regard to the pinch contributions themselves however, since the pinch technique is process-independent [93].

As it was the case in App. B, all pinch contributions for the CP-even sector have the structure of self-energies, i.e. they depend only on s , but not on any other Mandelstam variable, nor on any external fermion masses. If we denote with

$$Y_{h_i} := \begin{cases} Y_2 & , \text{ if } h_i = H^0 \\ Y_1 & , \text{ if } h_i = h^0 \end{cases} . \quad (\text{C.24})$$

the Yukawa coupling constants for the 2HDM, as defined in Sec. 8.2, then the coupling between the external (anti) muons and CP-even Higgses and the external (anti) bottom quarks and CP-even Higgses is given by

$$i\Gamma_{(p_1, p_2)}^{\mu\mu h_i} = \bar{v}(p_1) \frac{-iem_\mu}{2m_{WSW}} Y_{h_i} u(p_2) , \quad (\text{C.25})$$

$$i\Gamma_{(r_1, r_2)}^{bb h_j} = \bar{u}(r_2) \frac{-iem_b}{2m_{WSW}} Y_{h_j} v(r_1) . \quad (\text{C.26})$$

Applying the pinch technique to all box, triangle and self-energy diagrams of the CP-even sector reveals that all amplitudes can be cast into the form

$$i\mathcal{A}^i = [i\mathcal{A}^i]_{\xi=1} + i\Gamma_{(p_1, p_2)}^{\mu\mu h_i} \frac{i}{q^2 - m_{h_i}^2} i\Sigma_{h_i h_j}^i(q^2) \frac{i}{q^2 - m_{h_j}^2} i\Gamma_{(r_1, r_2)}^{bb h_j} , \quad (\text{C.27})$$

where the pinch parts $i\Sigma_{h_i h_j}^i(q^2)$ from the boxes, triangles and self-energies have to be assigned to the CP-even self-energies $i\Sigma_{h_i h_j}(q^2)$. The generic result in Eq. (C.27) is the 2HDM-analogue to Eq. (B.69).

We begin by considering the exemplary box diagram in Fig. C.4. We want to calculate the pinch contributions originating from this diagram explicitly in order to demonstrate the

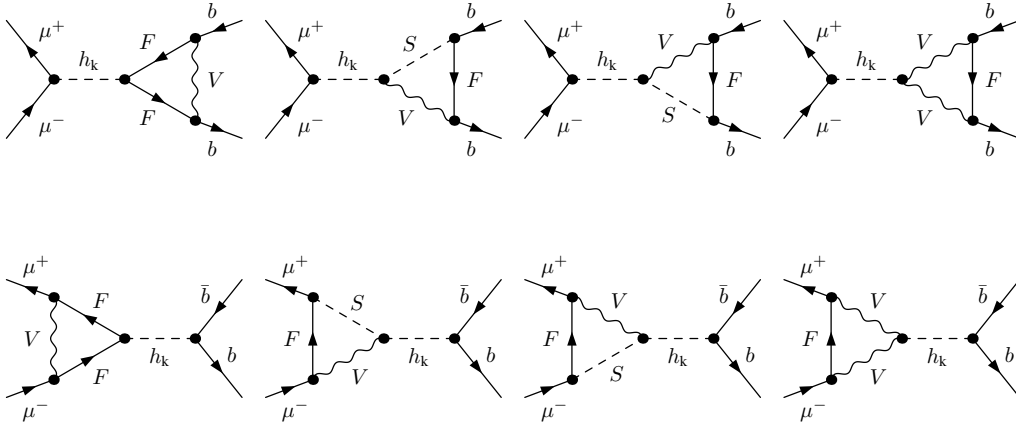


Figure C.6.: CP-even triangle contributions. Full set of one-loop triangle diagrams for our toy process that contain pinch contributions to the CP-even Higgs sector. The sum over both internal CP-even Higgs bosons $h_k \in \{h^0, H^0\}$ is taken. The diagrams consist of contributions from fermions F , gauge bosons V and scalar bosons S .

concept of the pinch technique in the 2HDM. With the kinematics given in the Feynman diagram, the amplitude reads

$$\begin{aligned}
i\mathcal{A}_1^{\text{box}, Z^0 A^0} &= \int_k \bar{v}(p_1) \frac{ie\gamma^\mu}{c_W s_W} \left[\left(\frac{1}{2} - s_W^2 \right) \omega_- - s_W^2 \omega_+ \right] iS(k-p_1) \frac{em_\mu Y_3}{2m_W s_W} \gamma_5 u(p_2) \\
&\quad \cdot \bar{u}(r_2) \frac{em_b Y_3}{2m_W s_W} \gamma_5 iS(k-r_1) \frac{ie\gamma^\nu}{6c_W s_W} \left[(3 - 2s_W^2) \omega_- - 2s_W^2 \omega_+ \right] v(r_1) \\
&\quad \cdot \frac{i}{(k-q)^2 - m_{A^0}^2} i\Delta_{\mu\nu}(k) \\
&= -\frac{e^4 m_\mu m_b Y_3^2}{24m_W^2 s_W^4 c_W^2} \int_k \bar{v}(p_1) \left[\left(\frac{1}{2} - s_W^2 \right) \omega_+ - s_W^2 \omega_- \right] \gamma^\mu S(k-p_1) \gamma_5 u(p_2) \\
&\quad \cdot \bar{u}(r_2) \gamma_5 S(k-r_1) \gamma^\nu \left[(3 - 2s_W^2) \omega_- - 2s_W^2 \omega_+ \right] v(r_1) \\
&\quad \cdot \frac{1}{(k-q)^2 - m_{A^0}^2} \frac{-1}{k^2 - m_Z^2} \left[g_{\mu\nu} - \lambda_Z \frac{k_\mu k_\nu}{k^2 - \xi_Z m_Z^2} \right] \\
&\equiv \left[i\mathcal{A}_1^{\text{box}, Z^0 A^0} \right]_{\xi_Z=1} + \left[i\mathcal{A}_1^{\text{box}, Z^0 A^0} \right]_{\lambda_Z}.
\end{aligned} \tag{C.28}$$

In the last line, we split up the amplitude into the term $\left[i\mathcal{A}_1^{\text{box}, Z^0 A^0} \right]_{\xi_Z=1}$, which contains no pinch contributions, and the term proportional to λ_Z which can be pinched:

$$\begin{aligned}
\left[i\mathcal{A}_1^{\text{box}, Z^0 A^0} \right]_{\lambda_Z} &= -\lambda_Z \frac{e^4 m_\mu m_b Y_3^2}{24m_W^2 s_W^4 c_W^2} \int_k \bar{v}(p_1) \left[\left(\frac{1}{2} - s_W^2 \right) \omega_+ - s_W^2 \omega_- \right] \not{k} S(k-p_1) \gamma_5 u(p_2) \\
&\quad \cdot \bar{u}(r_2) \gamma_5 S(k-r_1) \not{k} \left[(3 - 2s_W^2) \omega_- - 2s_W^2 \omega_+ \right] v(r_1) \\
&\quad \cdot \frac{1}{(k-q)^2 - m_{A^0}^2} \frac{1}{k^2 - m_Z^2} \frac{1}{k^2 - \xi_Z m_Z^2} \\
&\stackrel{(C.1)}{=} -\lambda_Z \frac{e^4 m_\mu m_b Y_3^2}{24m_W^2 s_W^4 c_W^2} \int_k \bar{v}(p_1) \left[\left(\frac{1}{2} - s_W^2 \right) \omega_+ - s_W^2 \omega_- \right] \gamma_5 u(p_2) \frac{1}{k^2 - \xi_Z m_Z^2} \\
&\quad \cdot \bar{u}(r_2) \gamma_5 \left[(3 - 2s_W^2) \omega_- - 2s_W^2 \omega_+ \right] v(r_1) \frac{1}{(k-q)^2 - m_{A^0}^2} \frac{1}{k^2 - m_Z^2} \\
&= -\lambda_Z \frac{ig^4 m_\mu m_b Y_3^2}{384\pi^2 m_W^2 c_W^2} \bar{v}(p_1) \left[\left(\frac{1}{2} - s_W^2 \right) \omega_+ + s_W^2 \omega_- \right] u(p_2) \\
&\quad \cdot \bar{u}(r_2) \left[- (3 - 2s_W^2) \omega_- - 2s_W^2 \omega_+ \right] v(r_1) \beta_{ZA^0}(q^2).
\end{aligned} \tag{C.29}$$

Note that when we applied the Ward identity from Eq. (C.1), we neglected all terms that introduce vertex-like pinch parts, i.e. parts that depend not only on the Mandelstam variable s , but additionally on the external bottom and muon masses. These terms would have to be assigned to the pinched 2HDM vertices. However, since we are only interested in the construction of pinched self-energies, we can neglect them.

We repeat the calculation for the other three box diagrams which contain one Z^0 and one A^0 boson, shown generically in Fig. C.5, and add the results of the calculations to Eq. (C.29), which yields

$$\begin{aligned}
\left[i\mathcal{A}^{\text{box}, Z^0 A^0} \right]_{\lambda_Z} &= \lambda_Z \frac{ig^4 m_\mu m_b Y_3^2}{384\pi^2 m_W^2 c_W^2} \bar{v}(p_1) \left[\left(\frac{1}{2} - s_W^2 \right) + s_W^2 \right] (\omega_+ + \omega_-) u(p_2) \\
&\quad \cdot \bar{u}(r_2) (\omega_+ + \omega_-) \left[- (3 - 2s_W^2) - 2s_W^2 \right] v(r_1) \beta_{ZA^0}(q^2) \\
&= \lambda_Z \frac{ig^4 m_\mu m_b Y_3^2}{256\pi^2 m_W^2 c_W^2} \bar{v}(p_1) u(p_2) \bar{u}(r_2) v(r_1) \beta_{ZA^0}(q^2) \\
&= -\bar{v}(p_1) \frac{-iem_\mu}{2m_W s_W} u(p_2) \lambda_Z \frac{ig^2 Y_3^2}{64\pi^2 c_W^2} \beta_{ZA^0}(q^2) \bar{u}(r_2) \frac{-iem_b}{2m_W s_W} v(r_1) \\
&= -\bar{v}(p_1) \frac{-iem_\mu}{2m_W s_W} (s_{\beta-\alpha} Y_1 + c_{\beta-\alpha} Y_2) Y_3 u(p_2) \lambda_Z \frac{ig^2}{64\pi^2 c_W^2} \beta_{ZA^0}(q^2) \quad (\text{C.30}) \\
&\quad \cdot \bar{u}(r_2) \frac{-iem_b}{2m_W s_W} (s_{\beta-\alpha} Y_1 + c_{\beta-\alpha} Y_2) Y_3 v(r_1) \\
&= \sum_{h_i, h_j} i\Gamma_{(p_1, p_2)}^{\mu\mu h_i} \left[-\lambda_Z \frac{ig^2 \mathcal{O}_{h_i h_j}^{(1)}}{64\pi^2 c_W^2} \beta_{ZA^0}(q^2) \right] i\Gamma_{(r_1, r_2)}^{bb h_j} \\
&\equiv \sum_{h_i, h_j} i\Gamma_{(p_1, p_2)}^{\mu\mu h_i} \frac{i}{q^2 - m_{h_i}^2} i\Sigma_{h_i h_j}^{\text{box}, Z^0 A^0}(q^2) \frac{i}{q^2 - m_{h_j}^2} i\Gamma_{(r_1, r_2)}^{bb h_j},
\end{aligned}$$

where in the last line, we have defined the complete pinch contribution of the $Z^0 A^0$ boxes,

$$i\Sigma_{h_i h_j}^{\text{box}, Z^0 A^0}(q^2) = \lambda_Z (q^2 - m_{h_i}^2)(q^2 - m_{h_j}^2) \frac{ig^2 \mathcal{O}_{h_i h_j}^{(1)}}{64\pi^2 c_W^2} \beta_{ZA^0}(q^2). \quad (\text{C.31})$$

In order to derive the pinch contributions in Eq. (C.30), we have used that the following relations hold independently of the 2HDM type:

$$1 = s_{\beta-\alpha} Y_1 + c_{\beta-\alpha} Y_2, \quad (\text{C.32})$$

$$c_{\beta-\alpha} Y_3 = s_{\beta-\alpha} - Y_1, \quad (\text{C.33})$$

$$s_{\beta-\alpha} Y_3 = -c_{\beta-\alpha} + Y_2. \quad (\text{C.34})$$

Additionally, we neglected in Eq. (C.30) every term which has not the correct Yukawa coupling structure according to Eqs. (C.25) and (C.26), since these terms do not yield pinch contributions to the CP-even self-energies.

The calculation of the pinch parts of all other box diagrams shown in Fig. C.5 is completely analogous. In total, the CP-even pinch contribution from the boxes reads

$$\begin{aligned}
i\Sigma_{h_i h_j}^{\text{box}}(q^2) &= \lambda_Z (q^2 - m_{h_i}^2)(q^2 - m_{h_j}^2) \frac{ig^2}{64\pi^2 c_W^2} \left[\mathcal{O}_{h_i h_j}^{(1)} \beta_{ZA^0}(q^2) + \mathcal{O}_{h_i h_j}^{(2)} \frac{\beta_{ZZ}(q^2) + \beta_{Z\xi Z}(q^2)}{2} \right] \\
&\quad + \lambda_W (q^2 - m_{h_i}^2)(q^2 - m_{h_j}^2) \frac{ig^2}{32\pi^2} \left[\mathcal{O}_{h_i h_j}^{(1)} \beta_{WH^\pm}(q^2) + \mathcal{O}_{h_i h_j}^{(2)} \frac{\beta_{WW}(q^2) + \beta_{W\xi W}(q^2)}{2} \right]. \quad (\text{C.35})
\end{aligned}$$

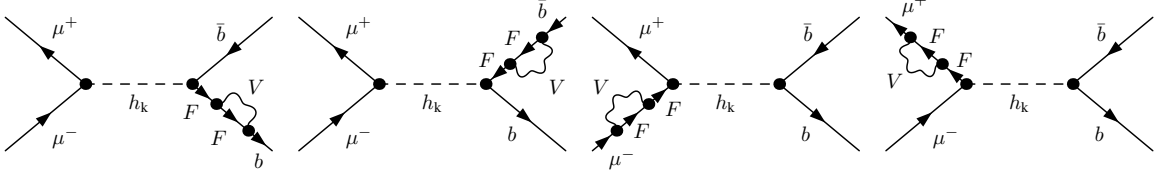


Figure C.7.: CP-even fermion self-energy contributions. Full set of one-loop fermion self-energy corrections for our toy process that contain pinch contributions to the CP-even Higgs sector. The sum over both internal CP-even Higgs bosons $h_k \in \{h^0, H^0\}$ is taken. The diagrams consist of contributions from gauge bosons V and fermions F .

The next pinch contributions we consider are the ones originating from the triangle diagrams shown in Fig. C.6. The calculation is completely analogous to the previous one, therefore, we state the resulting pinch parts directly. The sum of all pinch terms proportional to λ_V reads

$$\begin{aligned}
i\Sigma_{h_i h_j}^{\text{tri}}(q^2) &= \lambda_Z(2q^2 - m_{h_i}^2 - m_{h_j}^2) \frac{-ig^2}{128\pi^2 c_W^2} \left[\mathcal{O}_{h_i h_j}^{(2)} \left[(q^2 + 2m_Z^2) \beta_{ZZ} + q^2 \beta_{Z\xi Z} \right] \right. \\
&\quad \left. + \mathcal{O}_{h_i h_j}^{(1)} (2q^2 - 2m_{A^0}^2) \beta_{ZA^0} + \delta_{h_i h_j} \left(\frac{8}{3} s_W^2 - \frac{40}{9} s_W^4 - 2 \right) \alpha_Z \right] \\
&+ \lambda_W(2q^2 - m_{h_i}^2 - m_{h_j}^2) \frac{-ig^2}{64\pi^2} \left[\mathcal{O}_{h_i h_j}^{(2)} \left[(q^2 + 2m_W^2) \beta_{WW} + q^2 \beta_{W\xi W} \right] - 2\delta_{h_i h_j} \alpha_W \right. \\
&\quad \left. + \mathcal{O}_{h_i h_j}^{(1)} (2q^2 - 2m_{H^\pm}^2) \beta_{WH^\pm} \right] \quad (\text{C.36}) \\
&+ \lambda_\gamma(2q^2 - m_{h_i}^2 - m_{h_j}^2) \frac{5ie^2}{144\pi^2} \delta_{h_i h_j} \alpha_\gamma .
\end{aligned}$$

As it was the case for QCD in App. B.3.8, the triangle diagrams contain additional pinch contributions through longitudinal pinching momenta which are contained in the $\xi = 1$ parts of the amplitudes. The triangle diagrams in Fig. C.6 containing scalar-scalar-vector vertices have a Lorentz structure which allows these longitudinal pinching momenta to appear next to internal fermion propagators so that the latter can be pinched out. In total, these additional pinch contributions read

$$\begin{aligned}
i\Sigma_{h_i h_j}^{\text{add}}(q^2) &= \lambda_Z(2q^2 - m_{h_i}^2 - m_{h_j}^2) \frac{ig^2}{64\pi^2 c_W^2} \mathcal{O}_{h_i h_j}^{(2)} m_Z^2 \beta_{ZZ} \\
&+ \lambda_W(2q^2 - m_{h_i}^2 - m_{h_j}^2) \frac{ig^2}{32\pi^2} \mathcal{O}_{h_i h_j}^{(2)} m_W^2 \beta_{WW} \quad (\text{C.37}) \\
&- \frac{ig^2}{32\pi^2 c_W^2} \left(q^2 - \frac{m_{h_i}^2 + m_{h_j}^2}{2} \right) \left\{ \mathcal{O}_{h_i h_j}^{(1)} B_0(q^2; m_Z^2, m_{A^0}^2) + \mathcal{O}_{h_i h_j}^{(2)} B_0(q^2; m_Z^2, m_Z^2) \right. \\
&\quad \left. + 2c_W^2 \left[\mathcal{O}_{h_i h_j}^{(1)} B_0(q^2; m_W^2, m_{H^\pm}^2) + \mathcal{O}_{h_i h_j}^{(2)} B_0(q^2; m_W^2, m_W^2) \right] \right\} .
\end{aligned}$$

The last pinch parts originate from one-loop corrections to the external fermion legs depicted in Fig. C.7. Tadpole diagrams contributing to the external leg corrections are not depicted,

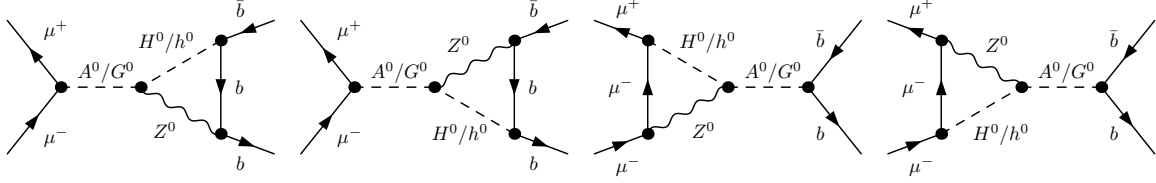


Figure C.8.: Additional pinch terms for the CP-odd sector. The $\xi = 1$ part of the triangle diagrams containing the scalar-scalar-vector vertices yield additional gauge-independent pinch contributions. Only the diagrams which contain pinch contributions to the off-diagonal self-energy $i\Sigma_{G^0 A^0}$ are shown.

since they yield no pinch contributions to the CP-even self-energies. The sum of all pinch parts is given by

$$\begin{aligned}
i\Sigma_{h_i h_j}^{\text{self}}(q^2) &= -\lambda_Z(2q^2 - m_{h_i}^2 - m_{h_j}^2) \frac{ig^2}{128\pi^2 c_W^2} \left(1 - \frac{8}{3}s_W^2 + \frac{40}{9}s_W^4\right) \delta_{h_i h_j} \alpha_Z \\
&\quad - \lambda_W(2q^2 - m_{h_i}^2 - m_{h_j}^2) \frac{ig^2}{64\pi^2} \delta_{h_i h_j} \alpha_W \\
&\quad - \lambda_\gamma(2q^2 - m_{h_i}^2 - m_{h_j}^2) \frac{5ie^2}{144\pi^2} \delta_{h_i h_j} \alpha_\gamma .
\end{aligned} \tag{C.38}$$

With all pinch parts at hand, we are able to create the pinched self-energy of the CP-even sector. It is given as the sum of the self-energy in the alternative tadpole scheme and all pinch parts derived in this subsection. Explicitly, the pinched self-energy reads:

$$\begin{aligned}
i\Sigma_{h_i h_j}^{\text{pinch}}(q^2) &= i\Sigma_{h_i h_j}^{\text{tad}}(q^2) + i\Sigma_{h_i h_j}^{\text{box}}(q^2) + i\Sigma_{h_i h_j}^{\text{tri}}(q^2) + i\Sigma_{h_i h_j}^{\text{self}}(q^2) \\
&\stackrel{\text{(C.14)}}{=} \left[i\Sigma_{h_i h_j}^{\text{tad}}(q^2) \right]_{\xi=1} + \left[i\Sigma_{h_i h_j}^{\text{tad}}(q^2) \right]_{\text{g.d.}} + i\Sigma_{h_i h_j}^{\text{box}}(q^2) + i\Sigma_{h_i h_j}^{\text{tri}}(q^2) + i\Sigma_{h_i h_j}^{\text{self}}(q^2) \\
&= \left[i\Sigma_{h_i h_j}^{\text{tad}}(q^2) \right]_{\xi=1} \\
&\quad - \frac{ig^2}{32\pi^2 c_W^2} \left(q^2 - \frac{m_{h_i}^2 + m_{h_j}^2}{2} \right) \left\{ \mathcal{O}_{h_i h_j}^{(1)} B_0(q^2; m_Z^2, m_{A^0}^2) + \mathcal{O}_{h_i h_j}^{(2)} B_0(q^2; m_Z^2, m_Z^2) \right. \\
&\quad \left. + 2c_W^2 \left[\mathcal{O}_{h_i h_j}^{(1)} B_0(q^2; m_W^2, m_{H^\pm}^2) + \mathcal{O}_{h_i h_j}^{(2)} B_0(q^2; m_W^2, m_W^2) \right] \right\} ,
\end{aligned} \tag{C.39}$$

All gauge-dependences of the CP-even self-energies cancel against the pinch contributions. The pinched self-energy is the sum of the self-energy in the alternative tadpole scheme and the additional gauge-independent pinch contributions from the triangle diagrams. Since Eq. (C.39) holds for *all* gauge-fixing-parameters $\xi \in \{\xi_Z, \xi_W, \xi_\gamma\}$, the pinched self-energy is manifestly gauge-independent.

C.3. The Pinch Technique in the CP-Odd and Charged Sectors

In order to derive the pinch terms for the CP-odd and charged scalar sector of the 2HDM, we repeat the calculations from the previous section to all diagrams that contribute to the respective self-energies. The demonstration of these calculations is beyond the scope of this thesis, since the number of diagrams which have to be considered is large. We want to note that the application of the pinch technique in the CP-odd and charged sector is significantly more involved than for the CP-even sector. After having derived the pinch contributions, we carefully have to allot them between all possible self-energies of the respective sector, e.g. the

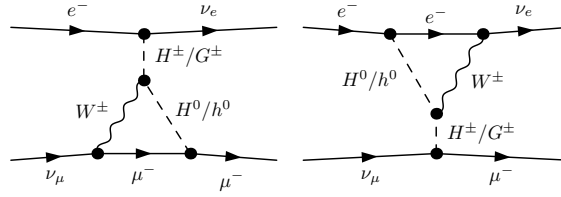


Figure C.9.: Additional pinch terms for the charged sector. The $\xi = 1$ part of the triangle diagrams containing the scalar-scalar-vector vertices yield additional gauge-independent pinch contributions. Only the diagrams which contain pinch contributions to the off-diagonal self-energy $i\Sigma_{G^\pm H^\pm}$ are shown.

pinch contributions of the charged sector have to be distributed amongst the self-energies of the charged Higgses H^\pm , of the Goldstones G^\pm and of the W^\pm bosons as well as amongst all mixed self-energies of all these particles.

Although we will not present the calculations explicitly within this thesis, we have shown that the gauge-dependences of all self-energies in the CP-odd sector are precisely cancelled by all gauge-dependent pinch contributions. For the derivation of these contributions, we used the same toy process as in App. C.2.2. The cancellation of all gauge-dependences in the charged sector is completely analogous. However, in this sector we considered the toy process $e^- \nu_\mu \rightarrow \nu_e \mu^-$ which contains the charged scalar propagators in the t channel.

For the purpose of stating a manifestly gauge-independent definition of the mixing angle counterterm $\delta\beta$, we only need the pinched versions of the CP-odd or charged off-diagonal self-energies $i\Sigma_{G^0 A^0}$ and $i\Sigma_{G^\pm H^\pm}$. All gauge-dependent pinch contributions cancel against the gauge-dependences of these self-energies. Analogous to the CP-even sector, the pinch technique furthermore yields additional gauge-independent pinch contributions from the $\xi = 1$ part of the triangle diagrams shown in Fig. C.8 for the CP-odd and in Fig. C.9 for the charged sector. In total, the pinched off-diagonal self-energies of the CP-odd and charged sectors read

$$i\Sigma_{G^0 A^0}^{\text{pinch}}(q^2) = \left[i\Sigma_{G^0 A^0}^{\text{tad}}(q^2) \right]_{\xi=1} + \frac{ig^2 s_{\beta-\alpha} c_{\beta-\alpha}}{32\pi^2 c_W^2} \left(p^2 - \frac{m_{A^0}^2}{2} \right) [B_0(p^2; m_Z^2, m_{H^0}^2) - B_0(p^2; m_Z^2, m_{h^0}^2)] , \quad (\text{C.40})$$

$$i\Sigma_{G^\pm H^\pm}^{\text{pinch}}(q^2) = \left[i\Sigma_{G^\pm H^\pm}^{\text{tad}}(q^2) \right]_{\xi=1} + \frac{ig^2 s_{\beta-\alpha} c_{\beta-\alpha}}{16\pi^2} \left(p^2 - \frac{m_{H^\pm}^2}{2} \right) [B_0(p^2; m_W^2, m_{H^0}^2) - B_0(p^2; m_W^2, m_{h^0}^2)] . \quad (\text{C.41})$$

Acknowledgement / Danksagungen

Mein besonderer Dank gilt Frau Prof. Dr. M. Margarete Mühlleitner für die spannende Themenstellung und die Möglichkeit, diese Masterarbeit am Institut für Theoretische Physik anzufertigen. Durch ihre offene und freundliche Art fühlte ich mich sowohl am Institut als auch in ihrer Arbeitsgruppe sofort willkommen. Die Zusammenarbeit war geprägt von zahlreichen fruchtbaren Diskussionen, welche es mir ermöglichten, innerhalb kurzer Zeit einen tieferen Einblick in ein spannendes und lehrreiches Forschungsfeld zu erlangen. Weiterhin möchte ich mich bei Frau Prof. Mühlleitner für die Teilnahme am DAAD-Programm bedanken, durch welches mehrere Forschungsaufenthalte in Portugal ermöglicht wurden.

I would like to express my gratitude to Prof. Dr. Rui Santos for agreeing to be the second referee of my master's thesis and for countless fruitful discussions. Additionally, I would like to thank him for his hospitality during my stay in Lisbon in the course of the DAAD exchange, as well as for the great time we had during the stay of our working group in Aveiro.

I express my gratitude to Dr. Marco Sampaio for providing me with countless input parameter sets for the decay processes considered in my thesis.

I would like to thank all members of the Institute of Theoretical Physics for the very nice time and the pleasant atmosphere. I especially enjoyed our countless interesting discussions at the coffee table about a huge variety of different topics.

Ein ganz besonderer Dank gilt der direkten Betreuerin meiner Masterarbeit, Hanna Ziesche, welche für sämtliche meiner Fragen rund um die Themenstellung der Arbeit stets ein offenes Ohr hatte. Durch die hilfreichen Diskussionen mit ihr wurde mir ein schneller Einstieg in die Aufgabenstellung meiner Arbeit ermöglicht.

Ich bedanke mich bei Robin Lorenz für zahlreiche Hilfestellungen und aufschlussreiche Erklärungen zu Beginn meiner Zeit am Institut. Weiterhin bedanke ich mich bei ihm dafür, dass er mir den Quellcode seines im Rahmen seiner Masterarbeit entwickelten Programms `CalcGamma` überlassen hat.

Ein Dank geht an Dr. Michael Rauch, welcher mich in die Subtilitäten der Berechnung von Ein-Schleifen-Integralen, insbesondere in besonderen Massen-Limites, einführte. Durch zahlreiche Diskussionen ermöglichte er mir einen tieferen Einblick in die analytische und numerische Berechnung der Integrale.

Ich bedanke mich bei Juraj Streicher, dass er mich auf die Existenz des \LaTeX -Pakets von `FeynArts` aufmerksam gemacht hat, durch welche ich die Vielzahl der Feynman-Diagramme in meiner Masterarbeit auf schnelle und elegante Weise erstellen konnte.

Ich danke Robin Roth, Nicolae Vasiliu, Alexander Wlotzka und Hanna Ziesche für das Korrekturlesen meiner Arbeit und das sehr hilfreiche Feedback, welches ich von ihnen bekommen habe.

Nicht zuletzt gilt ein besonderer Dank meiner Familie, welche mich während der gesamten Zeit meines Studiums sowohl seelisch wie auch finanziell in jeder Lage unterstützt hat. Ohne sie wäre es mir niemals möglich gewesen, mein Studium so frei zu verfolgen. Ich bedanke mich weiterhin bei meinen Freunden, schlicht und ergreifend für alles.

References

- [1] H. G. Liddell, R. Scott, and H. S. Jones, *A Greek-English lexicon*. Clarendon Press, Oxford [u.a.], 1996.
- [2] H. Kragh, *Quantum Generations: A History of Physics in the Twentieth Century*. History and philosophy of science. Princeton University Press, 2002.
- [3] D. Griffiths, *Introduction to Elementary Particles*. Physics textbook. Wiley, 2008.
- [4] L. H. Ryder, *Quantum Field Theory*. Cambridge Univ. Press, Cambridge, 1985.
- [5] M. E. Peskin and D. V. Schroeder, *An Introduction to quantum field theory*. Advanced book program. Westview Press Reading (Mass.), 1995.
<http://www.slac.stanford.edu/spires/find/books/www?cl=QC174.45%3AP4>.
- [6] S. L. Glashow, “Partial-symmetries of weak interactions,” *Nuclear Physics* **22** no. 4, (1961) 579 – 588.
<http://www.sciencedirect.com/science/article/pii/0029558261904692>.
- [7] S. Weinberg, “A Model of Leptons,” *Phys. Rev. Lett.* **19** (Nov, 1967) 1264–1266.
<http://link.aps.org/doi/10.1103/PhysRevLett.19.1264>.
- [8] A. Salam, “Weak and Electromagnetic Interactions,” *Conf. Proc.* **C680519** (1968) 367–377.
- [9] **CDF** Collaboration, F. Abe *et al.*, “Observation of top quark production in $\bar{p}p$ collisions,” *Phys. Rev. Lett.* **74** (1995) 2626–2631, [arXiv:hep-ex/9503002](https://arxiv.org/abs/hep-ex/9503002) [[hep-ex](#)].
- [10] **DO** Collaboration, S. Abachi *et al.*, “Search for high mass top quark production in $p\bar{p}$ collisions at $\sqrt{s} = 1.8$ TeV,” *Phys. Rev. Lett.* **74** (1995) 2422–2426, [arXiv:hep-ex/9411001](https://arxiv.org/abs/hep-ex/9411001) [[hep-ex](#)].
- [11] **DONUT** Collaboration, K. Kodama *et al.*, “Observation of tau neutrino interactions,” *Phys. Lett.* **B504** (2001) 218–224, [arXiv:hep-ex/0012035](https://arxiv.org/abs/hep-ex/0012035) [[hep-ex](#)].
- [12] P. W. Higgs, “Broken Symmetries and the Masses of Gauge Bosons,” *Phys. Rev. Lett.* **13** (Oct, 1964) 508–509. <http://link.aps.org/doi/10.1103/PhysRevLett.13.508>.
- [13] P. W. Higgs, “Broken symmetries, massless particles and gauge fields,” *Physics Letters* **12** no. 2, (1964) 132 – 133.
<http://www.sciencedirect.com/science/article/pii/0031916364911369>.
- [14] F. Englert and R. Brout, “Broken Symmetry and the Mass of Gauge Vector Mesons,” *Physical Review Letters* **13** (Aug., 1964) 321–323.
- [15] G. S. Guralnik, C. R. Hagen, and T. W. B. Kibble, “Global Conservation Laws and Massless Particles,” *Phys. Rev. Lett.* **13** (Nov, 1964) 585–587.
<http://link.aps.org/doi/10.1103/PhysRevLett.13.585>.

- [16] T. W. B. Kibble, “Symmetry Breaking in Non-Abelian Gauge Theories,” *Phys. Rev.* **155** (Mar, 1967) 1554–1561.
<http://link.aps.org/doi/10.1103/PhysRev.155.1554>.
- [17] **ATLAS** Collaboration, G. Aad *et al.*, “Observation of a new particle in the search for the Standard Model Higgs boson with the ATLAS detector at the LHC,” *Phys. Lett.* **B716** (2012) 1–29, [arXiv:1207.7214](https://arxiv.org/abs/1207.7214) [hep-ex].
- [18] **CMS** Collaboration, S. Chatrchyan *et al.*, “Observation of a new boson at a mass of 125 GeV with the CMS experiment at the LHC,” *Phys. Lett.* **B716** (2012) 30–61, [arXiv:1207.7235](https://arxiv.org/abs/1207.7235) [hep-ex].
- [19] **Tevatron Electroweak Working Group, CDF, DELPHI, SLD Electroweak and Heavy Flavour Groups, ALEPH, LEP Electroweak Working Group, SLD, OPAL, D0, L3** Collaboration, L. E. W. Group, “Precision Electroweak Measurements and Constraints on the Standard Model,” [arXiv:1012.2367](https://arxiv.org/abs/1012.2367) [hep-ex].
- [20] M. Baak, M. Goebel, J. Haller, A. Hoecker, D. Ludwig, K. Moenig, M. Schott, and J. Stelzer, “Updated Status of the Global Electroweak Fit and Constraints on New Physics,” *Eur. Phys. J.* **C72** (2012) 2003, [arXiv:1107.0975](https://arxiv.org/abs/1107.0975) [hep-ph].
- [21] M. Baak, M. Goebel, J. Haller, A. Hoecker, D. Kennedy, R. Kogler, K. Moenig, M. Schott, and J. Stelzer, “The Electroweak Fit of the Standard Model after the Discovery of a New Boson at the LHC,” *Eur. Phys. J.* **C72** (2012) 2205, [arXiv:1209.2716](https://arxiv.org/abs/1209.2716) [hep-ph].
- [22] **ATLAS** Collaboration, G. Aad *et al.*, “Study of the spin and parity of the Higgs boson in diboson decays with the ATLAS detector,” *Eur. Phys. J.* **C75** no. 10, (2015) 476, [arXiv:1506.05669](https://arxiv.org/abs/1506.05669) [hep-ex]. [Erratum: *Eur. Phys. J.* **C76**,no.3,152(2016)].
- [23] **CMS** Collaboration, V. Khachatryan *et al.*, “Precise determination of the mass of the Higgs boson and tests of compatibility of its couplings with the standard model predictions using proton collisions at 7 and 8 TeV,” *Eur. Phys. J.* **C75** no. 5, (2015) 212, [arXiv:1412.8662](https://arxiv.org/abs/1412.8662) [hep-ex].
- [24] **ATLAS** Collaboration, G. Aad *et al.*, “Measurements of the Higgs boson production and decay rates and coupling strengths using pp collision data at $\sqrt{s} = 7$ and 8 TeV in the ATLAS experiment,” *Eur. Phys. J.* **C76** no. 1, (2016) 6, [arXiv:1507.04548](https://arxiv.org/abs/1507.04548) [hep-ex].
- [25] **CMS Collaboration** Collaboration, S. Chatrchyan *et al.*, “Evidence for the direct decay of the 125 GeV Higgs boson to fermions,” *Nature Phys.* **10** (2014) 557–560, [arXiv:1401.6527](https://arxiv.org/abs/1401.6527) [hep-ex].
- [26] **CMS Collaboration** Collaboration, S. Chatrchyan *et al.*, “Study of the Mass and Spin-Parity of the Higgs Boson Candidate via its Decays to Z Boson Pairs,” *Phys. Rev. Lett.* **110** (Feb, 2013) 081803.
<http://link.aps.org/doi/10.1103/PhysRevLett.110.081803>.
- [27] A. D. Sakharov, “Violation of CP Invariance, c Asymmetry, and Baryon Asymmetry of the Universe,” *Pisma Zh. Eksp. Teor. Fiz.* **5** (1967) 32–35. [*Usp. Fiz. Nauk*161,61(1991)].
- [28] M. Persic and P. Salucci, “The baryon content of the Universe,” *Monthly Notices of the Royal Astronomical Society* **258** no. 1, (1992) 14P–18P,
<http://mnras.oxfordjournals.org/content/258/1/14P.full.pdf+html>.
<http://mnras.oxfordjournals.org/content/258/1/14P.abstract>.

- [29] E. M. Dolle and S. Su, “The Inert Dark Matter,” *Phys. Rev.* **D80** (2009) 055012, arXiv:0906.1609 [hep-ph].
- [30] M. A. Díaz, B. Koch, and S. Urrutia-Quiroga, “Constraints to Dark Matter from Inert Higgs Doublet Model,” arXiv:1511.04429 [hep-ph].
- [31] L. Fromme, S. J. Huber, and M. Seniuch, “Baryogenesis in the two-Higgs doublet model,” *JHEP* **11** (2006) 038, arXiv:hep-ph/0605242 [hep-ph].
- [32] J. F. Gunion, H. E. Haber, G. L. Kane, and S. Dawson, “The Higgs Hunter’s Guide,” *Front. Phys.* **80** (2000) 1–448.
- [33] G. C. Branco, P. M. Ferreira, L. Lavoura, M. N. Rebelo, M. Sher, and J. P. Silva, “Theory and phenomenology of two-Higgs-doublet models,” *Phys. Rept.* **516** (2012) 1–102, arXiv:1106.0034 [hep-ph].
- [34] J. Gunion, G. Kane, and J. Wudka, “Search techniques for charged and neutral intermediate-mass Higgs bosons,” *Nuclear Physics B* **299** no. 2, (1988) 231 – 278. <http://www.sciencedirect.com/science/article/pii/0550321388902842>.
- [35] A. Méndez and A. Pomarol, “t-quark loop corrections to neutral Higgs couplings in the two-Higgs-doublet model,” *Physics Letters B* **279** no. 1, (1992) 98 – 105. <http://www.sciencedirect.com/science/article/pii/0370269392918473>.
- [36] A. Freitas and D. Stockinger, “Gauge dependence and renormalization of tan beta in the MSSM,” *Phys. Rev.* **D66** (2002) 095014, arXiv:hep-ph/0205281 [hep-ph].
- [37] G. S. Guralnik, C. R. Hagen, and T. W. Kibble, “Global Conservation Laws and Massless Particles,” *Physical Review Letters* **13** (Nov., 1964) 585–587.
- [38] I. Masina and M. Quiros, “On the Veltman Condition, the Hierarchy Problem and High-Scale Supersymmetry,” *Phys. Rev.* **D88** (2013) 093003, arXiv:1308.1242 [hep-ph].
- [39] J. F. Gunion and H. E. Haber, “Higgs bosons in supersymmetric models (i),” *Nuclear Physics B* **272** no. 1, (1986) 1 – 76. <http://www.sciencedirect.com/science/article/pii/0550321386903408>.
- [40] P. Fayet, “Supersymmetry and weak, electromagnetic and strong interactions,” *Physics Letters B* **64** no. 2, (1976) 159 – 162. <http://www.sciencedirect.com/science/article/pii/0370269376903191>.
- [41] **Planck** Collaboration, P. A. R. Ade *et al.*, “Planck 2013 results. I. Overview of products and scientific results,” *Astron. Astrophys.* **571** (2014) A1, arXiv:1303.5062 [astro-ph.CO].
- [42] N. Cabibbo, “Unitary symmetry and leptonic decays,” *Phys. Rev. Lett.* **10** (Jun, 1963) 531–533. <http://link.aps.org/doi/10.1103/PhysRevLett.10.531>.
- [43] M. Kobayashi and T. Maskawa, “CP Violation in the Renormalizable Theory of Weak Interaction,” *Prog. Theor. Phys.* **49** (1973) 652–657.
- [44] M. Trodden, “Electroweak baryogenesis,” *Rev. Mod. Phys.* **71** (1999) 1463–1500, arXiv:hep-ph/9803479 [hep-ph].
- [45] K. Funakubo, A. Kakuto, and K. Takenaga, “The Effective potential of electroweak theory with two massless Higgs doublets at finite temperature,” *Prog. Theor. Phys.* **91** (1994) 341–352, arXiv:hep-ph/9310267 [hep-ph].

- [46] **Particle Data Group** Collaboration, K. A. Olive *et al.*, “Review of Particle Physics,” *Chin. Phys.* **C38** (2014) 090001.
- [47] D. Ross and M. Veltman, “Neutral currents and the Higgs mechanism,” *Nuclear Physics B* **95** no. 1, (1975) 135 – 147.
<http://www.sciencedirect.com/science/article/pii/055032137590485X>.
- [48] **CMS** Collaboration, D. Pedrini, “Search for the flavour-changing neutral current decay $D^0 \rightarrow \mu^+ \mu^-$ in pp collisions at $\sqrt{s} = 7$ TeV with CMS,” in *Proceedings, 5th International Workshop on Charm Physics (Charm 2012)*. 2012. [arXiv:1208.5908](https://arxiv.org/abs/1208.5908) [hep-ex].
<https://inspirehep.net/record/1182516/files/arXiv:1208.5908.pdf>.
- [49] **ATLAS, CDF, CMS, D0** Collaboration, E. Yazgan, “Flavor changing neutral currents in top quark production and decay,” in *6th International Workshop on Top Quark Physics (TOP2013) Durbach, Germany, September 14-19, 2013*, pp. 285–294. 2014. [arXiv:1312.5435](https://arxiv.org/abs/1312.5435) [hep-ex].
<https://inspirehep.net/record/1272845/files/arXiv:1312.5435.pdf>.
- [50] S. L. Glashow, J. Iliopoulos, and L. Maiani, “Weak Interactions with Lepton-Hadron Symmetry,” *Phys. Rev. D* **2** (Oct, 1970) 1285–1292.
<http://link.aps.org/doi/10.1103/PhysRevD.2.1285>.
- [51] J. F. Gunion, H. E. Haber, and J. Wudka, “Sum rules for Higgs bosons,” *Phys. Rev. D* **43** (Feb, 1991) 904–912. <http://link.aps.org/doi/10.1103/PhysRevD.43.904>.
- [52] A. Denner, “Techniques for calculation of electroweak radiative corrections at the one loop level and results for W physics at LEP-200,” *Fortsch. Phys.* **41** (1993) 307–420, [arXiv:0709.1075](https://arxiv.org/abs/0709.1075) [hep-ph].
- [53] J. M. Cline, K. Kainulainen, and M. Trott, “Electroweak Baryogenesis in Two Higgs Doublet Models and B meson anomalies,” *JHEP* **11** (2011) 089, [arXiv:1107.3559](https://arxiv.org/abs/1107.3559) [hep-ph].
- [54] U. Sarkar, *Particle and Astroparticle Physics*. Series in High Energy Physics, Cosmology and Gravitation. CRC Press, 2007.
- [55] T. Hahn, “Generating Feynman diagrams and amplitudes with FeynArts 3,” *Comput. Phys. Commun.* **140** (2001) 418–431, [arXiv:hep-ph/0012260](https://arxiv.org/abs/hep-ph/0012260) [hep-ph].
- [56] S. Kanemura, Y. Okada, E. Senaha, and C. P. Yuan, “Higgs coupling constants as a probe of new physics,” *Phys. Rev.* **D70** (2004) 115002, [arXiv:hep-ph/0408364](https://arxiv.org/abs/hep-ph/0408364) [hep-ph].
- [57] T. Hahn, *FeynArts 3.9 User’s Guide*. Thomas Hahn, 2015.
<http://www.feynarts.de/FA3Guide.pdf>.
- [58] M. Aoki, S. Kanemura, K. Tsumura, and K. Yagyu, “Models of Yukawa interaction in the two Higgs doublet model, and their collider phenomenology,” *Phys. Rev.* **D80** (2009) 015017, [arXiv:0902.4665](https://arxiv.org/abs/0902.4665) [hep-ph].
- [59] S. L. Glashow and S. Weinberg, “Natural Conservation Laws for Neutral Currents,” *Phys. Rev. D* **15** (Apr, 1977) 1958–1965.
<http://link.aps.org/doi/10.1103/PhysRevD.15.1958>.
- [60] L. D. Faddeev and V. N. Popov, “Feynman Diagrams for the Yang-Mills Field,” *Phys. Lett.* **B25** (1967) 29–30.

- [61] A. Zee, *Quantum Field Theory in a Nutshell: (Second Edition)*. In a Nutshell. Princeton University Press, 2010.
- [62] A. I. Miller, *Early Quantum Electrodynamics: A Sourcebook*. Cambridge University Press, 1995.
- [63] Y. Ne’eman and Y. Kirsh, *The Particle Hunters*. Cambridge University Press, second ed., 1996. <http://dx.doi.org/10.1017/CB09780511599880>. Cambridge Books Online.
- [64] T. S. Kuhn, *Black-body theory and the quantum discontinuity, 1894-1912*. Clarendon Press ; Oxford University Press Oxford : New York, 1978.
- [65] H. Kragh, *Dirac: A scientific biography*. Cambridge University Press, 2005. <http://www.cambridge.org/us/academic/subjects/physics/history-philosophy-and-foundations-physics/dirac-scientific-biography>.
- [66] F. J. Dyson, “Divergence of Perturbation Theory in Quantum Electrodynamics,” *Phys. Rev.* **85** (Feb, 1952) 631–632. <http://link.aps.org/doi/10.1103/PhysRev.85.631>.
- [67] K. Hagiwara, A. D. Martin, D. Nomura, and T. Teubner, “Improved predictions for $g-2$ of the muon and $\alpha(\text{QED}) (M^{*2}(Z))$,” *Phys. Lett.* **B649** (2007) 173–179, [arXiv:hep-ph/0611102](https://arxiv.org/abs/hep-ph/0611102) [hep-ph].
- [68] B. Odom, D. Hanneke, B. D’Urso, and G. Gabrielse, “New Measurement of the Electron Magnetic Moment Using a One-Electron Quantum Cyclotron,” *Phys. Rev. Lett.* **97** (Jul, 2006) 030801. <http://link.aps.org/doi/10.1103/PhysRevLett.97.030801>.
- [69] G. Gabrielse, D. Hanneke, T. Kinoshita, M. Nio, and B. Odom, “New Determination of the Fine Structure Constant from the Electron g Value and QED,” *Phys. Rev. Lett.* **97** (Jul, 2006) 030802. <http://link.aps.org/doi/10.1103/PhysRevLett.97.030802>.
- [70] S. S. Schweber and F. M. H. Villars, “QED and the Men Who Made It: Dyson, Feynman, Schwinger, and Tomonaga,” *American Journal of Physics* **63** no. 4, (1995) 383–384. <http://scitation.aip.org/content/aapt/journal/ajp/63/4/10.1119/1.17926>.
- [71] J. Polchinski, “Renormalization and Effective Lagrangians,” *Nucl. Phys.* **B231** (1984) 269–295.
- [72] C. G. Bollini and J. J. Giambiagi, “Dimensional Renormalization: The Number of Dimensions as a Regularizing Parameter,” *Nuovo Cim.* **B12** (1972) 20–26.
- [73] G. ’t Hooft and M. J. G. Veltman, “Regularization and Renormalization of Gauge Fields,” *Nucl. Phys.* **B44** (1972) 189–213.
- [74] D. Kreimer, “The Role of $\gamma(5)$ in dimensional regularization,” [arXiv:hep-ph/9401354](https://arxiv.org/abs/hep-ph/9401354) [hep-ph].
- [75] S. A. Larin, “The Renormalization of the axial anomaly in dimensional regularization,” *Phys. Lett.* **B303** (1993) 113–118, [arXiv:hep-ph/9302240](https://arxiv.org/abs/hep-ph/9302240) [hep-ph].
- [76] F. Jegerlehner, “Facts of life with $\gamma(5)$,” *Eur. Phys. J.* **C18** (2001) 673–679, [arXiv:hep-th/0005255](https://arxiv.org/abs/hep-th/0005255) [hep-th].
- [77] J.-B. Zuber and C. Itzykson, *Quantum Field Theory*. McGraw-Hill, Inc., 1980.

- [78] J. S. Feldman, T. R. Hurd, L. Rosen, and J. D. Wright, “QED: A proof of renormalizability,” *Lect. Notes Phys.* **312** (1988) 1–176.
- [79] R. Santos and A. Barroso, “On the renormalization of two Higgs doublet models,” *Phys. Rev.* **D56** (1997) 5366–5385, [arXiv:hep-ph/9701257](https://arxiv.org/abs/hep-ph/9701257) [hep-ph].
- [80] M. Thomson, *Modern particle physics*. Cambridge University Press, New York, 2013. <http://www-spires.fnal.gov/spires/find/books/www?cl=QC793.2.T46::2013>.
- [81] G. Kallen, “On the definition of the Renormalization Constants in Quantum Electrodynamics,” *Helv. Phys. Acta* **25** no. 4, (1952) 417. [,509(1952)].
- [82] H. Lehmann, “Über Eigenschaften von Ausbreitungsfunktionen und Renormierungskonstanten quantisierter Felder,” *Il Nuovo Cimento (1943-1954)* **11** no. 4, (2008) 342–357. <http://dx.doi.org/10.1007/BF02783624>.
- [83] A. Denner and S. Dittmaier, “The Complex-mass scheme for perturbative calculations with unstable particles,” *Nucl. Phys. Proc. Suppl.* **160** (2006) 22–26, [arXiv:hep-ph/0605312](https://arxiv.org/abs/hep-ph/0605312) [hep-ph]. [,22(2006)].
- [84] J. Fleischer and F. Jegerlehner, “Radiative corrections to higgs-boson decays in the weinberg-salam model,” *Phys. Rev. D* **23** (May, 1981) 2001–2026. <http://link.aps.org/doi/10.1103/PhysRevD.23.2001>.
- [85] S. Kanemura, M. Kikuchi, and K. Yagyu, “Fingerprinting the extended Higgs sector using one-loop corrected Higgs boson couplings and future precision measurements,” *Nucl. Phys.* **B896** (2015) 80–137, [arXiv:1502.07716](https://arxiv.org/abs/1502.07716) [hep-ph].
- [86] J. W. Van Holten, “Aspects of BRST quantization,” *Lect. Notes Phys.* **659** (2005) 99–166, [arXiv:hep-th/0201124](https://arxiv.org/abs/hep-th/0201124) [hep-th].
- [87] R. H. Bernstein and P. S. Cooper, “Charged Lepton Flavor Violation: An Experimenter’s Guide,” *Phys. Rept.* **532** (2013) 27–64, [arXiv:1307.5787](https://arxiv.org/abs/1307.5787) [hep-ex].
- [88] MEG Collaboration, J. Adam *et al.*, “New limit on the lepton-flavour violating decay $\mu^+ \rightarrow e^+ \gamma$,” *Phys. Rev. Lett.* **107** (2011) 171801, [arXiv:1107.5547](https://arxiv.org/abs/1107.5547) [hep-ex].
- [89] G. ’t Hooft, “Dimensional regularization and the renormalization group,” *Nuclear Physics B* **61** (1973) 455 – 468. <http://www.sciencedirect.com/science/article/pii/0550321373903763>.
- [90] F. Olness and R. Scalise, “Regularization, Renormalization, and Dimensional Analysis: Dimensional Regularization meets Freshman E&M,” *Am. J. Phys.* **79** (2011) 306, [arXiv:0812.3578](https://arxiv.org/abs/0812.3578) [hep-ph].
- [91] R. Lorenz, “Full One-Loop Electroweak Corrections to the Decays $H^+ \rightarrow W^+ h/H$ in the Two-Higgs-Doublet Model,” Master’s thesis, Karlsruher Institut für Technologie, Jun, 2015. <https://www.itp.kit.edu/prep/diploma/PSFiles/MasterRobinL.pdf>.
- [92] J. M. Cornwall, “Dynamical mass generation in continuum quantum chromodynamics,” *Phys. Rev. D* **26** (Sep, 1982) 1453–1478. <http://link.aps.org/doi/10.1103/PhysRevD.26.1453>.
- [93] D. Binosi and J. Papavassiliou, “Pinch Technique: Theory and Applications,” *Phys. Rept.* **479** (2009) 1–152, [arXiv:0909.2536](https://arxiv.org/abs/0909.2536) [hep-ph].
- [94] J. Papavassiliou, “Gauge Invariant Proper Selfenergies and Vertices in Gauge Theories with Broken Symmetry,” *Phys. Rev.* **D41** (1990) 3179.

- [95] J. M. Cornwall and J. Papavassiliou, “Gauge Invariant Three Gluon Vertex in QCD,” *Phys. Rev.* **D40** (1989) 3474.
- [96] J. Papavassiliou, “Gauge independent transverse and longitudinal self energies and vertices via the pinch technique,” *Phys. Rev.* **D50** (1994) 5958–5970, [arXiv:hep-ph/9406258](https://arxiv.org/abs/hep-ph/9406258) [hep-ph].
- [97] G. Degrossi and A. Sirlin, “Gauge-invariant self-energies and vertex parts of the standard model in the pinch technique framework,” *Phys. Rev. D* **46** (Oct, 1992) 3104–3116. <http://link.aps.org/doi/10.1103/PhysRevD.46.3104>.
- [98] N. Baro and F. Boudjema, “Automatised full one-loop renormalisation of the MSSM II: The chargino-neutralino sector, the sfermion sector and some applications,” *Phys. Rev.* **D80** (2009) 076010, [arXiv:0906.1665](https://arxiv.org/abs/0906.1665) [hep-ph].
- [99] R. G. Stuart, “Gauge invariance, analyticity and physical observables at the Z0 resonance,” *Phys. Lett.* **B262** (1991) 113–119.
- [100] J. R. Espinosa and Y. Yamada, “Scale independent and gauge independent mixing angles for scalar particles,” *Phys. Rev.* **D67** (2003) 036003, [arXiv:hep-ph/0207351](https://arxiv.org/abs/hep-ph/0207351) [hep-ph].
- [101] J. Honerkamp, “The Question of invariant renormalizability of the massless Yang-Mills theory in a manifest covariant approach,” *Nucl. Phys.* **B48** (1972) 269–287.
- [102] H. Kluberg-Stern and J. B. Zuber, “Renormalization of non-abelian Gauge Theories in a Background Field Gauge. I. Green Functions,” *Phys. Rev.* **D12** (1975) 482–488.
- [103] H. Kluberg-Stern and J. B. Zuber, “Renormalization of non-Abelian gauge theories in a background-field gauge. II. Gauge-invariant operators,” *Phys. Rev. D* **12** (Nov, 1975) 3159–3180. <http://link.aps.org/doi/10.1103/PhysRevD.12.3159>.
- [104] I. Y. Arefeva, L. D. Faddeev, and A. A. Slavnov, “Generating Functional for the s Matrix in Gauge Theories,” *Theor. Math. Phys.* **21** (1975) 1165. [Teor. Mat. Fiz.21,311(1974)].
- [105] A. Denner, G. Weiglein, and S. Dittmaier, “Gauge Invariance of Green Functions: Background Field Method versus Pinch Technique,” *Phys. Lett.* **B333** (1994) 420–426, [arXiv:hep-ph/9406204](https://arxiv.org/abs/hep-ph/9406204) [hep-ph].
- [106] A. Denner, G. Weiglein, and S. Dittmaier, “Application of the background field method to the electroweak standard model,” *Nucl. Phys.* **B440** (1995) 95–128, [arXiv:hep-ph/9410338](https://arxiv.org/abs/hep-ph/9410338) [hep-ph].
- [107] S. Bauberger, M. Böhm, G. Weiglein, F. A. Berends, and M. Buza, “Calculation of two-loop self-energies in the electroweak Standard Model,” *Nucl. Phys. Proc. Suppl.* **37B** no. 2, (1994) 95–114, [arXiv:hep-ph/9406404](https://arxiv.org/abs/hep-ph/9406404) [hep-ph].
- [108] D. Binosi, “Electroweak pinch technique to all orders,” *J. Phys.* **G30** (2004) 1021–1064, [arXiv:hep-ph/0401182](https://arxiv.org/abs/hep-ph/0401182) [hep-ph].
- [109] N. J. Watson, “Universality of the pinch technique gauge boson selfenergies,” *Phys. Lett.* **B349** (1995) 155–164, [arXiv:hep-ph/9412319](https://arxiv.org/abs/hep-ph/9412319) [hep-ph].
- [110] D. Binosi and J. Papavassiliou, “Gauge independent off-shell fermion selfenergies at two loops: the cases of QED and QCD,” *Phys. Rev.* **D65** (2002) 085003, [arXiv:hep-ph/0110238](https://arxiv.org/abs/hep-ph/0110238) [hep-ph].

- [111] S. Hashimoto, J. Kodaira, Y. Yasui, and K. Sasaki, “The Background field method: Alternative way of deriving the pinch technique’s results,” *Phys. Rev.* **D50** (1994) 7066–7076, [arXiv:hep-ph/9406271](#) [hep-ph].
- [112] G. Degrandi and P. Slavich, “On the NLO QCD corrections to Higgs production and decay in the MSSM,” *Nucl. Phys.* **B805** (2008) 267–286, [arXiv:0806.1495](#) [hep-ph].
- [113] J. A. Coarasa Perez, D. Garcia, J. Guasch, R. A. Jimenez, and J. Sola, “Quantum effects on $t \rightarrow H + b$ in the MSSM: A Window to ‘virtual’ supersymmetry?,” *Eur. Phys. J.* **C2** (1998) 373–392, [arXiv:hep-ph/9607485](#) [hep-ph].
- [114] R. Santos, A. Barroso, and L. Brucher, “Top quark loop corrections to the decay $H \rightarrow h_0 W^+$ in the two Higgs doublet model,” *Phys. Lett.* **B391** (1997) 429–433, [arXiv:hep-ph/9608376](#) [hep-ph].
- [115] K. E. Williams, H. Rzehak, and G. Weiglein, “Higher order corrections to Higgs boson decays in the MSSM with complex parameters,” *Eur. Phys. J.* **C71** (2011) 1669, [arXiv:1103.1335](#) [hep-ph].
- [116] M. Misiak *et al.*, “Updated NNLO QCD predictions for the weak radiative B-meson decays,” *Phys. Rev. Lett.* **114** no. 22, (2015) 221801, [arXiv:1503.01789](#) [hep-ph].
- [117] D. Ross and J. Taylor, “Renormalization of a unified theory of weak and electromagnetic interactions,” *Nuclear Physics B* **51** (1973) 125 – 144. <http://www.sciencedirect.com/science/article/pii/0550321373905051>.
- [118] R. Mertig, M. Bohm, and A. Denner, “FEYN CALC: Computer algebraic calculation of Feynman amplitudes,” *Comput. Phys. Commun.* **64** (1991) 345–359.
- [119] G. ’t Hooft and M. J. G. Veltman, “Scalar One Loop Integrals,” *Nucl. Phys.* **B153** (1979) 365–401.
- [120] T. Hahn and M. Perez-Victoria, “Automatized one loop calculations in four-dimensions and D-dimensions,” *Comput. Phys. Commun.* **118** (1999) 153–165, [arXiv:hep-ph/9807565](#) [hep-ph].
- [121] T. Kinoshita, “Mass singularities of Feynman amplitudes,” *J. Math. Phys.* **3** (1962) 650–677.
- [122] T. D. Lee and M. Nauenberg, “Degenerate systems and mass singularities,” *Phys. Rev.* **133** (Mar, 1964) B1549–B1562. <http://link.aps.org/doi/10.1103/PhysRev.133.B1549>.
- [123] N. Nakanishi, “General Theory of Infrared Divergence,” *Progress of Theoretical Physics* **19** (Feb., 1958) 159–168.
- [124] D. R. Yennie, S. C. Frautschi, and H. Suura, “The infrared divergence phenomena and high-energy processes,” *Annals Phys.* **13** (1961) 379–452.
- [125] L. Lewin, *Polylogarithms and associated functions*. North-Holland, New York, NY, 1981. <https://cds.cern.ch/record/100000>.
- [126] D. Lopez-Val and J. Sola, “Neutral Higgs-pair production at Linear Colliders within the general 2HDM: Quantum effects and triple Higgs boson self-interactions,” *Phys. Rev.* **D81** (2010) 033003, [arXiv:0908.2898](#) [hep-ph].
- [127] Wolfram Research, Inc., *Mathematica 10.3*. Wolfram Research, Inc., Champaign, Illinois, 2015.

- [128] **LHC Higgs Cross Section Working Group** Collaboration, S. Dittmaier *et al.*, “Handbook of LHC Higgs Cross Sections: 1. Inclusive Observables,” arXiv:1101.0593 [hep-ph].
- [129] **ATLAS, CMS** Collaboration, G. Aad *et al.*, “Combined Measurement of the Higgs Boson Mass in pp Collisions at $\sqrt{s} = 7$ and 8 TeV with the ATLAS and CMS Experiments,” *Phys. Rev. Lett.* **114** (2015) 191803, arXiv:1503.07589 [hep-ex].
- [130] R. Coimbra, M. O. P. Sampaio, and R. Santos, “ScannerS: Constraining the phase diagram of a complex scalar singlet at the LHC,” *Eur. Phys. J.* **C73** (2013) 2428, arXiv:1301.2599 [hep-ph].
- [131] P. M. Ferreira, R. Santos, and A. Barroso, “Stability of the tree-level vacuum in two Higgs doublet models against charge or CP spontaneous violation,” *Phys. Lett.* **B603** (2004) 219–229, arXiv:hep-ph/0406231 [hep-ph]. [Erratum: *Phys. Lett.*B629,114(2005)].
- [132] I. P. Ivanov, “Minkowski space structure of the Higgs potential in 2HDM,” *Phys. Rev.* **D75** (2007) 035001, arXiv:hep-ph/0609018 [hep-ph]. [Erratum: *Phys. Rev.*D76,039902(2007)].
- [133] M. Maniatis, A. von Manteuffel, O. Nachtmann, and F. Nagel, “Stability and symmetry breaking in the general two-Higgs-doublet model,” *Eur. Phys. J.* **C48** (2006) 805–823, arXiv:hep-ph/0605184 [hep-ph].
- [134] A. Barroso, P. M. Ferreira, I. P. Ivanov, and R. Santos, “Metastability bounds on the two Higgs doublet model,” *JHEP* **06** (2013) 045, arXiv:1303.5098 [hep-ph].
- [135] S. Kanemura, T. Kubota, and E. Takasugi, “Lee-quigg-thacker bounds for higgs boson masses in a two-doublet model,” *Physics Letters B* **313** no. 1, (1993) 155 – 160. <http://www.sciencedirect.com/science/article/pii/0370269393912052>.
- [136] A. G. Akeroyd, A. Arhrib, and E. Naimi, “Note on tree-level unitarity in the general two higgs doublet model,” *Physics Letters B* **490** no. 1–2, (2000) 119 – 124. <http://www.sciencedirect.com/science/article/pii/S037026930000962X>.
- [137] N. G. Deshpande and E. Ma, “Pattern of symmetry breaking with two Higgs doublets,” *Phys. Rev. D* **18** (Oct, 1978) 2574–2576. <http://link.aps.org/doi/10.1103/PhysRevD.18.2574>.
- [138] P. M. Ferreira, R. Guedes, M. O. P. Sampaio, and R. Santos, “Wrong sign and symmetric limits and non-decoupling in 2HDMs,” *JHEP* **12** (2014) 067, arXiv:1409.6723 [hep-ph].
- [139] M. E. Peskin and T. Takeuchi, “Estimation of oblique electroweak corrections,” *Phys. Rev. D* **46** (Jul, 1992) 381–409. <http://link.aps.org/doi/10.1103/PhysRevD.46.381>.
- [140] C. D. Froggatt, R. G. Moorhouse, and I. G. Knowles, “Leading radiative corrections in two-scalar-doublet models,” *Phys. Rev. D* **45** (Apr, 1992) 2471–2481. <http://link.aps.org/doi/10.1103/PhysRevD.45.2471>.
- [141] W. Grimus, L. Lavoura, O. M. Ogreid, and P. Osland, “The Oblique parameters in multi-Higgs-doublet models,” *Nucl. Phys.* **B801** (2008) 81–96, arXiv:0802.4353 [hep-ph].
- [142] H. E. Haber and D. O’Neil, “Basis-independent methods for the two-Higgs-doublet model III: The CP-conserving limit, custodial symmetry, and the oblique parameters S, T, U,” *Phys. Rev.* **D83** (2011) 055017, arXiv:1011.6188 [hep-ph].

-
- [143] **LEP, DELPHI, OPAL, ALEPH, L3** Collaboration, G. Abbiendi *et al.*, “Search for Charged Higgs bosons: Combined Results Using LEP Data,” *Eur. Phys. J.* **C73** (2013) 2463, [arXiv:1301.6065 \[hep-ex\]](#).
- [144] **ATLAS** Collaboration, G. Aad *et al.*, “Search for charged Higgs bosons decaying via $H^+ \rightarrow \tau\nu$ in top quark pair events using pp collision data at $\sqrt{s} = 7$ TeV with the ATLAS detector,” *JHEP* **06** (2012) 039, [arXiv:1204.2760 \[hep-ex\]](#).
- [145] **CMS** Collaboration, S. Chatrchyan *et al.*, “Search for a light charged Higgs boson in top quark decays in pp collisions at $\sqrt{s} = 7$ TeV,” *JHEP* **07** (2012) 143, [arXiv:1205.5736 \[hep-ex\]](#).
- [146] R. V. Harlander, S. Liebler, and H. Mantler, “SusHi: A program for the calculation of Higgs production in gluon fusion and bottom-quark annihilation in the Standard Model and the MSSM,” *Comput. Phys. Commun.* **184** (2013) 1605–1617, [arXiv:1212.3249 \[hep-ph\]](#).
- [147] P. Bechtle, O. Brein, S. Heinemeyer, G. Weiglein, and K. E. Williams, “HiggsBounds: Confronting Arbitrary Higgs Sectors with Exclusion Bounds from LEP and the Tevatron,” *Comput. Phys. Commun.* **181** (2010) 138–167, [arXiv:0811.4169 \[hep-ph\]](#).
- [148] R. Harlander, M. Mühlleitner, J. Rathsman, M. Spira, and O. Stål, “Interim recommendations for the evaluation of Higgs production cross sections and branching ratios at the LHC in the Two-Higgs-Doublet Model,” [arXiv:1312.5571 \[hep-ph\]](#).
- [149] T. Appelquist and J. Carazzone, “Infrared singularities and massive fields,” *Phys. Rev. D* **11** (May, 1975) 2856–2861.
<http://link.aps.org/doi/10.1103/PhysRevD.11.2856>.
- [150] J. F. Gunion and H. E. Haber, “The CP conserving two Higgs doublet model: The Approach to the decoupling limit,” *Phys. Rev.* **D67** (2003) 075019, [arXiv:hep-ph/0207010 \[hep-ph\]](#).